



Tomas Bata University in Zlín

Faculty of Technology

Doctoral Thesis

Study of poly(vinyl alcohol) solution for inkjet printing

Studium roztoku polyvinylalkoholu pro inkoustový tisk

Author: **Ing. Pavol Šuly**

Study programme: Chemistry and materials technology P2808

Study course: Technology of macromolecular compounds 2808V006

Supervisor: Assoc. Prof. Ing. et Ing. Ivo Kuřitka, Ph.D. et Ph.D.

Consultants: Assoc. Prof. Ing. Tomáš Sedláček, Ph.D.
Ing. Pavel Urbánek, Ph.D.

Zlín, July 2017

© Pavol Šuly, July 2017

ACKNOWLEDGEMENT

First and foremost, I would like to express my sincere gratitude to my supervisor Assoc. Prof. Ing. et Ing. Ivo Kuřitka, Ph.D. et Ph.D. for his guidance, advices and encouragement during my doctoral study.

I would like also to thank my consultants Assoc. Prof. Ing. Tomáš Sedláček, Ph.D. and Ing. Pavel Urbánek, Ph.D. for their contributions and assistance during my doctoral study.

My gratitude goes to all my colleagues, friends and every person who helped me throughout my doctoral study.

With special mention to Ing. Michal Machovský, Ph.D., Ing. Jan Mašlík, Ing. Petr Krčmář, doc. Ing. Michal Sedlačík, Ph.D., Ing. František Bílek, Ing. Michal Urbánek, Ph.D. and Ing. Pavel Urbánek, Ph.D. again for introducing me into measurement techniques and helping me with experimental work.

Special thanks belong to my family for its support, patience and endless love.

This dissertation work was supported by the following projects: CPS (CZ.1.05/2.1.00/03.0111), CPS+ (LO 1504), IGA/FT/2013/025, IGA/FT/2014/006, IGA/CPS/2015/006, and IGA/CPS/2016/007 in which I was working as a member of the research teams.

The financial support granted to my research work by the funding providers is partially addressed and acknowledged in the respective places in my published or submitted papers whenever the opportunity to do so was. Here, I would like to thank the Centre of Polymer Systems and the Faculty of Technology of the Tomas Bata University in Zlín for the financial support during my studies.

TABLE OF CONTENTS

Acknowledgement.....	1
Table of contents	2
Abstract.....	4
Abstrakt	5
Keywords / Klíčová Slova.....	6
1. Introduction	7
2. Inkjet Printing.....	9
2.1 Continuous Inkjet Printing.....	10
2.2 Drop-on-Demand Inkjet Printing	11
2.2.1 Thermal inkjet printing.....	12
2.2.2 Piezoelectric inkjet printing	14
2.2.3 Electrostatic inkjet printing	17
3. Inkjet Inks.....	19
3.1 Classification of Inkjet Inks.....	19
3.1.1 Water-based inkjet inks	20
3.1.2 Solvent-based (non-aqueous) inkjet inks	21
3.1.3 Phase change (Hot-melt) inkjet inks	22
3.1.4 UV curable inkjet inks.....	22
3.2 Crucial Ink Parameters	24
3.2.1 Viscosity	24
3.2.2 Surface tension and wettability	28
3.3 Ink Jetting Characteristics	31
3.3.1 Ink drop formation	31
3.3.2 Dimensionless criteria.....	33
3.3.3 Viscoelasticity in drop formation.....	36
4. Poly(vinyl alcohol)	42
5. Aims of the Thesis.....	44
6. Experimental Part.....	45
6.1 Materials and Sample Preparation.....	45
6.2 Experimental Methods.....	45
6.3 Notes on Data Statistics.....	47
7. Results and Discussion.....	48

7.1	Rational Selection of Polymer-Solvent Systems	48
7.2	Rheological Study	50
7.3	Determination of Solvation Effect: Viscometric Analysis of Solvent-Polymer System.....	56
7.4	Stability of PVA Solutions in Water/DMSO co-Solvent	60
7.5	Surface Tension.....	65
7.6	Analysis of Prepared Solutions and Printing Process with the Aid of Dimensionless Numbers within the Framework of Mainstream Viscous Fluid Models	68
7.7	Drop Ejection Analysis	77
7.8	Refinement of Dimensionless Analysis by Including the Viscoelasticity of the Polymer Solution.....	88
7.9	Characterization of Dimatix Fluid Cartridge	96
7.10	Printed Demonstration Patterns and Analysis Thereof.....	101
7.10.1	Substrate properties	101
7.10.2	Resolution of printed patterns.....	102
7.10.3	Effect of Polymer-Solvent System	103
7.10.4	Patterns Prepared from PVA in Water/DMSO Mixture.....	104
8.	Advices for Preparation of Polymer Based Ink – Step by Step.....	109
9.	Concluding Summary	111
10.	Closing Remarks.....	116
10.1	Contribution to Science and Practice	116
10.2	Ongoing Research and Future Prospective	117
	References	118
	APPENDIX – Supplementary data.....	137
	List of figures	145
	List of tables.....	149
	List of abbreviations	150
	List of symbols.....	151
	List of dimensionless numbers.....	153
	List of units	154
	List of publications.....	155
	Conference contributions	156
	Curriculum vitae	157

ABSTRACT

The thesis is focused on the preparation and characterization of water-soluble polymer-based ink. The poly(vinyl alcohol) (PVA) was chosen for preparation of the suitable polymer inks for a Dimatix material printer DMP-2800 Series working in the drop-on-demand mode. Drop-on-demand mode is one of the two most frequently used ways in inkjet printing technology, which represents a promising technique for simultaneously patterning and material deposition without a need of any master form or masks.

The work is divided into theoretical background and experimental part. In theory, a brief introduction to inkjet printing technology is provided, and followed by a description of the main ways of drops generation together with the device arrangement. The next section of the theoretical part is focused on a description of the basic groups of inkjet inks as well as on their crucial parameters, for example, viscosity and surface tension. Further, the interpretational framework based on dimensionless criteria for ink property evaluation is discussed including viscoelasticity assessment. A brief description of the polyvinyl alcohol is provided in the last section of theoretical part. The main aim and goals of this work are defined in accordance with hitherto achieved results of research conducted in the laboratories at our institution and with the aid of information gathered from a literature review summarized in previous sections. The experimental part is arranged in accord once the sequence of the performed experiments. The core section of the work contains 10 chapters discussing obtained results. At the beginning of this section, a selection of polymer-solvent system is discussed. The rheological and viscosity studies of the prepared solutions are shown and discussed including the stability and aging issue. In the next step, discussion of surface tension measurements follows. According to the obtained results, the suitability of prepared solution for inkjet printing was performed by calculating and evaluating of dimensionless criteria to find optimum solution properties correlating with a processing window. It was shown that the analytical apparatus does not fully cover the studied case, in spite of its improvement. Therefore, the next section is dedicated to study drop formation and analysis of this process resulting in a study of viscoelastic properties and their analysis with respect to ink drop formation. In the last step, other parameters (waveform, drop velocity) were optimized with respect to the used digital printing cartridge and modified polyethylene terephthalate. Consequently, the prepared demonstration patterns are characterised and presented mainly in the form of images captured by optical microscopy and data obtained by AFM and mechanical profilometry.

Gathered knowledge and experience were summarized in the concluding summary section and in a short advice for practical ink development procedure.

ABSTRAKT

Práce je zaměřena na přípravu a charakterizaci inkoustu na bázi vodě-rozpustného polymeru. Polyvinylalkohol (PVA) byl vybrán pro přípravu polymerního inkoustu vhodného pro materiálovou tiskárnu Dimatix DMP-2800 Series pracující v módu „drop-on-demand“, který je jedním ze dvou nejčastěji používaných v technologii inkoustového tisku, a který představuje slibnou metodu pro vzorování a ukládání materiálu současně bez potřeby použití tiskové formy anebo masky.

Práce je rozdělena na část teoretickou a část experimentální. Stručný úvod do technologie inkoustového tisku je popsán v teoretické části, za kterou následuje popis hlavních způsobů generace kapiček spolu s uspořádáním zařízení pro každý typ tvorby kapiček. Následující sekce teoretické části je zaměřena na popis základních druhů inkoustů, jakož i na jejich klíčové parametry, které jsou reprezentovány hlavně viskozitou a povrchovým napětím. Následně je diskutován interpretační rámec založený na bezrozměrných kritériích včetně posouzení viskoelasticity. Poslední sekce teoretické částí je věnována stručnému textu o polyvinylalkoholu. Poté jsou definovány hlavní cíle této práce v souladu s dříve dosaženými výsledky výzkumu prováděného v laboratořích naší instituce a s pomocí informací shromážděných v průběhu literární rešerše. Experimentální část je uspořádána v souladu s posloupností provedených experimentů. Základní část práce obsahuje 10 kapitol zabývajících se získanými výsledky a jejich diskusí. Na začátku této části je diskutován výběr vhodného systému polymer-rozpouštědlo. Dále jsou uvedeny a diskutovány reologické a viskozimetrické studie připravených roztoků včetně záležitosti ohledně jejich stability a stárnutí. Poté následuje diskuse stanovení povrchového napětí. Na základě naměřených hodnot byla stanovena vhodnost připravených roztoků pro inkoustový tisk pomocí vypočtení a vyhodnocení bezrozměrných kritérií. Ty přes zlepšení mohou být využity pro nalezení vhodných vlastností inkoustu, které by odpovídaly zpracovatelskému oknu. Bylo prokázáno, že analytický přístroj zcela nepopisuje studovaný případ. Další sekce je proto věnována studiu tvorby kapičky a analýze tohoto procesu, který vyžaduje studium visko-elastických vlastností a jejich analýzu s ohledem na tvorbu kapičky. V posledním kroku byly optimalizovány ostatní parametry (waveforma, rychlost kapičky) pro použití digitálního tisku definované inkoustové kazety a konkrétní model flexibilního substrátu z poly(ethylentereftalátu). V návaznosti na to jsou připravené demonstrační vzory charakterizovány a prezentovány zejména ve formě obrázků zachycených pomocí optické mikroskopie a dat získaných z AFM a mechanické profilometrie.

Získané znalosti a zkušenosti byly shrnuty krok za krokem v části závěrečné shrnutí a v krátkém shrnujícím doporučení pro praktickou přípravu a vývoj inkoustu.

KEYWORDS / KLÍČOVÁ SLOVA

English

Poly(vinyl alcohol); solution; polymer; solvent; viscosity; surface tension; surface energy; rheology; viscoelasticity; relaxation time; ink; inkjet; Rayleigh breakup; velocity; drop; printability; stability; gel; digital printing; resolution; pattern; substrate;

Czech

Polyvinylalkohol; roztok; polymer; rozpouštědlo; viskozita; povrchové napětí; povrchová energie; reologie; viskoelastická; relaxační čas; inkoust; inkjet; Rayleighova nestabilita; rychlost; kapka; tisknutelnost; stabilita; gel; digitální tisk; rozlišení; vzor; podklad;

1. INTRODUCTION

Printing process has been known for a long period. The first written evidence came from the Far East. The earliest printed text, images and patterns were prepared by woodblock printing technique during the Tang Dynasty (618 – 906) in China. The “*Diamond Sutra*” is the first printed book with illustrations and text. The patterns were printed by hand-carved wooden blocks. The writing ink was composed by lamp-black and gum dissolved in water. This method remained unique for the next 1,300 years and was identified as the letterpress process following the invention of other printing processes. The first paper mills were opened in France and Germany in 1338 and 1390, respectively. Metal plates were for the first time used for printing in the middle of the 15th century by Johannes Gutenberg. Gutenberg printed the Bible subsequently after invention of the printing press with metal plates. Richard Hoe invented the cylinder press, which printed 8,000 sheets per hour in the middle of 19th century. Photogravure printing was invented by Klic at the end of 19th century. The modern printers were introduced in the second half of the 20th century by Xerox, Hewlett-Packard, Epson, and Canon. [1, 2]

In principle, the printing process allows to duplicate a predefined text, picture, pattern, functional group (material deposition) onto printed medium with use of ink. In other words, it is a special type of surface patterning.

The main types of printing processes include offset lithographic, flexographic, gravure, letterpress, screen printing, inkjet printing process and toner printing system. [1] The major part of the mentioned processes is based on roll-to-roll principle and each of them is specific for certain application. However, only a few of them are suitable for surface functionalization, especially for surface treatment of solid polymer materials or polymer deposition because of their thermal, mechanical, and functional properties.¹

Additionally, polymers represent a unique group of material that could be divided according to their density, flexibility, and cost-effectiveness. However, the special properties are required in industrial applications. These requirements are often attributed to their surface properties, wettability, biocompatibility, adhesion, gas permeability and other. Hence, the surface properties are often modified to obtain desired features. [4] Shi *et al.*[5] provided short description of

¹ The term polymer is derived from the Greek words meaning “many parts.” The polymer is prepared by a process known as polymerization, which involves the chemical combination of many small chemical units known as monomers. The repeating units may be either single atoms as in sulphur molecules or groups of atoms such as methylene units. Polymers have a linear, branched or cross-linked structure. [3]

micro- and nano-patterning of polymers. Their work included the patterning via special structural arrangement of polymers; phase separation of copolymers; special physical properties, and other methods.

Moreover, some kinds of polymers could be processed in liquid form (solution or dispersion). In this case, polymers are used for preparation of special devices such as light-emitting diodes.[6]

Hence, according to the required properties or purpose, the various patterns of other materials could be printed and deposited onto polymers surface. On the other hand, some kinds of polymer could be used for preparation of special functional devices. In this case, the inkjet printing seems to be an appropriate printing process for polymer patterning.

Although the inkjet printing seems to be relatively simple process of deposition, there are several important conditions that should be fulfilled for good printing performance. They include the requirements on inkjet ink, substrate properties, drop formation, and on the printing algorithm, as can be seen in Figure 1. Each part plays an important role in a whole inkjet printing process. Inkjet ink requirements include its properties, such as viscosity and surface tension; for substrate, the crucial parameters involve wettability, surface energy and surface structure; and the printing procedure, actuator type, drop size represent characteristic parameters of printing platform and drop generation.[7]

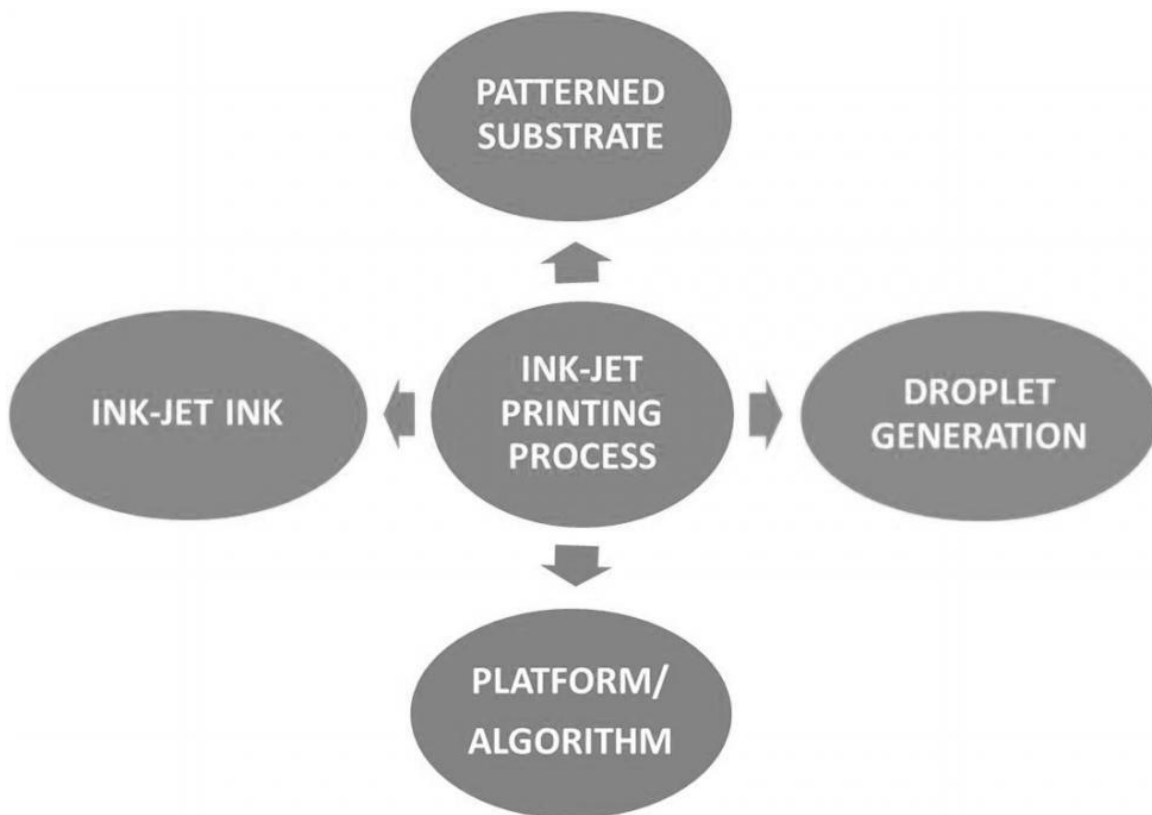


Figure 1. Major parts of inkjet printing process. [7]

2. INKJET PRINTING

Inkjet printing (IJP) technology allows controlled material deposition and patterning without need of any master form or masks. Moreover, it is a non-contact deposition technique based on computer-controlled ejection of fluid (ink) drops from print-head nozzle to a pre-defined substrate position. [8, 9] Technique is suitable for preparation of several patterns, whose shape and size depend on a specific application. In this case, IJP represents a versatile method, which can find application in various industrial sectors.

Although the IJP is still used for decoration, mainly, of textile substrates, the latest applications include preparation of printed electronics such as sensors [10, 11], partially or all-inkjet printed organic thin film transistors and capacitors [12, 13], or ionic actuators [14]; organic, or polymer light-emitting diodes (OLED or PLED) [6, 15, 16]; fabrication of polymer lenses [17]; and biological applications, e.g. cell-patterning [18-20]. Although inkjet printing may be used for preparation of different patterns or/and devices, this technique could be also used together with other deposition techniques to obtain a required functionalized device, such as a pixel-like capacitive vapour micro-sensor [21] or an organic thin film transistor [22]. Additionally, three-dimensional printing represents a method for rapid prototyping that aims to prepare a complex shape pattern directly from a computer by overprinting (slice after slice). Main advantages of inkjet printing are low ink consumption, possibility to manufacture very fine and precise structures, i.e. it is a cost-saving process. On the other hand, the technique is suitable for low viscosity inks (include polymer solutions, dispersions and others) [23]. Other limitations may come from thermal and chemical stability of device parts that are in contact with the used ink.

Actually, the writing with drops of ink is the most critical step of the process. Moreover, the distance between two adjacent drops (drop spacing) defines a final resolution of printed patterns. On the other hand, morphology and quality of deposited patterns depend on stability of printed lines, appropriate printing parameters, convenient drying conditions and other factors. An alteration of appearance of the printed pattern, in this case, basic line, was described by Soltman and Subramanian [24]. They found that a “coffee-ring effect” and its topology may be reduced by controlling the substrate temperature. A similar study, which focused on the influence of drop spacing and drying conditions on the electrical properties of printed carbon nanotubes network, was performed by Wang *et al.*[25]. Furthermore, the effect of pulse voltage drops on inkjet printing of a silver nano-powder suspension and deionized water was investigated by Tsai *et al.*[26], who found the range of pulse voltages, which is needed for recombination of ejected drops, for both silver suspension as well as deionized water.

In practice, the resolution is characterized by abbreviation “DPI - Dots per Inch”. The relationship between resolution and drop spacing is shown in Figure 2, which manifests that resolution is inversely proportional to the drop spacing.

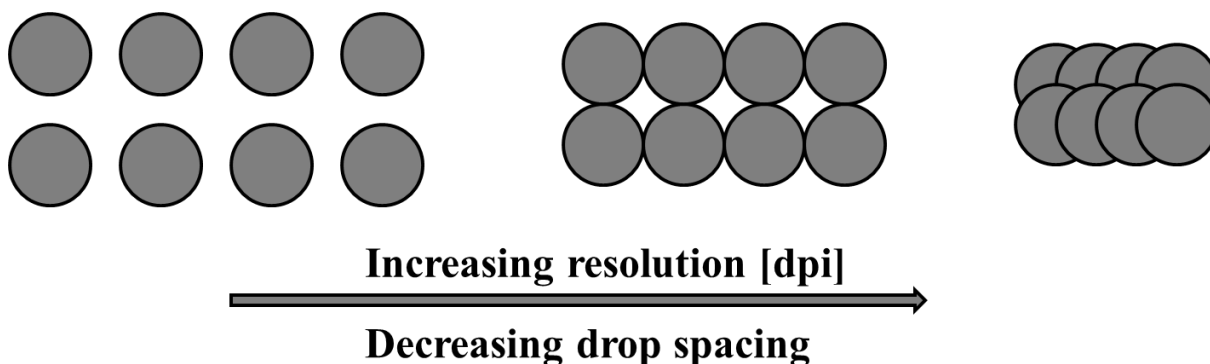


Figure 2. Scheme of relationship between resolution and drop spacing.

The inkjet printing methods can be divided according to drop generation modes into two groups, namely continuous inkjet printing (CIJ) and drop-on-demand (DOD). The DOD modes can be later divided into several subgroups. [9] In this work, the only CIJ, thermal DOD and piezoelectric DOD will be described in detail due to their use in practice.

2.1 Continuous Inkjet Printing

The first inkjet printing technology, which will be described, is continuous inkjet printing (CIJ). Figure 3 illustrates the process of drops generation and deposition onto substrate according to Li *et al.*[9] A stream of liquid is broken up into stream of drops of a size and quantity determined mainly with the surface tension of liquid, the pressure applied to it and, of course, the nozzle diameter. The more regular drops are obtained with regular pressure pulses, which are applied continuously to the ink at suitable frequency that can be controlled with setting of high-frequency alternating voltage on a piezoelectric crystal. [1] Then, particularly formed drops are electrostatically charged by an electrode. The intensity of charge depends on voltage applied to the electrode in the moment of drops separation from the nozzle. Further, the drops pass through the parallel deflection plates, where charged drops are deflected. In this stage, there are two possibilities. First, the required drops with charge are deflected and deposited onto patterned substrate, while the position on substrate is defined by charge intensity; the drops without charge are collected in a gutter and ink can be therefore reused. In the second case, the uncharged drops deposited onto substrate and the drops, which carry charges, are deflected to gutter. The stepped voltage pulses applied to the charging electrode are gated by signals that define the character matrix and

allow drops to be printed.[1, 27] The second type of discussed drops deflection and deposition is illustrated in Figure 3.

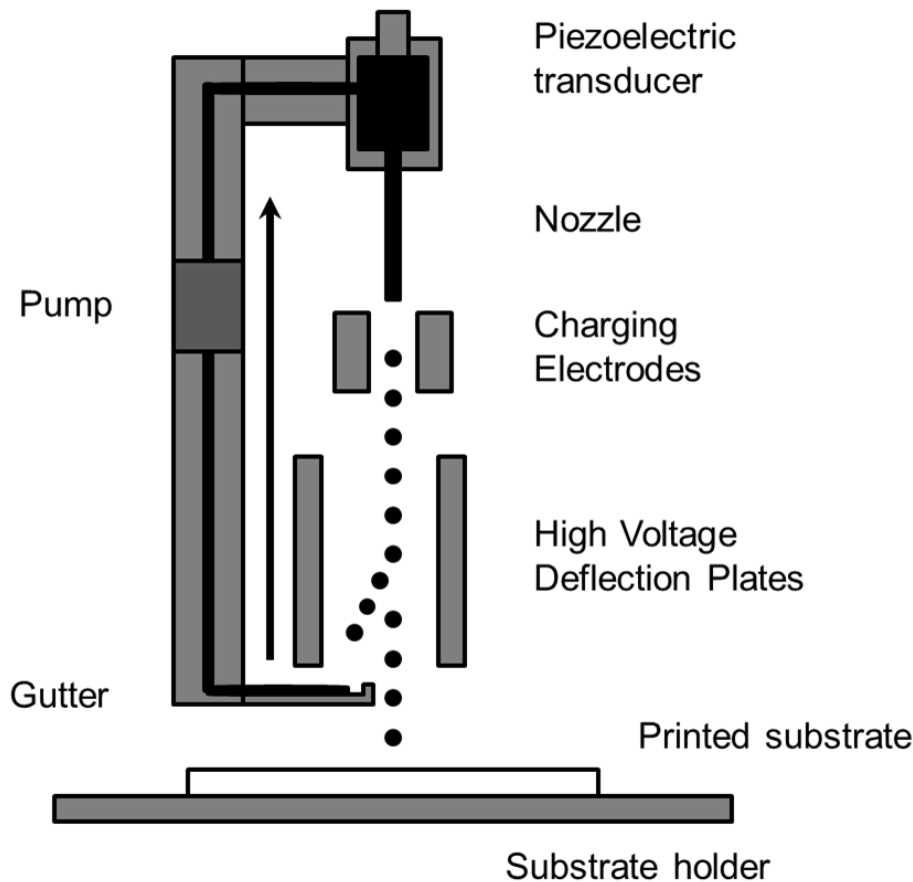


Figure 3. Scheme of continuous inkjet printing.[9]

The applications of CIJ include mainly the marking and coding of products and packages. The benefits of this system are: printing at high-speed (drop velocity is up to 25 m/s); printing nozzle is not easily clogged; and a use of volatile inks allow their rapid drying. On the contrary, the major disadvantages involve: the use of inks that can be charged, relative low print resolution due to the high-speed printing, high maintenance, and the perception that the technology is environmentally unfriendly due to the use of solvent-based fluids.[9, 28]

2.2 Drop-on-Demand Inkjet Printing

Another inkjet printing technology is drop-on-demand (DOD). In this case, the drops are generated and deposited only when required. The main subcategories of DOD inkjet printing are thermal, piezoelectric and others (for example electrostatic). Hence, drops are formed in dependence on the initial impulse, which is evoked by piezoelectric or heating element.

2.2.1 Thermal inkjet printing

Thermal inkjet (TIJ) technology was invented by the Canon and Hewlett Packard companies in late 1970s and early 1980s. This printing method is still used in home as well as in office printers. [29] The basic principle of TIJ is shown in Figure 4. As can be seen, the print-head contains the integrated thin film resistor (heater) inside the nozzle chamber. The vapour bubble generation is induced by rapid heating of this resistor. Following expansion of vapour bubble results in displacement of liquid (ink) inside the print-head and finally, the ejection of drop from nozzle is put into effect. The vapour bubble collapses when the atmospheric pressure is reached. Then the whole process, which lasts several micro-seconds, repeats again.[30]

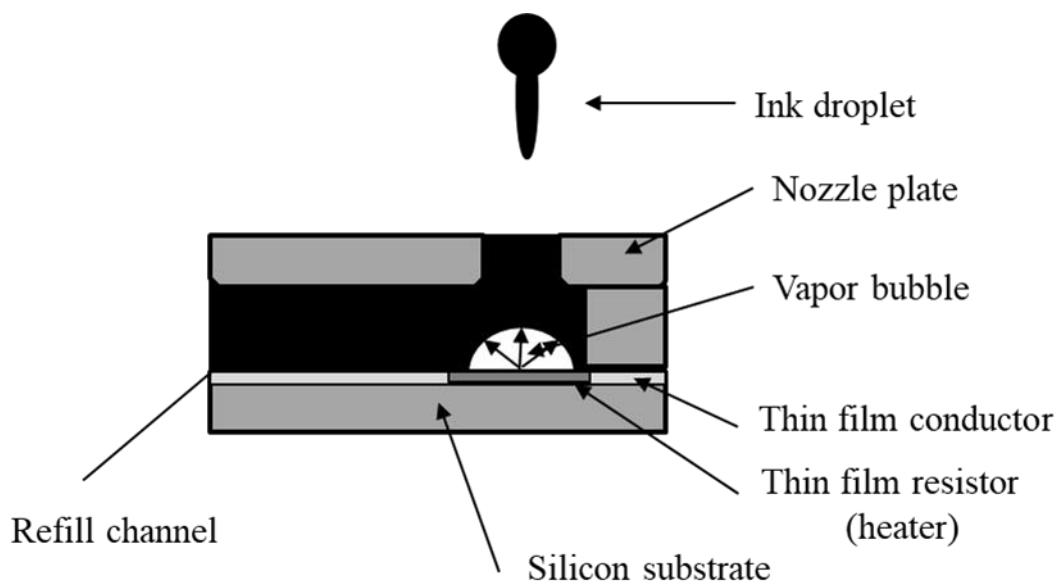


Figure 4. Basic principle of the thermal inkjet printing process.[30]

The process of drop generation can be described in more details, as it is illustrated in Figure 5. At the beginning, an electric pulse that lasts few micro-seconds, increases the temperature of resistor by more than 300 °C. As a consequence of the rapid heating, the superheating limit of liquid is reached, which results in the inertial pressure of bubbles that acts on the entire heat-transfer surface as an impulse force. This force induces the growth of bubbles, moreover, the expansion of bubbles continues due to inertia that leads to the drop ejection. The inertial pressure of bubbles is of a vacuum state, falling below atmospheric pressure. The bubbles stop their movement and start collapsing because of the differences with the external atmospheric pressure and fluid resistance. When the bubbles disappeared, the high-speed gas-liquid interface of the ink collides with the surface of heater element and impulse force starts acting once again. This

effect can be explained as a cavitation phenomenon occurring in the place of bubbles disappearance (in the heater centre). [9, 31]

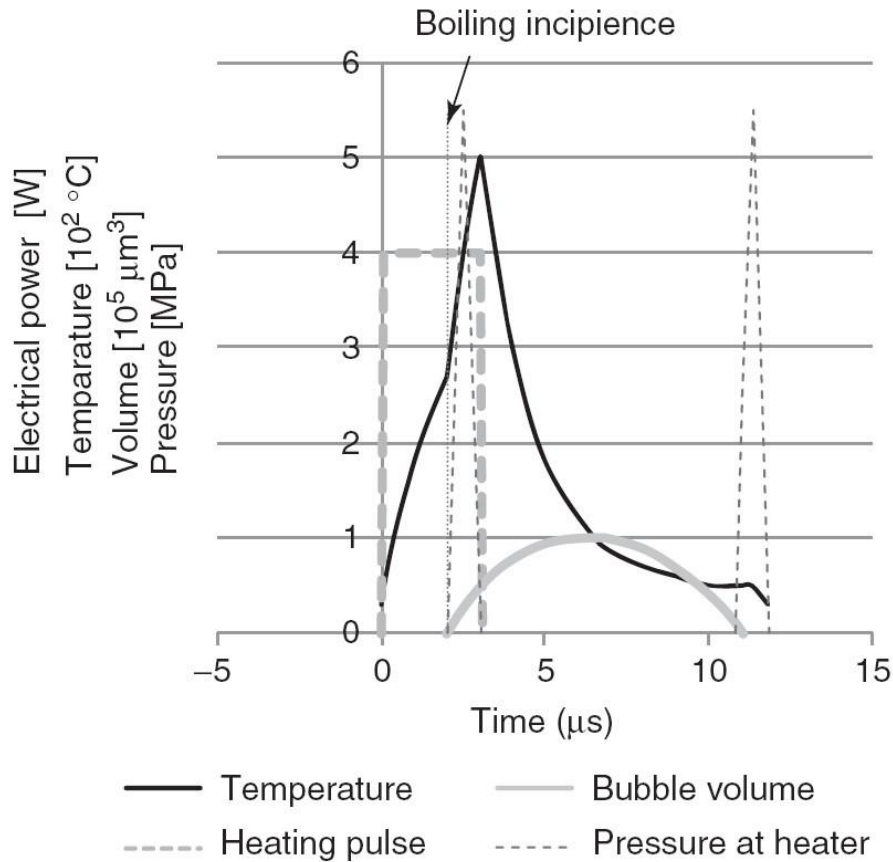


Figure 5. Mechanism of jetting in thermal inkjet printing in relation with different parameters.[31]

The main advantages of this technique include the high nozzle density, small drop size, and lower print-head and product costs. On the other hand, the great attention is related to ink requirements. In special cases, the ink can lose their functionality because of high temperature during printing (delicate fluids or polymers).[28]

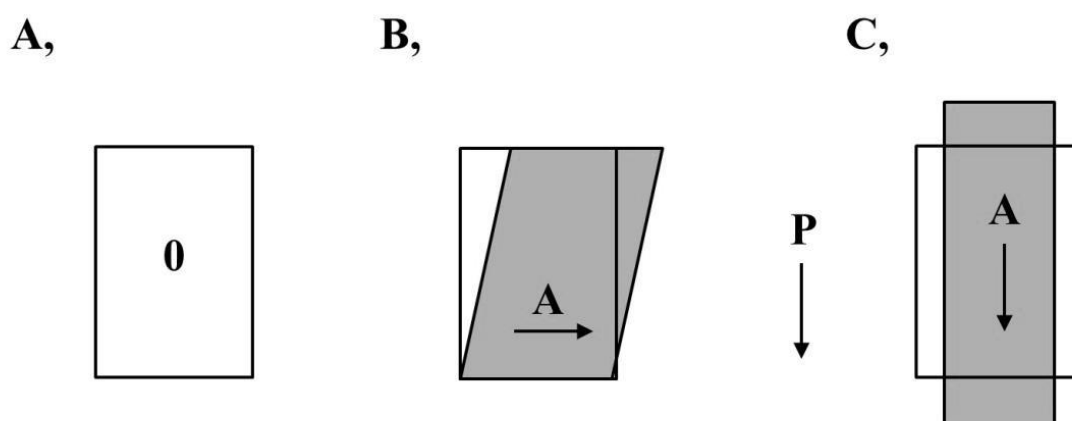
In the recent years, the original printers based on thermal drops generation have been continuously implemented into biological applications such as biosensors and cell patterning. Setti *et al.*[32] used TIJ printer for preparation of a horseradish peroxidase based amperometric biosensor for detection of a hydrogen peroxide as well as for preparation of a prototype of glucose biosensor onto ITO-coated glass [33]. Cui and Boland [34] demonstrated the fabrication of human microvasculature based on bio-ink composed from human microvascular endothelial cells and fibrin. Moreover, they found that the simultaneous printing of above mentioned compounds can promote proliferation and microvasculature formation. Of course, the whole printing process was performed with a sterile modified cartridge as well as the thermal printer. Neural cell structure and their viability and electrophysiology were investigated by Xu *et al.*[35]. They also used

the modified thermal inkjet printer that was sterilized before using. They demonstrated a capability of preparation of a three-dimensional structure by printing layer-by-layer as well as potential of inkjet printing, which can be applied in neural tissue engineering.

2.2.2 Piezoelectric inkjet printing

Piezoelectric inkjet printing (PIJ) is another technique, in which the drops are formed only when they are required. In this case, the heating element is replaced with piezoelectric element.

The piezoelectric element (usually based on Lead Zirconium Titanate - PZT) is a material that exhibits a unique property - piezoelectric effect. It is the ability of certain materials to generate an electric field in a response to mechanical strain (applying pressure/stress), and more precisely, it is called *direct piezoelectric effect*. Oppositely, if this material is exposed to an external electric field, the asymmetric displacement or deformation of its crystal structure occurs, which is called *indirect piezoelectric effect*. [36] The piezoelectric effect is anisotropic; the material will change shape depending upon the relative orientation of the applied field as well as the poling direction. Figure 6 shows the effect of poling direction and applied field direction in the piezoelectric element. At the beginning, the PZT is in the standby position (Figure 6-A). Then, if the applied field is perpendicular (Figure 6-B) to the poling direction, the element will shear. If the applied field is in the same (opposite) direction as poling field, the piezo element will expand (or contract) along that direction and contract (expand) in orthogonal direction (Figure 6-C). [29]



P: Poling field; A: Actuation field

Figure 6. The effects of electric field and poling direction in piezoelectric material. Standby position (A); shear mode (B); and thickness deformation mode (C).[29]

The PZT represents a key and most important unit in all inkjet printers operating in this mechanism of drop generation. It could be expected that the drops will be generated and ejected as a result of distortion of this element.

This piezo element is used for conversion of an electrical driving voltage into a mechanical deformation of an ink chamber resulting in pressure generation required for drop formation and ejection from the nozzle. [37] There are many possibilities, which describe the incorporation of the piezo element in the print-head. Figure 7 shows the structure of print-head with piezo crystals on both sides of ink chamber. At the beginning, piezo elements are in the initial (standby) position (Figure 7-A). The electric field is generated when – voltage and + voltage are applied. There are two cases how the field can be applied; in the first case (Figure 7-B), the field result in opening of the nozzle walls. In the second case (Figure 7-C), the reverse electric field is generated that makes the nozzle walls curve in the closing direction, near to the nozzle, and causes the formation and ejection of ink drop. Then, the nozzle walls are returned back to the initial (standby) position (Figure 7-D). This sequence of operations describes the shear mode of piezo elements.[38]

The print-heads with the piezo element contain several numbers of nozzles, which can share the PZT or not. In the cases where the walls of ink channels are shared, they must work synchronically. Thus, the drop is ejected from one channel, and another drop cannot be ejected at the same time from the adjacent channel. [29]

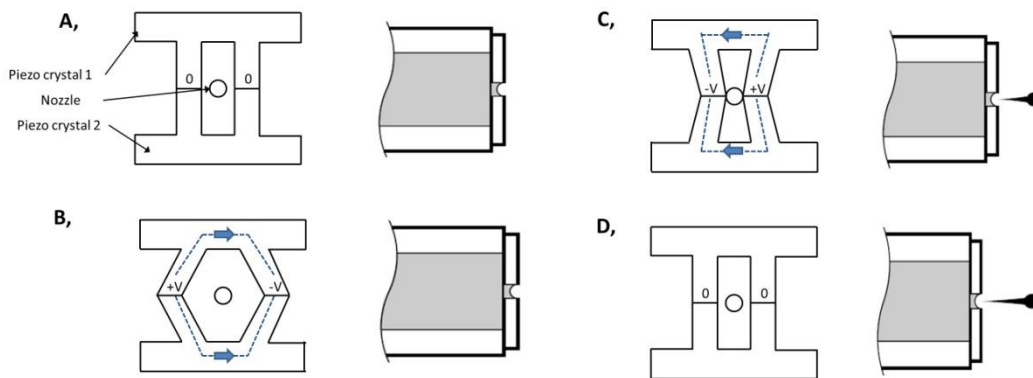


Figure 7. Principle of print-head with piezoelectric crystal on both sides of the ink pressure chamber.[38]

The process of drop ejection and the work of PZT are discussed above. However, it is necessary to describe the actual process of PZT deformation in detail. The deformation of PZT is defined by voltage of pulse waveform. The waveform can be divided into several segments.

The example of one proposed waveform is illustrated in Figure 8-A together with the print-head nozzle with PZT located in the wall (Figure 8-B). The actual position of PZT corresponds to a “START” (or Standby) phase on waveform. In the phase 1, the voltage decreases to zero volts, which results in returning PZT back to a neutral position in the wall. In this phase, the chamber is filled with ink from a reservoir; moreover, the ink is also pulled from nozzle or meniscus at the same time, which results in maximum volume of the ink inside the chamber. Then, the applied voltage leads to compression of pumping chamber and also to drop ejection due to generated pressure (Phase 2). Consequently, the deflected PZT is returned back to the initial (standby) position. Thus, the voltage decreases back to the initial level (Phases 3 and 4). In this step, the motion of PZT is controlled during drop break-off.[39]

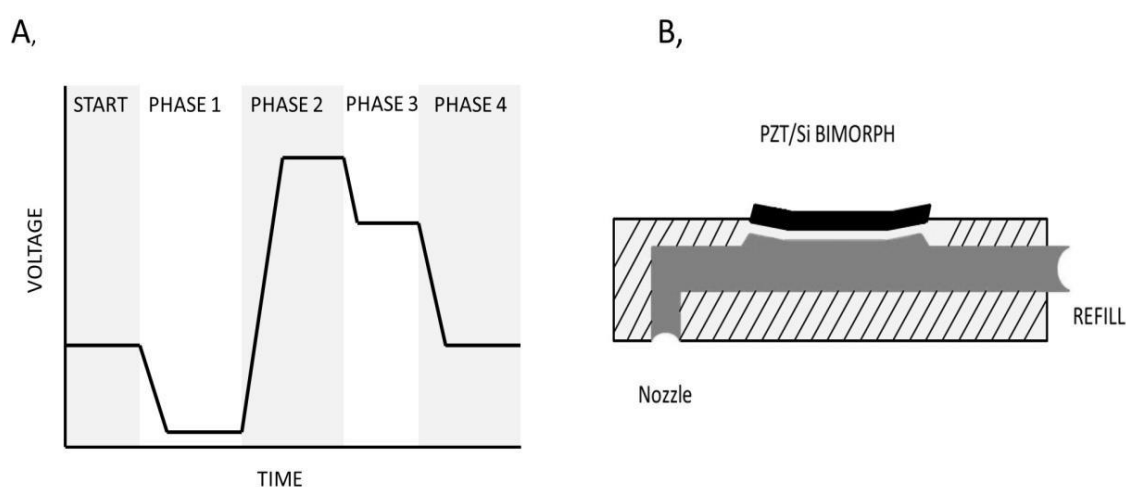


Figure 8. The proposed segments of pulse waveform (A), and the pumping chamber of piezoelectric print-head (B).[39]

The “PULL-PUSH” drive principle is described in previous situation (Figure 8-B). It is based on already deflected piezo element in the standby position. Moreover, this principle is often used in commercially available piezoelectric printers. However, Yamaguchi *et al.* [40] used a “PUSH-PULL” principle for cell patterning. In this case, the piezo element is not deflected in the initial position. In the next step, the PZT is deflected resulting in drop ejection from the nozzle (push). At the end of jetting cycle, the piezo element is returned back to the initial position; this process is joined with refilling of pumping chamber by inks (pull). It was found that an arbitrary number of cells can be deposited in a desired position at high speed. Moreover, three-dimensional tissue structures can be achieved by piling up these cell layers.

Structure of waveform can be changed to obtain stable drops ejection and formation. Additionally, uniform drops velocity can be achieved by changing waveform parameters such as level, duration and slew rate. These parameters can

be modified independently on each other in the case, when the each nozzle (ink channel) contains its own piezo element (in the case of the Dimatix cartridges and print-head with 16 nozzles). [39]

There are also several examples, in which their authors investigated the effect of pulse waveform on the printing process. Cummins *et al.* [41] investigated the influence of the above mentioned parameters (voltage level, slew rate, and duration) on the preparation of Greek cross patterns from novel platinum organometallic inks. A study focused on a reduction of drop volume by controlling actuating waveform, was performed by Gan *et al.*[42]. They studied the effect of unipolar, bipolar, M-shape and W-shape waveforms. The most important parameters were investigated in order to determine both ink jetting behaviour and required volume of ejected drops. The proposed waveforms were tested on a Newtonian fluid (deionized water) as well as on a non-Newtonian fluid (Poly(3,4-ethylenedioxythiophene)-PEDOT polymer ink). The influence of similar parameters on printing of water using computer-aided analysis system (FLOW-3D) was investigated by Liu *et al.*[43]. Their research was focused on the characteristic times of the uniform waveform. The simulated results were later compared to the experimental observed data. The results provide the relation between first slope, duration, and the final period of uniform waveform and the formation of satellite drops, over-suction of liquid around the nozzle, and the drops velocity. Only one piezo actuator was considered in the previously described studies. The authors Kim *et al.* [44] presented a development of inkjet nozzle driven by double PZT. In this case, the important parameters are the pulse width and the time delay between piezo transducers. The optimized pulse widths and time delays between transducers were determined for applied bipolar waveform. Inkjet nozzle containing the double PZT can be used for jetting various kind of ink, from low to high viscosity liquids. However, more parameters must be controlled in comparison with a single transducer nozzle.

The inks for PIJ must not contain the vaporizable compounds in comparison with TIJ and, therefore, various types of ink can be used in this technique. In addition, the print-heads have longer life because of omission of heating element. On the other hand, the limitation can be attributed to the cost of print-heads and the associated hardware.[28]

2.2.3 Electrostatic inkjet printing

Electrostatic inkjet printing technique is the third major subcategory of DOD inkjet printing. An ability to eject very fine drops, simple structure of fabricated device, and precision in extraction are the most important advantages over the above described methods (TIJ and PIJ). The electrostatic method is based on protruding through the nozzle induced by an electrostatic field, which forms a meniscus called the Taylor cone. [45] In other words, the drops are drawn through the orifice under applied electrostatic field. In fact, the applied electrostatic field

attracts the free charge within the ink to its surface in such a way that the drops are produced when this field pull exceeds the surface tension of the liquid. [28] Figure 9 shows the experimental set-up of constructed electrostatic inkjet printing. As can be seen, this method requires a presence of two electrodes; a pin electrode and a metal plate electrode. Substrate is put on the metal electrode. A gap between the nozzle tip and the plate can be controlled by mechanical stage. In this case, a current-voltage characteristic of the pin electrode filled by ion-conductive water was measured and compared with metal pin electrode. The constructed apparatus was suitable for film formation, three-dimensional printing, and electrostatic circuit printing, but it was elemental and not satisfactory for practical applications. [46]

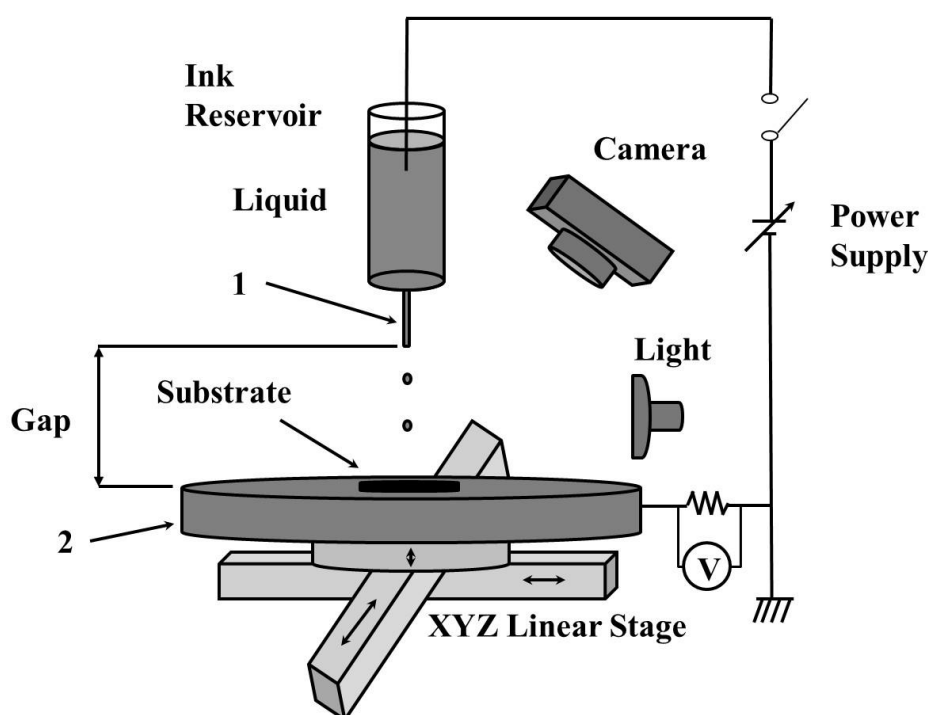


Figure 9. Experimental set-up of electrostatic ink-jet printing. (1-pin electrode, insulating capillary tube filled with liquid, 2-metal plate electrode).[46]

The similar configuration was also investigated by Choi *et al.*[47]. In their study, the substrate is put under bottom electrode; the ejected nano-silver drops are then delivered onto substrate through a hole in plate electrode. The parameters (optimal conditions, such as voltage, pulse, and flow rate) were also investigated because they are needed for obtaining tiny drops.

As has already been mentioned above, the electrostatic inkjet printing offers, in comparison with TIJ and PIJ, the following benefits, which are simplicity of structure, ability to eject fine drops, and use of more concentrated inks. On the contrary, the limitations include the use of conductive fluids only. [28]

3. INKJET INKS

The basic inkjet principles as well as drop ejections were described in previous section. The inkjet printing process is not only about the printing modes. The other requirements come from ink properties. The inkjet inks classification and their basic composition will be described in this part.

3.1 Classification of Inkjet Inks

The inks suitable for inkjet printing can be divided into four major groups. These groups are shown in Figure 10. Each group, except UV curable, can be found in alternative term in literature, for example water or aqueous ink, solvent or non-aqueous ink, and phase change or hot melt inks. Generally, the ink could be described as a system consisting of functional material and a liquid vehicle (carrier medium). The liquid vehicle usually contains different additives. Additives can improve the ink processing, visibility of prepared motives, ink adhesion, for example. These additives are surfactants, plasticizers, colorants, co-solvents, and other compounds. [48]

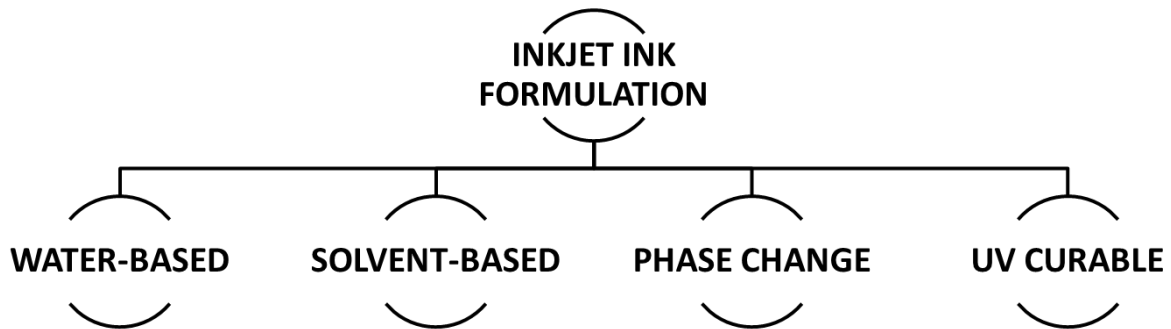


Figure 10. The main classifications of inkjet ink.[48]

The appropriate ink formulation (composition) depends on final application of ink. The water-based and solvent-based inks include a solution or dispersion of functional material in carrier medium. The low viscosity inks are used in inkjet printing because of their transport through the nozzle, drop formation, and the drop integrity. The viscosity represents only one of the crucial properties of the inks. Other important properties are for example surface tension (SFT), density, and conductivity in the case of preparation of conductive patterns. In addition, the conductivity of inkjet ink is important in CIJ printing. [48, 49]

3.1.1 Water-based inkjet inks

The first type of inkjet ink is a water-based (or aqueous) ink. This kind of ink is mostly used in office and home printers because of its inexpensive and environmentally friendly properties. [48] The major component is water and inks could be prepared in form of solution, dispersion or micro-emulsion. [49] The example of water-based inkjet ink composition is listed in Table 1. As can be seen, the aqueous ink contains a lot of other additives such as colorant, co-solvent, buffer and other additives. The function of each component is described in Table 1. Colour is provided by dyes or pigments. The main advantages of dyes over pigments include a large number of chromophores that can be fine-tuned to deliver the specific colour needs in required applications. On the other hand, the dyes generally, in comparison with pigments, do not display good light and ozone fastness. Therefore, the pigments offer high colour density (especially for black text), and the permanence of the image. Good water fastness and excellent resistance to fading by ozone or light are observed in this case. [50]

Table 1. The general composition of water-based inkjet ink. [50]

Ink component	Component amount [wt%]	Component function
Deionised Water	60 - 90	Aqueous carrier medium
Co-solvent/ Humectant	5 - 30	Controls the viscosity of the ink and inhibits an evaporation
Colorant	1 - 10	Provides colour
Surfactant	0.1 - 10	Improves surface tension, wetting, and penetration
Biocide	0.05 - 1	Prevents bacterial growth
Buffer	0.1 - 0.5	Controls pH of the ink
Other	> 1	Include chelating agents, charging agent, binders, and other additives

Of course, Table 1 showed only a typical composition of aqueous ink. The real ink does not have to contain all compounds listed in Table 1. Moreover, the water-based inkjet inks may be in form solutions, dispersions or micro-emulsions as already mentioned. There are many articles, in which the inkjet printing of metallic nanoparticles (silver and copper based aqueous ink) or aqueous titania suspension are described. [51-53] There is also the example of patent focused on aqueous inkjet ink [54] as well as the example for water-based polymer thick film conductive ink [55]. Other applications include the preparation of a brightly luminescent film based on aqueous ZnS:Mn nanoparticles. [56] The ink was deposited onto various substrates including glass, foil, photo-paper, and other substrates. Isopropanol was used as surfactant due to reduction of SFT. The ink

also contained other additives such as humectant and co-solvent. Special example of deposition of stable oil-in-water micro-emulsion was demonstrated by Kamyshny *et al.* [57] In this case, the micro-emulsion, containing water-insoluble functional organic molecules, represents system that behaves as water-based dye ink before printing process and as water-based pigment ink after inkjet printing. They demonstrated that evaporation of the micro-emulsion drops leads to formation of ordered arrays of organic nanoparticles at the rim of the drop in some cases.

3.1.2 Solvent-based (non-aqueous) inkjet inks

Solvent-based inkjet inks are the next kind of inks. However, organic solvents are usually used as a carrier medium in this case. Table 2 shows the typical formulation of solvent-based ink compositions for both CIJ and DOD inkjet system. As can be seen, the major part is carrier solvent or mixture of miscible solvents in both cases. Moreover, there are only little differences in composition of inks for CIJ and DOD ink-jet printing.[58, 59]

Table 2. Solvent-based ink formulation for both CIJ and DOD inkjet printing.[58, 59]

Ink component	Component amount [wt%]	Component function
Continuous inkjet		
Solvent	85.5	Non-aqueous carrier medium
Colorant	5	Provide colour
Polymer	8	Adjust viscosity and adhesion
Surfactant	0.5	Adjust surface tension and wettability
Conductive salt	1	Provide conductivity for drop charging and deflection
DOD inkjet		
Solvent	1 - 40	Carrier medium
Co-solvent	10 - 90	Adjust viscosity, SFT and evaporation
Polymer/resin	0.1 - 10	Binder
Wetting agent	0.1 - 10	Adjust surface tension and wettability
Pigments	0.1 - 10	Provide colour
Plasticizers	0.1 - 10	Enhance flexibility
Other	0 - 5	Include light stabilizers, anti-static agents, control agent of corrosion and other component

Ketones are usually used as an active solvent because of their solvency for different substrates such as vinyl and plastic substrates. Other appropriate solvents include alcohols, propylene carbonate, ethyl acetate and other. Moreover, the better ink properties can be achieved with mixture of solvents (mixture of carrier medium and co-solvent). The mixture of solvents can affect the viscosity, SFT, and the rate of evaporation. As has been already mentioned, the conductivity is important properties in CIJ printing. Therefore, a conductive salt is added into ink composition. In special cases, dyes provide their own conductivity via a counter ion or residual salt. [48, 59] Brown *et al.* [60] describe the formulation of solvent-based inks with different additives such as resin, surfactant, and colorant in their patent.

The main advantages of solvent-based inks include the ability to adhere to various substrates and ability to use both pigments and dyes as colorant. Disadvantages include cleaning process of print-head nozzles because of fast drying process, which can result in clogging of print-head nozzles. Moreover, the solvent-based inks are not environmentally friendly. [28]

3.1.3 Phase change (Hot-melt) inkjet inks

The next group represents the hot-melt or phase-change inks. The characteristic feature of these inks is a solid state of ink at ambient temperature. The ink changes the state from solid to liquid at the moment of printing, and reversibly, they solidified when the surface of substrate is obtained. The promptly solidification prevents the ink from spreading or penetrating into a printed media. The inks are usually composed from the components such as wax (carrier medium), and resin (representative of tackifiers). They can contain also other components such as plasticizers, antiscratch additives, corrosion inhibitors, antioxidants and other ingredients. Pigments and dyes could be used in this type of inks as well.[61]

Printing temperature of this system is usually in the range of 50-120 °C. The main benefits of phase-change inks include the rapid drying (solidifying) process, inks are environmentally friendly. The main deficiencies include the low durability and poor abrasion resistance. [48]

Pekarovicova *et al.* [49] presents various ink formulations depending on inkjet system. Their work contains the list of components that can be used in hot-melt inks together with the description of their function and quantity (concentration).

3.1.4 UV curable inkjet inks

The last group represents UV curable inkjet inks. Final patterns or motives are formed after UV curing process in this case. The preparation of motives can be divided into two steps. The final motives are prepared by printing, then the motives are exposed to ultraviolet (UV) light, which result in polymerisation of

the reactive components in ink formulation. The ink formulations contain the following materials: monomers or oligomers, photo-initiators, colorants (pigments or dyes dispersed or dissolved in liquid vehicle) and other additives. The pigment particle size should be smaller than 1 μm to achieve good printability. The final properties of prepared motive are given by used monomers or oligomers. The ink often contains mixture of mono-, di-, tri-, tetra- and penta-functional monomer with respect to polymerising groups. Table 3 shows the influence of functionality of acrylate monomer molecule on selected properties. For example, the mono- functional monomer are usually characterised by low viscosity and low cure speed, giving films with good flexibility, but with poor solvent resistance and poor hardness. On the other hand, multi-functional monomer offers faster curing time, the good hardness and solvent resistance, but the obtained films are brittle. All these properties must be taken into account during the ink formulation. The polymerisation process (the curing process) can be performed either by “free radical” or “cationic” mechanism. [48, 50]

Table 3. Typical UV-curable monomer properties as a function of acrylate functionality.[50]

Property	Functionality of acrylate molecule	
	Mono-	Penta-
Cure speed	Slow	Fast
Flexibility	Flexible	Brittle
Hardness	Soft	Hard
Solvent resistance	Less	Best
Shrinkage	Low	High

Zhai *et al.* [62] demonstrated the preparation of water-based UV curable conductive inks for flexible electronics. The ink contains silver nano-colloids and water-based UV resin. The preparation of conductive pattern was divided into several steps: inkjet printing of UV conductive inks on flexible substrate (I), evaporation of water (II), UV curing (III), and sintering the metal nano-particles (IV). The printing process was carried out by CIJ printer. The effects of different content of silver nano-colloids, thickness and sintering temperature were investigated to obtain the optimal conductivity performance. Karim *et al.* [63] demonstrate the inkjet printing of biodegradable heat-sensitive poly(lactic acid) fabrics using UV curable ink because of its potential degradation at high temperature as well as the rigid inter-fibre bonding. The rigid-fibre bonding occurred with thermal curing at high temperature. They prepared a single jersey poly(lactic acid) knit fabrics with UV curable and thermal pigment ink. They observed that the UV curable inks with higher acrylate functionalities in their formulation provided better overall colour fastness, higher colour strength and comparable colour difference to thermally cured system.

UV curable inks usually do not contain volatile organic chemicals or air pollutants, so the inks are environmentally friendly. Moreover, the inks offer high durability and abrasion resistance of printed patterns because of its cross-linked nature. The limitations include cost of materials and requirements of the UV curing hardware. [48]

3.2 Crucial Ink Parameters

The inkjet inks compositions were described in previous parts. As was shown, the ink can contain different additives that can affect the ink properties during printing. Thus, the most important properties of inkjet inks will be discussed in this part. These properties include mainly viscosity and surface tension. Of course, specific techniques may require inclusion of other ink properties, for example, conductivity in continuous inkjet printing.

3.2.1 Viscosity

The first important property of each printing fluid is its viscosity. However, the viscosity of ink can be affected by many parameters such as additives, surfactants, polymer concentration, and solvent composition and other. It can be also affected by other physical parameters, such as temperature, and pressure for a given fluid system. The viscosity of inkjet ink is usually very low, usually below 20 mPa·s, depending on a print-head. It is very important parameter for its performance during jetting and spreading on substrate. [64, 65]

Rheology studies the flow/deformation behaviour of material. Generally, the materials can exhibit Newtonian or non-Newtonian behaviour. The basic flow curves of time-independent materials are shown in Figure 11. The simplest (Newtonian) behaviour represents the curve “A”, in which shear stress is directly proportional to shear rate. Thus, an apparent viscosity is constant in a graph of viscosity against shear rate (it is not showed). In other words, the viscosity is independent on the shear rate. Many low molecular weight liquids behave in accordance with Newton`s Law of viscosity described by equation (3.1) [65, 66]

$$\tau = \eta \cdot \dot{\gamma} \quad (3.1)$$

where τ is the shear stress, η is the shear viscosity and $\dot{\gamma}$ is the shear rate.[65]

But for high molecular weight liquids, which include polymer melts and solutions, the shear stress and shear rate are not proportional over all ranges of shear stress and shear rate. Such liquids exhibit non-Newtonian behaviour and they can be characterised as pseudo-plastic fluid (shear thinning fluid showed in Figure 11, curve “C”) and dilatant fluid (shear thickening fluid showed in Figure 11, curve “B”). Typical examples of pseudo-plastic fluid are polymer melts and

solutions. Dilatant behaviour can be demonstrated by adding water to starch and stirring it.[66]

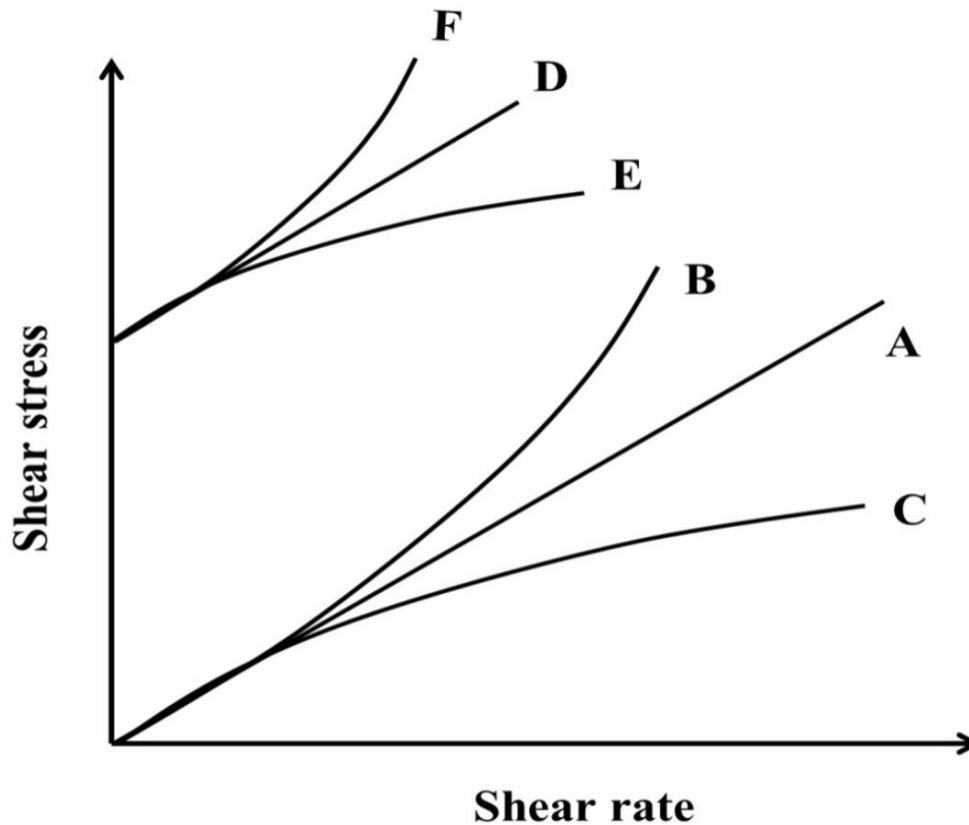


Figure 11. Flow curves for various time-independent materials. A represents Newtonian fluid; B, a dilatant fluid; C, a pseudo-plastic fluid; D, a Bingham fluid; E, a pseudo-plastic fluid with yield stress; and F, a dilatant fluid with yield stress.[65]

Sochi [65] summarized a description of large number of models for flow of non-Newtonian fluids in porous media. Behaviour of these fluids can be described by the following equation also called the Herschel-Bulkley model:

$$\tau = \tau_0 + \eta \cdot \dot{\gamma}^n \quad (3.2)$$

where τ is the shear stress; τ_0 is the yield stress; η is the shear viscosity; $\dot{\gamma}$ is the shear rate; and n is the flow behaviour index.[65]

The equation 3.2 can be used for describing all materials exhibiting Newtonian as well as non-Newtonian behaviour. The all possible cases are summarized in Table 4.

Table 4. Values of yield stress (τ_0) and flow behaviour index (n) for various materials. [65]

Flow behaviour	Yield stress τ_0	Index n	Curve in Figure 11
Newtonian	0	1	A
Pseudo-plastic	0	<1	C
Dilatant	0	>1	B
Bingham	>0	1	D
Pseudo-plastic with yield stress	>0	<1	E
Dilatant with yield stress	>0	>1	F

The pseudo-plastic fluid with yield stress is also known as the Casson fluid, which is assumed to have an infinite viscosity at zero shear rate, and the zero viscosity at an infinite shear rate. In other word, the Casson fluid exhibits no flow below yield stress. The examples of Casson fluid include human blood, honey, tomato sauce, and jelly.[67]

Fluids can be also classified according to their time-dependent behaviour at constant shear rate and constant temperature. The fluids are either rheopectic (shear hardening) or thixotropic (shear softening). The shear stress of rheopectic fluids increases with time, on the other hand, the shear stress of thixotropic fluids decreases with time. [65]

The shear rate-dependent as well as time-dependent behaviour of fluids has been already described. Other parameters such as molecular weight, temperature and polymer concentration can also affect the viscosity of polymer solution.

The effect of temperature and polymer concentration on viscosity of polymer solution will be explained on an example of metallocene linear low density polyethylene polymer solution in cyclohexane. These effects were demonstrated by Al-Shammari *et al.*[68] They observed the following conclusions: (1) the viscosity of solutions decreased with increasing temperature, however, a decrease is better visible at lower shear rates (from zero to 100 s^{-1}) than at higher shear rates (above 200 s^{-1}); (2) the viscosity of solution increased with increasing polymer concentration at same temperature during measurement. The viscosity was changed slightly for concentration from 1,000 ppm to 3,000 ppm at room temperature. The essential change occurred at concentration 4,000 ppm, when the jump in viscosity appeared.

The similar study was performed by Munoz *et al.*[69]. Their study was focused on rheological properties and surface tension of *Acacia tortuosa gum* aqueous dispersion with preservative agent. The similar trends were also observed in case of dispersions. For increasing concentration (15-40 w/v %) of *Acacia tortuosa* the viscosity of dispersion increased as well for the same temperature. Moreover, the

pseudo-plastic behavior of dispersion was observed in the range of shear rate of 0.4-100 reciprocal seconds. On the other hand, as the temperature increased the viscosity decreased as well for the same concentration.

Similar results of dependency of polymer concentration or/and temperature were published by many other authors. [70-73]

The next parameter is molecular weight of polymer. Figure 12 depicts the effect of molecular weight and concentration on solution viscosity for cellulose ester in γ -butyrolactone. As can be seen, the viscosity is higher for solutions with higher molecular weight in contrast to the solutions with lower molecular weight at the same mass concentration.[50]

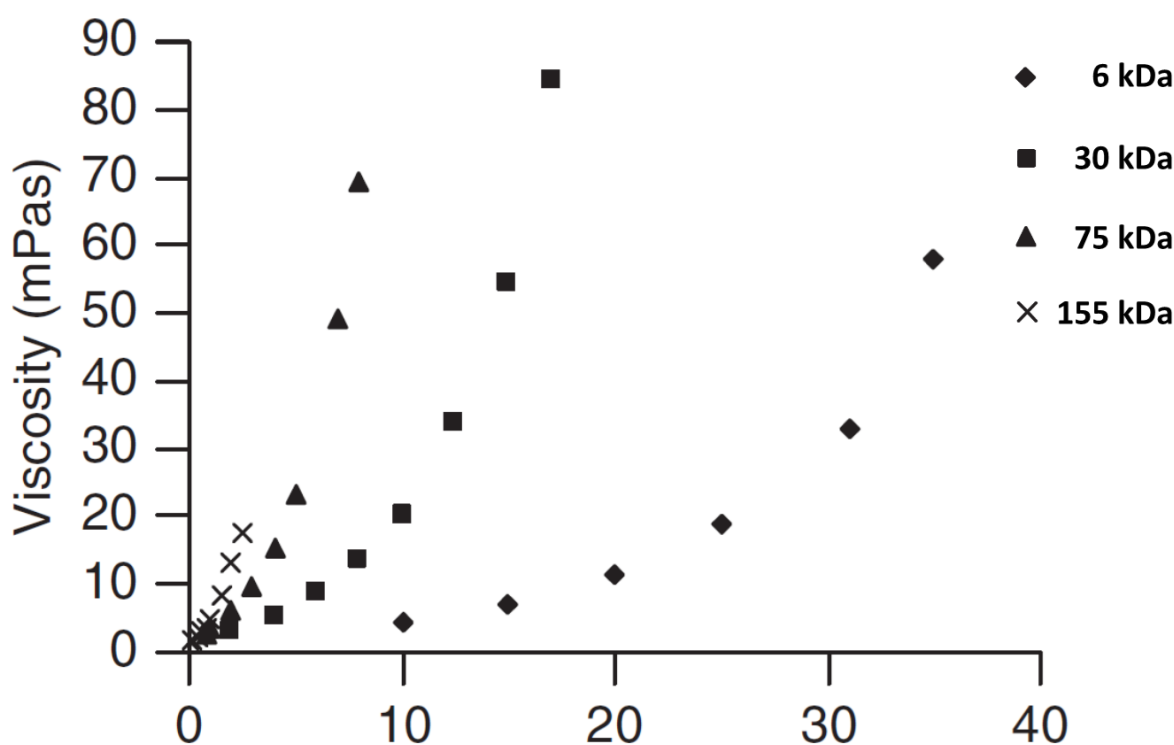


Figure 12. Effect of polymer molecular weight and concentration on viscosity of cellulose ester in γ -butyrolactone.[50]

González-Tello *et al.* [74] derived similar conclusions for concentrated aqueous solutions of polyethylene glycol with three different average molecular mass. Another study performed by Jakubka *et al.*[75] was focused on a comparison of single-wall carbon nanotubes dispersion selectivity of different weight average molecular weight conjugated polymers prepared in various aromatic solvents. The authors proposed that solution viscosity is one of the factors influencing the apparent selectivity by changing a re-aggregation rate of the single-wall carbon nanotubes.

In summary, the viscosity of inkjet ink plays important role in printing process. However, it can be affected by temperature, polymer concentration, and polymer molecular weight. Therefore, the rheological studies are necessary for better understanding of ink flow behaviour.

3.2.2 Surface tension and wettability

The next discussed crucial parameter of inkjet inks is surface tension (SFT). Surface tension is a reversible work needed to create a unit surface area in a substance. Sometimes it is also called the specific surface energy, the intrinsic or true surface energy [76]. All liquids are made up of molecules close to one another and exerting attractive forces. These mutual attractions produce this universal property. In other words, SFT is a result of a cohesive interaction (forces) in the liquid. The molecule in the bulk of liquid senses the same attractive forces in all directions, whereas these attractions are lacking in one direction for the molecules at the surface. Every liquid has a specific SFT value. Liquid with higher SFT (for example water) demonstrates a high intramolecular attraction and a strong tendency to form a sphere. On the other hand, liquids with lower SFT have a weak tendency toward sphere formation that is overcome by countering forces. The SFT for liquids is expressed in the units of mN/m.[77, 78]

The relationship between the surface tension and the cohesive forces in the liquid, as described by solubility parameter (δ) is [78]:

$$\gamma = C \cdot \delta^2 \cdot V^{1/3} \quad (3.3)$$

where V is the molar volume of liquid and C is the constant.

A value of surface tension is also affected by temperature. Figure 13 illustrates the effect of temperature on SFT of poly(ethyleneglycol) (PEG) aqueous solution at different concentrations. The number-average molecular weight of PEG attained 300. As can be seen, the surface tension of all polymer concentrations decreases with increasing temperature. Effect of polymer concentration is also demonstrated. Higher polymer concentration results in lower surface tension at same temperature. The obtained results were compared with the calculated values. The comparison is presented in Figure 13 as the lines for the highest and lowest concentrations. The data were fitted by the following relation:

$$\sigma = a + b \cdot w + c \cdot T \quad (3.4)$$

where σ is the surface tension in mN/m at the measured temperature, w is the mass fraction of polymer in solution, T is the solution temperature in K, a, b in mN/m and c in mN/m°C are the experimental parameters. [79]

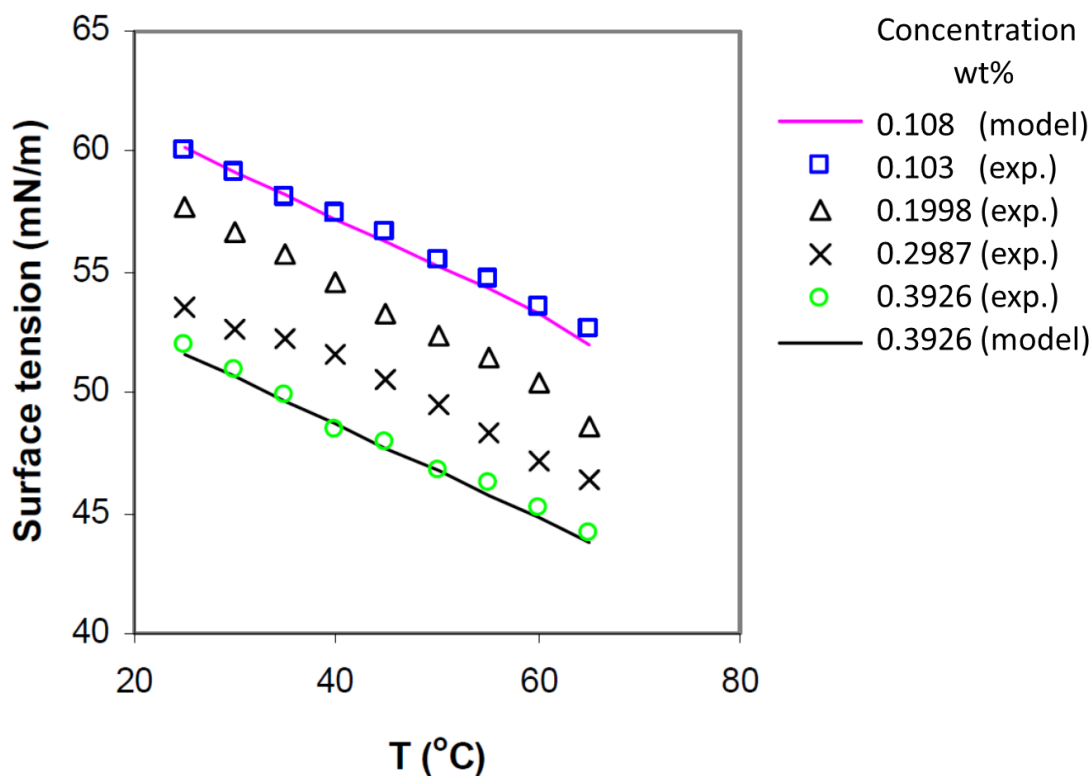


Figure 13. Surface tension of PEG 300 in water at different temperatures and concentrations. [79]

Many studies focused on the effect of temperature on SFT value. In some cases, the surface tension measurements were performed with pure water [80], or with the polymer solution in water [81, 82]. Mohammad *et al.* [83] focused on the effect of temperature on a binary system of polymer in 1-alkanols.

Khan *et al.* [84] published the study focused on the measurements of SFT, density and viscosity of oxoethylene-oxobutylene di-block copolymers in water at different temperatures. They found that the STF decreases with increasing amount of polymer in solution up to a specific concentration and beyond which, no prominent decrease in surface tension was observed. The observed specific concentration represents the critical micelle concentration point (CMC). It was also observed that the CMC decrease with increasing temperature in both aqueous polymer solutions.

Khan *et al.* [85] studied the interactions between different polymer solutions and surfactants by measuring their conductivity and SFT. They analysed the effect of polymer concentration on SFT of pure surfactant solution. They found that the increasing polymer concentration resulted in higher SFT of surfactant solutions except the system of xanthan gum and sodium dodecyl sulphate. The surface tension of surfactant solution decreases with increasing polymer concentration in the system composed of xanthan gum and sodium dodecyl sulphate. They also documented that maximum interaction occurred between the critical aggregation concentration and the polymer saturation point.

Surface and interfacial tensions play important role in wetting, coating, corrosion and adsorption processes. A better wettability may be obtained either by modification of the SFT of liquids or by modification of a functional group on substrate surface. In the first case, the better wettability is obtained by using a surface active compound (surfactant) or similar compound, which results in lower surface tension of liquid. In the second case, the required functional groups are incorporated onto surface of solid substrates by different surface treatment techniques. These new functional groups are capable to interact with liquids resulting in better or tailored wettability.[86, 87]

The surface energy of solid polymers surfaces is in most cases determined from the contact angle measurement, in which a drop is positioned on the sample surface. The contact angle depends on three co-existing interfacial interfaces: interface between solid and liquid phase, solid and vapour phase and liquid and vapour phase. The equilibrium contact angle is related to various interfacial tensions by well-known Young equation:

$$\gamma_{sv} = \cos\theta \cdot \gamma_{lv} + \gamma_{sl} \quad (3.5)$$

where γ_{sv} , γ_{lv} , and γ_{sl} represent the solid-vapour, liquid-vapour, and solid-liquid interfacial tensions, respectively, and θ is the contact angle.[86, 88]

Figure 14 shows the illustration of contact angle (θ) on homogeneous solid substrate.

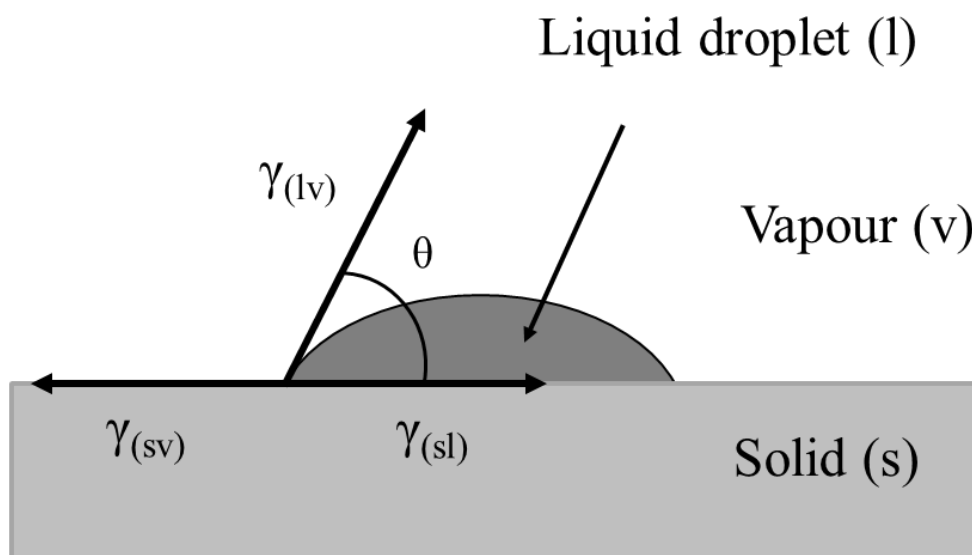


Figure 14. Illustration of a contact angle formed by a sessile drop on smooth homogeneous solid surface. [88]

The contact angle is usually determined by the sessile drop method as cosine of the contact angle ($\cos \theta$) that is an empirical index for the wettability of the solid surface by liquid. The wettability can be characterized in a dependence on θ

value. The contact angles lower than 90° correspond to better wettability, while the angles higher than 90° correspond to poor wettability.[88]

For better explanation of the relation between wettability and the contact angle is suitable to rearrange the preceding relation (3.5) into:

$$\cos\theta = (\gamma_{sv} - \gamma_{sl})/\gamma_{lv} \quad (3.6)$$

The better wettability could be obtained either by decreasing the surface tension of liquids or by increasing the surface energy of solid. If the solid surface is completely wetted by the liquid, the contact angle becomes zero (i.e., $\cos \theta$ is one). The $\cos \theta$ takes negative value for truly non-wetting surfaces. The many polymeric surfaces show the partial wettability to liquid such that $\cos \theta$ has a value in the range from zero to one.[87]

To summarize, the role of surface tension of ink is twofold. First, it is important parameter influencing the printing process, namely the drop formation. Next, the lower surface tension of the ink results in better wettability of substrate.

3.3 Ink Jetting Characteristics

3.3.1 Ink drop formation

As has been already mentioned, the creation of patterns with precise shape and required quality is obtained by deposition of several hundreds or thousands of ink drops. Therefore, one of the important steps in inkjet printing process is ejection and formation of spherical drops without existence of any several smaller drops known as „satellite drops“.

Controlling drop formation and break up of filament of ink is a complex process that depends on many factors including the rheology of ink. Besides properties of ink such as viscosity, surface tension and inertia, the phenomenon of viscoelasticity must be considered. Viscosity and elastic stresses resist a necking of liquid filament and the surface tension and inertia have also influence on the final shape and form of the drops. [89, 90] The breakup of Newtonian fluid is known very well since Rayleigh pioneering studies [91] and his followers. Rayleigh type of axisymmetric varicose instabilities is adequate for a description of the inkjet printing process of viscous fluids. [92] More complicated phenomena of lateral kink break ups and ramified jet break ups occur beyond the range of processing conditions common in this technique and may apply for other processes, namely electrospinning. [93] Figure 15 illustrates the three break-up modes.

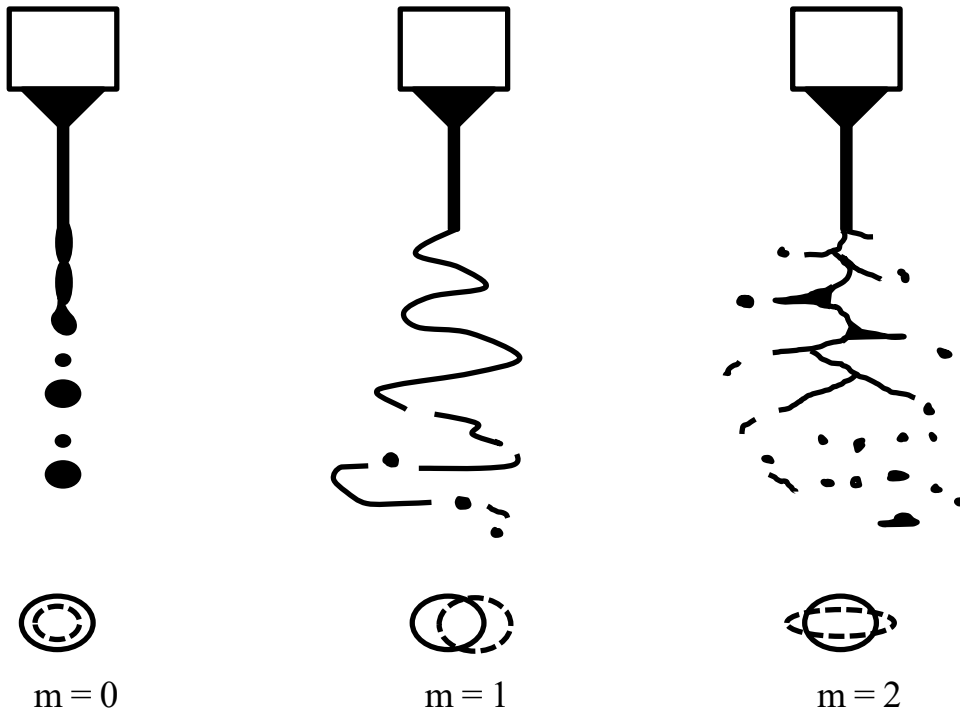


Figure 15. Three jet break-up modes, the axisymmetric varicose break-up ($m=0$), the lateral kink break-up ($m=1$), and the ramified jet break-up ($m=2$). [93]

The jet break up theory by Rayleigh induces the time constant for drop formation. [93]

$$\tau_d = \left(\frac{r_{jet}^3 \cdot \rho}{\sigma} \right)^{1/2} \quad (3.7)$$

Drop generation in DOD printing process is a repeated pulse process. Single pulse can be generally divided into five stages: (1) ejection and stretching of liquid, (2) pinch-off of liquid thread from nozzle exit, (3) contraction of liquid thread, (4) break up of liquid thread into primary drop and satellites, and (5) recombination of primary and satellite drops. In ideal case, no break up appears and the last (fourth) stage may be described as spherical drop formation and travel. [92, 94]

The drop generation is illustrated in Figure 16. As can be seen, liquid passes through the nozzle and ejects to free space (stages 1-3). The pinch-off of liquid occurred in the next step (stage between 3 and 4). Then, the liquid thread is contracted during flight (stages 4-6) up to the time when the break up occurred (stage between 6 and 7). After break up, the primary drop is formed; moreover, the rest of thread continues in contraction resulting in formation of secondary (satellite) drop (stages 7-8). If the satellites drop velocity is high enough, the recombination or merge of satellite and primary drop occurs (stages 8-11). Finally, a final single drop travels until delivered onto patterned substrate (stage 11).

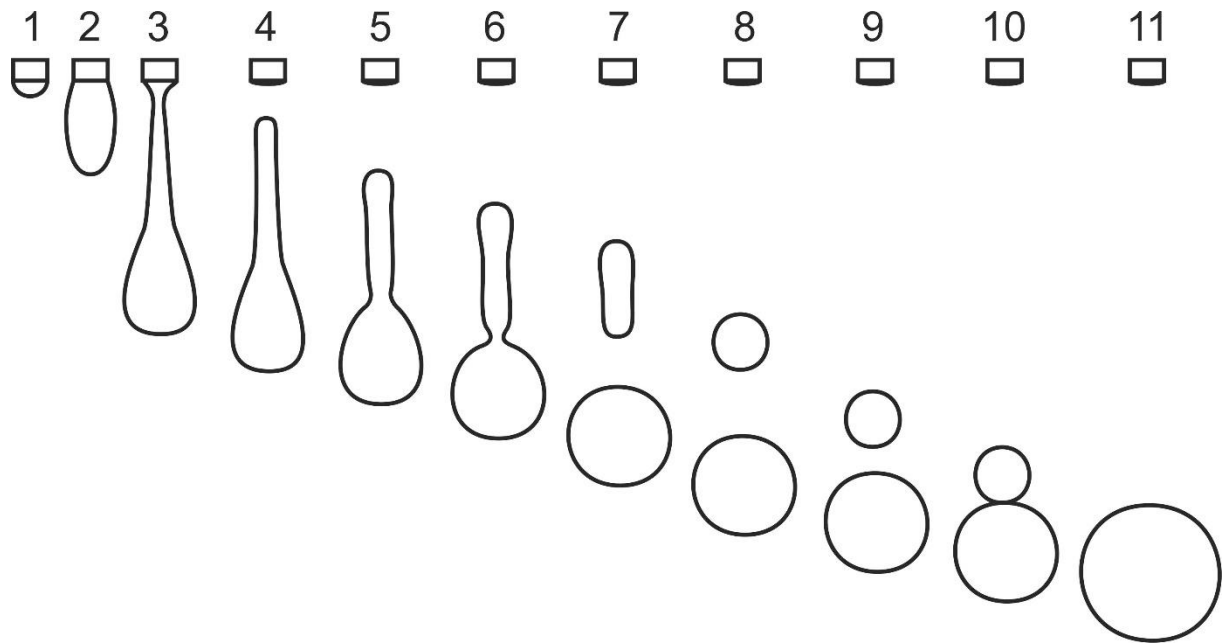


Figure 16. Illustration of drop ejection and formation.

Ink jetting is characterized by noncontact printing, so that the nozzle must be separated from the substrate during the print process. The distance between the nozzle and the substrate, that is the stand-off distance, is the distance over which all the described process must be accomplished. The conditions of a printing process can be considered as being in optimum printability state when a single drop is formed either directly without second pinch-off (break up) or the satellite drop merges with the main drop within its travel distance forming thus a single drop before hitting the patterned surface. This distance defines also the minimum stand-off distance (MSD) which is necessary to be kept in the printing process. Printing performed at a distance of less than the MSD results in the deposition of drops having tails and satellites, degrading the printing resolution. In praxis, stand-off about 1 mm is used in digital printing normally. The critical value is arbitrarily set to be 20 times the printing nozzle diameter. It is based on general experience that if the MSD is less than 20 times the diameter, the printing error is sufficiently small, i.e. smaller than the drop radius and the printing quality on the sub-millimetre scale is acceptable for highest achievable real resolution. [95]

3.3.2 Dimensionless criteria

Besides the important process parameters, the properties of inks, mainly the viscosity, surface tension, and density could be considered for the main factors that affect the drop formation and the printability as well. The drop formation is the key step of the process and its complexity can be characterized by a number of dimensionless groupings of physical constants, namely by the Reynolds (Re), the Weber (We), and the Ohnesorge (Oh) number. The number Z is defined as reciprocal value of the Ohnesorge number. [95, 96]

$$\text{Re} = \frac{v \cdot \rho \cdot A}{\eta} \quad (3.8)$$

$$\text{We} = \frac{v^2 \cdot \rho \cdot A}{\sigma} \quad (3.9)$$

$$\text{Oh} = \frac{\sqrt{\text{We}}}{\text{Re}} = \frac{\eta}{\sqrt{\sigma \cdot \rho \cdot A}} = Z^{-1} \quad (3.10)$$

where η , ρ and σ are the dynamic viscosity, the density, and the surface tension of polymer solution (polymer ink) respectively, v is the drop velocity and A is the characteristic length corresponding to the inert diameter of the nozzle.

The number Z was implemented by Fromm [97] who performed the fundamental work focused on understanding drops generation. Moreover, Fromm suggested that stable drop generation occurred for $Z > 2$ and that for a given pressure pulse the drop volume increases with an increasing value of Z as well. [8] Later, this prediction was refined by Reis & Derby [98] who found that stable drop formation occurred for Z values between 1 and 10. They also determined that low Z value impedes drop ejection due to viscous dissipation, whereas at high values, the primary drops are accompanied by satellite drops. [96] Jang *et al.* [95] monitored the behaviour and drop formation dynamics of various fluid based on water, ethylene glycol and diethylene glycol at different volume fraction. They adjusted the Reis & Derby's printable range characterized by Z values into the following form $4 < Z < 14$ by considering the characteristics of printing as single drop formability, the minimum stand-off distance, positional accuracy and maximum allowable jetting frequency.

Although the Z number is widely used for the basic printability characterization of inks, there are also other dimensionless criteria that have to be considered because velocity “ v ” terms describing dynamic effects are cancelled in its fraction formula (equation 3.10) and only material constants and characteristic length remain.

This problem can be solved by an introduction of second parameter which includes the velocity to construct a plot of Oh against this criterion. McKinley and Renardy [99] redrew the schematic diagram originally constructed by Derby [96] to show the field of parameter values for stable operation of DOD inkjet printing by using logarithmic coordinate system defined by plotting Ohnesorge against Reynolds number. The diagram defines a region, in which the particular fluids are printable and single drop formation may be achieved. The diagram is shown in Figure 17 providing that any printable fluid must not be too viscous, i.e. the Ohnesorge number must be lower than 1 but its value must not be lower than 0.1 otherwise satellite drops will be formed and complicate the printing process. From the other side of view, the fluid must have sufficient energy for drop formation

which defines the lower borderline from 3 (for $Oh = 1$) to 30 (for $Oh = 0.1$) in Reynolds number space. The upper Re limit is given by a line of demarcation with the splashing onset region from 20 (for $Oh = 1$) to 130 (for $Oh = 0.1$).

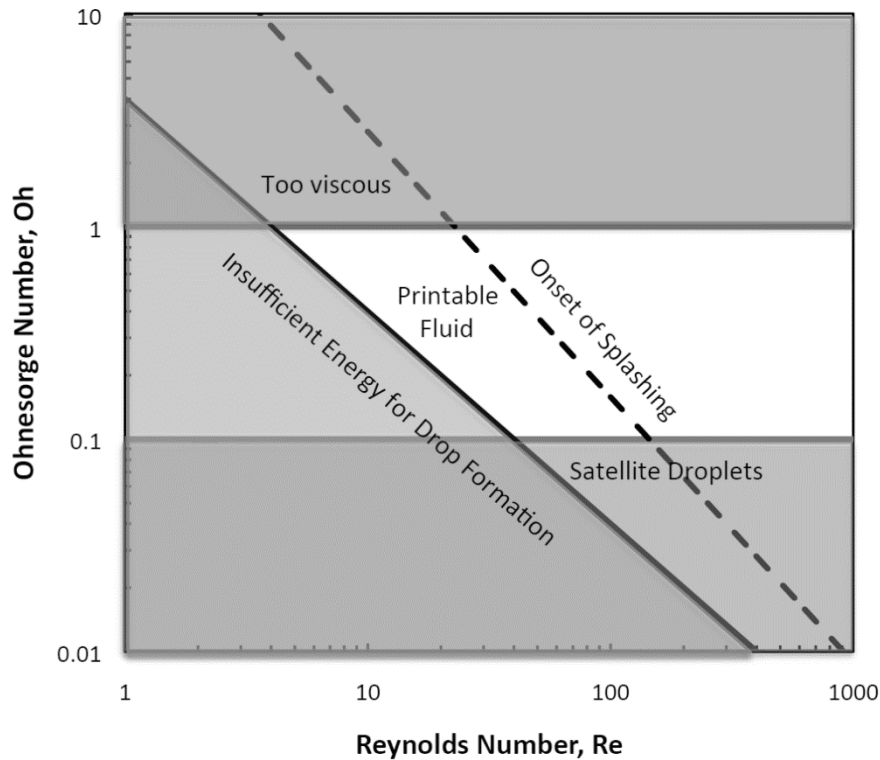


Figure 17. Original schematic diagrams showing the operating regime for stable operation of DOD ink-jet printing according to McKinley and Renardy. [99]

Other approach relies on the introduction of another dimensionless number which includes velocity. The Capillary number (Ca) is one of these other numbers. It is defined as follows:

$$Ca = \frac{We}{Re} = \frac{v \cdot \eta}{\sigma} \quad (3.11)$$

Indeed, Kim and Baek [92] found that the Z number alone is insufficient for describing the drop formation dynamics. On the other hand, the characteristic length and density are not included in the Ca number. Hence, they used Ca taking into account the drop velocity during printing and demonstrated the printability window based on the Capillary number plotted against the Weber number. They also divided the printability window into several sectors according to drops behaviour during printing and created thus a fundamental road-map covering the space of operation parameters in inkjet printing technology. The graph is shown in Figure 18. White polygon (regime I) in the middle of the graph is the printability region, within which a single drop is formed either directly without second pinch-off or the satellite drop merges with the main drop within its travel distance less

than 20A forming thus a single drop. On the right side of this white area, a grey polygon marking regime II can be found. Typically, one or more satellite drops are generated, but they do not recombine with the main drop. If one continues the graph inspection anticlockwise, regime III is found at large Ca and We , where the pinch-off typically occurs after a relatively longer pinch-off time, but very thin and long-lasting threads generate a fine satellite drop that does not merge with the main drop. The fourth area at large Ca and small We applies for the regime IV, where viscosity effect dominates inertial forces and the fluid fails to eject. The last regime V is then found close to the graph origin at small Ca and small We when surface tensional forces dominate both viscous and inertial forces thus the fluid fails to eject too.

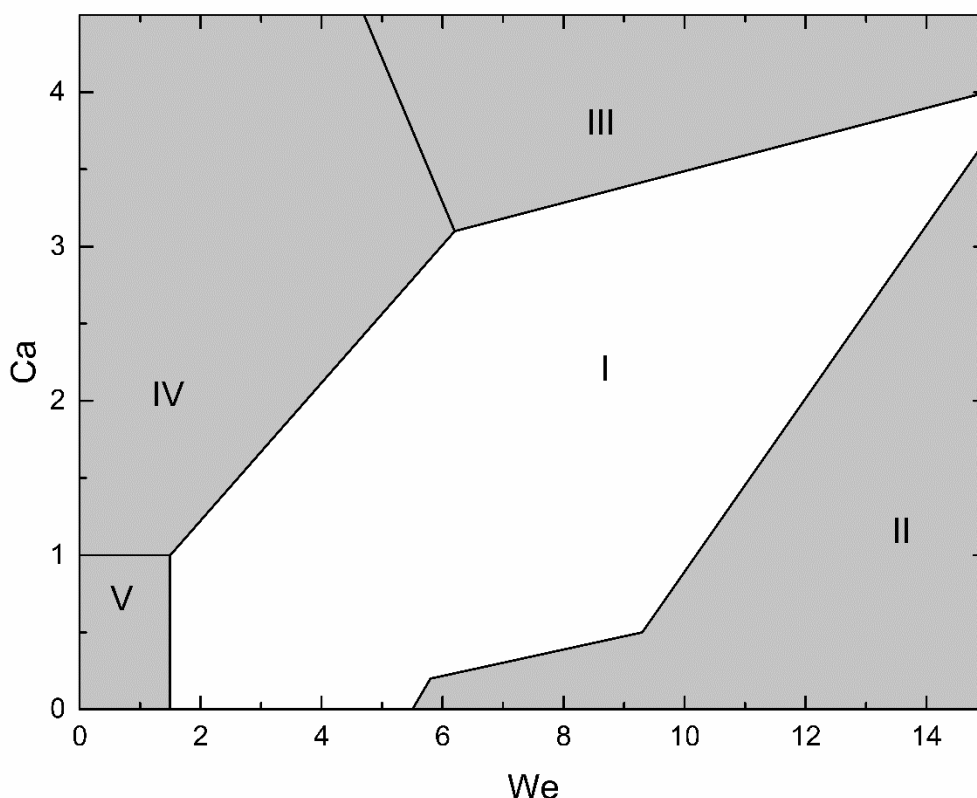


Figure 18. Original Kim and Baeks Capillary-Weber diagram.[92]

Based on this approach, Nallan *et al.* [100] developed and successfully experimentally validated the printing window within a Capillary number – Weber number space for metallic nanoparticle-based ink.

3.3.3 Viscoelasticity in drop formation

Indeed, the Rayleigh model holds perfectly for viscous liquids and it works with limited success for printable viscoelastic liquids as well. Further considerations are necessary for investigated solutions because the addition of small amount of polymer to the ink has significant effect on the break up dynamics. The polymer addition results in the formation of long-lived filaments

(or thin threads), connecting the ejected drops with the nozzle of printer. Length and lifetime of filament increase with both molecular weight and concentration of polymer. Above a certain concentration, the capillary force is not able to break the filament resulting in elastic retraction of ejected drops back to nozzle by filament. [101, 102]

Morrison and Harlen [89] demonstrated the jet behaviour in their work. The break up dynamics of Newtonian jets was compared with non-Newtonian jets, in which the jet behaviour was varied with respect to different viscoelastic parameters such as concentration, Deborah number, and molecule extensibility. In Newtonian jets, the ligament is breakaway shortly from the nozzle. This ligament is then break up into several smaller drops due to Rayleigh instability that is attributed to grow of a capillary wave along the filament. In the presence of polymer, the breakaway from nozzle is delayed, moreover, the speed of primary drops is reduced and the distribution of satellite drops is different. They also demonstrated the special case, in which the primary drop is never formed as elastic forces within the fluid pull the protruding jet back to the nozzle. This behaviour occurs at large value of molecule extensibility.

The process of drop formation in DOD inkjet mode could be represented by five sections [94] as mentioned in the chapter 3.3.1. *Ink drop formation*; even when the viscoelasticity is taken into account. Four of these process stages (stretching of liquid, pinch-off, contraction, and finally break up of the thread) belong to a sub-group of free-surface flows called self-thinning. There is no external driving force, or in other words, external forcing is much slower than any internal dynamics that develops spontaneously in the fluid. The process of jet thread formation, its thinning and break up develop under action of capillary forces. Once the system is virtually left alone to develop itself freely after an initial impulse, the velocity as the process parameter may be eliminated by a proper choice of the dimensionless parameters used for description and analysis of such system. In general, the self-thinning processes are governed by three time scales: a viscous time scale, the polymeric time scale and an inertial or Rayleigh breakup time scale. [103]

Nevertheless, other experimental studies include the utilization of extensional rheometers. Tuladhar and Mackley [90] demonstrated the filament thinning response of low viscosity Newtonian, polymer and inkjet fluids by using a variant of a multipass rheometer (MPR). This rheometer consists of two independently controlled pistons. The pistons displacement is controlled by servo-hydraulic movement. Moreover, in its conventional forms, the rheometer can be also used for measurements of high-shear rheology of inks. Vadillo *et al.* [104] demonstrated the similar device to determine the filament stretching and break up, however; in this case, the device did not use the servo-hydraulic driven pistons. The rotation of a stepper motor drive cause that both pistons are moved in synchronization with each other in “Trimaster”. CaBER™ test - Capillary break up extensional rheometry [105] is another used variant of the extensional

rheometric characterization. Classical oscillation mode rheometry (cone plate) can be utilized as well, until the liquid parameters do not make the technique impractical. All these techniques give useful yet slightly indirect information about the measured system (see discussion of extensional and linear viscoelastic relaxation times). The main advantage of camera utilization is that there is no need to transfer or scaling of obtained results into processing conditions because it is the process itself what is watched. On the other hand, no forces are measured by image analysis therefore it is surpassed by all rheometers.

A high shear rates or high extension rates necessitates for inkjet printing process. If we consider the polymer solution behaviour in these high rates, the polymer is not necessarily in its thermodynamically stable Gaussian coil chain configuration and may undergo a transition to a rigid-rod-type configuration. A coil-stretch process could be characterized by Weissenberg number, (Wi), in which a stress relaxation time is considered together with the applied shear rate (or elongation rate). [106]

$$Wi = \lambda \cdot \dot{\gamma}_{crit} \quad (3.12)$$

where λ is the relaxation time and $\dot{\gamma}_{crit}$ is the shear rate.

However, Wi number could be rewritten into the form:

$$Wi = \frac{\lambda \cdot v}{A} \quad (3.13)$$

where λ is the relaxation time, v and A are the characteristic velocity and length, respectively. [103]

During coil-stretch transition of polymer, the shear stress is then placed on its backbone and there is an entropic driving force for the polymer to return to the thermodynamically stable coil configuration, which is the molecular mechanism of observed elasticity. The transition from coil to stretched molecule occurs at a critical value of Weissenberg number ($Wi = 0.5$) for solutions of linear polymers. [107] However, the mechanical straining can lead to the irreversible polymer M_w degradation as well. [106]

Later, the Wi could be used for calculation of the Elasticity number (El) defined as:

$$El = \frac{Wi}{Re} = \frac{\lambda \cdot \eta}{\rho \cdot A^2} \quad (3.14)$$

where Re is the Reynold number, η and ρ are the viscosity and density of tested fluids, respectively. [103]

As can be seen, the Elasticity number, similarly to the Capillary number, does not depend on the imposed kinematics; it only considers the process geometry and fluid properties. For example, extrusion of polymer melts corresponds to $El \gg 1$, whereas the spin coating or other processes for dilute polymer solution correspond to $El \ll 1$. [103]

The Elasto-Capillary number, Ec , is defined as a ratio between Weissenberg and Capillary numbers allowing to compare contributions of viscous and elastic effects in a (theoretically infinitely long) fluid cylinder expressing thus a competition between the energy of elastic strain in the bulk and capillary forces that both work against viscous effects. [103]

$$Ec = \frac{Wi}{Ca} = \frac{\lambda \cdot \sigma}{\eta \cdot A} \quad (3.15)$$

This number also does not include velocity and is a function of fluid rheology (relaxation time - λ , surface tension - σ , and viscosity - η) and the characteristic length (A).

Time scales related with flow relevant for inertial effect and viscosity depend on simply measurable variables and they are sufficiently discussed above. However, successful treatment of elasticity needs careful assessment of the relaxation timescale of the fluid under investigation (i.e. our polymer solution). In other words, calculation of the Elasticity number requires estimation of intrinsic relaxation time which cannot be approached directly by measurement. Zimm relaxation time, (λ_Z), is considered as the longest relaxation time for a macromolecule in polymer solution. Its definition is shown in the following equation (3.16). [102, 106]

$$\lambda_Z = \frac{\eta_s \cdot [\eta] \cdot M_w}{R \cdot T} \quad (3.16)$$

where $[\eta]$ is the intrinsic viscosity, η_s is the solvent viscosity, M_w is the weight average molecular weight, R is the gas constant, and T is the absolute temperature.

However, the Zimm relaxation time distribution is actually an extrapolation for infinitely dilute polymer solution hence it holds for highly diluted solutions only where the mutual interactions between macromolecules are negligible. Therefore, we can consider this relaxation time λ_Z as an estimation of the lowest limit to determine the polymeric time scale expectable in our case.

Mun *et al.* [101] estimated the elasticity of dilute polymer solutions based on poly(ethylene oxide) with different nominal molecular weight by the Rouse model. The longest relaxation time according to Rouse theory, (λ_R), is shown in the next equation (3.17).

$$\lambda_R = \frac{6}{\pi^2} \cdot \frac{\eta_s \cdot [\eta] \cdot M_v}{R \cdot T} \quad (3.17)$$

where η_s is the solvent viscosity, $[\eta]$ is the intrinsic viscosity, M_v is the viscosity average molecular weight, R is the gas constant, and T is the absolute temperature.

It can be seen that λ_R differs from λ_Z by the type of used molecular weight average as well as by the factor $6/\pi^2$. The geometry factor is approximately 0.608 and this difference can be considered less important with respect to the studied problem. Round value of Zimm relaxation time ($\lambda_Z \approx 0.7 \mu s$) is a good approximation of this time scale for PVA MowiolTM 4-98.

Another approach using real polymer chain description (in terms of Kuhn length), which seems to hold better for less dilute solutions, was examined too. The relaxation time was calculated according to the relation used by Bazilevskii *et al.* [108]:

$$\lambda_k = \frac{2 \cdot \pi \cdot \eta \cdot z_0^3}{k_B \cdot T} \quad (3.18)$$

where $k_B \cdot T$ is the Boltzmann temperature, η is the viscosity of the solution, and the parameter z_0 defined as:

$$z_0 = b_K \cdot N^{1/2} = b_K \cdot \left(\frac{M_w}{\left(\frac{b_K}{a} \right) \cdot M_{mer}} \right)^{1/2} \quad (3.19)$$

which is nothing else than real polymer chain end-to-end dimension, where a is the monomer (actually a mer) length, b_K is the length of Kuhn segment, N is the number of Kuhn segments in macromolecule, and M_{mer} is the molar mass of a monomer (mer) unit.

The relative balance between the time scales discussed above could be described by two dimensionless criteria, namely by the Ohnesorge number (viscous and inertial time scales) and by the Deborah number (De) (polymeric and inertial time scales) defined by the following equation (3.20) and representing the balance between polymeric and inertial time scales. [103]

$$De = \frac{\lambda}{t_c} = \frac{\lambda}{\sqrt{\frac{\rho \cdot A^3}{\sigma}}} \quad (3.20)$$

where t_c represent the inertial time scale, λ is the relaxation time, ρ and σ are the density and surface tension of tested fluid, respectively, and A is the characteristic length. [103]

Elastic properties (can be manifested at high impact rate processes, if any) of common molecular liquids normally considered as viscous only do not play any role in printing due to their very short relaxation time while printing process is much slower. The elastic solid or viscous liquids behaviour of viscoelastic material could be considered according to Deborah number, which depends on the material response time and its relation to the time scale of the experiment or observation. [109]

$$De = \frac{\lambda}{t_0} \quad (3.21)$$

where λ is the relaxation time and t_0 represents the observation time.

A long response time relative to the observation time (a high De) implies the solid behaviour or, on the other hand, the low value of De indicates the viscous (or fluid) behaviour. In other words, the greater Deborah number, the more solid like material is and oppositely. [109, 110]

According to Bazilevskii *et al.* [108] the characteristic break up time can be estimated with utilization of the Raleigh-Weber mechanism by the following equation:

$$t = t_c + t_v \quad (3.22)$$

where t_c corresponds to the inertial component of break up time, and t_v is attributed to the viscous component of breakup time.

Each component is described as follows:

$$t_c = \sqrt{\frac{\rho \cdot A^3}{\sigma}} \quad (3.23)$$

$$t_v = \frac{3 \cdot \eta \cdot A}{\sigma} \quad (3.24)$$

where ρ , η , γ , correspond to solution density, viscosity, and surface tension, respectively. The parameter A corresponds to the nozzle diameter.

4. POLY(VINYL ALCOHOL)

Poly(vinyl acetate), the precursor of Poly(vinyl alcohol), (PVA), was discovered by F. Klatte in 1915. The preparation of PVA was firstly described by W. O. Herrmann and W. Haehnel in 1924. The stoichiometric saponification of polyvinyl acetate with caustic soda was used for preparation of PVA. [111] It cannot be prepared by traditional polymerisation way because its monomer vinyl alcohol is not stable and rearranges readily to acetaldehyde. Therefore, it is usually manufactured by hydrolysis of polyvinyl acetate. Hydrolysis of acetate groups involves partial or total replacement of the ester groups of vinyl acetate by hydroxyl groups, under defined condition (for example alkaline methanolysis). Then, the poly(vinyl alcohol) is precipitated, washed and dried. Properties of resulting product depend on the length of polymer chain (polymerisation degree, PD) and on the degree of hydrolysis (DH). Quite high DH (above 70 %) is commonly achieved to consider the product as PVA otherwise it would be closer to the original polymer and rather considered just a modified or partially hydrolysed poly(vinyl acetate). Poly(vinyl alcohol) is an example of water-soluble semi-crystalline synthetic polymer. However, it is slightly soluble in ethanol and insoluble in other organic solvents. The higher degree of hydrolysis and polymerisation degree of prepared PVA, the lower solubility in cold water. [112]

It can be noted that DP and DH of polymer are the most important parameters, which affect the properties of prepared PVAs. Polyvinyl alcohols are usually classified according to DH into fully (98-99 mol.%), intermediate (93-97 mol.%), and partially (85-90 mol.%) hydrolysed grades. The melting point of fully hydrolysed PVA grade (228 °C) is higher than melting point of partially hydrolysed grade of PVA (180-190 °C). [113, 114]

Characteristic properties for polyvinyl alcohol with higher DH and DP include, for example higher viscosity, better adhesion to hydrophilic surfaces, better resistance to water and solvent. On the other hand, the properties of PVA with lower DH and DP include for example better solubility and flexibility. [113]

As has been already mentioned, the solubility of PVA is affected by DH and DP. High solvent temperature (above 90 °C) is necessary for dissolving the fully hydrolysed PVA in water due to strong intra- and intermolecular hydrogen bonding between PVA's hydroxyl side groups. On the other hand, the residual acetate groups weaken the hydrogen bonds and therefore, the partially hydrolysed PVAs are better soluble at lower temperature. Except DH and DP, the viscosity of PVA solution depends on polymer concentration, temperature, stereoregularity of polymer chains, and thermal history. [113] Of course, the viscosity can be also affected by addition of additives.

PVA represents a versatile polymer available for many different applications in various ranges of industries. The applications include for example the

preparation of water-soluble films, packaging films and coating, blended PVA films, fibres, adhesives and other. Other application includes for example preparation of belts and canvases. In this case, PVA can be extruded by using the mixtures such as PVA (33%), water (50%), plasticizers, fillers, and pigments followed by drying and elongation. Another example includes the preparation of poly(vinyl butyral). PVA is used a chemical intermediate in the reaction with aldehydes in the presence of small amounts of mineral acid, in this case. [113]

Poly(vinyl alcohol) is used in topical pharmaceutical and ophthalmic formulation. It is used in artificial tears and contact lens solutions for lubrication purposes, in transdermal patches and other. [114]

The literature on PVA properties as a large scale produced polymer is very rich and large amount of various details is ubiquitously available in handbooks. Therefore, the general introduction of PVA is kept short on the obligate level only. Reasonably large literature exists also on PVA solutions focused on spinning, namely electro-spinning processes. However, the use of PVA water solutions for inkjet printing is not notorious and small number of publications is available. Concerning specific solvent system used in the presented work, very little is known. To date, two articles focused on inkjet printing of poly(vinyl alcohol) were released. In the first work, the printability of PVA was investigated by Yun *et al.* [115] for construction of 3D structures at micro-scale. In their work, the PVA was dissolved in mixture water/DMSO (4/1 v/v). However, it is not clear, which type of both poly(vinyl alcohol) and DMSO were used in their study. In the second work, Salaoru *et al.* [116] investigated several numbers of inks composed from PVA with different both mass molecular weight and degree of hydrolysis. In this case, PVAs were dissolved in purified water at 60 °C in the first step. Then, the humectant (glycerine or mono propylene glycol) and pigments were added to prepared solutions.

5. AIMS OF THE THESIS

The thesis aims at a development of an ink based on water-soluble polymer for DOD digital printing for patterning of polymer surfaces. Besides that specific goal, the polymer system shall be treated as an exemplary case and lessons shall be drawn at each step of the work. It is possible to acquire not only new practical experience with material printing but also strengthen general knowledge in the field of polymer solution dispensing and improve the ink formulation development method. This aim has been defined in accordance with hitherto achieved results of research conducted in laboratories at our institution and with the aid of information gathered from literature review summarized in previous sections.

The aim of this Thesis may be achieved by pursuing following goals:

- Choice of proper solvent system and grade of Poly(vinyl alcohol) with respect to potential application for temporary patterns printing on polymer (PET) substrate.
- Research of PVA solution properties relevant to its use as an ink for DOD printing including stability (aging) issues including tuning of the solution properties by additives/co-solvents and finding optimum temperature for processing.
- Evaluation of prepared solution on the base of mainstream printability assessment methods with the use of dimensionless numbers. Critical reconsideration of these approaches and eventual improvement.
- Study of ink drop formation as the key step in printing process. What can be learned from it?
- Research in the field of specific features related with polymer solutions, namely viscoelasticity, if the Newtonian model does not apply. Critical reconsideration of these approaches and eventual improvement.
- Demonstration of the suitability of prepared ink for printing.
 - Research and development of printing method in laboratory scale on model substrate together with optimization of individual steps of printing process.
 - Preparation and characterization of testing patterns on model substrate (SiO_2 coated polymer substrate made from PET with surface energy of $49 \text{ mJ}\cdot\text{m}^{-2}$).
- Summarization of practical advices for preparation of polymer based inks based on experience gathered during the work.

6. EXPERIMENTAL PART

6.1 Materials and Sample Preparation

A commercial poly(vinyl alcohol) (PVA) that represents a water-soluble polymer was purchased from Sigma-Aldrich under trade name Mowiol[®]. The experimentally investigated material in this work was Mowiol[®] 4-98. Degree of hydrolysis (DH) of this PVA was in the range from 98.0 to 98.8 mol %, polymerization degree (PD) around ~ 600 and weight-average molecular weight (M_w) around ~ 27,000 as declared by the producer. Also other PVA brands were tested at the beginning of the preliminary material selection for ink formulation, namely Mowiol[®] 6-98 that had DH in the range from 98.0 to 98.8 mol %, DP around 1,000 and weight-average molecular weight around ~ 47,000. Other initially tested materials was Mowiol[®] 8-88 that had weight-average molecular weight around ~ 67,000, DH ~ 86.7-88.7 mol %, DP ~ 1,400.

Dimethyl sulfoxide (DMSO) for UV spectroscopy grade, ≥ 99.8 % (GC), was also purchased from Sigma-Aldrich. Demineralised water was used as a major solvent. The water was obtained from in home deionization unit, its conductivity was always in order of 10^{-7} S·cm.

As a surfactant, laboratory grade of Triton[™] X-100 was also purchased from Sigma-Aldrich.

Polymer PET substrate selected for printing (NOVELE[™] IJ-220) was supplied from Novacentrix (USA).

The reference PVA solutions at different concentration were prepared by dissolving of granulated PVA in distilled water at 85 °C and continual stirring. Next, the PVA was dissolved in mixture of distilled water/DMSO in volume ratio 2:1 (v/v) at the same concentrations as reference solutions. DMSO was used for decreasing of surface tensions of PVA solutions. Moreover, prepared mixture water/DMSO has higher boiling point than water. All solutions were passed through a syringe filter “LUT Syringe Filters PTFE” (Labicom s.r.o., Czech Republic) with pore size 0.24 μm to eliminate insoluble particles and other solid impurities.

6.2 Experimental Methods

Crucial parameters of each inkjet inks are viscosity and surface tension. Measurements of the rheological properties of prepared solutions were carried out using a rotational rheometer (Bohlin Gemini, Malvern Instruments, UK), with coaxial cylinder geometry (length of 27.4 mm, inner cylinder of 14 mm in diameter and the outer cylinder separated by a 0.7–mm gap). All steady-shear tests were performed in the shear rate range of 10-50 s^{-1} (controlled shear rate mode). Additionally, the samples of PVA were measured in temperature range between

10 and 40 °C at 7 different temperatures with 5 °C increments. Before the measurement at given temperature, the sample was tempered for 2 minutes.

Intrinsic viscosity, $[\eta]$, was determined by measuring the relative viscosities, η_{rel} , of a series of PVA solutions of different concentrations at 25 °C. The measurements were carried out by using a Lovis 2000 M/ME viscometer (Anton Paar) based on the rolling ball made from steel and diameter of 1.5 mm. The measuring angle was 70°. Density measurements of liquids were performed at required temperatures by density meter DMA5000M (Anton Paar). The surface tension (SFT) was estimated using force tensiometer K100 from KRÜSS (GmbH Germany) by plate method (also called Wilhelmy plate method). In this assessment, the plate is oriented perpendicularly to the interface, and the force exerted on it is measured. The measurements of viscosity and SFT were performed for various temperatures as it was not known at the beginning of the work which temperature is optimal for printing. Besides that, temperature dependences enriched interpretational framework of present study.

Solution with suitable (optimum) properties were filled into cartridges (type: piezo-driven jetting device with integrated reservoir and heater) and printed by Dimatix Materials Printer DMP-2800 series (Fujifilm Dimatix) onto coated PET foil (NOVELE™ IJ-220). The cartridge with ink was put on a wet cloth for 10 minutes before installing into cartridge holder. The printer head nozzles were heated and their temperature controlled at 35 °C. The substrate temperature was set to 45 or 47 °C. The print-head angle was appropriately set for any needed resolution of patterns. The print-head nozzles were purged for 1 μ s after every 8 run to ensure freshness of ink.

The surface energy of coated PET foil was determined using Surface Energy Evaluation System (See system) (Advex Instruments). System allows the measurement of contact angle by determining a tangent angle of a liquid drop with solid surface (Sessile drop technique).

Printed demonstration patterns were analysed by optical microscope LEICA DVM2500 Digital Camera (LEICA MICROSYSTEMS) and by atomic force microscope (AFM) Dimension ICON (Bruker) under ambient condition. The mechanical profilometer (Bruker) was used for determination of high profile of prepared motives. The structure of cartridge was determined by compact x-ray micro-tomography SKYSCAN 1174 (Bruker). The material cartridge was also characterized by scanning electron microscope Nova NanoSEM (FEI, the Czech Republic). The common high vacuum condition throughout the column and specimen chamber was used with the ETD optional HiVac detector. The images were scanned in SE operational mode with maximum magnification 20 000 x. The sample was cut and fixed onto a holder and all measurements were kept in 5 mm range.

6.3 Notes on Data Statistics

A number that follows the \pm sign is a standard error (s.e.) of the mean in Tables 6, 7 and 8, otherwise it is always a standard deviation (s.d.) calculated with the help of $(n-1)$.

Standard error is calculated according to equation:

$$s.e. = \sqrt{\frac{\sum (x - \bar{x})^2}{n \cdot (n-1)}} \quad (6.1)$$

Standard deviation is calculated according to equation:

$$s.d. = \sqrt{\frac{\sum (x - \bar{x})^2}{(n-1)}} \quad (6.2)$$

Relative standard deviation corresponding to each data point in graphs in Figures 21-23 and 25 are in order of 2-3 %, therefore the error bars are not shown in graphs as they would graphically merge with the data point symbols. Each set of data points in graphs in Figures 19, 20 represent a single value in graphs in Figures 21 and 22.

In the case of graphs in Figures 23, each data point measurement was repeated three times for the same solution and the results differed at fourth digit only, hence the variability of these data points due to repeatability is negligible in comparison with other sources of variation manifested in these graphs.

Statistics related to the substrate surface energy estimation with the help of Surface Energy Evaluation (See) system is described in corresponding part of the text of chapter 7.10.1 *Substrate properties*.

7. RESULTS AND DISCUSSION

7.1 Rational Selection of Polymer-Solvent Systems

Polyvinyl alcohol was chosen as a representative synthetic hydrophilic polymer. PVA is used in various applications, to illustrate: it is used as a stabilizer for polymer dispersions, a thickening agent in inks and stamping colours, as optical brightener carrier of choice in paper/paperboard coatings, to preparation of thin water-soluble films in packaging and fibres for textile products and others. [117, 118] Biocompatibility and non-toxicity increase its attractiveness for sophisticated applications even more. [119] PVA is characteristic due to highly polar -OH side groups attached to every second carbon in the main chain. But, it also contains certain amount of acetyl groups that are still bound to the polymer backbone after hydrolysis process of poly(vinyl acetate). The degree of hydrolysis (DH) expresses the percentage of hydrolysed mer units while the value $100\% - DH$ represents the residual acetyl group fraction. Polymerization degree (DP) and DH are the most important characteristics affecting properties of the polymer. Therefore, PVA can be purchased in fully or partially hydrolysed grades for each DP according to different purposes. Both parameters have an important effect on solubility of polymer in water and other solvents. The viscosity of PVA solution is governed mainly by DP and concentration while temperature and DH have weaker effect. The viscosity of a polymer solution with higher DP is significantly bigger than the viscosity of a polymer solution with lower DP at the same concentration because longer polymer chains have more opportunities to form inter and intramolecular hydrogen bonds. Similarly increasing concentration causes enhancement of namely intermolecular hydrogen bonding creation due to decreasing distance between polymer chains which again has larger effect in the system with longer chains. The influence of DH is much less pronounced and generally small at low concentrations, i.e. in dilute solutions. The bigger DH the more hydroxyl groups are available to be involved in hydrogen bonding and increase of viscosity is observed. Increasing concentration enhances this effect too but less than in the former case. Obviously, the viscosity of all these water based systems decreases with increasing temperature with activation energy estimated from Arrhenius equation in order of 10-20 kJ/mol in water solutions. The size of energy barrier testifies for the important role of hydrogen bonds in the system. [118, 120, 121]

Many experiments were performed at the beginning of this work. Firstly, the PVA with higher molecular weight (Mowiol[®] 6-98) was used for preparation of aqueous solutions. Generally, the surface tension of aqueous solutions and dispersion is too high because of high surface tension of water itself. Therefore, the ethanol was added to aqueous solutions to decrease surface tension. Moreover, the addition of ethanol diluted the origin concentration of PVA solutions; on the other hand, the addition increased their viscosity. Nevertheless, the origin

solutions as well as the modified by ethanol did not lead to a stable jetting of drops from cartridge, probably due to clogging of the print-head. The clogging of nozzle could be caused by low boiling point and faster evaporation of ethanol or by use of PVA with too high polymerization degree. The using of surfactants was also investigated in the prepared PVA solutions. The available surfactant Triton X-100 was added to origin PVA solutions, but it precipitated in PVA solution. The polyvinyl alcohol with lower degree of hydrolysis was also tested (Mowiol® 8-88). The advantage of lower degree of hydrolysis was better dissolving process in comparison with almost fully hydrolysed PVA 6-98, but the limitation of this PVA is its gel forming tendency that resulted in conversion from solution into quazi-gel form inside of cartridge.

After previous experiences, following experiments were performed on almost fully hydrolysed PVA 4-98 with low polymerization degree in the next step. Moreover, it has been already found, that although co-solvents with lower boiling point (case of ethanol) decrease the SFT, its evaporation at lower temperatures can cause clogging of the nozzle. Therefore, another co-solvent miscible with water was searched. Examples of solvents miscible with water are listed in Table 5 together with their selected properties such as boiling point, density, surface tension, and viscosity at certain temperature. The primary alcohols as well as acetone were excluded because of their low boiling point. The properties of acetic acid is similar to water (except surface tension), thus, the improvement of printability was not expected. The DMSO was chosen as co-solvent from remain compounds. The dynamic viscosity of ethylene glycol and diethylene glycol is too high; on the other hand, dimethylformamide is toxic.

Table 5. The most common polar solvents and their selected properties such as boiling point, density, surface tension and dynamic viscosity [122-124]

Solvent	Boiling point [°C]	Density at 20 °C [g·cm⁻³]	Surface tension at 20 °C [mN·m⁻¹]	Dynamic Viscosity at 25 °C [mPa·s]
Water	100.0	0.998	72.6	0.890
Ethylene glycol	197.0	1.115	46.5	16.8
Diethylene glycol	245.0	1.118	48.5	30.0
Dimethylformamide	153.0	0.948	36.8	0.794
Dimethyl sulfoxide	189.0	1.101	43.7	1.996
Acetone	56.1	0.790	23.3	0.306
Acetic acid	118.0	1.049	27.4	1.115
Ethanol	78.3	0.789	22.3	1.074
Methanol	64.7	0.791	22.6	0.545

A co-solvent has multiple roles. Although water is a relatively good (i.e. not the worst) choice with respect to its evaporation rate the ink must not dry at the nozzle / atmosphere interface therefore, high boiling solvents should be added as humectants. Viscosity is another parameter modified by additions of substantial amounts of co-solvents although the dissolved polymer contributes largely too. The surface tension is a parameter that is sensitive to small concentration of additives if they have surface activity within the chosen system. On the other hand, mixing of water with reasonable amount of the co-solvent dictates the surface tension too. Other co-solvents and additives may be responsible for antimicrobial protection of the ink, dispersion stabilization etc. Mutual effects of components used for making the ink formulation are of very complex and complicated nature. [48]

The first attempts to prepare printed PVA patterns were based on empirical trial and error approach mainly [125] but this work is focused on formulation of a polymer ink in a rational way. Fully hydrolysed material was chosen because its application potential and moreover the use of homopolymer makes studied problems more tractable than in case of co-polymers. DMSO was chosen as a single satisfactorily appropriate and compatible ink modifying compound. As printed PVA pattern might find its applications in highest demanding fields, there is strong motivation to keep the ink composition as simple as possible in order not to deal with inevitable residual additives in printed material after drying, e.g. surfactants.

7.2 Rheological Study

The flow behaviour was investigated with the use of the rotary rheometer. Solutions of PVA in water and water/DMSO were prepared in concentrations that are relevant for practical deposition of material by inkjet printing (i.e. several weight percents) with emphasis put on more dilute solutions. Figure 19 shows the plots of shear stress against shear rate (left part), and viscosity against shear rate (right part) of PVA solutions in water at 25°C. Simultaneously, the Figure 20 shows the same plots for PVA solutions at same temperature and concentrations, but the solutions were prepared in water/DMSO (2:1 v/v) mixture. In short, all diluted solutions showed the Newtonian behaviour in the measured range. Additionally, the higher polymer concentration the higher viscosity values were determined. The generally higher level of viscosities of PVA solutions prepared in water/DMSO mixture is caused by the presence of DMSO. The role of co-solvent system is discussed in detail in the next section.

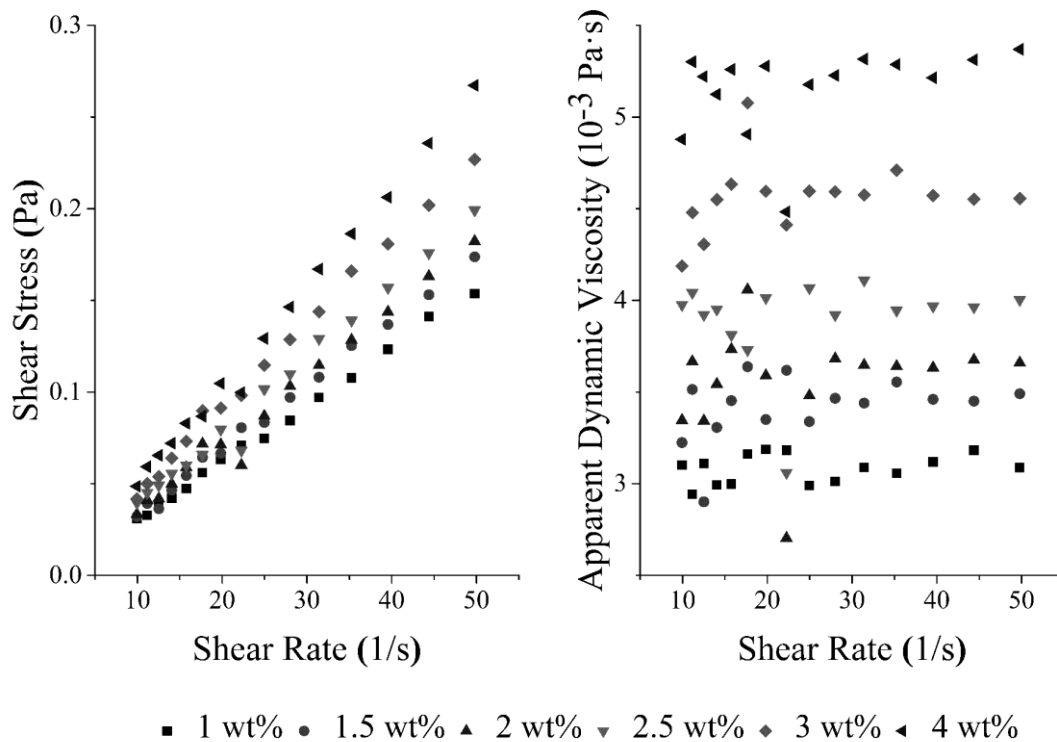


Figure 19. Shear stress vs. shear rate (left) and viscosity vs. shear rate (right) plots of aqueous PVA solutions at 25 °C.

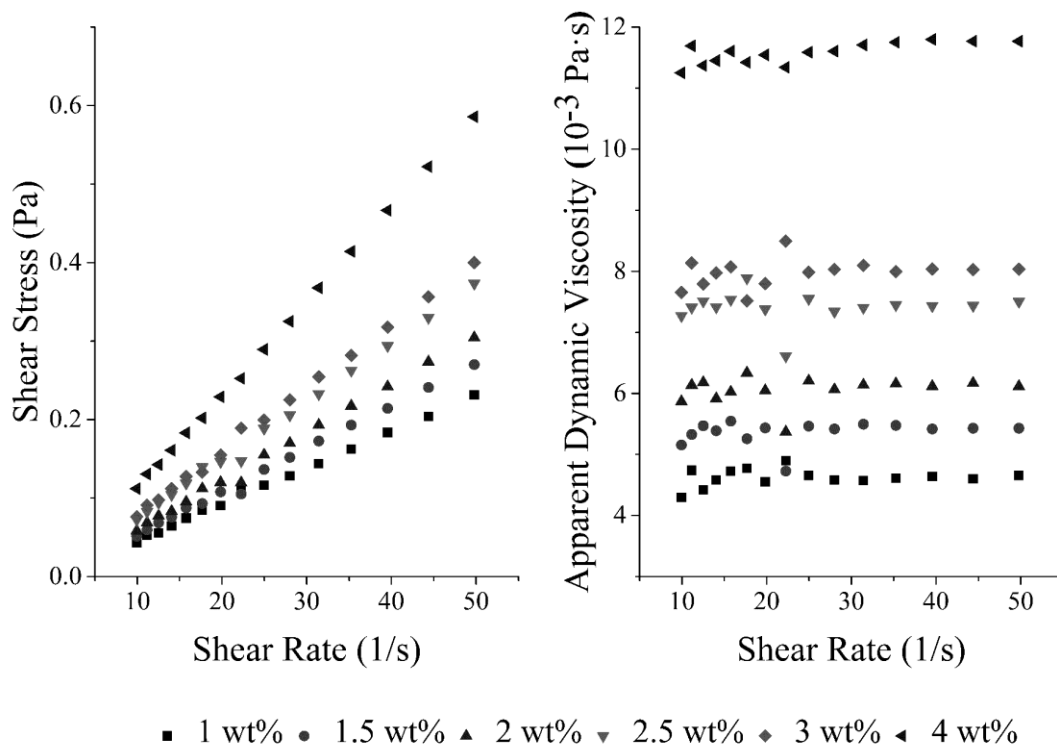


Figure 20. Shear stress vs. shear rate (left) and viscosity vs. shear rate (right) plots of PVA solutions prepared in mixture of water/DMSO at 25 °C

Temperature-dependent behaviour of solutions' viscosity was also determined, because the jetting temperature can be controlled during printing process. Figure 21 shows the temperature dependence of apparent dynamic viscosity of PVA solutions in water as well as in the mixture of water/DMSO. Similar data series as shown in Figures 19 and 20 were recorded for all tested concentrations and temperatures. Newtonian behaviour was experienced in all cases in measured range of shear rates. Therefore, dynamic viscosity (each one point in graphs in Figure 21) was calculated as an average over the whole shear rate range measured for each concentration-temperature combination representing thus extensive experimental data matrix. Similar general trends were observed for both types (water and water/DMSO) of solutions as follows: the solution with highest concentration of PVA at lowest temperature shows the highest viscosity. Viscosity decreases with decreasing concentration and increasing temperature. The overall viscosities for solutions prepared in pure water (Figure 21 left panel) and in water/DMSO (Figure 21 right panel) are in ranges 2.5-8 mPa·s and 3-21 mPa·s, respectively. The original measured data of shear-stress vs. shear rate and viscosity vs. shear rate data for PVA in water as well as for water/DMSO is visible in the Appendix of this work.

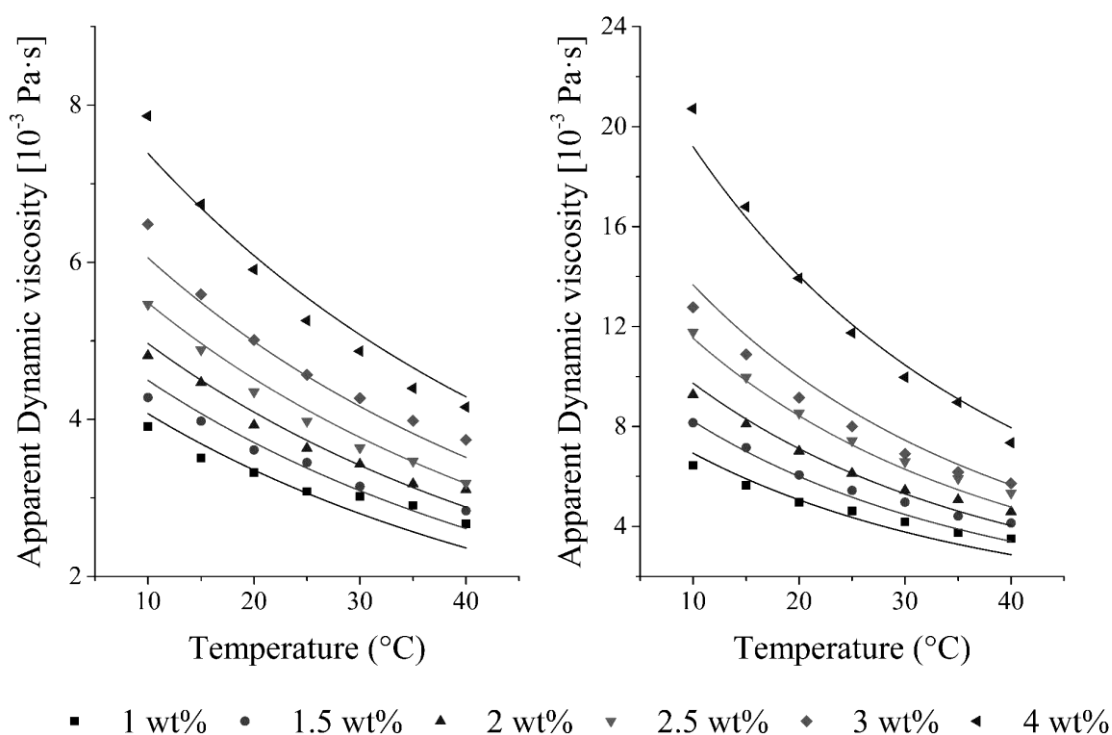


Figure 21. Temperature dependence of apparent dynamic viscosity of PVA solutions (left) in water, and (right) in water/DMSO mixture. Multiple lines show result of theoretical global fits of unlimited region of experimental data by equation (7.2).

Al-Farris and Al-Zahrani [126] investigated the rheological behaviour of dilute aqueous polymer solutions. They proposed a correlation equation for the viscosity of dilute polymer solution as a function of temperature, shear rate and concentration. The equation can be used for prediction the viscosity of polymer solution at different concentration and temperature.

$$\eta = A_1 \cdot [\exp(B_1 / T)] \cdot \dot{\gamma}^{C_1} \cdot [\exp(D_1 \cdot C)] \quad (7.1)$$

where η is the viscosity of polymer solution, A_1 , B_1 , C_1 , D_1 are the constants, T is the temperature in K, $\dot{\gamma}$ is the shear rate in 1/s, and C is the concentration in ppm.

The equation was successfully applied by Al-Shammari [68] to predict the viscosity of mLLDPE solutions in cyclohexane. A relationship using the same formalism was also applied in this study to describe rheological behaviour of PVA solutions at different temperature and different concentration too.

The equation was little adjusted and simplified into the following form:

$$\eta = K \cdot \exp \left[(B_1 / T) + (D_1 \cdot w) \right] \quad (7.2)$$

where w is the concentration in mass percent ($100 \text{ wt}\% \cdot m_{\text{dissolved polymer}} / m_{\text{total of the solution}}$), T is the temperature in K, the constant K has the dimension of mPa·s and includes the parameters A_1 and shear rate $\dot{\gamma}^{C_1}$. This simplification is possible, as it was experimentally observed for tested range of parameters that viscosity does not depend on shear rate implying that C_1 is 0. Therefore, in this study, the shear rate term is virtually cancelled or can be considered for a constant (with the value 1) hidden in K due to consistency of units, because the solutions behave as Newtonian fluids in measured range. The equation represents actually a product of two terms. The first exponential which includes K and B_1/T is nothing else but the Arrhenius equation for viscosity dependence on temperature where B_1 is defined as E_a/R (E_a is activation energy and R is the universal gas constant) and K is the frequency factor. The second term includes $\exp(D_1 \cdot w)$ which phenomenologically describes inter and intramolecular interactions in the system. Multi-data fit (global) mode of non-linear curve fitting with shared optimized parameters procedure included in OriginPro software was used for mathematical analysis of experimental data. Obtained results for PVA solutions in water and water/DMSO mixture are shown in Figure 21. The equation was always fitted into the whole set of data, obtaining thus a set of fitting curves with only one value for each parameter for the two types of solution. Results are listed in Table 6.

Activation energy E_a can be obtained from B_1 constant by simple multiplying it by R . Obtained values agree with literature data (see first paragraph of this section). Hence the model can be useful to predict an approximate solution viscosity at certain temperature and concentrations over the range of investigated parameters.

Table 6. Model parameters for PVA solutions obtained by using equation (7.2) fitted into full data range shown in Figure 21.

Solvent	K [10^{-4} mPa·s]	B_1 [K]	E_a [kJ/mol]	D_1 [-]
Water	110 ± 20	1600 ± 60	13.3 ± 0.5	0.198 ± 0.007
Water/DMSO	5.0 ± 1.5	2600 ± 80	21.6 ± 0.5	0.339 ± 0.009

However, values for extreme temperatures (10 °C and 40 °C) and the highest as well the lowest concentration data sets were intentionally omitted in the fitting procedure to define area where the equation (7.2) holds best on. The fitted selected range is shown in Figure 22. Then, Table 7 shows the model parameters obtained for data fitting in selected range.

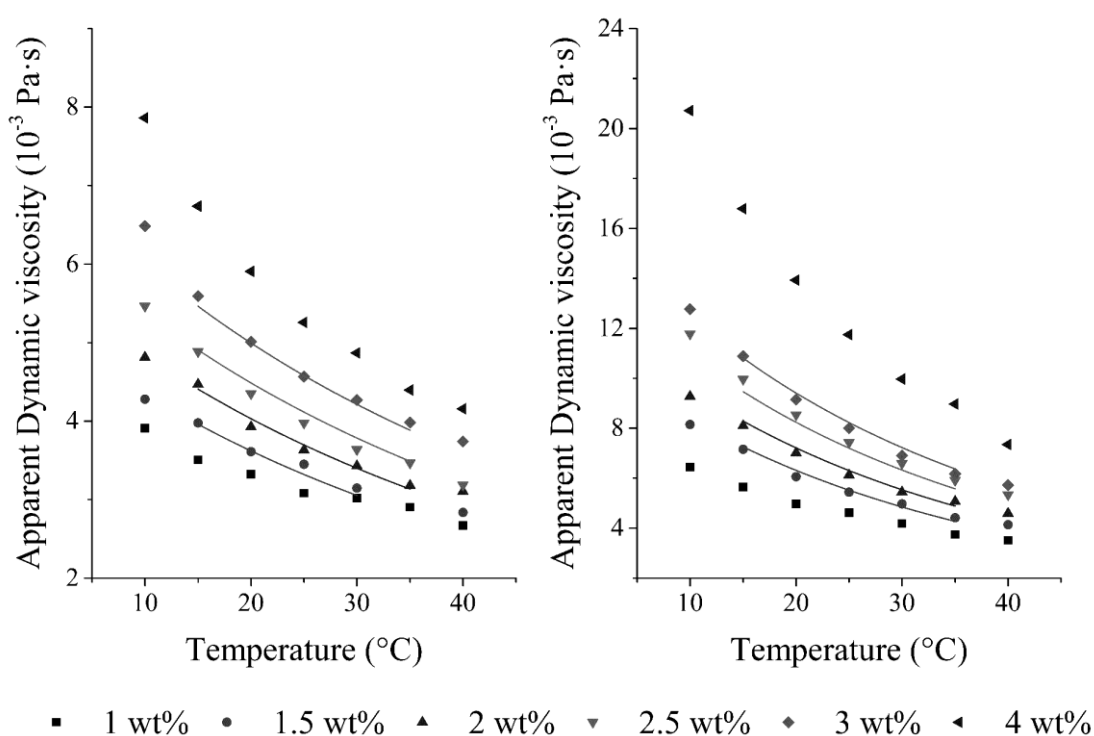


Figure 22. Temperature dependence of dynamic viscosity of PVA solutions (left) in water, and (right) in water/DMSO mixture. Multiple lines show result of theoretical global fits of selected region of experimental data by equation (7.2).

Table 7. Model parameters for PVA solutions obtained by using equation (7.2) fitted into the selected data range shown in Figure 22.

Solvent	K [10^{-4} mPa·s]	B_1 [K]	E_a [kJ/mol]	D_1 [-]
Water	150 ± 30	1510 ± 70	12.6 ± 0.5	0.215 ± 0.010
Water/DMSO	14 ± 5	2350 ± 100	19.5 ± 0.8	0.266 ± 0.015

The optimum recommended viscosity for the inkjet printer used in this study is in the range of 10-12 mPa·s [39]. Fluids with slightly smaller viscosities can be jetted with success too, therefore concentrations of 2.5 wt% and 3 wt% of PVA in water/DMSO mixture seem to be most suitable among tested solutions judging preliminary on rheological measurements only. However, the data were obtained for low shear rates only because it has not available instruments working at high shear range at such very small viscosities. In practice, high shear rates are experienced during the inkjet printing process. Based on Wang's study [127] and calculations according to following equation (7.3), the expectable shear rate can exceed $1 \times 10^5 \text{ s}^{-1}$.

$$\dot{\gamma} = \frac{4 \cdot \dot{Q}}{\pi \cdot R^3} \quad (7.3)$$

where $\dot{\gamma}$ is the apparent shear rate, \dot{Q} is the volumetric flow rate, and R is the capillary radius of the printer head nozzle.

Although high-shear rates are achieved in printing process, low-shear rate viscometers are still used for basic characterization of inkjet inks in inkjet industry as well as in academia due to their availability.[128-131] Thus, the data obtained by ordinary viscometers is considered sufficient enough for characterization of prepared inks and their further processing and evaluation. The main idea behind this concept is that the investigated liquid flows in laminar regime although the shear rate is so extremely large. It is the Reynolds number which allows to judge about the suitability of this approach in each individual case. It will be shown in a later section of this article that all prepared solutions under used conditions fall deeply into laminar flow regime.

It should be noted that laminar flow in pipe occurred, when the $Re \leq 2320$. It is also the condition of validity of Hagen-Poiseuille law, which is valid only for stable laminar flow, in the other word, at fully developed velocity profile. However, this velocity profile can be obtained, when the fluid cover great deal of pipe region called the "Entrance or inlet length". The inlet length is usually defined by Boussinesq equation (7.4) or Schiller equation (7.5), respectively. [132, 133]

$$\frac{x_r}{d} \geq 0.065 \cdot Re \quad (7.4)$$

$$\frac{x_r}{d} \geq 0.025 \cdot Re \quad (7.5)$$

where the x_r is the inlet length, d is the pipe diameter, and Re is the Reynolds number.

Direct rheological measurements of inkjet inks at high shear rates are possible using instruments based on the flow of the liquid through a microchannel. As an example, a microfluidic slit rheometer VROCTM (fabricated by RheoSense Inc.)

can be referred. The slit is made from Pyrex mounted on a gold-coated silicon base. The base of the microchannel contains three flush mounted Micro-Electro-Mechanical Systems (MEMS) pressure sensors. The rheometer has been already successfully applied for experimental measurements performed up to 10^5 s^{-1} shear rates. [134-136] However, either this or similar instrument was not available for this study.

7.3 Determination of Solvation Effect: Viscometric Analysis of Solvent-Polymer System

A limiting viscosity number, or intrinsic viscosity $[\eta]$, is an important parameter for polymer characterization, but it depends on several parameters such as concentration and size of dissolved macromolecules, solvent quality, temperature, and other. A viscometer based on the rolling ball method was used for all viscometric measurements. The unit of intrinsic viscosity used in this work is cm^3/g according to IUPAC recommendations [137] although it can be any reciprocal of mass concentration unit in general. Intrinsic viscosity is usually used for determining of molecular weight of macromolecules compounds through the Mark-Houwink equation with known constants K and a . [138] Values 3.19×10^{-4} for K and 0.717 for a were obtained from viscometric data for PVA with DH = 99 % by Benlian Wang *et al.* [139] with the aid of Ubbelohde viscometer at 25 °C. Tacx *et al.* [140] found 6.51×10^{-4} and 0.628 for PVA with DH \geq 99.6 % at 30 °C. Moreover, estimation of $[\eta]$ can be also used for determining of solvation efficiency and the interaction between polymer and solvent. The thermodynamic quality of the solvent for certain polymer is often evaluated on the basis of Huggins constant (also called Huggins viscosity coefficient), K_H , which reflects both hydrodynamic and thermodynamic interactions in polymer-solvent system in the Huggins equation describing the specific viscosity η_{sp} as a product of dimensionless concentration $[\eta]c$.

$$\eta_{sp} = [\eta] \cdot c + K_H \cdot [\eta]^2 \cdot c^2 + K_2 \cdot [\eta]^3 \cdot c^3 + \dots \quad (7.6)$$

The value of K_H is obtained by Huggins original method neglecting higher terms in the virial expansion (7.6) from plotting the reduced viscosity against mass concentration of the polymer in solution c (defined as mass of the polymer / volume of the solution, the unit is g/cm^3) by extrapolation of equation (7.7) linear fit into observed data to zero polymer concentration and its slope. The intercept is the $[\eta]$ itself. [141-144] The Huggins constant is dimensionless and its value is usually in the range of 0.3-0.5 in good solvent and in the range of 0.5-1 for theta solvent. Values in range 0.35-0.5 are reported for PVAs in literature too, however in polar (aqueous) solvents the constant value tends to be higher than 0.5. Lower

values are expectable for PVAs with lower DH while higher values are experienced for highly hydrolysed PVAs due to their higher content of OH groups imparting them more hydrophilic nature and susceptibility to hydrogen bond formation as shown by Lewandowska *et al.* in [145] and references therein. Moreover, the dependence of reduced viscosity against concentration does not have to be always linear, but it may be deflected in the upward direction, especially for polymers with higher molecular weight and higher values of intrinsic viscosity. Therefore, the Schulz-Blaschke equation (7.8) was introduced to evaluate intrinsic viscosity from a dependency of reduced viscosity on the specific viscosity. [142] Schulz-Blaschke equation works in wider concentration range and Schulz-Blaschke constant (K_{SB}) values vary in the range from 0.27 to 0.4. [146-148] The equations for Huggins and Schulz-Blaschke methods for evaluation of $[\eta]$ can be defined as:

$$\frac{\eta_{sp}}{c} = [\eta] + K_H \cdot [\eta]^2 \cdot c \quad (7.7)$$

and

$$\frac{\eta_{sp}}{c} = [\eta] + K_{SB} \cdot [\eta] \cdot \eta_{sp} \quad (7.8)$$

where c is the concentration, η_{sp} is the specific viscosity, $[\eta]$ is the intrinsic viscosity, and K_H and K_{SB} are the Huggins and the Schulz-Blaschke constants, respectively.

There are other methods of $[\eta]$ determination available, for example Kraemer's [143] and Heller's [144] methods. Abdel-Azim *et al.* [147] discussed the determination of intrinsic viscosity by single specific viscosity measurement and described different equations leading to intrinsic viscosity. Their equations were proposed by derivation or combination of the original Huggins's and Schulz-Blaschke equations. However, the single point measurement method is practically applicable only for serial measurements of systems with known reliable constant value for given pair polymer-solvent.

The intrinsic viscosity measurement was performed in order to achieve better understanding why the water/DMSO mixture performed better in preparation of water-soluble inkjet ink based on PVA. The results are shown in Figure 23 and obtained values are summarized in Table 8. As can be seen, the observed dependency of reduced viscosity on mass concentration for PVA in solvent mixture has bigger slope than the plot of data for PVA in water (Figure 23-left). The same trend can be seen in Schulz-Blaschke graph (Figure 23-right).

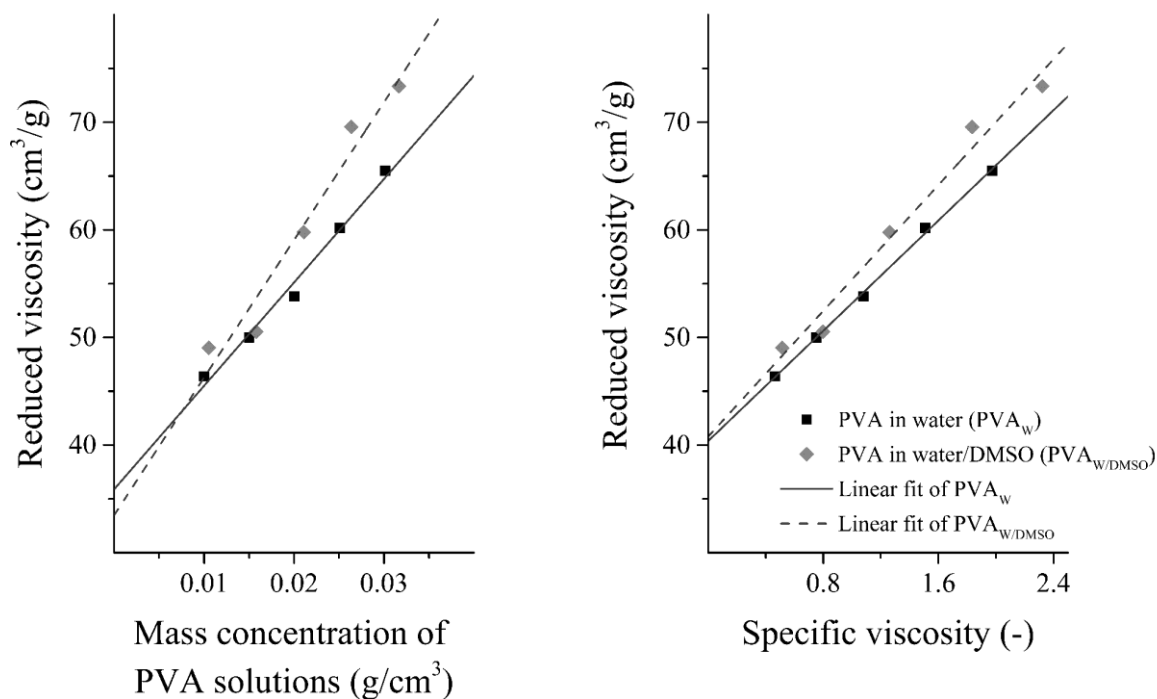


Figure 23. Plots of reduced viscosity against mass concentration of PVA solutions (left-Huggins plot) and reduced viscosity against specific viscosity (right-Schulz-Blaschke plot), respectively.

Table 8. The observed data from determination of intrinsic viscosity as slope, intercept, correlation coefficient, Huggins (K_H) and Schulz-Blaschke (K_{SB}) constants for PVA.

Solvent	Huggins equation			
	Slope [cm ⁶ /g ²]	Intercept; [η] [cm ³ /g]	R^2	K_H [-]
Water	960 ± 60	35.9 ± 1.4	0.9824	0.75 ± 0.06
W/DMSO	1280 ± 160	33 ± 4	0.9424	1.14 ± 0.20

Solvent	Schulz-Blaschke equation			
	Slope [cm ⁶ /g ²]	Intercept; [η] [cm ³ /g]	R^2	K_{SB} [-]
Water	12.8 ± 0.3	40.4 ± 0.4	0.9979	0.317 ± 0.008
W/DMSO	14.6 ± 1.3	40.8 ± 1.9	0.9713	0.360 ± 0.035

According to the theory mentioned above, water may be considered as a theta solvent for used PVA with the Huggins constant $K_H = 0.75$. The value $K_H = 1.14$ obtained for PVA in water/DMSO is apparently slightly above ideal range, however the value of K_H may be affected by polymer concentration, molecular weight, degree of branching, and solvent composition in non-trivial way. Despite

of the higher value of the Huggins constant for solution in mixture of water/DMSO, this mixture could be still considered as theta solvent although it needs additional analysis. Schoff [146] listed Huggins and Schulz-Blaschke constants for several polymers in different solvents confirming large variability in the K_H value observed for PVAs. On the other hand, the values of Schulz-Blaschke constants obtained for the same PVA in water and water/DMSO mixture differ within one s.e. range only which testifies for the same quality of both solvents with respect to used PVA. It is known, that Schulz-Blaschke method is more robust with respect to higher concentrations of the polymer in solution. On the other hand, Huggins method approaches its utilization limits due to polymer-polymer interactions in the solution if the solutions cannot be considered as diluted enough, which is most likely true in case of water/DMSO as discussed below. Other reasons for observed value can be found in specific solvent-polymer interactions that are not experienced in purely water solution as discussed further.

The mixture water/DMSO is specific mainly due to mutual strong interaction between their molecules. This interaction occurs already in mixing process which was confirmed by heat generation during mixing of two volumes of water with one volume of DMSO. The molar fraction of DMSO in used water/DMSO (2:1 v/v) co-solvent is 0.113. The behaviour of whole solvent system depends on concentration of each substance. Wong *et al.* [149] described in their work that there are two dominant different structures governing resulting properties of water/DMSO solution. In DMSO-rich solution, water will be preferentially involved in bridging two DMSO molecules by hydrogen bond and, of course; the water-water hydrogen bonds also exist and their number increase proportionally with water content. In a water-rich solution, water will have a tetrahedral hydrogen bond structure that may lead to local structures consisting of one molecule of DMSO and two molecules of water. Additionally, the hydrogen bonds are stronger with DMSO's oxygen than with water's oxygen.

The strong interactions between DMSO and water were also discussed by Tacx *et al.* [140] Moreover, they studied the dissolution behaviour of PVA in three different solvent. They found that intrinsic viscosity increased considerably in order water, ethylene glycol and DMSO. They concluded that the strong interactions exist in presence of two low molar mass components between themselves resulting in smaller interaction with PVA. Also, the increasing dilution of DMSO leads to decreasing of intrinsic viscosity. From another point of view, this may be reconsidered as having the same effect as (apparent) increase of PVA concentration because the number of water molecules interacting with PVA molecule is decreased by those water molecules which enter interaction with DMSO being bonded in the supramolecular complex.

Wright *et al.* [150] investigated the dilute solution of PVA two different molecular weights because of their effect on the properties of solid-state film prepared by casting. They studied the rheological properties of solution and the relationship between these and mechanical and swelling properties and other

parameters. Nevertheless, the improvement of solvent quality has been observed by using various co-solvents mixed with water. They compared solutions of PVA in mixtures of water with DMSO, N-Methyl Pyrrolidone, 2-Pyrrolidone, N-Ethyl Pyrrolidone, Propylene Glycol and Dipropyleneglycol. The mixture of water-DMSO showed better solvent quality than water alone. However, DMSO in dilute solutions offers poorer performance for coil expansion in comparison with other co-solvents because of strong interaction between DMSO and water molecules (cononsolvency effect, as is discussed in the next section). The complex formed by DMSO/(water)₂ molecules results to little interactions of whole solvent system with polymer, and therefore, the fully extended state of polymer chain cannot be reached (in other words, an overcome of the intramolecular polymer interactions was not reached).

According to Vollmert [148], the slope ($K_H \cdot [\eta]^2$), obtained from the plot of reduced viscosity against concentration, should be considered for an indicator of energy interaction level between polymer and solvent. The sharper slope the better solvation of macromolecules is reached.

In conclusion, the used water/DMSO mixture (2:1 v/v) offers better solvation effect than water alone in used system. Used composition of water/DMSO was such that the mixture did not fail into composition region of thermodynamically poor solvent causing collapse of polymer coils of the used PVA.

7.4 Stability of PVA Solutions in Water/DMSO co-Solvent

Tested PVA concentration range spans from dilute to semi-dilute region. Table 9 summarizes prepared PVA solutions in water/DMSO (2:1 v/v) with the help of dimensionless concentrations. Based on the viscometric data, the critical concentration (c^*) was calculated from both Hugging and Schulz-Blaschke intrinsic viscosity $[\eta]$. These values of c^* are 0.0303 g/cm³ ($=1/[\eta]=1/33$) for Huggins and 0.0245 g/cm³ ($=1/40.8$) for Schulz-Blaschke, respectively.

The first critical concentration is c^* defined as $[\eta] \cdot c = 1$. It represents the border between infinite dilute and hydrodynamic screening region. In this region, interactions between macromolecules will begin to influence the behaviour of polymer chains in the solution. If the dimensionless concentration exceeds the second critical value c^{**} (representing the chain overlapping concentration limit in the semi-dilute region) defined as $[\eta] \cdot c = 4$, the polymer coils begin to overlap and intermolecular interactions are strongly manifested in this semi-dilute entangled regime.

Table 9. Dimensionless concentrations of prepared solutions PVA in water/DMSO (2:1 v/v) mixture.

Mass fraction, w [wt%]	Mass concentration, c [g/cm ³]	Dimensionless concentration, Huggins $[\eta] \cdot c$	Dimensionless concentration, Schulz-Blaschke $[\eta] \cdot c$
1.0	0.01052	0.347	0.429
1.5	0.01579	0.521	0.644
2.0	0.02109	0.696	0.860
2.5	0.02637	0.870	1.076
3.0	0.03167	1.045	1.292
4.0	0.04232	1.397	1.727

According to the requirements of inkjet technology, the solution must allow formation of single drops and thereby the polymer concentration shall be below critical gel concentration, which is normally the low concentration limit for solutions used in electrospinning technology where rich literatures on this topic exist. [106, 151-154] On the other hand, the concentration of polymer in the ink must be high enough for a drop to carry sufficient amount of material to the place where it needs to be delivered. Formation of a gel in the ink would be critical for the printing process and ultimately can cause clogging the nozzles in printing head. The determination of viscosity and surface tension (see next section) were carried out no later than two days after preparation of samples to avoid ageing, because the long storage time (two-three weeks or more) of PVA water/DMSO solutions can lead to formation of a gel according to already available experience. Hoshino *et al.* [155] reported interesting features of PVA gel prepared from solutions with the addition of DMSO. They observed at 23 °C, that no gel was formed if the DMSO concentration was below 20 wt% and above 80 wt%. The gel was formed when DMSO composition was in range from 20 to 80 wt% for the content of polymer over 2 wt%. Next, they found that the transparency or opacity of PVA gels depends on water/DMSO co-solvent composition too. PVA solutions of higher concentration than 2 wt% in co-solvents with DMSO concentration between 20 to 30 wt% form transparent gel readily from a clear solution while solutions with DMSO concentration between 40 to 80 wt% form opaque gels. The opacity develops in gel slowly for original solutions with DMSO concentration ≤ 60 wt% while formation of a gel in solutions with DMSO concentration $\geq 70\%$ is preceded by formation of turbid liquid dispersion. The appearance of turbid dispersions is described by the term clouded in their study as well. Solutions with the DMSO composition between 40 to 80 wt% with 1 wt%

PVA were found to form clouded dispersion but no gel. The water/DMSO co-solvent contained 35.5 wt% of DMSO in this work. Hence, the PVA solution stability is a serious issue over tested range of parameters. Prepared samples of solutions were closed into vials and kept in dark for 52 days at laboratory temperature to simulate common shelf storage conditions for inks. The observations are summarized in Figure 24 and shown in Table 10. The results obtained by naked eye observation are in accord with the already published data. It is evident, that all studied materials were unaffected by ageing during the first three days after dissolution which was our time window for performance of all other experiments. It can be seen that the time of three weeks is the maximum safe storage time for prepared inks up to 2.5 wt% PVA concentration. Moreover, it was not observed either clouds or gel formation for solutions below 1.5 wt% over the whole ageing experimental time span.

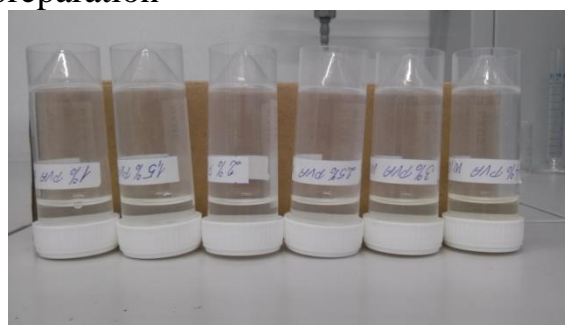
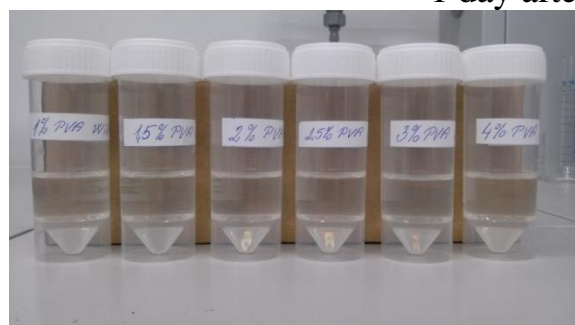
Time (days)	52	-	-	turb	turb	gel	gel
	22	-	-	-	-	gel	gel
	14	-	-	-	-	turb	turb
	8	-	-	-	-	turb	turb
	3	-	-	-	-	-	-
		1	1.5	2	2.5	3	4
		Concentration of PVA (wt%)					

Figure 24. Turbidity of PVA solutions in water/DMSO obtained by naked eye observation. The “-” sign means no change, “turb” stands for turbidity and “gel” indicates formation of a gel)

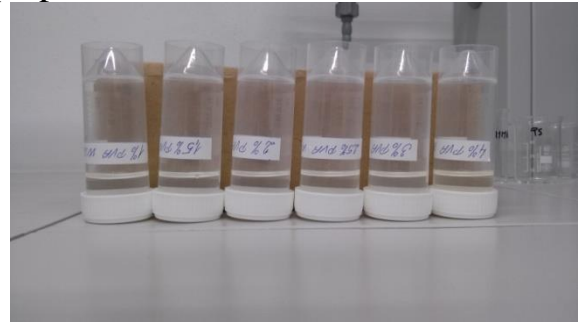
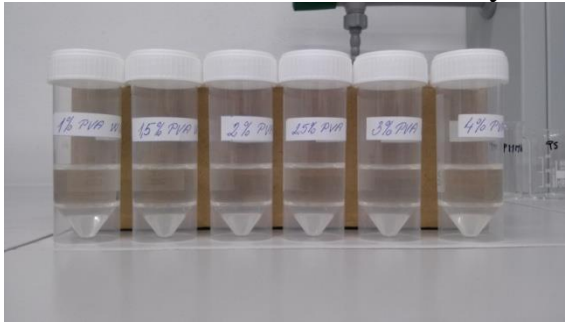
Table 10. The gelation of PVA solutions prepared in solvents mixture water/DMSO.

Pictures of PVA solution in water/DMSO mixture at selected time after preparation

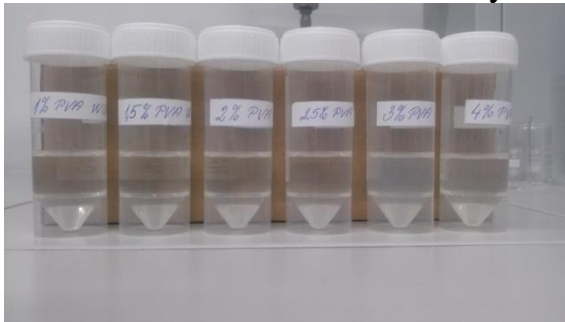
1 day after preparation



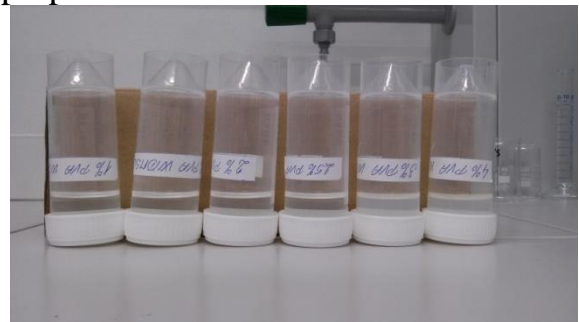
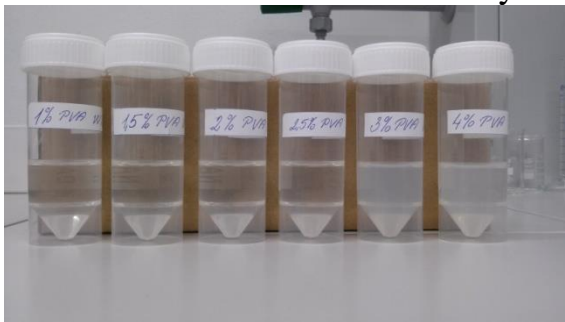
3 day after preparation



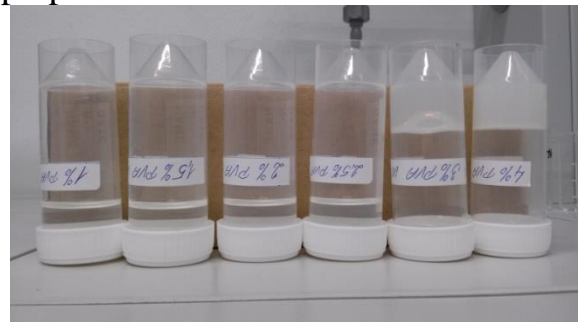
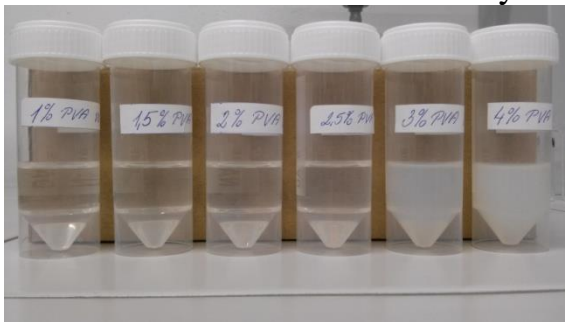
8 day after preparation



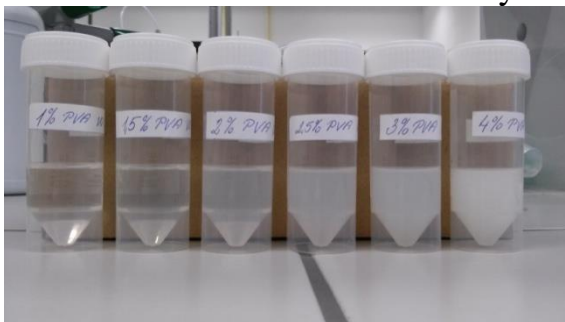
14 day after preparation



22 day after preparation



52 day after preparation



Formation of turbid solutions was observed always before gelation which can be used as a simple criterion of the ink usability by checking its appearance prior printing. This apparent contradiction with literature can be caused by the used gelation time estimation technique. Hoshino *et al.* [155] used extrapolation of inverse viscosity vs. time while we stick on the naked eye observation and manual touch by a glass rod technique. It can be hypothesized that their method underestimates the gelation time and our method may tend to overestimation.

The gel obtained from PVA in water/DMSO solution is of physical nature with PVA crystallites as crosslinking points between polymer chains. According [155], it is expected that in turbid solutions high crystallization rate produces bigger crystals (possibly fibrils in nature) while smaller crystals are formed in water rich solutions which results into a formation of an apparently clear gel followed by crystallite growth in gel phase turning the gel from clear to opaque. Our experience with the solution in the co-solvent in the water rich region is different although the X-ray scattering experiments of Hoshino *et al.* [155] are not taken in doubts. The turbidity appearance prior gel formation can be ascribed to a formation of a microgel before the system reaches complete gelation point where the crosslinking points are created by small crystallites. Shi-Jie Hong *et al.* [156] studied in detail kinetics and thermodynamics of PVA gel formation in water/DMSO co-solvent too. They studied the problem as an example of spinodal decomposition. Obtained results can be refined with respect to their work. They also performed a set of experiments with different water/DMSO composition and various PVA concentrations. First, they studied the co-solvent system itself. Parameters such as excess volume, excess mixing enthalpy, and relative viscosity show maximum or minimum values for molar fraction of DMSO 0.33 in the solution. They observed that gelation rate is maximal at DMSO molar fraction about 0.33 for 10 g/dl PVA solution at 25 °C. Additionally, at this molar fraction of DMSO, there are only slight amount of free water and free DMSO molecules in mixture, therefore a preferential adsorption coefficient is equal to be 0 indicating that most of DMSO and water molecules form DMSO/(water)₂ complexes. Lower DMSO molar fraction than 0.33 means the preferential adsorption of water to PVA molecules with an extreme at molar fraction of 0.07. On the other hand, higher DMSO molar fraction than 0.33 means preferential adsorption of DMSO to PVA molecules and increase of co-solvent quality. In fact, they found experimentally the lowest value of intrinsic viscosity for DMSO molar fraction 0.28 for dilute solutions which means the poorest solvent quality. A local maximum of intrinsic viscosity was found at DMSO molar fraction 0.07 (which is close to 0.113 specific for system used in this work) showing ideal behaviour. The part of their study performed on semi-dilute solutions confirmed the effects of co-solvent composition with extremes at the same concentrations.

Takahashi *et al.* [157] also studied the rates of gelation and phase separation of PVA solutions in mixtures of water and DMSO at different solvents compositions. They found that gelation rate increase rapidly by adding DMSO to water up to

DMSO volume fraction around 0.60 (which equals to molar fraction 0.303) and then decrease with increasing amount of DMSO, while gelation was not observed in both pure water and pure DMSO solvents. They studied the effect called “cononsolvency”, in which poor solvent is formed by mixing of two good solvent. However, this effect was observed only at specific solvent compositions. They found that the mixture of DMSO and water is poorest at DMSO volume fraction of 0.66 (corresponding to DMSO molar fraction of 0.33). If the molar fraction is lower than this value, the added DMSO molecules form a 1:2 association complex with water molecules. The rest of free water molecules are possible to form hydrogen bonds with hydroxyl groups in PVA to solve PVA. The number of free water molecules decreases with increasing the fraction of DMSO. At molar fraction of DMSO 0.33, all DMSO molecules form the 1:2 association complexes with two molecules of water which theoretically result in no hydrogen bonds with PVA. The hydrogen bonds of DMSO with PVA could be formed with further increase of DMSO fraction so that mixture represent better solvent than the mixture with volume fraction of DMSO of 0.66.

Shi-Jie Hong *et al.* [158] in other work studied again both the gelation behaviour and phase separation of PVA/DMSO/water ternary system focusing on gelation rate of PVA at different concentration (dilute, semi-dilute and concentrated region). They found that phase separation due to spinodal decomposition competes with aggregate behaviour due to hydrodynamic screening of polymer chains occurring when the molar fraction of DMSO in solvent mixture is between 0.2-0.33. The effect of crystallization would outshine that of phase separation on gelation when the PVA concentration and DMSO molar fractions were increased. When the mixture contains small amount of DMSO (molar fraction ~ 0.07) the size of PVA coil is slightly extended in this system in comparison with dimension of PVA coil in pure water. It was suggested that addition of DMSO led to disruption of tetrahedral structure of water molecules at the position close to the polar sites (i.e. at S=O groups). As a result, the PVA-solvent affinity was a bit increased because of more free water molecules. This was confirmed for molar fraction of DMSO between 0.05-0.10 (corresponding to volume ratio near to 2/8 \sim 3/7) by the measurements of diffusion coefficient implying that PVA chains may become more extended at this mixture composition. Explanation for the poorest solvent quality of the co-solvent with DMSO molar fraction about 0.25-0.28 was found by formation of DMSO/(water)₃ complexes.

7.5 Surface Tension

The second most important parameter of inkjet inks is surface tension; the SFT measurements were carried out by Wilhelmy plate method, where the force acting on a vertically immersed plate is measured and then recalculated to surface tension.

Table 11 shows the determined surface tension of PVA solutions prepared in water/DMSO mixture at 25 °C.

Table 11. Surface tension of PVA solutions prepared in water/DMSO mixture at 25 °C.

Concentration of PVA solutions [wt%]	Surface tension [mN·m⁻¹]
	PVA in water/DMSO
1	46.36 ± 0.31
1.5	49.85 ± 0.24
2	51.95 ± 0.11
2.5	46.44 ± 0.26
3	46.76 ± 0.17
4	45.06 ± 0.13

Table 12 shows the determined surface tension of aqueous PVA solutions at same concentrations of polymer only at ambient temperature (28 °C). The SFT of pure solvents (distilled water and DMSO) and their mixture (2:1 v/v) were measured, too. These measurements were carried out due to comparison how much SFT decrease after addition of DMSO. As can be seen, DMSO additions decrease the original SFT of water as well as the surface tension of aqueous PVA solutions.

Table 12. Surface tension of aqueous PVA solutions as well as used solvents measured at laboratory temperature of 28 °C.

Samples	Surface tension [mN·m⁻¹]
Water	72.06 ± 0.04
Dimethyl sulfoxide (DMSO)	43.22 ± 0.04
Water/DMSO [2/1 v/v]	53.5 ± 0.6

Concentration of PVA solutions [wt%]	PVA in water
1	59.79 ± 0.16
1.5	58.60 ± 0.12
2	60.80 ± 0.19
2.5	59.14 ± 0.15
3	59.96 ± 0.19
4	60.41 ± 0.22

The temperature dependency of surface tension was tested only for samples of PVA prepared in mixture of solvents which showed to be worthy of choice for further ink development. The obtained results are shown in Figure 25. The surface

tension of solutions clearly decreased with increasing temperature generally by $10 \text{ mN}\cdot\text{m}^{-1}$ at each solution when the temperature was increased from 20 to 40 °C.

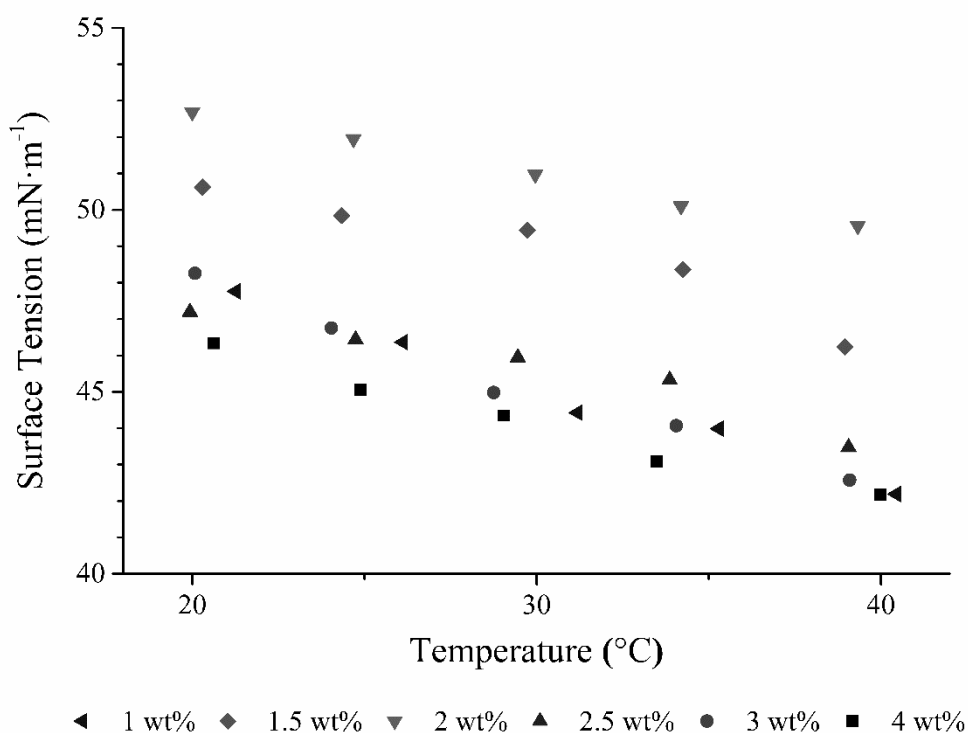


Figure 25. Temperature-concentration dependence of surface tension of prepared PVA solutions in water/DMSO mixture.

According to our experience, the achieved SFTs approached values low enough to allow formation and ejection of drops from printer head nozzles. Value of SFT may be further manipulated by printing temperature and improved by its proper setting.

On the other hand, no simple trend in concentration-dependence of SFT of PVA was observed and we consider the little variations between recorded curves as a result of experimental error. Theoretically, there should be a trend of decreasing SFT with increasing concentration of PVA however the effect is strongly manifested only at low concentrations of PVA below 0.1 wt% for water solutions where a decrease from cca $72 \text{ mN}\cdot\text{m}^{-1}$ (pure water) to cca $65 \text{ mN}\cdot\text{m}^{-1}$ was observed for fully hydrolysed PVA. Then, relatively flat dependence with a very small slope of SFT on PVA concentration was observed for higher concentrations, resembling thus the effect of surfactants. [120, 121] Therefore, we concluded that the contribution to variability of results expectable due to small steps in concentration of measured PVA solutions was overlaid by the statistically random variability of experimental conditions. The optimum recommended range of SFT for the inkjet printer used in this study is 28-42 mN/m. [39] SFT values higher

than $70 \text{ mN}\cdot\text{m}^{-1}$ usually limits the jetting process. [159] In this work, it means higher temperature is needed to improve the operating performance of printing process. On the other hand, vapour partial pressure increases with elevated temperatures which may cause processing complications. Therefore, the operating temperature $35 \text{ }^\circ\text{C}$ was chosen as the best guess. Values of SFT of PVA in water/DMSO recorded for 25 and $35 \text{ }^\circ\text{C}$ are listed in Table 11 and in Table 13.

7.6 Analysis of Prepared Solutions and Printing Process with the Aid of Dimensionless Numbers within the Framework of Mainstream Viscous Fluid Models

Suitability of prepared PVA solutions in water/DMSO mixture as inks for digital printing process was evaluated by group of dimensionless numbers based on performed measurements. The attention is paid to better understanding of liquid ejection, drop formation and printability of inks. Viscosity, SFT and density experimental input data are summarized in Table 13. The measurements were performed at $35 \text{ }^\circ\text{C}$ because this was the temperature used at the printing process.

Table 13. Experimental values of viscosity (η), SFT (σ) and density (ρ) of PVA in water/DMSO all obtained at 35°C . Density is expressed with 5 valid digits as this precision is given by the specification of the producer (Anton Paar.)

PVA concentration [wt%]	Viscosity [mPa·s]	Surface tension [mN·m⁻¹]	Density [kg·m⁻³]
1	3.74 ± 0.10	44.0 ± 0.4	1045.4
1.5	4.4 ± 0.3	48.4 ± 0.3	1046.0
2	5.07 ± 0.13	50.10 ± 0.12	1047.3
2.5	5.9 ± 0.2	45.3 ± 0.3	1048.2
3	6.2 ± 0.3	44.1 ± 0.2	1050.0
4	8.97 ± 0.17	43.09 ± 0.16	1053.0

The drops ejection rate was considered as the drop velocity (also drop impact velocity according to [160], in this case $5.4 \text{ m}\cdot\text{s}^{-1}$; it was determined by drop-watcher camera integrated in the printer machine (see next section “*Drop Ejection Analysis*”). The characteristic length (A) was derived from the nozzle geometry as its equivalent diameter by a general formula:

$$A = 4 \cdot \frac{S}{O} = 4 \cdot \frac{A^2}{4A} \quad (7.9)$$

where S is the area of nozzle, and O is the wetted perimeter of non-circular geometry which gives A as the size of a side of the square shaped nozzle orifice. [161]

Used nozzles have the side size around 21.5 μm . The size has been confirmed by electron microscopic analysis (images are not shown, 10 pL cartridges are commercially available by the supplier). The same value is used throughout the literature for this kind of equipment e.g. [115]. Calculated results are shown in Table 14.

Table 14. Calculated dimensionless criteria: the Reynolds number (Re), the Weber number (We), the Ohnesorge number (Oh), the Z-value and the Capillary number (Ca) of prepared solutions of PVA in water/DMSO mixture for 35 °C.

PVA concentration [wt%]	Re [-]	We [-]	Oh [-]	Z [-]	Ca [-]
1	32.4	14.9	0.12	8.4	0.46
1.5	27.5	13.6	0.13	7.5	0.49
2	24.0	13.1	0.15	6.6	0.55
2.5	20.6	14.5	0.19	5.4	0.71
3	19.7	14.9	0.20	5.1	0.76
4	13.6	15.3	0.29	3.5	1.12

It must be noted, that the characteristic length derived from the nozzle geometry holds precisely for initial stage of the liquid ejection only. Dimensionless numbers obtained in this way are said to be “global” and are used for overall assessment of the jet thread development dynamics. Thread thinning with the accent put on the word thinning is important part of this process which means that the characteristic length scale changes with time. The problem can be treated inversely and “local” critical radius of the fluid thread can be calculated under otherwise given material and processing characteristics. [103, 162] The former approach is used primarily throughout this work as we used a real yet laboratory size printer and did not develop a detailed experimental model study with high accuracy of image capture and analysis where the latter approach would be more beneficial. The printability ranges cited in this article have been developed by experiments and simulations using global criteria. Nevertheless, thought experiment of the type “what happens if” playing with the thread radius is discussed in order to speculate potential consequences of thinning in cases where the actual global dimensionless number value is assessed with respect to the critical transition. It is especially useful in situations when the global number value is close to the critical value. Finally, it must be noted that among the numbers used in this study the Capillary number depends not on A .

According to McKinley and Renardy [99], prepared solutions are all but one in the printability window lying very close to the border where the fluids become energy enough to form drops. *Oh* number is always bigger than 0.1. The solution with 4 wt% of PVA is below limit with *Re* value being too small. According to that, all solutions but the last one should be printable in the optimum single drop regime which is actually not the case (see analysis and discussions below). The original schematic diagram constructed by Derby [96] uses Weber and Reynolds numbers to mark the operating regime for stable drop formation in inkjet printing. According to that, the prepared solutions are in printability region too. However, satellite drop formation should be expected. Indeed, this was confirmed by observation as shown in other section below.

Assessment of fluid printability based on the *Z* number had been recently widely accepted. [97] All prepared solutions meet the range given originally by Reis & Derby [98]. Nevertheless, too dilute solutions (concentration 1.5 wt% and lower) could cause dipping of ink from the cartridge, opposite; more concentrated solutions (concentration 4 wt% and more) could led to clogging of nozzles. [115] The printability *Z*-range has been refined by Jang *et al.* [95] and again the 4 wt% PVA solution does not reach the lower printability limit ($Z = 4$). Jang's study was performed on similar system but without polymer addition. If the *Z* value is high (*Oh* number is close to 0.1), the jet will form a large number of satellite drops. Therefore, solutions with concentration range from 2 to 3 wt% seem to be most suitable for inkjet printing. The viscosity of 2 wt% PVA solution is relatively low and it has the biggest surface tension in comparison with other PVA solutions. On the other hand, 3 wt% concentration is closer to critical concentration hence 2.5 wt % PVA solution scores as the best candidate for printing.

Although all above discussed still apply, the printability cannot be defined either only by material properties of the ink or by *Z*-value alone yet including the nozzle geometry. Kim and Baek [92] revolutionized the analytical framework for the printing process and employed the whole triad of material–tool–process parameters which must be taken into account to describe drop formation dynamics and printability range in DOD printing. They used *Ca* and *We* numbers to map various regimes that may occur during printing with respect to drop formation and other flow instabilities. The Weber number (*We*) scales with square of the drop velocity (v^2) which is a dynamic process parameter, then with the ratio of the fluid density and its surface tension (ρ/σ) which are the material parameters and finally with the characteristic length (*A*) which is a tool (nozzle geometry) related parameter. The Capillary number scales with drop velocity (*v*) and with the ratio between the fluid viscosity and its surface tension (η/σ) while it does not include the characteristic length. Figure 26 shows extended Kim and Baek's plot of *Ca* vs. *We*. The left part of the graph demonstrates original Kim and Baek's division of the space given by the two dimensionless parameters into five different regions corresponding to possible regimes of printing process. Description of their original graph can be found in the chapter 3.3.2. *Dimensionless Criteria*.

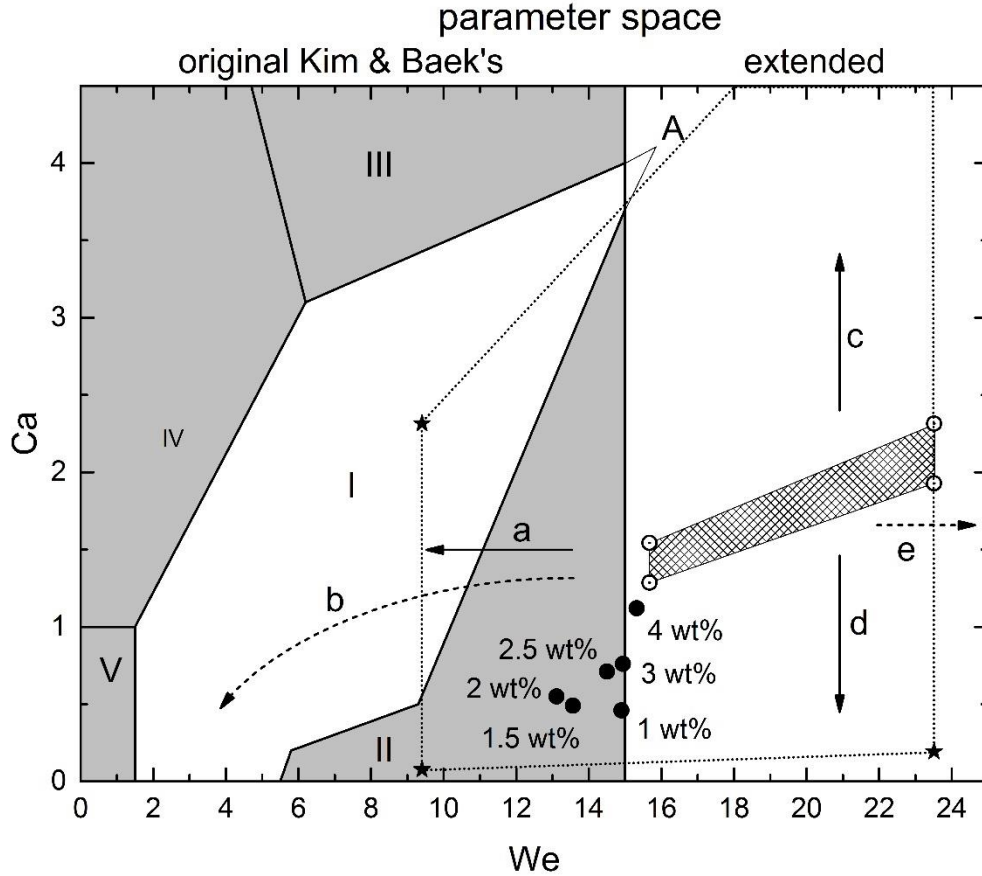


Figure 26. Capillary-Weber diagram showing the position of prepared PVA solution in water/DMSO.

The parameter space had to be extended in the We number axis direction in order to analyse our case, however a general lesson can be taken from this too. First, the area of the regime I was completed by extrapolation of its borderlines to the point A. In order to demonstrate the scale of the problem, the processing window of the used Dimatix material printer [39] was plotted into the graph with the use of typical values for investigated inks to draw generalized results. It must be noted that the characteristic length A cannot be changed as it is simply a part of the printer cartridge nozzles design. The recommendation for operational parameters for the inkjet printer equipped with the nominal 10 pL printing head used in this study is to keep the ink fluid viscosity in the range 10-12 mPa·s and its surface tension in range 28-42 mN·m⁻¹. The printer producer suggest using drop velocity in the range 7-9 m/s as the first guess [39], however, according to literature and experience in this study, velocities about 6 m/s are commonly used. [41, 163, 164] The obtained value of $v = 5.4$ m/s was therefore used in following calculation. Density about 1 g/cm³ can be considered as a good approximation for the whole class of polymer solution based inks and many other printable fluids. A rounded value 1.05 g/cm³ for ρ is taken from our examples. The processing window calculated on the base of these parameters is marked with the patterned tetragonal area having circles with a central dot in the points. It is obvious, that

the area is quite small and far from the optimum printability regime I. To demonstrate effect of material parameters on the printer processing window, range of viscosity and surface tension was extended up to maximum acceptable values for printing with Fujifilm Dimatix materials printer DMP-2800 Series, i.e. viscosity range from 1 mPa·s for water-like fluids up to 30 mPa·s which is declared as the highest viable for the printer. Similarly, surface tension about 70 mN·m⁻¹ represents the upper limit for printing with given machine. [159] This value is close to that of water without any additives and normally would be smaller for solution based polymer inks. On the other hand, lower limit 28 mN/m was not changed, as fluids with lower surface tension could leak from the nozzles resulting into dripping. The extremely extended range is shown in the Figure 26 as the region marked by asterisk symbols connected with a short dot line. The fourth asterisk symbol is out of the graph range (coordinates We : 23.51, Ca : 5.79) and it is not necessary to be shown. Full line arrows indicate the directions of the processing window area extension. Effect of increased surface tension is marked by arrows **a** and **d** as both We and Ca numbers scales with $1/\sigma$. A decrease of surface tension was not demonstrated because the lower limit 28 mN/m seems to hold for almost all cases, moreover it would increase both numbers in a wrong way, i.e. retreat from the printability regime I. Increase of viscosity extends the area upwards in the direction of arrow **c** as only $Ca \sim \eta$. On the other hand, a decrease of viscosity characteristic for dilute solutions and dispersions or for the use of surfactants causes extension of the processing windows downwards in the direction of the arrow **d**. In other words, the large area marked by asterisks and short dot line shows processing window based approximately on extreme parameters of water used as the solvent with the assumption that the surface tension of a water solution will not be adjusted below 28 mN/m.

The last material parameter to be discussed is the density. As $We \sim \rho$, increase of density causes shift of the whole processing window to the right side as indicated by arrow **e** (short dash line style). It must be stressed out, that increase of density multiplies inertial forces (actually increases kinetic energy term, $\rho \cdot v^2$) e.g. doubling the density doubles the Weber number causing considerable shift of the whole processing window away from the printability regime I, which can be a quite common situation for dense dispersions of nanoparticles that are often made from metals (silver is a good example) or oxides (e.g. ITO, TiO₂ or many other). Typical density of commercially available suspensions of this kind is about 1.5 g/cm³. Halogenated solvents can be given as another example of dense liquids. Thus, the role of density can be an important issue to be dealt with.

Thus, it seems, the most important parameter change, which can shift the processing window towards the regime I area, is the decrease of drop velocity, which is also the only one considered processing parameter. Since $Ca \sim v$ and $We \sim v^2$, the Weber number decreases much faster than the Capillary number and the processing window area is shifted to the left and bottom side of the graph in direction of arrow **b** (short dash line style, the shape indicates parabolic

dependence). If the drop velocity decreases twice, We decreases four times while Ca decreases only two times, however velocities in the range 2-3 m/s are hard to be achieved with the used printer for low viscosity fluids. Moreover, the slower is the velocity the lower is the jetting frequency and generally slower printing process. Hence, the use of velocities as high as possible is preferred until the printability regime applies.

Positions of tested solutions at the used velocity for the given printing nozzle size in the Ca versus We graph are marked by black full circles in Figure 26 and labelled by the PVA concentration. It can be seen that they are quite far from the Dimatix printer optimum, but they still fall into the extended printability range of the printer and they are in the area of the printing regime II. As analysed in more detail in the next section, satellite formation was observed but, surprisingly, obtained good printouts due to the merging of satellite with the main drop. The PVA solution with the concentration 2.5 wt% occupies central position within the cloud of experimental points far from all extremes which confirms its choice as the best candidate for printing of testing motives.

The free surface flows of Newtonian liquids can be characterized by the Reynolds and the Capillary numbers too. According to McKinley [103] and Clasen [162], Re can be plotted against Ca with advantage. The graph is shown in Figure 27. Both, Re and Ca scale linearly with the velocity thus the slope of straight lines going through the graph origin (zero) is independent on imposed velocity and is given by inverse square of the Ohnesorge number (Oh^{-2}) which is a number that depends on geometry and fluid properties alone. Additionally, the Oh^{-2} is nothing else but the Laplace number (La); also known as the Suratman number (Su). Hence a series of isolines for constant (Oh^{-2}) value resembles fan ribs.

$$La = Oh^{-2} = \frac{Re}{Ca} = \frac{\rho \cdot \sigma \cdot A}{\eta^2} \quad (7.10)$$

The graph usefully visualizes the trajectories in this plane (by the short dot lines), that indicate relative effects of the velocity change under given fluid properties and characteristic length. For example, if v is doubled the distance of the corresponding point from the origin increases 2 times in the trajectory direction marked by the arrow **a** (keeping all other parameters constant). Similarly, if the velocity decreases twice the given point shifts along the line towards the graph origin in the direction marked by the arrow **b** and its distance from the origin is halved. This can be helpful in case of processing parameters optimization. Moreover, a set of contour lines along which the We number has constant value was added to the plot. It is possible because:

$$Re = \frac{We}{Ca} \quad (7.11)$$

which gives a set of simple hyperbolic isolines. Doubling the velocity v changes the value of We number value by factor of 4. On the contrary, halving the velocity v changes the value of We by factor of $\frac{1}{4}$. Such plot involves all material (η , σ , ρ), process (v) and tool (A) parameters into one complex graphic representation which enables not only evaluation of printing process of tested solution with specific nozzle diameter, but also a reconsideration of all above discussed printability limits.

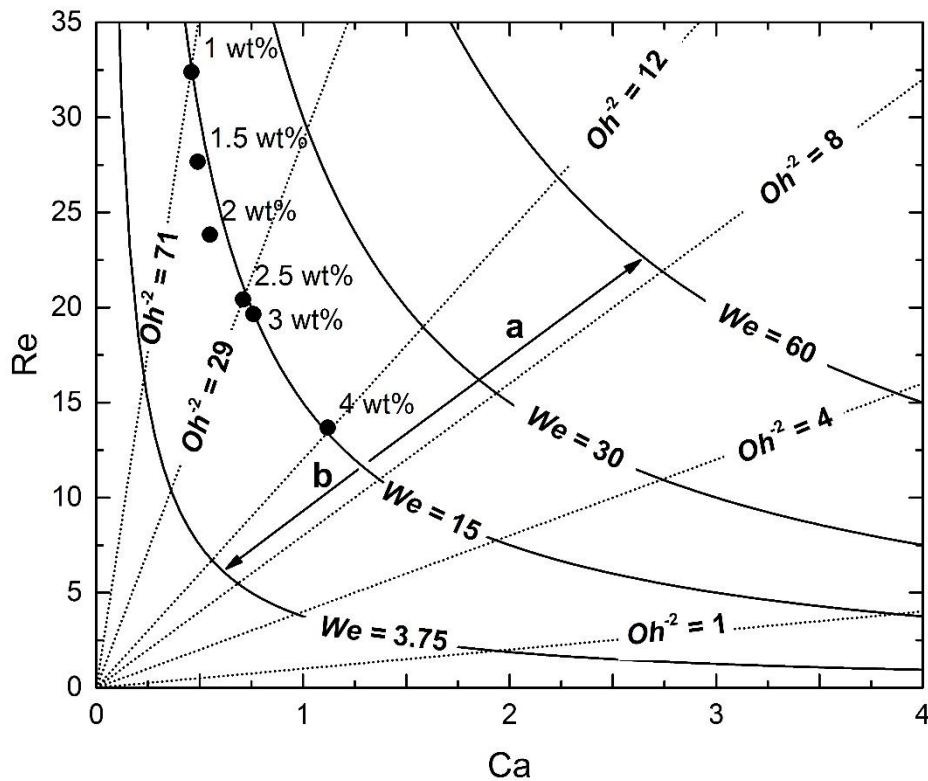


Figure 27. Reynolds-Capillary number diagram 1

The points representing experimental printing of tested PVA solutions at the velocity 5.4 m/s through the nozzle with characteristic size 21.5 μm are shown in the graph (Figure 27) by full black circles labelled by PVA solution concentration. It can be seen, that they do not form a chaotic cloud but they are aligned along the contour line with $We = 15$. They do not differ much in density and surface tension as can be expected due to their very simple composition variation. While keeping the value of We constant, the value of Oh^{-2} varied significantly from cca 12 for the most concentrated solution to 71 for the 1 wt% PVA solution. The best candidate (2.5 wt% PVA solution) was found at the moderate value of $Oh^{-2} = 29$.

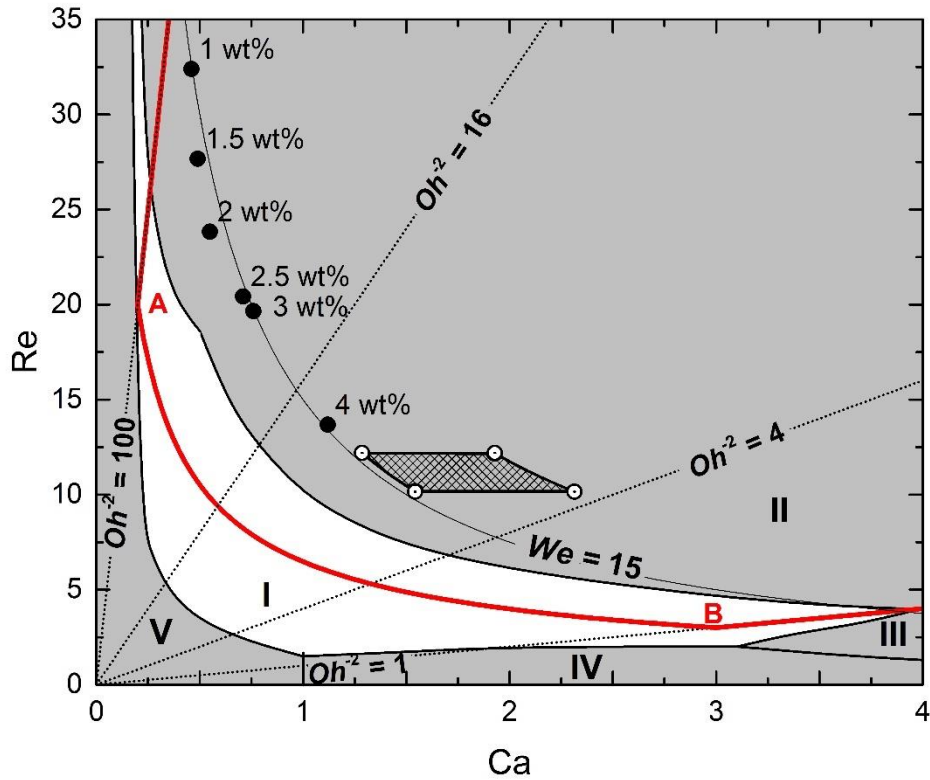


Figure 28. Reynolds-Capillary number diagram 2.

To draw a generalized view on the printing process of inks, the Kim & Baek's map of printing regimes was replotted into the space given by Re vs. Ca coordinates. Again, it is possible because $Re = We/Ca$. The graph is shown in Figure 28. Also here, the printability region I is the white area surrounded by other fields (coloured gray) corresponding to the other regimes, using the same notation by roman numerals as in the original context. The number Oh^2 scales with $1/\eta^2$, hence viscous threads formation is typical for its values lower than 1 and indeed, the areas for regimes III and IV can be found stuck close to the x-axis. On the other hand, the regime V that can be found at low Ca and We values close to the origin of the Kim & Baek's graph is characterized by the domination of surface tensional forces over both viscous and inertial forces thus the fluid fails to eject. This can be true for the region with small Ca and small Re too. Close to the transition line between regime I and V but still at the side where surface tension forces do not prevail there must be region of so called dripping which is spontaneous leaking and dropping off of the fluid drops from the printing nozzle. Another situation may occur, if the value of Re increases while Ca remains low, which must result into inviscid flow for high values of Re at low Ca that was not possible to see in the original Ca vs. We plot. The transition border line between these two kinds of behaviour cannot be plotted simply. It can be noted that drop formation is a free-boundary problem which means that any flow with Reynolds

number >1 will have significant inertial effects in addition to viscous effects. On the other hand, high Re in inviscid fluid means high fluid velocity. The Ca number contains the fluid velocity in the nominator as well while the ratio σ/η representing so called capillary velocity is in the denominator. Therefore, the capillary velocity must be very high to keep the value of Ca number low which requires low viscosity and high surface tension.

The regime II area occupies the largest part of the graph. It is a sector spanning to right upper corner of the graph. It can be said in other words, that the transition from regime I to regime II is just that, what happens if the initially well-setup jetting velocity is increased beyond the printability limit and exceeds the critical value of v for given Oh^{-2} (cross-section of the area I upper border and the constant Oh^{-2} trajectory).

The graph in Figure 28 can be used for re-analysis of previous printability regime assessment rules based on Z number easily because the square of Z is actually Oh^{-2} . Therefore, Fromm's original suggestion that stable drop generation occur when $Z > 2$ and that for a given pressure pulse the drop volume will increase with increasing value of Z as well [8] is simply represented by the sector of the Re vs. Ca first quadrant for $Oh^{-2} \geq 4$. The difference from Kim and Baek [92] is evident. Reis and Derby [98] found that stable drop formation occur when Z value is between 1 and 10 which can be visualized here as the sector between lines for $1 \leq Oh^{-2} \leq 100$ which seems to overlap with Kim and Baek's prediction to a large extent, although it does not imply regimes II and V. The printability range defined by Jang *et al.* [95] by Z values into following form $4 < Z < 14$ shows the worst agreement with the Kim and Baek's I regime region. The sector given by $16 \leq Oh^{-2} \leq 196$ covers less than 1/3 of the white area in the graph.

Printability region marked by McKinley and Renardy [99] showing the operating regime for stable operation of DOD inkjet printing by using the coordinate system defined by the Ohnesorge and Reynolds number can be replotted into the graph in Figure 28, too. Their original borderlines given by Oh values 0.1 and 1 can be easily marked as the sector limited by the Oh^{-2} lines 100 and 1. The low Re limit in their original $\log Oh$ vs. $\log Re$ space was replotted into prepared graph by the curve between the points A and B. The upper Re limit is beyond the scale of the graph. Hence, the overlap with the Kim and Baek's I regime region is only partial and the transition line is shifted to higher fluid velocities although it has the right hyperbolic shape. Moreover, the Kim and Baek's regime II area is included into the printability region remaining thus unresolved by McKinley and Renardy's approach.

If one inspects the Reynolds-capillary diagram in Figure 28 carefully once again, it can be noticed, that the optimum printability area has a banana-like shape that could be roughly delimited just by two properly selected We -isolines. In other words, it means that achievement of the printability optimum regime does not virtually depend on viscosity at all, at least over a very large range. This is actually contra-intuitive as viscosity is considered as the first and foremost

important parameter of any liquid and one would guess the viscosity is the main parameter of the ink considered all previous analysis and efforts spent to the description of the liquid flows during printing process we were able to find. However, if we remind the definition of good printability when “a single drop is formed either directly without second pinch-off or the satellite drop merges with the main drop within its travel distance less than $20A$ forming thus a single drop” we can realize that there is nothing said directly about viscosity but it means that there must be a mechanism causing either such cohesion of the ejected liquid volume, that it forms only one drop, or that the mechanism causing the break up is too weak so the lack of the break up is experienced or that there is a mechanism (possibly of the same cohesive physical nature) which causes acceleration of satellite drop such that it can catch up the main drop and merge with it forming one final drop that travels to the place where the ink should be delivered. Indeed, there is one material property in We number related to the cohesion (and break up too) – in other words surface relaxation – which is the surface tension σ . Hence, the relaxation time related to surface perturbation governs the process. Next, it can be seen on the processing window recommended for used Dimatix printer as well as on our experimental points that it is simply possible to achieve good printability even beyond the limit estimated purely by the We numbers. Therefore, a second cause besides the surface energy must produce this effect and the only plausible is the elastic energy. These phenomena are investigated in next sections.

7.7 Drop Ejection Analysis

The fluid ejection process is controlled by the so called ‘pulse waveform’ – a programmed voltage pulse that drives the piezoelectric system in the cartridge printing head nozzles. There are 16 nozzles in the printing head and each one can be independently programmed to achieve optimum jetting. The waveform consists of several stages that are defined by slew rate, duration, and magnitude (level) of pulse voltage. The particular segments need to be carefully adjusted so that uniform drops velocity to be achieved.

Drop formation and ejection was analysed in the next step. A good drop ejection performance can be obtained by using an appropriate waveform. It was proposed a suitable waveform for prepared polymer solution. The proposed waveform is showed in Figure 29. As can be seen, it is the unipolar waveform.

The jetting voltage and other setting of cartridge are shown in Figure 30. It must be notice, that showed settings have only informative character, the actual parameters need to be almost always adjusted with respect to prepared ink. Other settings include, for example, selection of the nozzles using for printing, or cleaning cycles to ensure freshness of ink, or substrate temperature.

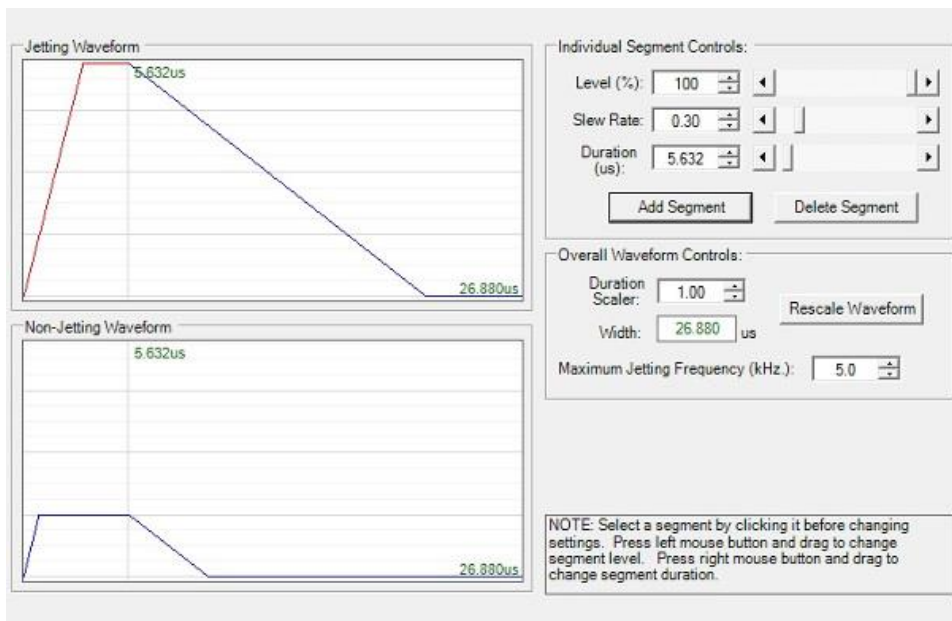


Figure 29. The waveform used for inkjet printing of 2.5 wt% PVA solution in water/DMSO.

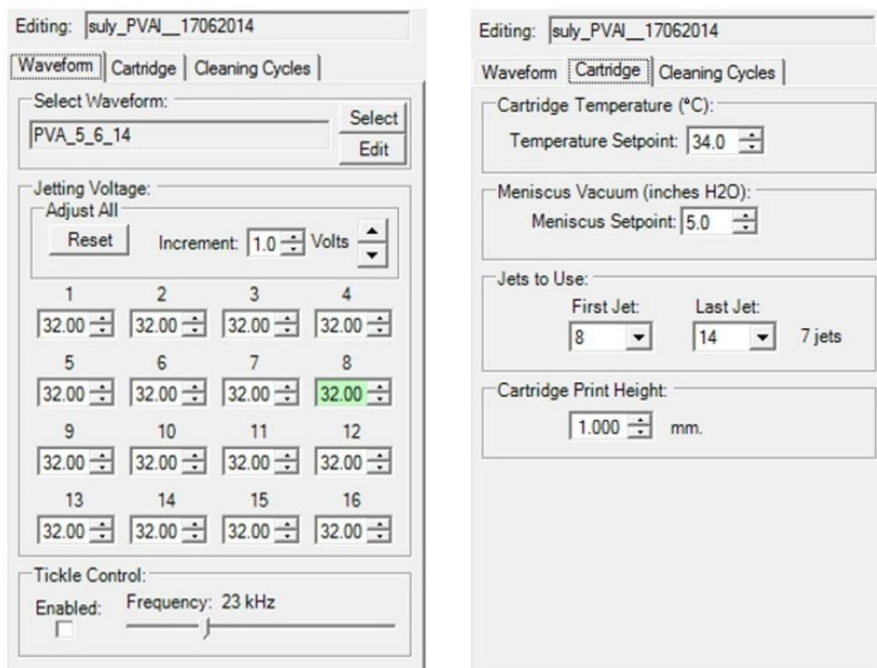


Figure 30. Cartridge settings for inkjet printing of 2.5 wt% PVA solution in water/DMSO.

Distance from nozzle	0 μm					
	100 μm					
Time	200 μm					
	300 μm					
Distance from nozzle	400 μm					
	0 μm					
Time	100 μm	6 μs	11 μs	20 μs	25 μs	31 μs
	200 μm					
Distance from nozzle	300 μm					
	400 μm					
Time	0 μm	35 μs	41 μs	49 μs	56 μs	63 μs
	100 μm					
Distance from nozzle	200 μm					
	300 μm					
Time	400 μm					
	500 μm					
Distance from nozzle	600 μm					
	700 μm					
Time	800 μm	118 μs	137 μs	157 μs	176 μs	
	900 μm					
Distance from nozzle	1000 μm					

Figure 31. Drop formation and ejection of 2.5 wt% of PVA in water/DMSO mixture, firing (jetting) voltage 34 V, cartridge temperature 35 °C.

Figure 31 shows the set of images capturing the drop formation and ejection for the PVA solution with 2.5 wt% concentration in the mixture water/DMSO. A drop velocity about 5.4 m/s was found to be low enough to assure the regime-I-like printability characteristics for our ink system and printing machine. As can be seen, a satellite drop is formed (around 41 μs) but during flight, this satellite drop is joined with the main drop (first touch around 56 μs), and a single drop (fully merged at 63 μs) then travels until delivered onto the substrate surface. Although break up occurred, the created satellite drop recombine with the main drop over the travel distance range from 350 μm (joining of drops) to 400 μm (achievement of full spherical shape of merged drop) which is in the range of 20A as defined by Kim and Baek [92] for the optimum printability regime I. The recombination process of drops was obtained by fine adjusting of the pulse waveform. The jetting conditions for process depicted in Figure 31 included a cartridge temperature 35 °C, and jetting voltage of 34 V at nozzle. Lower pulse voltage led to deflection of drops. However, the drop velocity control is not always ideal and undergoes small

variations between individual nozzles on one cartridge; therefore, the velocity as well as drops formation are often tailored by adjusting of jetting voltage at each nozzle or/and by changing of the segment level of the waveform. Based on the captured images the overall drop velocity was evaluated, in this case around $5.4 \text{ m}\cdot\text{s}^{-1}$ (as can be seen in Figure 32). This is the velocity that was used for calculation of dimensionless numbers throughout this work.

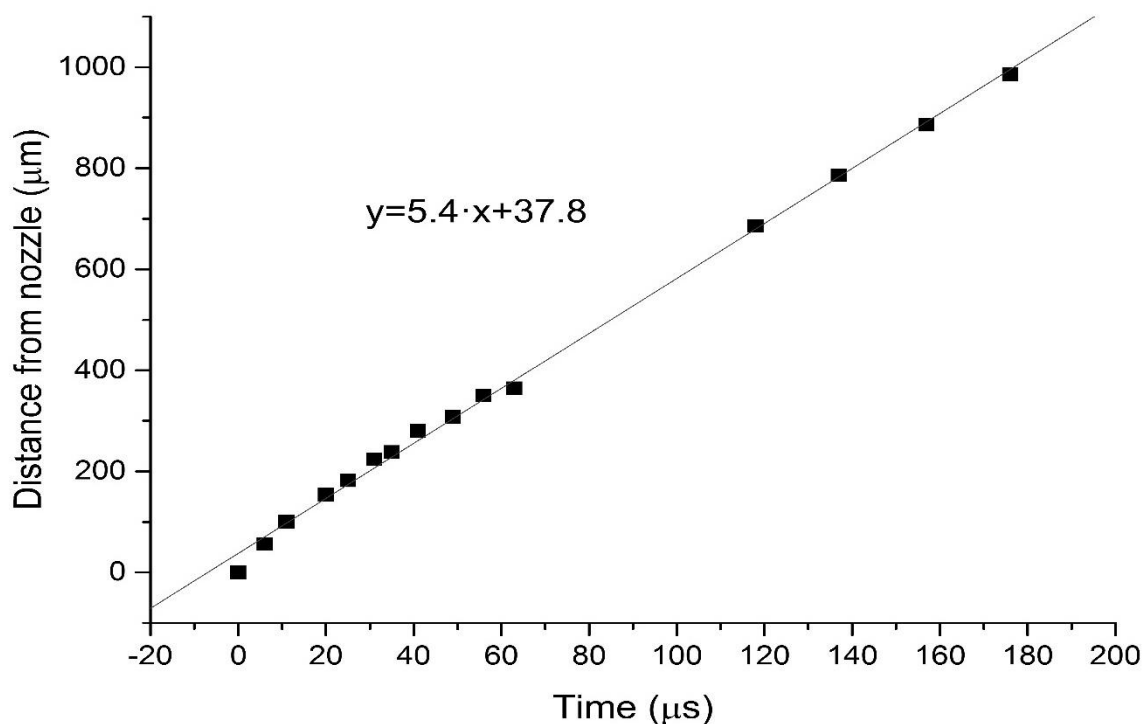


Figure 32. Relationship between drop distance from nozzle against time in the case of 2.5 wt% PVA solution prepared in water/DMSO.

Dong *et al.* [94] studied the conditions of drops recombination. This process of single drop formation could be considered as an improvement from industrial perspective in comparison with situation, in which the merge of primary and satellites drops do not occurred. They demonstrated that the velocity of satellite drops should be higher than the velocity of primary drops if the recombination process should be occurred. Many other authors investigated the evolution and break up behaviour of drops. For example, He *et al.* [165] studied an effect of drop velocity under different time gaps and printing voltage. Moreover, they also studied the influence of substrate temperature and drop spacing on the morphology of printed polycaprolactone patterns. Tsai and Hwang [166] performed the study focused on drop formation of alcohol and ethylene glycol which have different viscosities and surface tension coefficients. The liquids were tested at different conditions with emphasis on pulse voltage. They observed that formation of single drop or drops recombination occurred directly only in defined range of pulse voltage. If this voltage is higher the velocity of main drops is too

high which avoid to satellite to catch it up. Other approach includes the simulation of printing process under different condition. Wu and Lin [167] present a numerical analysis of a piezoelectric actuated drop generator. They showed the various drop formations by applying a pressure waveform (at different parameters such as positive and negative pressure amplitudes, operating period and acceleration of the positive pressure). They presented that a longer tail length, faster drop velocity and larger drop volume could be observed when (I) the amplitude of positive pressure is increasing, (II) acceleration of the positive pressure is increasing, and (III) the pressure pulse operation time is increasing. On the other hand, increasing the amplitude of the negative pressure could result in shorter tail length, shorter break up time and smaller drop volume.

Good printability was achieved in this work by fine tuning of process parameters (i.e. the pulse waveform programming) although the operation points are not inside of the best printing regime area in the Kim & Baek's graph. The best results were obtained for 2.5 wt%. The discrepancy between prediction and observed behaviour can be explained by introduction of an effect that was not taken into account in the Kim & Baek's analysis, since their work holds perfectly for viscous only fluids. There must be a factor that causes relative increase of the satellite drop velocity or decelerate the main drop so that they can recombine. Since the air drag force decelerates smaller drops more than bigger ones, it works against observed phenomena of drops merging. Indeed, it was assessed as having relatively low importance in the problem in general. [94] Moreover, presented calculations of energy balance indicate that the energy loss caused by air drag under turbulent condition at travelling velocity of the drop being about $5 \text{ m}\cdot\text{s}^{-1}$ would be about $4 \times 10^{-25} \text{ J}$ on the distance of $100 \text{ }\mu\text{m}$ taking into account classical Newtonian formula for spherical objects.

$$F_{AD} = \frac{1}{2} \cdot \rho_{Air} \cdot v^2 \cdot C_{FD} \cdot S \quad (7.12)$$

where F_{AD} is the air drag force, ρ_{Air} is the density of air (1.15 kg/m^3), v is the velocity of the drop, C_{FD} is the fluid drag coefficient, and S is the cross-sectional area. In our case of a sphere, C_{FD} equals to 0.5 and the radius of drop is about $15 \text{ }\mu\text{m}$. The deceleration of the drop was not taken into account and air drag force was considered as constant for the sake of simplicity. The energy loss on the $100 \text{ }\mu\text{m}$ trajectory is then calculated for linear motion as F_{AD} multiplied by traveling distance. The kinetic energy of the same drop estimated from the traveling velocity ($5.4 \text{ m}\cdot\text{s}^{-1}$) and its mass is about 220 pJ which is incomparably higher value than the estimated losses due to air drag.

The importance of gravity was found negligible in previous studies too. The Bond number (Bo) which correlates gravity and capillary effects, is defined as [92, 168]

$$Bo = \frac{\rho \cdot g \cdot A^2}{\sigma} \quad (7.13)$$

Using a typical ink density $\rho = 1.05 \text{ g/cm}^3$, the given characteristic length $A = 21.5 \text{ }\mu\text{m}$, a rounded value of standard gravity $g = 9.807 \text{ m/s}^2$ and the surface tension $\sigma = 28 \text{ mN}\cdot\text{m}^{-1}$ as the most extreme case, the formula yields $Bo = 1.70 \times 10^{-4}$. Indeed, this extremely small value confirms gravity effects to be irrelevant in this work. Eventual decrease of the characteristic length during fluid thread thinning would even decrease the local Bo value progressively as it scales with the square of the thread diameter. From another point of view, the characteristic length is about 1.65 mm for the Bo value 1 which implies that gravity effects do not play any role in microfluid technology such as our inkjet process. From another point of view, the importance of the effect of gravity can be judged on the base of energy balance calculation. The energy gain of one typical drop (with the volume 15 pL hence weight of about 15 ng) due to the free fall acceleration on the distance of 100 μm can be theoretically estimated about $1.5 \times 10^{-14} \text{ J}$, which is four orders of magnitude lower value than the kinetic energy of the drop (220 pJ). Moreover, all bodies fall freely with the same acceleration due to gravity. Hence, the gravity was not taken into account in performed physical analysis of the problem and energy balance calculations.

Surface tension is the only form of energy that works against the purely Newtonian fluid thread prolongation playing in some aspects the role of a spring-like element (cohesion energy). On the other hand, it is engaged in development of instabilities that promotes thread break up through generation of capillary pressure. Nevertheless, any possible contracting effect of the surface tension is indirect as it is not a true elastic element working through the material volume but its effect arises from the surface area minimization. If we step out from the field of Newtonian fluids into the group viscoelastic liquids, another reason for observed catch up and merging of the satellite with the main drop can be found in energy storage and its release due to partial elastic property of the material. The force accelerating liquid in the tail is exerted through the volume due to elasticity of the liquid. Among possible approaches to the physical analysis of the problem, i.e. kinematic, dynamic and energetic, (i) the energy balance is a general description using simplest calculations taking boundary conditions into account, (ii) dynamics goes most deeply into the physical understanding of the problem and requires identification and quantitative description of forces and momentums which is accompanied by quite demanding calculations and (iii) kinematics requires comprehensive (total) quantitative description of actual velocities, accelerations and trajectories all moving bodies using most demanding voluminous mathematical description. Although the integrated drop-watch camera quality (image capture frequency and resolution) is not such to assure similar information depth as in other studies of drop formation [94] it still allows to analyse the problem from the point of energy transformations, to some extent at least at the energy approach level.

The key condition for good printing is that the satellite drop (once formed) must catch up the main drop and merge with it so the ink is precisely delivered to the

required place in a single drop only. The concept of surface energy and elastic energy acting in the tailed drop is shown in Figure 33. According to the images captured by the drop-watch camera, the shape of tailed drop can be simplified and replaced by a sphere and capped cylinder. It is obvious, that no external force is exerted on the liquid volume after pinch-off (considering gravity and air drag negligible). Therefore, the centre of gravity of the whole liquid volume moves uniformly linear as seen by an external observer while different parts of the liquid volume may move relatively to each other (and oscillate around the common centre of gravity). Surface energy and elastic energy may contribute to the liquid flow and shape changes. The role of surface energy is conceptualised in the left part of the Figure 33. Surface tension is transferred through the zone of the liquid surface which creates border between the upper tail and lower main drop. The surface tension induces bigger internal pressure in the tail than in the main drop because the tail has smaller radius of curvature than the main drop, hence the acceleration and flow of the liquid from the tail towards the main drop is induced. The process starts from the free end of the tail where the surface has the shape of spherical cap hence is curved in two perpendicular directions. The right part of the schematic in the Figure 33 analyses the mode of elastic energy action. Elastic forces working through the whole liquid volume can be conceptualised as a spring between the centres of mass of the two liquid volume compartments while the frame of reference is attached to the common centre of mass of the whole liquid volume. If we adopt the illustration from the Figure 33 literally, the spring is loaded during liquid ejection and prolongation of the thread and released by the pinch-off. Then the liquid in the upper volume part (long tail) accelerates (a_S) towards the main drop due to the elastic force F_S which causes shortening of the tail and movement of the centre of gravity of the satellite M_S towards the centre of gravity of the main drop M_{MD} . The same size force F_{MD} of opposite direction accelerates the main drop too, but due to much larger mass of the drop in comparison with the tail, the main drop has much larger inertia and therefore the acceleration a_{MD} is much smaller and the relative displacement of the main drop towards the tail is much smaller too. It must be noted, that any effect of a_{MD} is manifested as deceleration of the main drop observable in the frame of reference of an external observer. The elastic forces can act between the liquid volume parts only when they are in contact and the interaction between these two volumes of liquid stops at the break up. The same holds for the surface tension effect too.

After the break up, no forces of either kind can act between the two mutually liberated volume parts any more until they merge again. Remaining excess of surface and elastic energy may then contribute to the further contraction of the dumbbell satellite and/or oscillations of drops, however this is beyond the scope and capability of instrumentation used in this analysis. On the other hand, the momentum of the liquid in the tail is increased by the contribution of either of the two forces or by both of them. The momentum increase of the tail liquid volume causes that it attains higher velocity than the main drop and it continues after

forming of the satellite drop with higher velocity than the main drop after break up and therefore the satellite is able to catch up the main drop. The contribution of main drop deceleration is much less manifested, although it consumed equal part of elastic energy as it was invested into the velocity increase of the satellite.

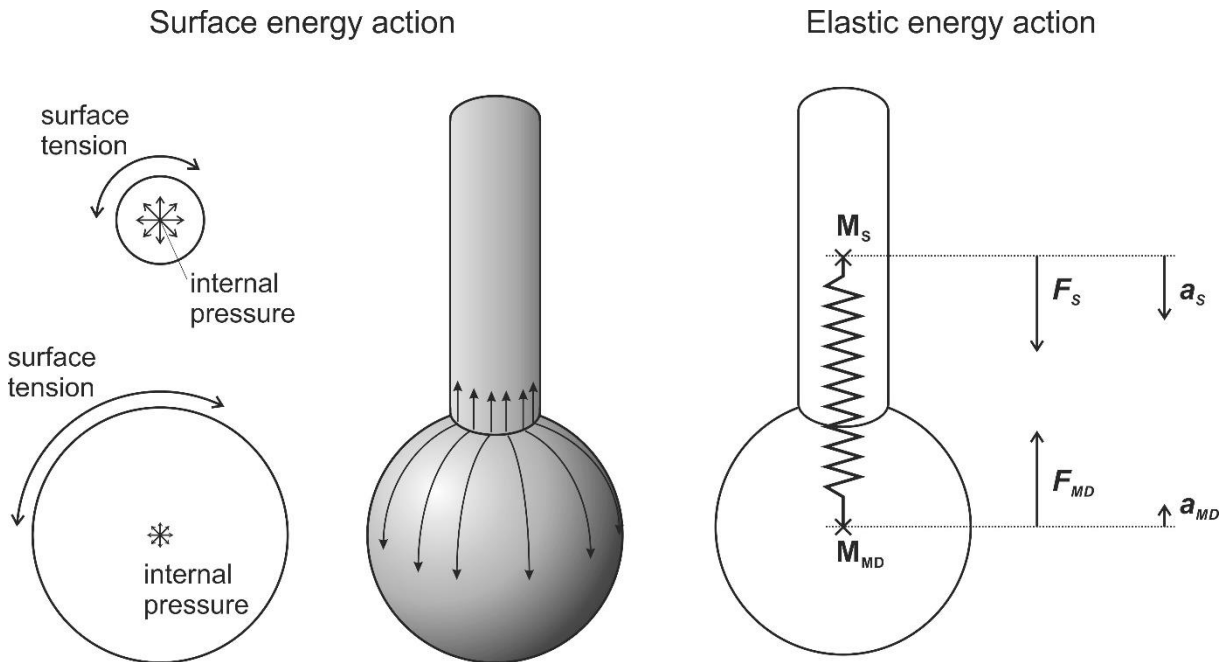


Figure 33. The analysis of surface energy and elastic energy

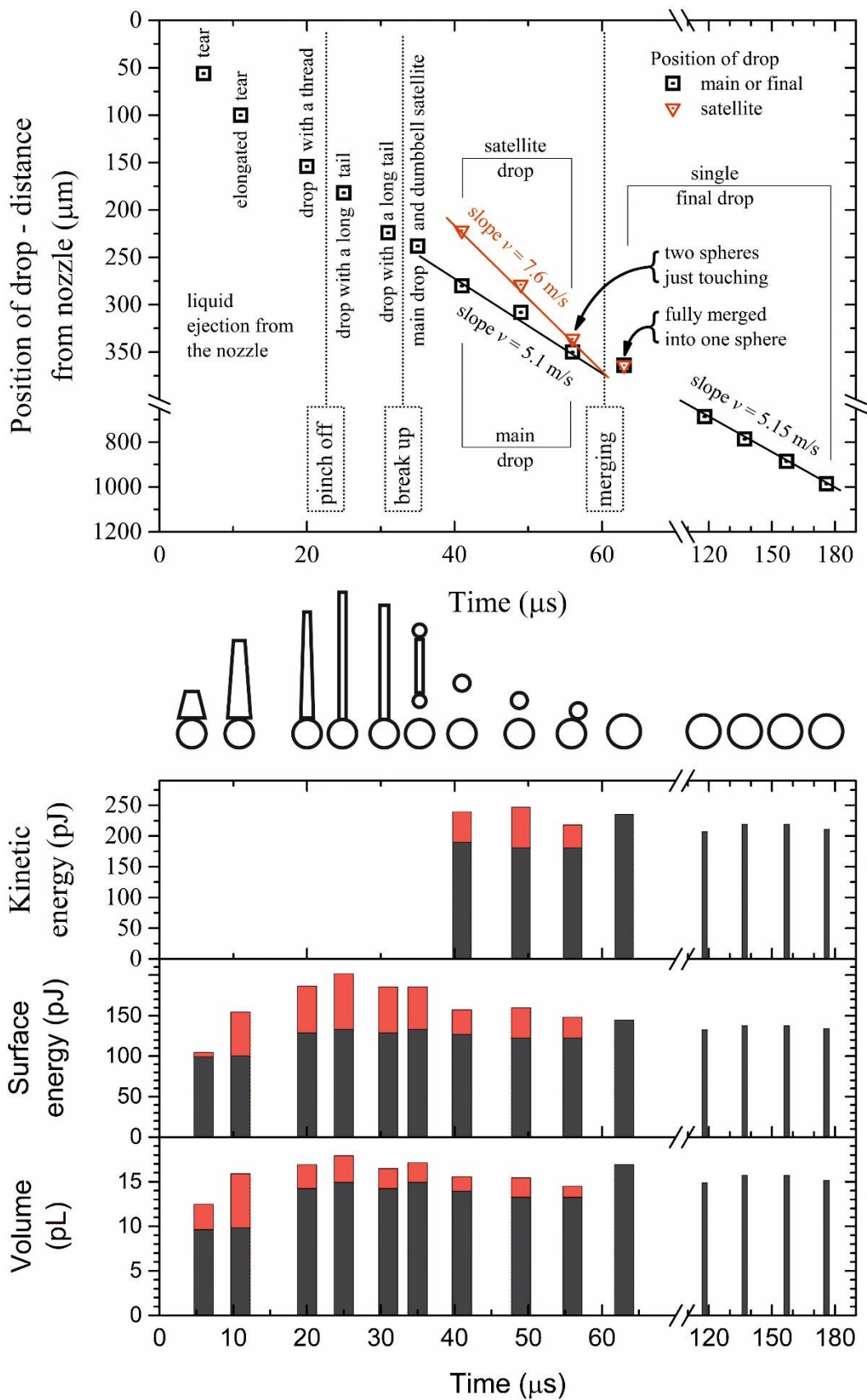


Figure 34. Analysis of drop ejection and formation based on captured images (in Figure 31). Upper graph shows the position of the center of the main or final drop (open square with central dot) and satellite drop (open triangle with central dot) once formed. The middle gallery shows schematics of simplified geometric shapes used for image analysis.

Lower graph: stacked bars show the volume and surface energy for the main drop (evaluated as a sphere, represented by grey bar) and its tail, thread, dumbbell or satellite (represented by red bar). The final drop property is than represented by the grey bar only after merging (from 63 μ s). The kinetic energy is shown for main (grey bar) and satellite drop (from 41 μ s, i.e. after its formation), the energy of the final drop is represented by the gray bar only after 63 μ s. The time x-axis is common for both graphs.

Figure 34 summarizes analysis of drop generation images shown in Figure 31. It must be noted that a single set of images was analysed, but a typical drop development and travel event was recorded. The upper graph panel describes position of the ejected liquid volume as the travelling distance of the spherical part centre (drop) from the nozzle. In order to do this and other quantifications, the real shapes of the liquid were replaced by simple geometric bodies as indicated in the middle part of the Figure 34. Sphere for drop - represented by a circle in 2D, truncated frustum represented by the trapezoid, thread or tail by a cylinder represented by the tall rectangle, and contracting thread virtually replaced by a dumbbell consisting from two spheres joined by a cylindrical rod, i.e. two circles and a rectangle in 2D. This allowed calculating volume and surface of all observed objects. However, due to relatively poor quality of images, the estimation error is about 10-15%. Due to error propagation, it can be seen, that largest variance is present in the volume analysis as the volume depends on third power of the diameter (linear dimension). Actually, the total volume should be constant after ejection of all liquid. Nevertheless, the first three bars present fairly the increase in volume of the ejected liquid until pinch-off between 20 and 25 μ s. It can be seen, that the main drop is formed first - shape of the tear, then the tail hanging on the nozzle prolongs into a thread and increases in volume during ejection which is then followed by thinning of the tail prior pinch-off when the liquid must flow from the tail into the main drop during thread formation as seen from the decrease of the tear-tail to thread volume and increase of the drop volume. The total volume of the ejected liquid is about 15.5 pL. It can be seen, that the actual value varies around this average, regardless to whether it is calculated for two geometrical bodies or for single sphere after merging of drops at about 60 μ s. The surface area of observed objects is not shown for the sake of brevity; however, the surface energy is collinear with the surface and shown directly. It was obtained as a product of the estimated free surface area and the surface tension measured for the used solution. The stacked bar graph shows contributions of the main spherical part and the satellite and other eventual secondary parts (tail, thread, and dumbbell). These data can be evaluated within the conceptual framework (Figure 33) given above. Indeed, it is reasonable to expect, that the acceleration of the satellite drop which is formed from the upper liquid volume part (tail) in comparison with the main drop stems from energy released between pinch-off and break up, as in that and only that time the energy stored in the surface of the upper part of the liquid (tail) as well as in the strained elastic liquid volume (if any

elasticity present, this is just the issue we elaborate) transforms into kinetic energy increase of this tail liquid volume part manifested in its acceleration towards the much heavier main drop. This energy transformation finishes at the moment of break up with the loss of contact (hence loss of force interaction) between the two volume parts of the liquid. The surpassing energy of the tail liquid volume part is conserved in the increase of the kinetic energy of the satellite, which can be roughly estimated from the satellite velocity increase in comparison with the main drop which is a necessary approximation as the deceleration of the main drop is so small that it cannot be efficiently evaluated. The best opportunity to measure this energy is at the stage of the process when both drops can be considered being spherical. Kinetic energy is shown in the upper graph panel of the lower graph window in Figure 34. Considering velocities of the main and satellite drops as shown in the upper graph ($v_{\text{satellite}} = 7.6 \text{ m}\cdot\text{s}^{-1}$, $v_{\text{main drop}} = 5.1 \text{ m}\cdot\text{s}^{-1}$) and taking into account estimated volumes from the lowest graph panel (at $\rho = 1.048209 \text{ g/cm}^3$) the energy difference can be calculated according to the formula:

$$\begin{aligned}\Delta E &= \frac{1}{2} \cdot m_{\text{satellite}} \cdot v_{\text{satellite}}^2 - \frac{1}{2} \cdot m_{\text{satellite}} \cdot v_{\text{main drop}}^2 = \\ &= \frac{1}{2} \cdot V_{\text{satellite}} \cdot \rho \cdot (v_{\text{satellite}}^2 - v_{\text{main drop}}^2)\end{aligned}\tag{7.14}$$

These calculations were performed for three cases from images captured at times 41, 49 and 56 μs , and give the energy difference about 28 pJ in average. The difference between surface energy of the satellite liquid volume part at the pinch-off and at the break up can be roughly estimated as 14 pJ (between situation in time 25 μs and average between 31 and 35 μs) seeing that the surface energy of the main drop (main volume compartment) remains nearly unchanged. Then it can be concluded, that there must be another contribution to the acceleration of the satellite with respect to the main drop, although it cannot be quantified precisely (the estimations are very rough but still reasoned, we expect 50 % error), just it can be estimated to be of comparable size with the surface energy contribution and this can be only due to elasticity effect. The fact, that the liquid elasticity effect is not negligible is the reason why the printing process was successful even in our case, having the working points in the second region of Kim & Baek's analysis (see graph in Figure 26), that has been drawn for viscous liquids only. On the base of this experience, it can be proposed a general conclusion, that viscoelastic solutions (suitable for printing, which means having still prevailing character of viscous liquid rather than elastic body) have extended region of good printability in the direction of increasing We number in both Kim & Baek's and Re vs. Ca graphs (see again Figures 26 and 28). Moreover, these results confirmed that introduction of used small concentration of polymers into tested solutions increases the elastic response of the fluid which is most likely responsible for observed behaviour. The issue of viscoelasticity is analysed more in the next section.

7.8 Refinement of Dimensionless Analysis by Including the Viscoelasticity of the Polymer Solution

Controlling drop formation and break up of filament of ink is a complex process that depends on many factors including the rheology of ink.

Taking the viscoelasticity effect into account, the process of drop formation in DOD inkjet mode could be represented by five sections. [94] Exactly this was observed in performed experiments as can be seen in Figure 31 and the sequence sections including time intervals was as follows (1) ejection and stretching of liquid: 0-20 μs , (2) pinch-off of liquid thread from nozzle exit: 20-25 μs , (3) contraction of liquid thread: 25-35 μs , (4) break up of liquid thread into primary drop and satellite: about 41 μs , and (5) recombination of primary and satellite drops: about 56 μs .

According to Bazilevskii [108], the characteristic break up time was estimated with utilization of the Raleigh-Weber mechanism. The break up time of a drop (pinch-off) was estimated for 2.5 wt% PVA solution in water/DMSO at 35 $^{\circ}\text{C}$:

$$t_c = \sqrt{\frac{\rho \cdot A^3}{\sigma}} = \sqrt{\frac{1048.2 \cdot (2.15 \cdot 10^{-5})^3}{(4.53 \cdot 10^{-2})}} \text{ s} = 15.2 \cdot 10^{-6} \text{ s}$$

$$t_v = \frac{3 \cdot \eta \cdot A}{\sigma} = \frac{3 \cdot (5.92 \cdot 10^{-3}) \cdot (2.15 \cdot 10^{-5})}{(4.53 \cdot 10^{-2})} \text{ s} = 8.4 \cdot 10^{-6} \text{ s}$$

$$t = t_c + t_v = (15.2 \cdot 10^{-6} \text{ s} + 8.4 \cdot 10^{-6} \text{ s}) = 23.6 \cdot 10^{-6} \text{ s} \approx 24 \mu\text{s}$$

The calculation for 25 $^{\circ}\text{C}$ gives similar values differing mostly due to change of viscosity.

$$t_{c,25^{\circ}\text{C}} = 15.025 \cdot 10^{-6} \text{ s}, t_{v,25^{\circ}\text{C}} = 10.342 \cdot 10^{-6} \text{ s}, t_{25^{\circ}\text{C}} = 25.367 \cdot 10^{-6} \text{ s} \approx 25 \mu\text{s}$$

It must be noted, that the calculated result of pinch-off time is in good agreement with the drop formation and ejection determined by the CCD camera integrated in the used printer which is discussed in previous section. The use of visualization systems is well established for this purpose. [102, 108, 169, 170]

Time scales related with flow relevant for inertial effect and viscosity depend on simply measurable variables and they are sufficiently discussed above. However, successful treatment of elasticity needs careful assessment of the relaxation timescale of the fluid under investigation (i.e. used polymer solution), in other words, calculation of the Elasticity number requires estimation of intrinsic relaxation time which cannot be approached directly by measurement. Zimm relaxation time, (λ_z), is considered as the longest relaxation time for a macromolecule in polymer solution. [102, 106]

Although the inkjet printing process was carried out at 35 °C, the Zimm relaxation time is calculated for PVA in water/DMSO at 25 °C, because the intrinsic viscosity was determined at that temperature. The viscosity of solvent necessary for this calculation was also taken for corresponding temperature.

$$\lambda_Z = \frac{\eta_s \cdot [\eta] \cdot M_w}{R \cdot T} = \frac{(1.9593 \cdot 10^{-3}) \cdot 33.5 \cdot 10^{-3} \cdot 27}{8.314 \cdot 298.15} = 7.149 \cdot 10^{-7} \text{ s} \cong 7.15 \cdot 10^{-7} \text{ s}$$

Similarly, to the previous case, the temperature 25 °C is used in the calculation for the 2.5 wt% PVA solution in water/DMSO. Kuhn length for PVA is taken from [171].

$$z_0 = b_K \cdot N^{1/2} = b_K \cdot \left(\frac{M_w}{\frac{b_K}{a} M_{mer}} \right)^{1/2} = (0.62 \cdot 10^{-9}) \cdot \left(\frac{27000}{2.47 \cdot 44} \right)^{1/2} \text{ m} = 9.77 \cdot 10^{-9} \text{ m}$$

$$\lambda_K = \frac{2 \cdot \pi \cdot \eta \cdot z_0^3}{k_B \cdot T} = \frac{2 \cdot \pi \cdot (7.44 \cdot 10^{-3}) \cdot (9.77 \cdot 10^{-9})^3}{(1.38064852 \cdot 10^{-23}) \cdot 298.15} \text{ s} = 1.06 \cdot 10^{-5} \text{ s}$$

This value of relaxation time ($\lambda_K \approx 10 \mu\text{s}$) can be considered as the upper estimation limit of the polymeric time scale. The real manifestation of elastic effects as a pinch-off in observed process with (Rayleigh) timescale about t_c , 25 °C $\approx 15 \mu\text{s}$ for inertia effects and timescale about 7-10 μs for viscous effects testifies that this later value (λ_K) of polymeric relaxation timescale is more realistic. Experimental verifications have been already published although it was demonstrated on polystyrene solutions in diethyl phthalate [172, 173], relaxation time estimations from oscillatory measurements in linear viscoelasticity response range (linear relaxation time, λ_{LVM}) are found to approach the Zimm time (λ_Z) in the dilute limit, which means that the use of (λ_Z) holds on for highly dilute solutions. The ratio $\lambda_{LVM} / \lambda_Z$ has 1 as theoretical asymptotic value for zero reduced concentration (c/c^* , where c is the mass concentration and c^* is the critical concentration in other expression reduced concentration is identical with dimensionless concentration $[\eta] \cdot c$). The ratio approached 1-1.5 for reduced concentrations below 0.1. Intermolecular interactions increase with increasing polymer concentration which prolongs the relaxation time exponentially. The value of λ_{LVM} can be higher than λ_Z by one or two orders of magnitude while the solution is still considered as a dilute one. Moreover, the ratio of this linear relaxation time (λ_{LVM}) to Zimm relaxation time (λ_Z) reduced significantly with increasing M_w keeping the concentration constant. Extensional rheometry was used for extensional relaxation time (λ_E) estimation also. Although it works beyond the linear viscoelasticity limit, λ_E was in agreement with λ_{LVM} for higher values of M_w . The ratio $\lambda_E / \lambda_{LVM}$ grows with increasing polymer concentration (while keeping the M_w constant) and also grows with decreasing M_w (while

keeping the concentration constant). This behaviour can be generalized and explained by increasing role of intramolecular interactions in the system with increasing M_w . Interactions between distant segments on a very long molecule can substitute to some extent the intermolecular interactions with respect to observed macroscopic relaxation. It is obvious that these effects will be more pronounced in the non-linear viscoelasticity regime and λ_E will tend to be higher than λ_{LVM} . Considering these studies and observations embodied in this Thesis, the choice of the Kuhn length model which is generally linked to the reptation mechanism seems to be fully rationalized.

Within this framework, Weissenberg and Elasticity numbers can be interpreted.

$$Wi = \frac{\lambda \cdot v}{A} \quad (7.15)$$

and

$$El = \frac{Wi}{Re} = \frac{\lambda \cdot \eta}{\rho \cdot A^2} \quad (7.16)$$

Using λ_z , one obtains 0.18 for Wi and 0.0109 for El . These values imply relatively suppressed manifestation of relaxation processes in the liquid judging on the Weissenberg number, however, the elasticity is largely underestimated and viscous flow would dominate the process totally. In such case, the liquid would follow the Kim & Baek analysis of printability [92], which is not exactly what was observed. Using λ_K , the value of Wi is 2.66 which testifies for importance of the molecular relaxation in terms of the Kuhn segments modelling real polymer chain. For $Wi > 0.5$, stretched molecules rather than random coils should be present in the liquid under stress. The value of El is 0.162 indicates moderate but still not prevailing contribution of elasticity. The Kuhn relaxation time scale proved as appropriate choice from this point of view also and λ_K should be used in this and possibly all similar cases. Considering decrease of jet fluid thread diameter during the break up process, the contribution elasticity may even increase locally. This interpretation is in agreement with observed characteristics of the solution exerted to applied jetting conditions. Another general lesson may be taken from the comparison of relaxation time scales. Since Wi scales with $1/A$ the local decrease of the fluid thread diameter will result into the coil stretching even for the most dilute solutions. Moreover, as $El \sim 1/A^2$, this number grows much more rapidly and the manifestation of elasticity can make the process otherwise assessed globally as viscous force governed one to be more complex than expected even for highly diluted polymer solutions.

According to [162], the critical value of E_c is 4.7015 when the velocities of viscosity controlled thinning and elasticity controlled thinning equal.

$$Ec = \frac{Wi}{Ca} = \frac{\lambda \cdot \sigma}{\eta \cdot A} \quad (7.17)$$

Viscosity controlled filament thinning dynamics are expected for $E_c < 4.7015$ and elastic effects for $E_c > 4.7015$. Calculated value of E_c using λ_K is 3.07 at 25 °C and 2.91 at 35 °C, respectively. It means that viscous effects still prevail however elasticity effects cannot be omitted. If considered that thinning causes shrinking of the jet thread diameter in comparison with the initial nozzle orifice side size, one can expect increased local value of the E_c testifying for increased role of elasticity effects. The use of λ_Z yields $E_c = 0.207$ (at 25 °C) which points deeply towards the solely viscous flow regime controlled by the balance between capillary pressure caused by surface tension and viscous stress with almost no influence of elasticity. The critical border between viscosity and inertia dominated regimes in dispensing liquids is characterized by the value of the Ohnesorge number $Oh = 0.2077$. For $Oh < 0.2$ inertia effects will dominate thinning while it will be controlled by viscous effects for $Oh > 0.2$. The values of Oh calculated for investigated set of polymer solutions varied from 0.12 up to 0.29. It indicates that neither effect will dominate the process. The best candidate solution (2.5 wt% PVA) has the value $Oh = 0.19$. Since Oh scales with $1/A$, it can be judged that viscous effects will tend to prevail over inertial ones due to local effect of the fluid thread thinning. A summary of discussed numbers for all tested solutions (calculated with the help of λ_K for 35 °C) is in the right part of Table 15.

Table 15. Calculated viscoelastic criteria: the Rayleigh time (t_c), the Relaxation time according to Kuhn segment (λ_K), the Deborah number (De), the Ohnesorge number (Oh), the Elasticity number (El), and the Elasto-Capillary number (Ec) of prepared solutions of PVA in water/DMSO mixture for 35 °C.

PVA concentration [wt%]	t_c [μ s]	t_v [μ s]	λ_K [μ s]	De [-]	Oh [-]	El [-]	Ec [-]
1	15.4	5.5	5.2	0.336	0.12	0.040	2.82
1.5	14.7	5.9	6.1	0.415	0.13	0.056	3.10
2	14.4	6.5	7.0	0.485	0.15	0.073	3.21
2.5	15.2	8.4	8.2	0.538	0.19	0.100	2.91
3	15.4	9.0	8.5	0.553	0.20	0.108	2.82
4	15.6	13.4	12.4	0.793	0.29	0.228	2.76

Criterion, that binds the timescale of polymer relaxation and the Rayleigh timescale for capillary breakup is the intrinsic Deborah number (De). To examine the impact of polymer relaxation time scale estimation on analysis of studied case, the relaxation time was calculated utilising the Zimm theory according to [106] and [102] also. Although the inkjet printing process was carried out at 35 °C, the value of relaxation time (hence the value of Deborah number too) is calculated for PVA in water/DMSO only at 25 °C, because the intrinsic viscosity was

determined at that temperature. The viscosity of solvent necessary for this calculation was also taken for given temperature.

The Deborah number calculated first using the Zimm relaxation time (for PVA in water/DMSO at 25 °C):

$$De = \frac{\lambda_z}{t_{c,25^\circ C}} = \frac{\lambda_z}{\sqrt{\frac{\rho \cdot A^3}{\sigma}}} = \frac{7.15 \cdot 10^{-7} s}{15.025 \cdot 10^{-6} s} = 0.04758$$

It can be compared with the second case which was found more appropriate (see discussion above) when the relaxation time was calculated according to relation defined by Bazilevskii *et al.* [108]:

$$De = \frac{\lambda_K}{t_{c,25^\circ C}} = \frac{\lambda_K}{\sqrt{\frac{\rho \cdot A^3}{\sigma}}} = \frac{1.06 \cdot 10^{-5} s}{15.025 \cdot 10^{-6} s} = 0.705$$

Using appropriate relaxation time λ_K , a value of De number was obtained that testifies for relative importance of the elastic component in the prepared ink. On the other hand, the value is such that viscous and capillary effects are not dominated by the elasticity of the solution. This becomes obvious as the ratio between De and Oh is the Elasto-Capillary number discussed above:

$$Ec = \frac{De}{Oh} \quad (7.18)$$

The conceptual diagram in Figure 35 was originally sketched by McKinley in [103]. The plot of De against Oh is highly illustrative and may serve to fast assessment of any viscoelastic fluid. The ovals indicating applicability fields of various polymer solutions, liquids, dispersions and melts are localized very roughly and serve rather to classification of polymer based fluids than to the quantification of various processing regimes. The elastically dominated processes and viscously dominated self-thinning and necking processes are demarcated by the rising line with slope 1. Since $Oh \sim t_v / t_c$ and $De \sim \lambda_K / t_c$ the line can be easily rationalized as $\lambda_K > t_c > t_v$ which means $De > 1 > Oh$ for elastically dominated systems and $t_v > t_c > \lambda_K$ (i.e. $Oh > 1 > De$) for systems with prevailing viscous effects. The situation is simply interpreted as governed by the relative size of viscous and elastic timescales (as indicated by the previous analysis of Ec number) which again results intuitively into the borderline at $Ec = 1$. [103] Taking into account numerical prefactors resulting from the cylindrical shape of the fluid filament [162], the correct critical value of Ec for studied case was 4.7015 as already mentioned above. This line was added to the original McKinley's graph. Moreover, it seems that the Rayleigh time scale is cancelled in all these estimations. In fact, it is not fully true. At any given ratio De/Oh , a straight line of that slope going through the origin can be plotted in the graph and one can virtually slide along it moving towards the graph origin with increasing t_c and far

from the origin with decreasing t_c , which means for macroscopic quantities that the square root of the ratio between the solution density and surface energy can be varied for given nozzle geometry or for the same solution the nozzle geometry can be changed which results into the change of the Rayleigh time.

A much more important drawback of this approach is that it is independent of the process kinematics. However, no better trial for printability map has been drawn yet for viscoelastic inks.

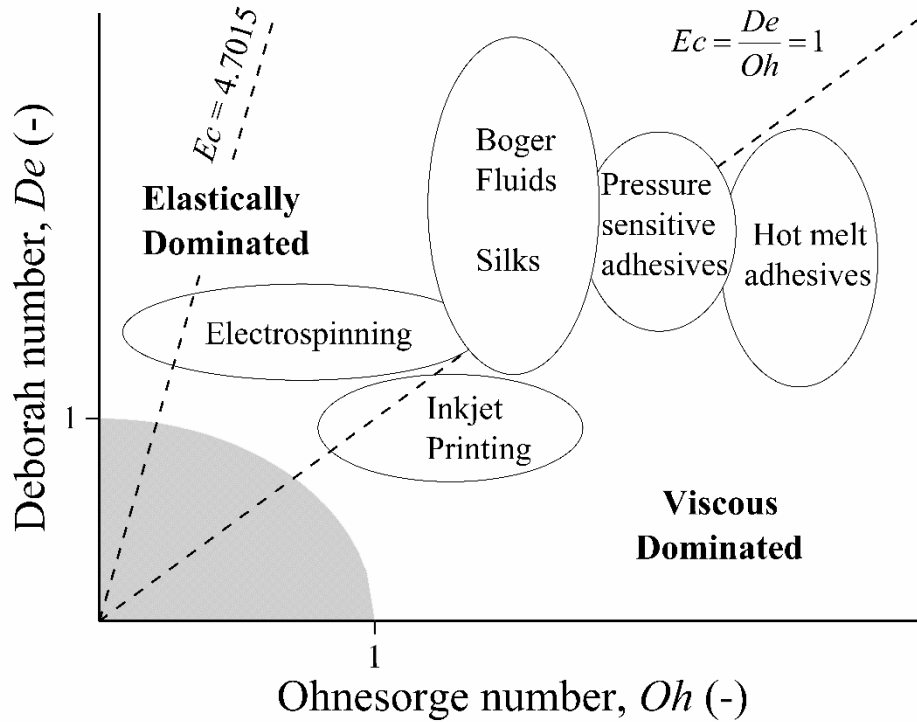


Figure 35. Diagram of Deborah number against Ohnesorge number sketched by McKinley. [103]

According to Table 15, it is evident that prepared inks falls into the area, where Caber tests are considered being impractical. It can be expected, that this will be the case of many inks similar to studied case and prepared for the use with the Dimatix printer. Therefore, the graph was replotted in Figure 36 showing isolines for $Ec = 1, 3$ and 4.7015 and a set of hyperbolic isolines for the Elasticity number was inserted as

$$De = \frac{El}{Oh} \quad (7.19)$$

In terms of physical quantities, it means, that for given El number, (i.e. sliding along El isoline) the surface energy can be changed (varying Ec) and for constant Ec (sliding along straight Ec isolines) the density may be changed. It seems, this space gives less freedom than that derived previously for Newtonian fluids which is due to the lack of processing dynamic.

It can be seen, that experimentally obtained points corresponding to characteristics of prepared inks aligned again along a suitable isoline, this case along the one for $Ec = 3$ while the best performing ink of concentration 3 wt% has the value of $El = 0.1$ and lays in the middle of the group.

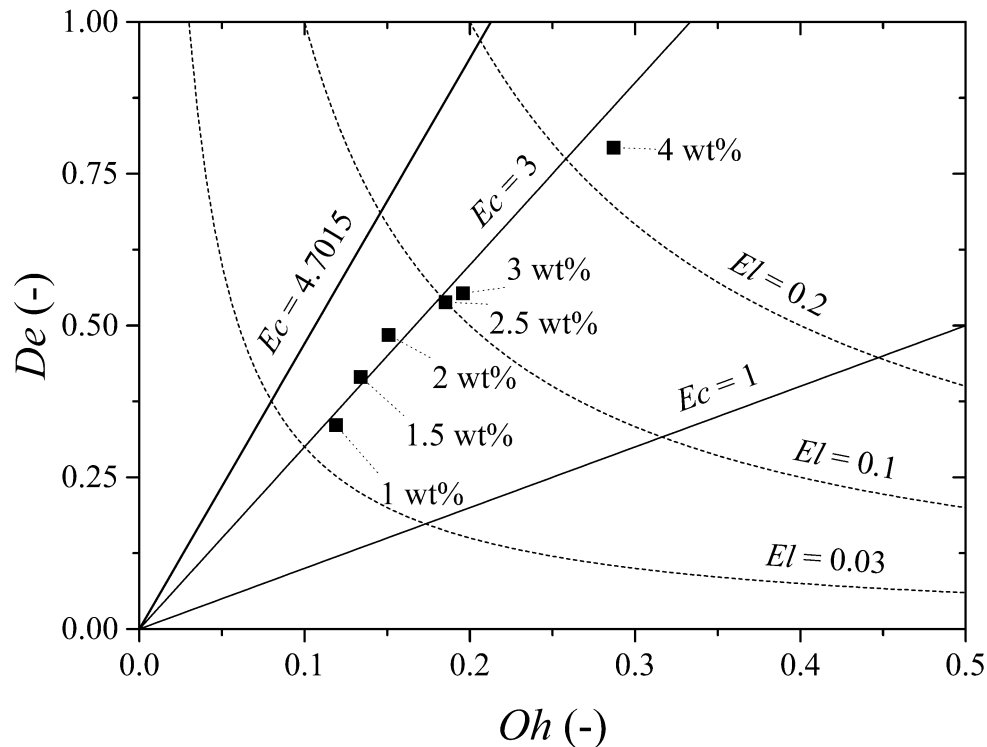


Figure 36. Replotted diagram of De number against Oh number showing the position of prepared solutions of PVA in water/DMSO.

The graph in Figure 36 has been developed to create a stepping stone for future studies of printability of viscoelastic inks. Two very different approaches were clearly demonstrated as useful yet each one limited tool if applied alone for handling the issue of polymer solution based inks. It seems there is a huge gap between them in the field of fluids for inkjet printing. The latest efforts in the field of viscous systems most likely reached their limits; on the other hand, viscoelastic liquids are relatively poorly understood in theory, although being massively used in praxis. It can be speculated that it is due to some peculiarities in their experimental characterisation, namely micro-capillary viscometers are not yet available in every laboratory. If we turn attention to the theoretical framework, the weakest point of contemporary state of the art including the advances present in this thesis can be seen in the use of the intrinsic Deborah and the Ohnesorge numbers. Neither De nor Oh grouping of quantities includes the process kinematics. Similarly to the situation in viscous liquids, all the triad of material-tool-process characteristics must be taken into account. The Deborah number is often treated as equivalent to the Weissenberg number, but they quantify different effect and can be treated as interchangeable in special cases only. [174] With

respect to the case studied in this Thesis, it must be pointed out that Wi is actually a ratio of polymer relaxation and convective timescales (since A/v is the timescale for the fluid flow). One may suggest unifying the approaches to viscous and viscoelastic liquids. All relevant timescales must be taken into consideration. Recently, use of three dimensionless criteria was introduced to build up a three dimensional space that allows to understand dripping/jetting transition. The two numbers Oh and De were completed with Ec to a triplet which describe dispensing operations in terms of the material-property based non-dimensional criterions. The dynamic numbers Ca , We and Wi define paths within this operation space. The six numbers are interrelated and any dispensing operation can be fully described by any set of two material-property based and one dynamic non-dimensional groups while the remaining groups can be calculated (for example for known Oh , De , and We one obtains $Ca = Oh \cdot We^{1/2}$, $Wi = De \cdot We^{1/2}$, and $Ec = De/Oh$). The diagram of the operating space helps to anticipate problems when wanting to dispense rheologically complex fluids however the broad field of dispensing of complex fluids is not yet fully understood, in particular with regard to flow phenomena as deformation-thickening, yielding thixotropy or rheopexy, and requires more in-depth experimental as well as computational studies to bring our understanding to the level of what is currently known about dispensing of Newtonian fluids. [162] The authors developed a classification of typical fluid classes and identified transition between dripping and jetting which is typical behaviour occurring at dispensing. However, inks with properties similar to those studied in this Thesis do not fall into any typical region. Another objection can be also raised against the focus on dripping/jetting transition while other modes of printing are not taken into account and processing windows for optimum printing regime were not delimited within this model.

Ideally, any ink should be described by a consistent formalism which takes elasticity into account and within which framework the purely viscous liquid would be just a limiting (special) case. The description should be also presentable and readable in 2D space (as a practical map) and should be fine enough to distinguish different printing modes. At least a good promise can be seen in the fact that all involved relaxation processes for studied DOD inkjet printing class of solutions have comparable time scale in microseconds but there is still a lot more that needs to be done.

7.9 Characterization of Dimatix Fluid Cartridge

The print-head nozzle and the print-head channel was also studied to verify claims of its producer in real product. Its shape was determined by optical and electron microscopy and compact x-ray camera (X-ray tomography). As an example, four nozzles in a row are clearly visible in Figure 37. For square ducts, the equivalent diameter (characteristic length in this case) is equal to the side size.

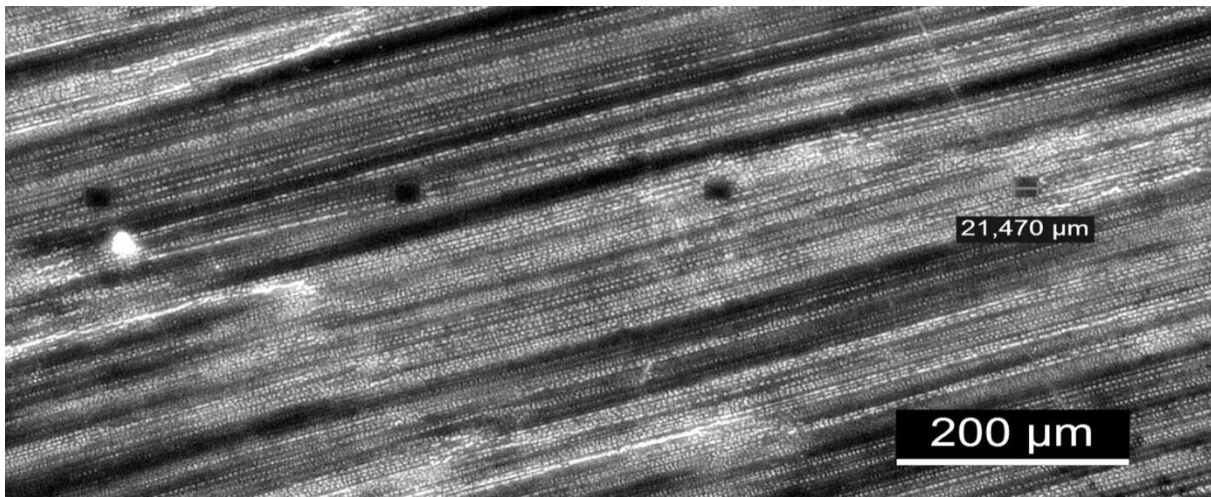


Figure 37. Shape of the nozzles as seen by optical microscopy.

The shape nozzle orifice was confirmed to be a square, but it is of certain interest to know the geometry of the ink channel. Therefore, the part of cartridge containing the ink channels was subjected to a more detailed analysis. This part was cut in the first step, and then grinded mechanically, which led to breaking off and snapping of part containing the nozzles. The obtained results are shown in Figures 38-41.

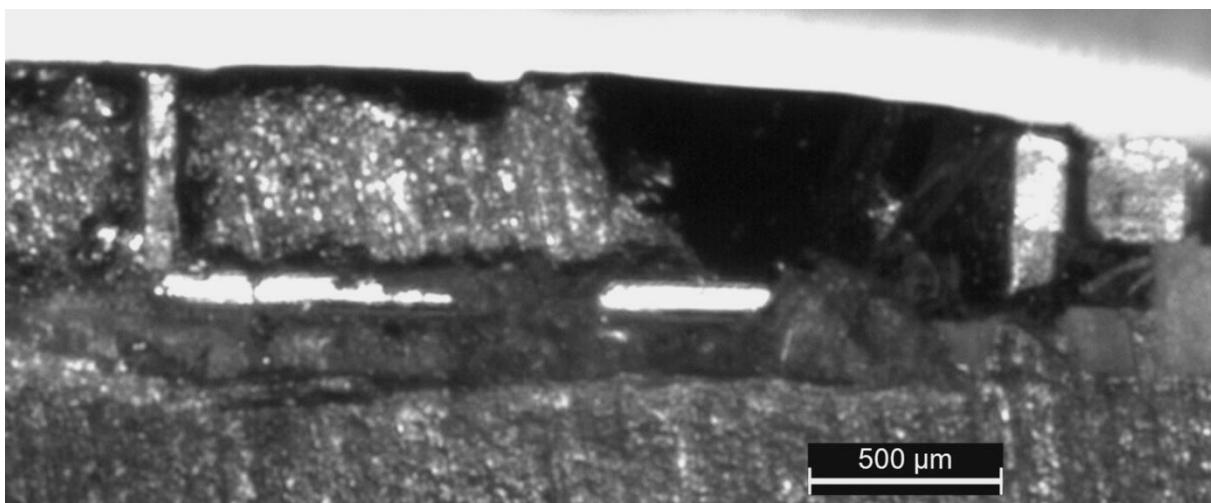


Figure 38. Cross-section of cartridge part containing the profile – optical microscopy.

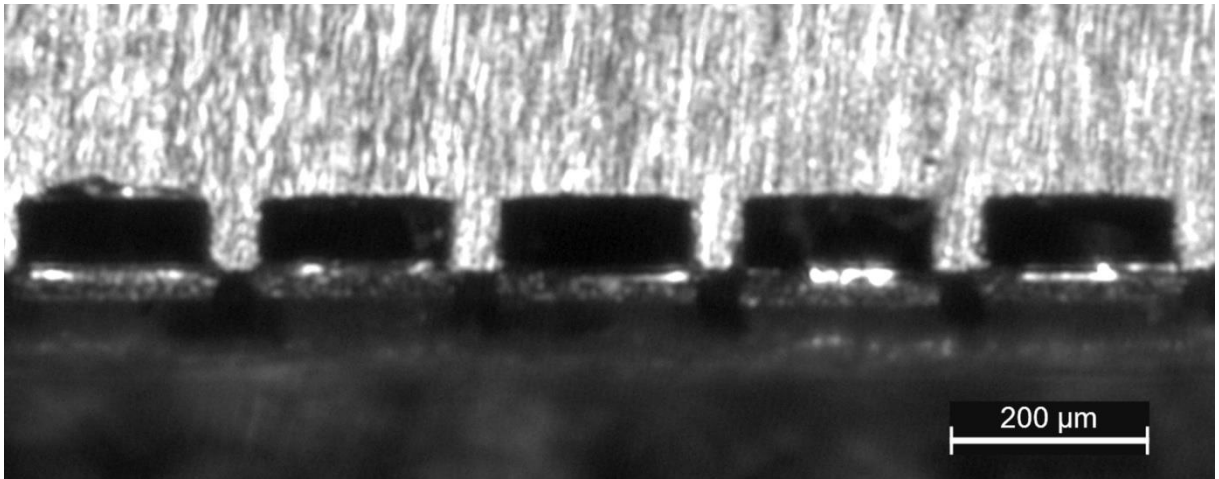


Figure 39. The shape of ink channel in the bottom part of prepared sample – optical microscopy

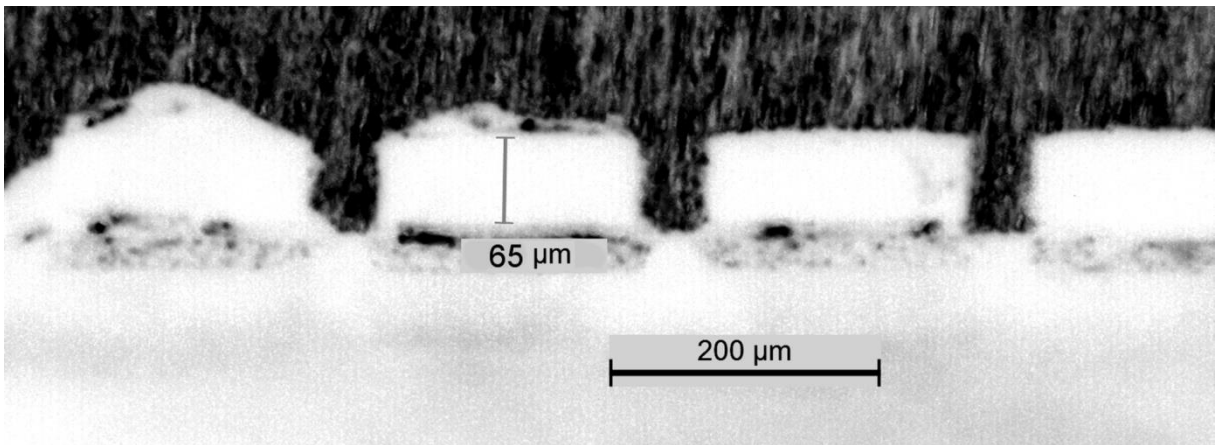


Figure 40. The shape of ink channel in the bottom part of prepared sample – optical microscopy.

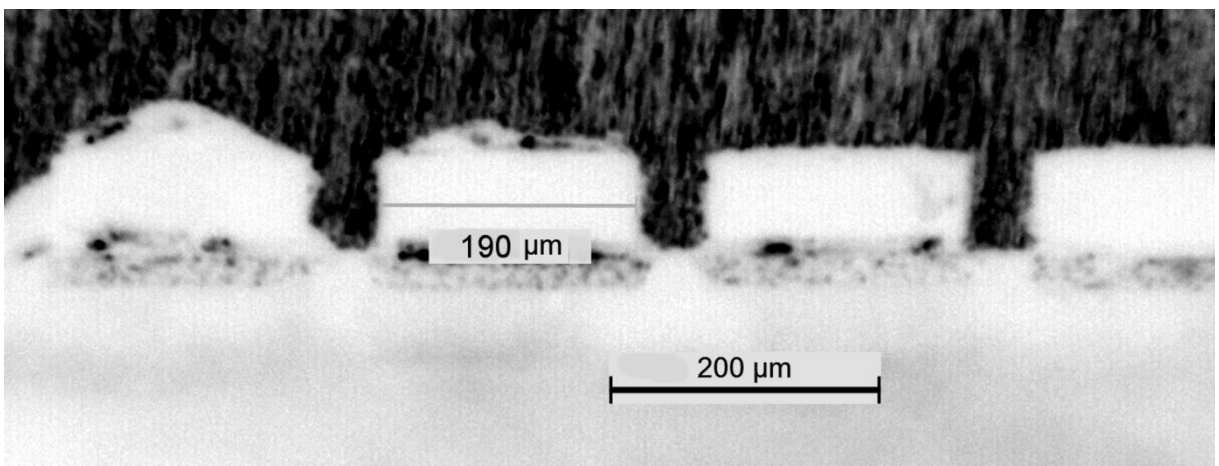


Figure 41. The shape of ink channel in the bottom part of prepared sample – optical microscopy.

As can be seen, the ink channels have a rectangular shape in the bottom part with size of (190 x 65) μm. This width of channel has been partially visible on results

obtained by x-ray camera (Figure 42). Nevertheless, other measurements were required for better dimension analysis due to low resolution of the X-ray tomograph (Figures 42-44).

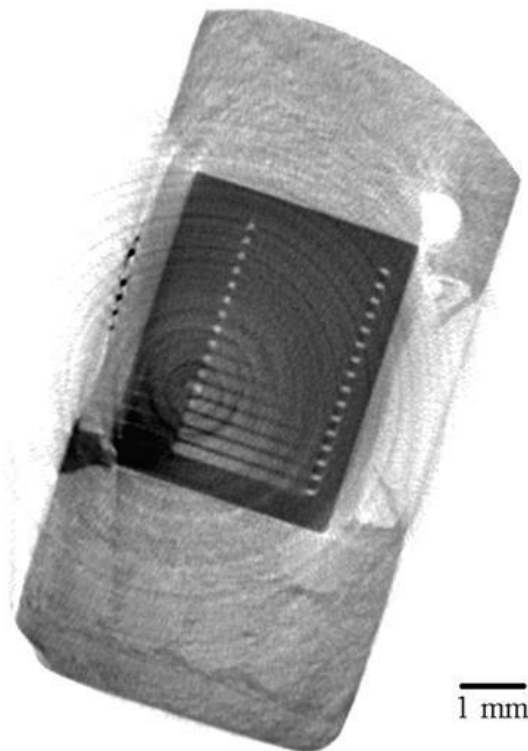


Figure 42. The picture of cartridge part containing ink channels captured from the top view (X-Y axes) obtained by x-ray analysis.

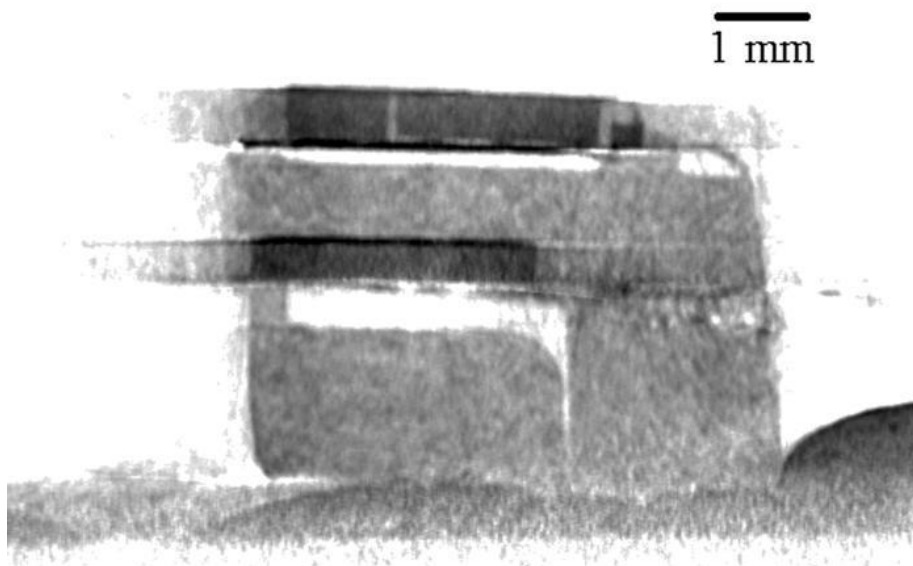


Figure 43. The picture of cartridge part containing ink channels captured from the side view (X-Z axes) obtained by x-ray analysis.

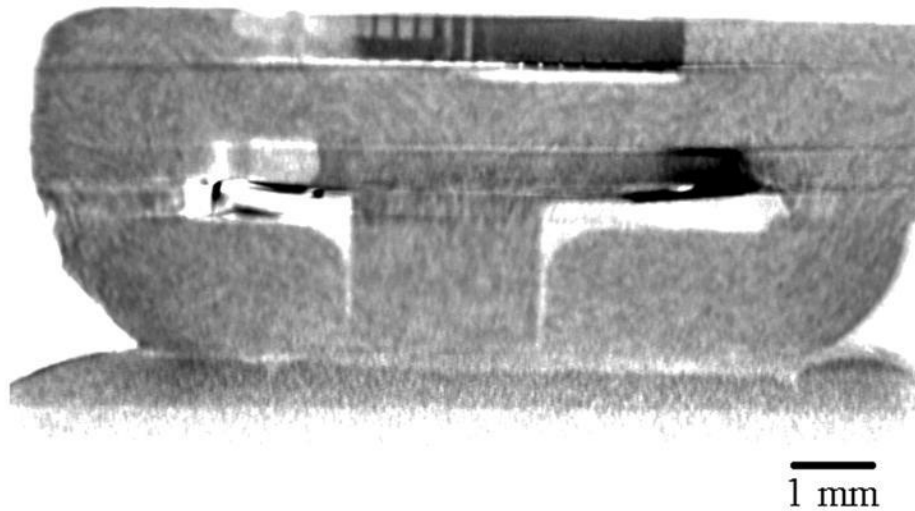


Figure 44. The picture of cartridge part containing ink channels captured from the side view (Y-Z axes) obtained by x-ray analysis.

It has been demonstrated that the nozzle diameter is around $21.5\ \mu\text{m}$, but the width of ink channel is bigger in the bottom part. Therefore, more precise investigation has been performed in the place of a nozzle and its connection to its ink channel. Figure 45 shows the image of the ink channel in silicon substrate determined by SEM. As can be seen, a lot of defects are visible around the channel. These defects were observed because of snapping and breaking off the silicon substrate.

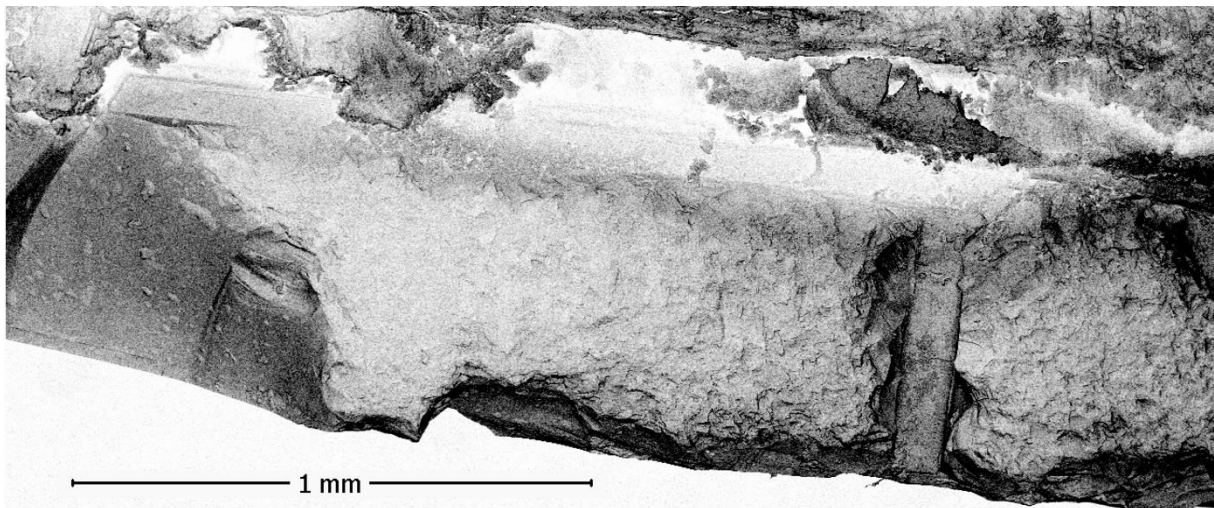


Figure 45. Ink channel determined by SEM.

A distance measurement tool of SEM device was used for determination of channel width in this part. Its width is around $100\ \mu\text{m}$ (results is not showed). It ends in the small piece of silicon substrate so that the nozzle has shape of a truncated pyramid as can be best seen in Figure 46. The liquid must pass through

the nozzle by pressure created inside ink channel during deflection of piezoelectric element that is shown in Figure 47.

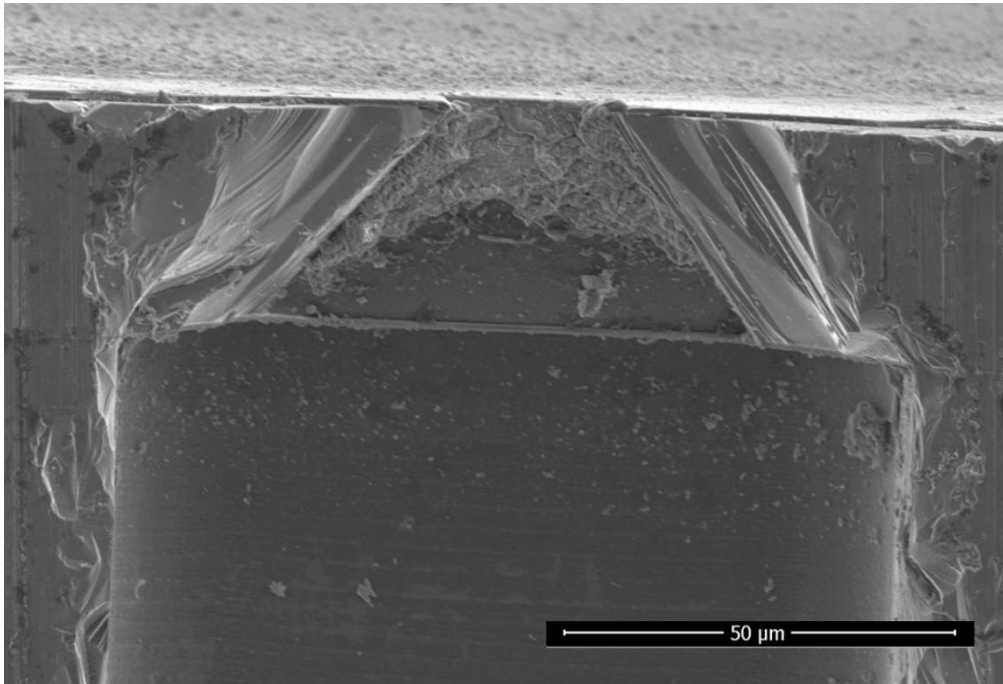


Figure 46. Ending of ink channel and its connection to nozzle captured by SEM. D

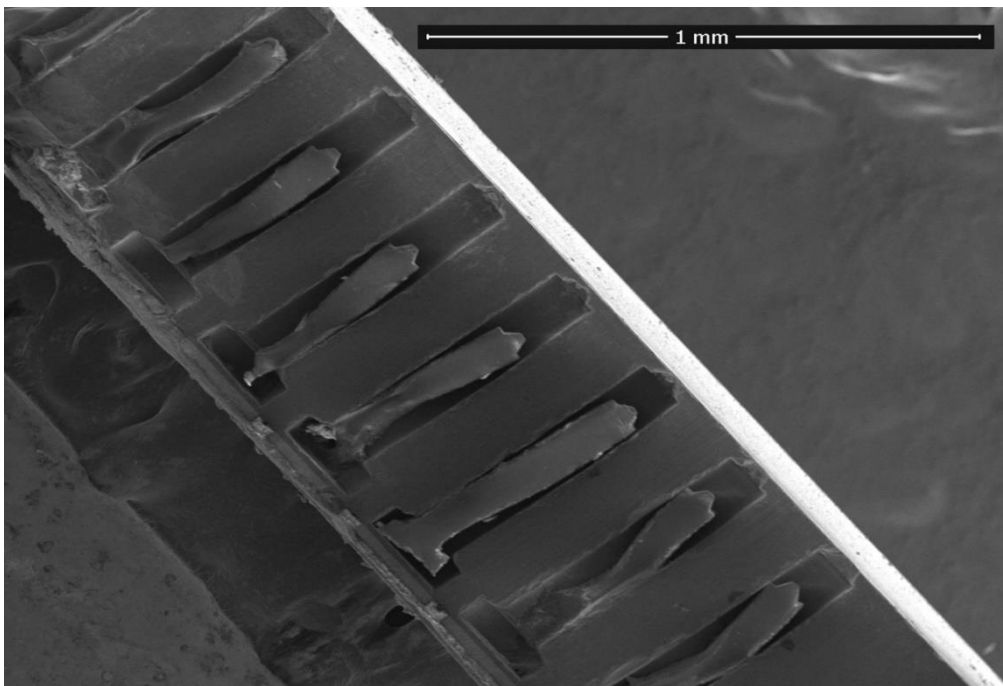


Figure 47. Ink channel outlets with piezoelements captured by SEM. E

To sum this section, Figure 48 shows cross-section schematics of cartridge containing the ink channel. The arrows show the direction of ink flow.

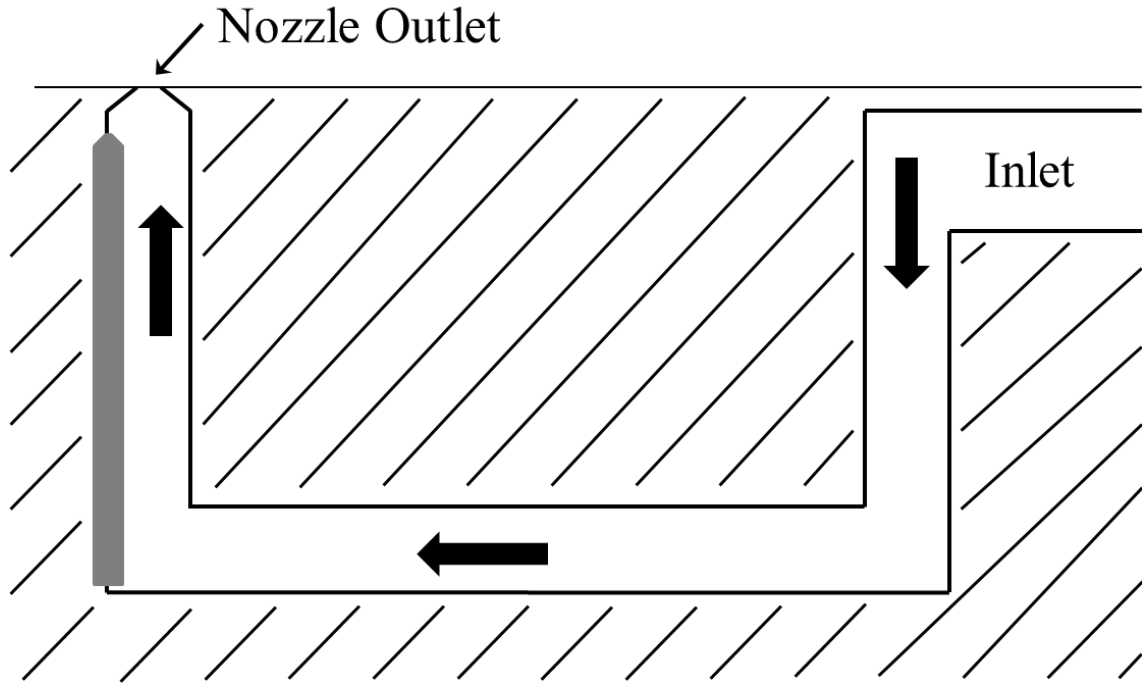


Figure 48. The scheme of cross-section of cartridge part containing ink channel. The grey filled area stands for the piezoelectric element. Arrows show the liquid flow direction.

7.10 Printed Demonstration Patterns and Analysis Thereof

The printed patterns could be prepared in variety of motives; for example, by the using of the pre-defined testing motives (single dots, dot arrays, single line or set of lines) or motives prepared individually with respect to intended function (more complicated shapes for sensors, circuits and other applications). Moreover, three-dimensional structure can be prepared by overprinting.

7.10.1 Substrate properties

The PVA solution (2.5 wt%) was confirmed as the best candidate for patterns preparation in previous section. The surface energy of patterned substrate could be calculated according to various mathematic models. In this work, the Lifshitz-Van der Waals/acid-base (LW/AB) theory was employed to obtain the total surface energy of the substrate using the following equation:

$$g_i^{total} = g_i^{LW} + g_i^{AB} \quad (7.20)$$

where g_i^{LW} and g_i^{AB} refer to the apolar (Lifshitz-van der Waals) and the polar (acid-base) components of surface energy of i-th material, respectively. The polar

component can be divided into the acid (g_i^+) and the base (g_i^-) part according to the relation:

$$g_i^{AB} = 2 \cdot \sqrt{g_i^+ \cdot g_i^-} \quad (7.21)$$

The method is described in detail in reference [175]. The total surface energy of PET substrate and its components are listed in Table 16.

To quantify the variability of obtained values of the surface energy and its components, Sg+ and Sg- are estimated. Sg+ represents the difference between the energy value calculated for the biggest measured contact angles and the energy calculated from average contact angles. Similarly, Sg- represents the difference between the energy value calculated for the smallest measured contact angles and the energy calculated from average contact angles. Hence, Sg+ and Sg- delimit interval experimentally estimated extremes around average value.

Table 16. Surface energy of printed media PET substrate evaluated by See systems.

	g	Sg-	Sg+
g^{Total}	48.99	4.66	9.80
g^{LW}	45.16	1.02	1.34
g^{AB}	3.83	3.64	8.45
g⁺	0.08	0.08	0.56
g⁻	44.10	10.32	14.27

The unit of listed partial surface energies is mJ/m².

7.10.2 Resolution of printed patterns

When these basic features are defined, then required patterns could be selected. The patterns could be pre-defined (for example, dot array, single lines and other) or could be firstly prepared in various graphics design software's, and later converted into required file type by available printer software. These patterns often include more complex images that can be used as circuit, sensors, and others. Then, the required resolution of printed patterns must be defined. This resolution is defined by drop spacing and a print-head angle. The example of relationship between resolution, drop spacing, and print-head angle is shown in Table 17, of course, the values are valid for Dimatix material printer DMP-2800 Series.

Table 17. Resolutions relationship of Dimatix material printer DMP-2800 Series.[39]

Resolution [dpi]	Sabre angle [°]	Drop spacing [μm]
5080.00	1.1	5
2540.00	2.3	10
1693.33	3.4	15
1270.00	4.5	20
1016.00	5.6	25
846.67	6.8	30
317.50	18.4	80
203.20	29.5	125
100.00	90.0	254

7.10.3 Effect of Polymer-Solvent System

The effect of co-solvent can be demonstrated by printing of strips (bands). Figure 49 shows the printed lines of PVA aqueous solution. As can be seen, the edges of printed lines are not smoothly; moreover, the bulging effect was observed in random part of lines. It suggested that the properties of prepared ink were sufficient for drop formation, but delay time was insufficient to eliminate this instability effect. The widths of printed layers are about 200 μm.

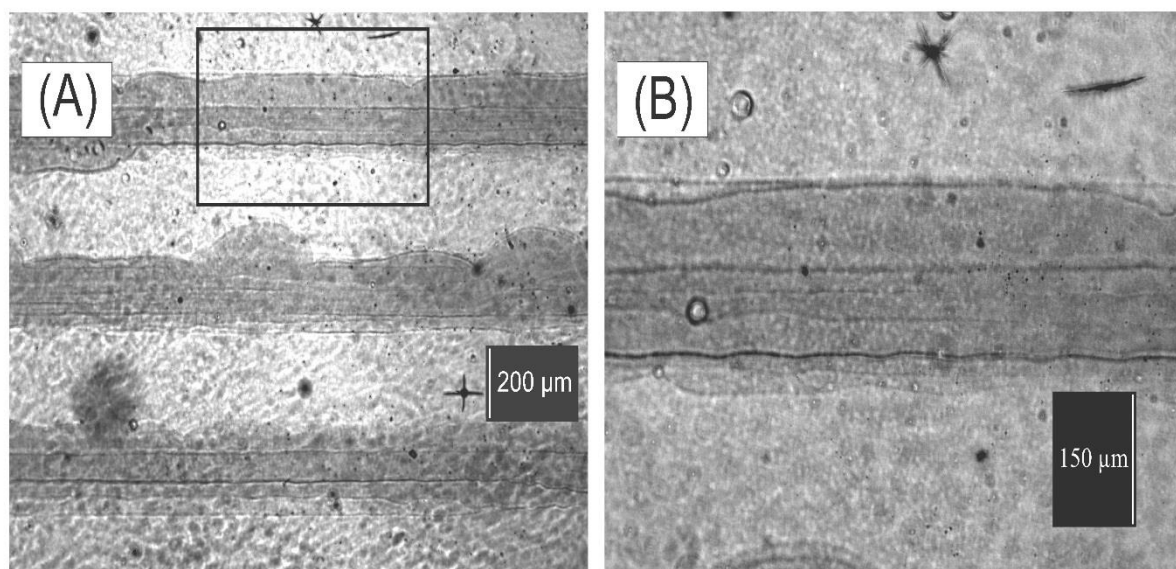


Figure 49. The set of bands printed from 3 wt% aqueous polymer solution PVA 4-98, magnified (A) 40 times, and (B) 100 times, respectively.

The same pattern was also prepared from solution of PVA 4-98 dissolved in water/DMSO mixture (Figure 50). As can be seen, the patterns are more smoothly with good visible edges. The width of these lines is about 250 μm and more, which

could be caused by better wettability of substrate by ink with lower surface tension. Moreover, the instabilities were not observed. The both motives were printed at drop spacing of 24 μm , which correspond to resolution around 1,060 dpi. The temperatures of cartridge and substrate were 33 $^{\circ}\text{C}$ and 45 $^{\circ}\text{C}$, respectively.

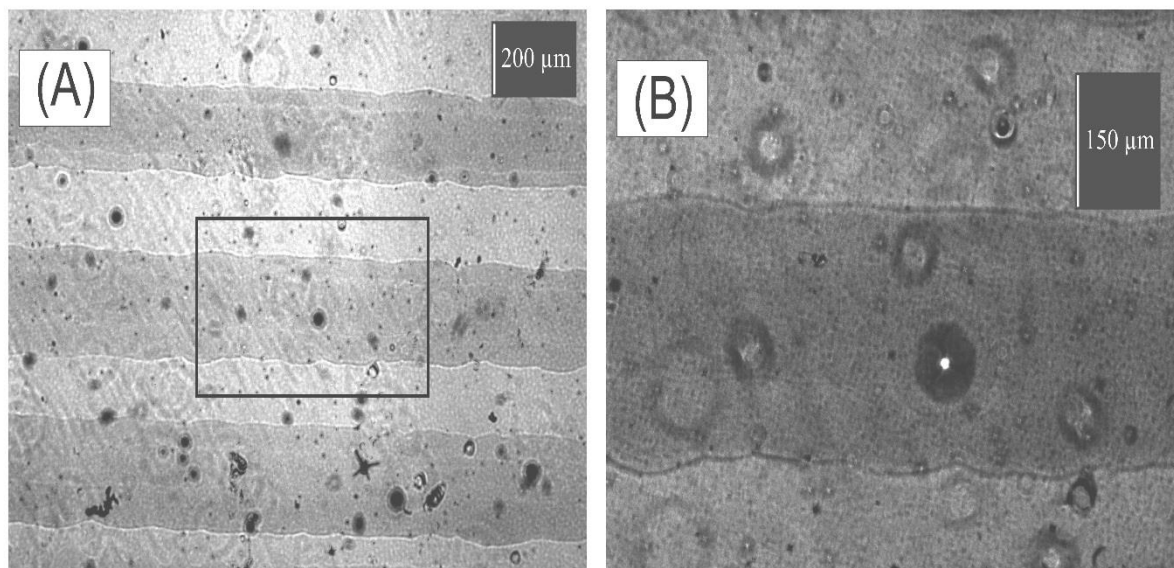


Figure 50. The set of bands printed from 2.5 wt% polymer solution PVA 4-98 in water/DMSO mixture, magnified (A) 40 times, and (B) 100 times, respectively.

7.10.4 Patterns Prepared from PVA in Water/DMSO Mixture

Based on the obtained results, the mixture of solvents (water/DMSO) showed the better covering of patterned substrate as the single solvent system. Thus, the next patterns were prepared from system created by two solvent.

The printed patterns could be evaluated by the use of either pre-defined testing motives (single dots, dot arrays, single line or set of lines) or motives prepared individually with respect to intended function (complex shapes for sensors, circuits and other applications for illustration). Moreover, three-dimensional structure can be prepared by overprinting. Firstly, the effect of different resolution and overprinting was investigated. Figure 51 shows the images of selected area rectangular-shape printed patterns with different resolutions (drop spacing) as well as with number of layers. Drop spacing describes the distance between centers of two dots. The influence of resolution seems to be clear, when two different resolutions are compared (for example figures 51-A and 51-C, patterns with drop spacing 10 μm (2540 dpi) and 17 μm (around 1495 dpi) respectively). As can be seen, when the drop spacing is smaller (higher resolution in dpi) there is larger dot overlapping and higher amount of ink is placed per surface unit resulting in thicker film preparation, but problems with drying of the layer may

occur. On the other hand, when the distance between two adjacent dots is too big, the layer is thin and becomes non-uniform. In that case, movement direction of the print head over substrate is manifested in morphology resembling rows of a potato field. However, more uniform layers may be reached by overprinting (Figures 51-B and 51-D). Printing conditions include in this case the cartridge and substrate temperature of 34 °C and 47 °C, respectively.

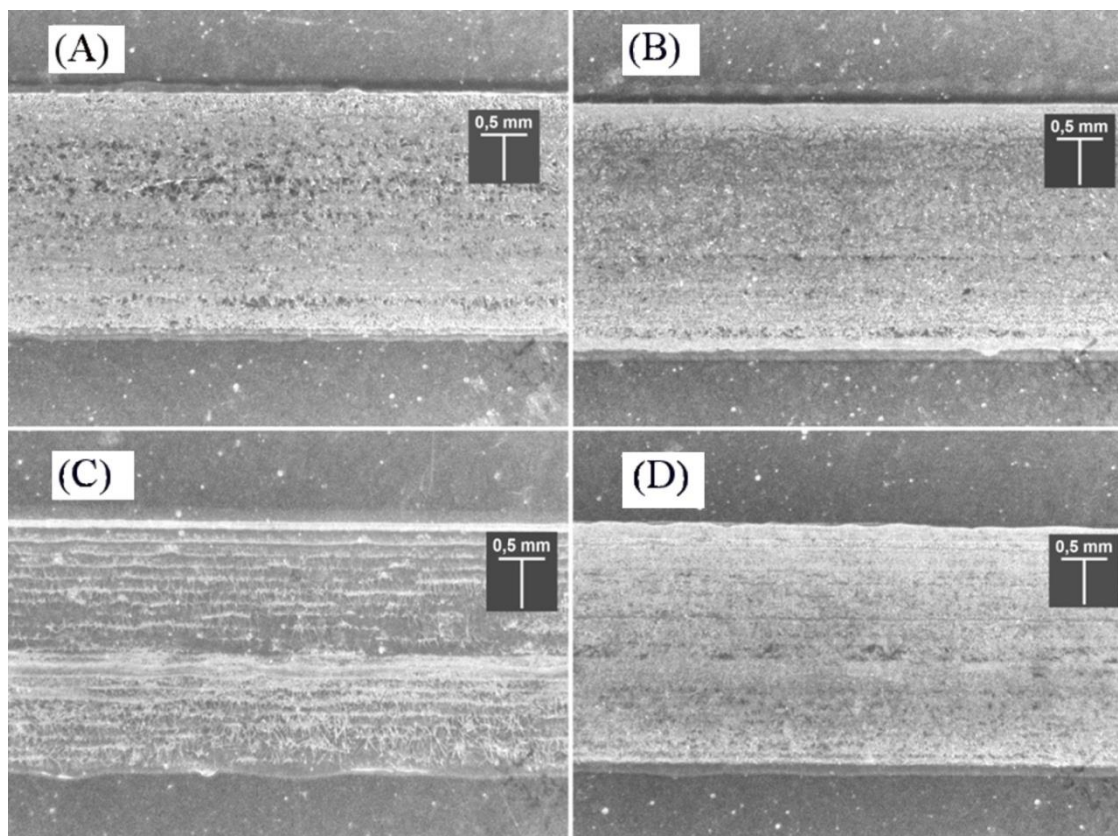


Figure 51. Set of patterns prepared from 2.5 wt% PVA solution in mixture of water/DMSO with different drop spacing and number layers: 10 μm – one run (A), 10 μm – overprint (B), 17 μm – one run (C), and 17 μm – overprint (D).

In the next step, a grid-shape pattern was prepared at same cartridge and substrate temperatures. Figure 52 shows the grid-shape patterns printed at 10 μm drop spacing. As can be seen, vertically oriented lines are overprinted sufficiently. Some of horizontally oriented lines seem to be of lower quality. It can be noticed (without showing results) that among observed PVA solution printing process instabilities, the most frequent was bulging for pure aqueous solutions. To find more detailed information on instabilities in inkjet printing process, the reader is referred to Soltman and Subramanian [24]. The wettability of PET foil was also better for mixture of solvents according to measured width of lines. The thickness of vertically oriented lines was determined at selected area. The height profile is shown in Figure 53. The total average step height (ASH) of each line is over 1 μm .

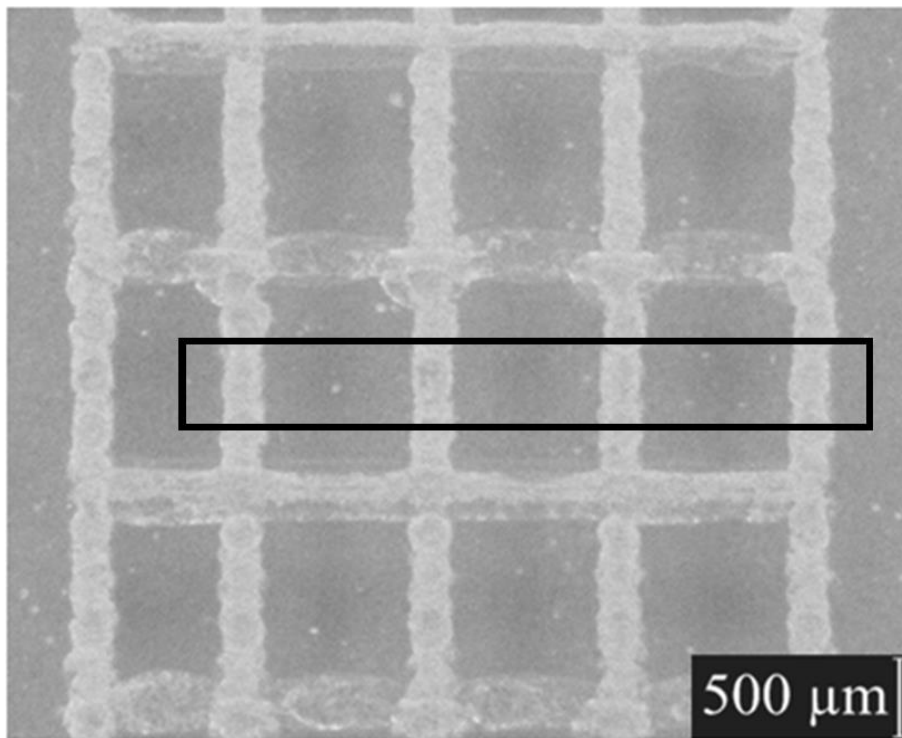


Figure 52. Grid-shape pattern prepared from 2.5wt% PVA solution in mixture of water/DMSO. The black border rectangle shows area, where the profilometry measurement was performed.

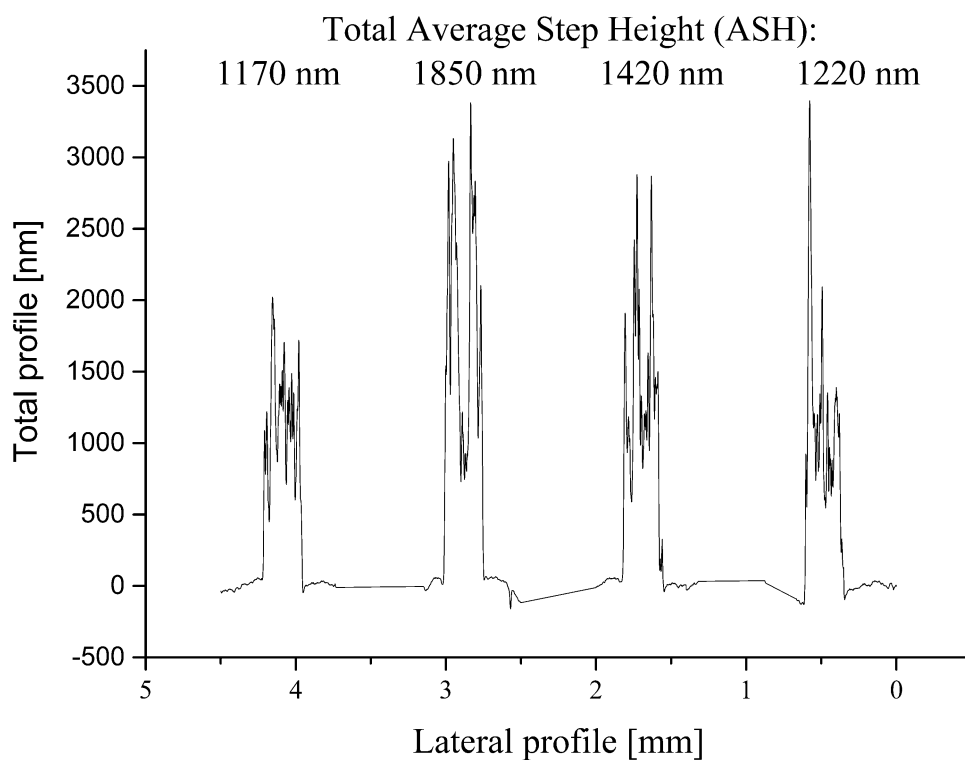


Figure 53. A height profile of grid-shape pattern determined in the selected area.

Although the foil with patterns was attached to metallic plate during profile measurements; the differences in height could be influenced by flexible nature of substrate. Therefore, the measurement was carried out two times at the same place with similar results.

Except the rectangle-shape patterns, the formation of dot arrays or separate dots could be of interest for certain applications. Thus, the dot arrays patterns were also printed. Figure 54 shows the image of printed single drop at 79 μm (A) and 254 μm (B) drop spacing, respectively. Observed drops look like circles or ellipses of little eccentricity. Images of drops were captured by digital optical microscope and their diameters were analysed by measuring tools involved in software. The diameter of drop in both cases varied from 60 μm to 70 μm . Then, a surface topography of prepared drops was determined.

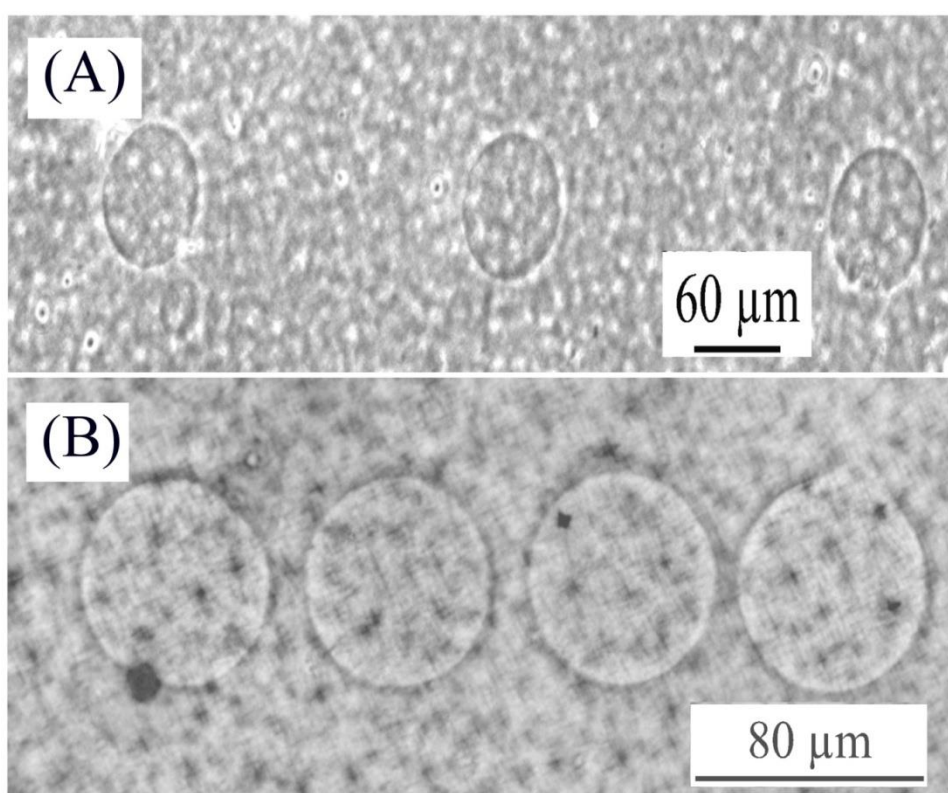


Figure 54. Single drops patterns prepared at 254 μm (A) and 79 μm (B) drop spacing, respectively.

Figure 55 shows an AFM topographic image of a single drop (left) with the corresponding cross-section (right) at position of 45 μm in y axis. This drop example was selected from a dot array, where the distance between two dot centres was 254 μm . The diameter of the analysed drop is about 55 μm ; its height varies from 200 nm at minimum point up to 480 nm at the highest point. The dot shape look like a shallow maar or a cake due to the so-called “coffee-ring effect”, that was observed and reported by many authors. This shape was formed during the drying process, when the polymer mass accumulated at the edge and was

depleted at the centre [115]. However, it could be controlled by substrate temperature to some extent [24] and the substrate temperature of 47 °C was used. The printer does not offer an option of atmosphere humidity and carrier gas flow control that would be most likely the best way how to control the drying process. Several prominent morphologies in the otherwise low relief surrounded by the rim of the dot may be created by polymer crystals however this hypothesis would need to be verified by other methods being behind the scope of this work.

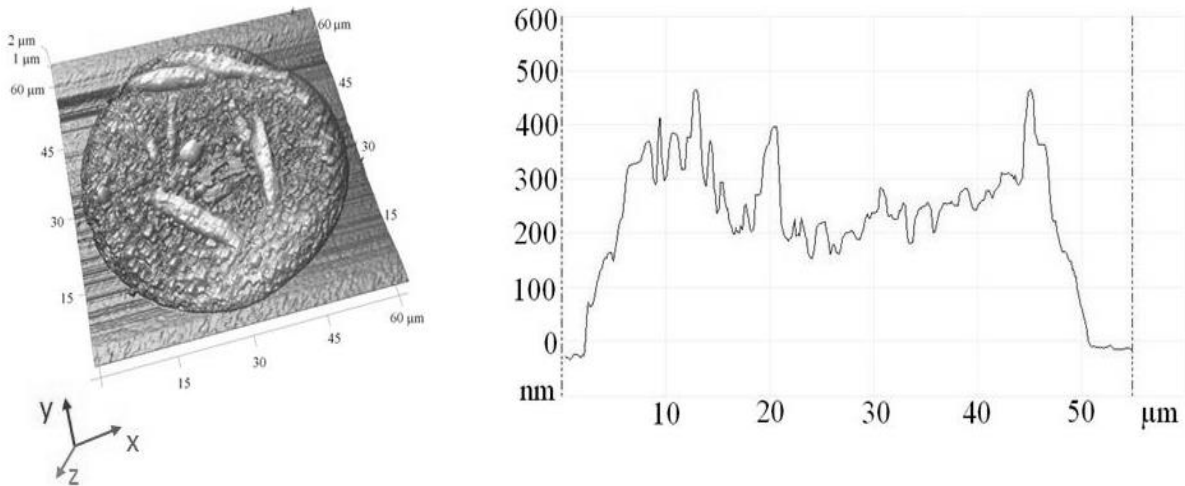


Figure 55. AFM topographic images of single drop of PVA printed on polymer substrate (left) with the cross-sectional profile (right) at 45 μm position in y axis.

8. ADVICES FOR PREPARATION OF POLYMER BASED INK – STEP BY STEP

1. **Choose a polymer** – properties such as polymer functional groups, stability, solubility, properties of the patterned substrate, bio-compatibility in the case of cell deposition and other must be considered.
2. **Choose a solvent** – choose an appropriate solvent according to selected polymer. Consider volatility of the solvent. The solvent should not react with the material of cartridge, in the other case; it could lead to fatal damage. If it is necessary, co-solvents or humectants could be used. Think about the surface energy of the substrate you will use.
3. **Additives** – the addition of other additives depend on the final application of prepared inks. To name a few examples, additives such as surfactants, colorants, biocides, plasticizers, buffers and others can be used.
4. **Basic characteristics** – prepare stock mixtures if using mixture of solvents, prepare enough of stock solution for dilution studies, use any polymer concentration units as you wish but always measure density and use polymer mass concentration for analysis, work fast and avoid degradation, observe ageing, estimate intrinsic viscosity, calculate c^* as you may expect concentration of your ink to be close to semi-dilute limit, perform the rheological study of proposed polymer solution without additives; investigate the viscosity, surface tension, and eventually other important properties (e.g. pH) in dependence on concentration and temperature. Newtonian or Newtonian-like character of your solution is an advantage. Evaluate Re , We , Ca and other dimensionless groupings for Newtonian fluids. Judge viscoelasticity on the base of De and Oh , consider Wi and Ec . For polymer relaxation time estimation, do not use models valid solely for infinite diluted solutions if you do not work with such dilutions.
5. **Modification of proposed ink** – change the primary properties either by changing of concentrations of already present compounds (polymer, solvent, co-solvents), or by addition of new compounds (additives) that improve the properties of the ink. Observe and analyse induced changes. The goal is to limit the number of tested formulations to those, which fit to the processing window of your printer. Consider property ranges recommended by the producers and your own accumulated experience.
6. **Drop formation** – study drop formation. It is a key step of your process as you add velocity of the ejected solution to the parametric space governing the process. Material parameters you know and tool parameters you most likely cannot change (given by the printing head). Find suitable pulse waveform for good drops generation; the uniform drops velocity can be achieved by slightly adjusting of voltage at nozzle. Follow your

experimental experience, rules of thumb in the printer manual and adopt knowledge from literature. The finding of a good drop formation regime can be accomplished faster by investigating the dimensionless numbers and adjusting the ink properties so that the ink lies in printability regime.

7. **Optimization of printing condition (parameters)** – After achieving good drop formation, other parameters should be set. Then it is possible to prepare first set of tested motives, adjust the resolution of printed motives and other parameters.
8. **Analysis and testing** – Testing of expected functional properties of prepared printouts.

9. CONCLUDING SUMMARY

Inkjet printing represents a promising technique for patterning and material deposition simultaneously without need of any master form or masks. However, the printing process depends on the type of inkjet printer as well as on the ink formulation. This Thesis provides description of experience and findings gathered during the work on preparation of water-soluble polymer inkjet ink. Poly(vinyl alcohol) (PVA) was chosen for preparation of the suitable polymer ink for the Dimatix material printer DMP-2800 Series working in drop-on-demand manner. Viscosity, density, and surface tension are generally considered crucial physical properties of each inkjet ink. The main problem of each water-based ink is its high surface tension coming from water. Hydrophilic polymers decrease the surface energy of their solutions however, it was experienced in this case that it was not enough to match the solution with the surface energy of chosen flexible substrate. Another requirement on the ink composition was to keep the formulation as simple as possible, ideally without any additives. Therefore, the ink properties were adjusted by choice of co-solvent system water/DMSO. The polymer solution with the best properties was used for preparation defined patterns on a typical flexible substrate (coated PET foil).

Firstly, the conclusions relating to PVA solution preparation will be summarized. According to empirical experience gained in first performed experiments, the polymer with lower weight-average molecular weight is more suitable for printing than polymer with bigger one. Other important parameter includes the degree of hydrolysis (DH). Although, dissolution of PVA with lower DH in carrier medium was easier than for higher DH, the gel forming tendency of solution avoided the ink being properly ejected through nozzle. Therefore, the almost fully hydrolysed PVA with lower M_w was chosen (Mowiol 4-98, $M_w \sim 27$ kg/mol, DH = (98.0-98.8) %, DP ~ 600). However, SFT of simple aqueous PVA solutions was too high. Addition of an available surfactant was tried without success due to interactions of the surfactant with the polymer (precipitation). Anyway, the use of surfactants was reconsidered and abandoned due to their inevitable residual content in printed material. Therefore, the decrease of SFT was reached via using co-solvent miscible with water. Ethylene glycol was tried in hope it will work as humectant simultaneously, however, its addition increased enormously viscosity of the ink. Ethanol was tried as an alcohol with possibly disinfecting effect and desired decrease of SFT was achieved. Nonetheless, its high volatility resulted into fast nozzle clogging making such solution impracticable. As the last solvent, DMSO was tried because of its capability to modify SFT, serve as a humectant and not increase the viscosity dramatically. The rheological study was performed on both aqueous and solvent based solutions. It was observed, that addition of DMSO into the solvent system influenced SFT of the solutions in a positive manner while viscosity was increased to acceptable

value only. Co-solvent composition water/DMSO (2:1 v/v) was selected as sufficiently performing and having positive implications towards PVA dissolution based on available literature too. Indeed, the mixture showed better solvation effect in comparison with aqueous solutions, which was evaluated according to the Huggins and the Schulz-Blaschke constants obtained by intrinsic viscosity evaluation. The temperature dependence of both viscosity and SFT was also determined because the optimum printing process temperature is not known at the beginning of ink development. Obtained results of analysis of the dependence of viscosity on temperature were in good relation with theoretical behaviour of polymer solutions. The viscosity increased with increasing polymer concentration and the higher temperature, the lower viscosity of solution is observed. Activation energy for viscosity of water based solution was in accordance with literature values, while the values for water/DMSO were obtained for the first time and both the activation energy and interaction parameter were found to be significantly higher which testifies for stronger polymer-solvent as well as for stronger polymer inter- and intramolecular interactions. Within this framework, study of aging and shelf-life of prepared solutions was interpreted. The use of PVA in water/DMSO co-solvent system is limited to three weeks before being deteriorated by microgel formation manifested by turbidity appearance of the ink. If stored longer, the solution may turn to gel. The second most important parameter for ink formulation is its surface tension (SFT) that was characterised for both water and water/DMSO solutions however, detailed study of SFT temperature dependence in the range from 20 to 40 °C was performed for the latter system only as it showed be worthy of choice for further ink development. It was observed that SFT of solutions decreased with increasing temperature generally by 10 mN·m⁻¹ at each solution when the temperature was increased while there was not observed significant trend in dependence on concentration over the tested concentration range. It was found that higher temperature is needed to push SFT towards optimum processing window of printing. On the other hand, viscosity and vapour partial pressure increases with elevated temperatures which may cause processing complications. Therefore, the operating temperature 35 °C was chosen as the best condition.

In the next part of Thesis, the attention was focused on the properties of PVA water/DMSO system at the temperature 35 °C. Results obtained by viscometric and rheological studies were analysed within the mainstream framework which approaches the ink as Newtonian fluid (or just having small deviations from Newtonian behaviour). Dimensionless numbers Re , We , Oh , Ca , Z , and Oh^{-2} ($= La$) were used for characterization of the system with the aim to find proper ink concentration to achieve optimum or at least satisfying quality regime of printing. It must be noted, that so called overall criteria were used, as the characteristic length the nozzle side size was taken into account and no local dimension based calculations were done. Application of dimensionless groupings helps to better understanding of liquid ejection and drop formation which is the key processing step of liquid dispensing and DOD printing. It can be said, that these approaches

are highly developed for Newtonian fluids and have long history. Nevertheless, the main ink printability evaluation schemes (criteria) available from the literature were applied to our dataset and besides finding the best candidate solution concentration for printing also weak sides of these concepts were identified. Definitely, all triad of material-tool-process parameters must be taken into account and the use of material-property only developed approaches is limited, as they do not take fluid velocity into account. The most advanced recent approach of Kim&Baek's Ca vs. We plot mapping of DOD printability regimes [92] was adopted together with their definition of good printability when "a single drop is formed either directly without second pinch-off or the satellite drop merges with the main drop within its travel distance less than 20 times characteristic length forming thus a single drop". However, extension of their original graph was found to be needed by extrapolation towards higher We values to cover both investigated solutions and processing window advised by the printer producer. The processing window of ink material properties and jetting velocity suggested by the printer producer outliers significantly the optimum printing area similarly as experimentally obtained positions for solutions prepared in this study. Nevertheless, good printing was achieved. To understand, why it is possible, main trends and pathways in dependence on variations of prepared inks (viscosity, SFT, density) and change of processing (jetting velocity) parameters were described, while little (but still some) attention was paid to the tool parameter, as the nozzle size is fixed in studied case. It was found that the printing regime map can be replotted in other coordinates with advantage. Re vs. Ca graph covers the Kim&Baek's map [92] but also all criteria derived by their predecessors can be easily plotted into this space and printing regime evaluation systems can be easily compared. Using this plot, it may create feeling that velocity is somewhat cancelled from consideration, however, a series of We isolines and iso- La straight lines conceptualize all necessary pathways in this graph. Reinspection of this newly created graph revealed that the borderlines of optimum printing regime have more or less hyperbolic shape and that they may be roughly approximated by a pair of We number values, i.e. by two We isolines. To remind, Weber number assesses the relative importance of the inertia of the fluid compared to its surface tension. This notice brought attention to the fact, that viscosity could be not necessarily the main parameter governing the ink behaviour from the point of printability but that it is SFT (surface energy) and relaxation time related to surface perturbation which governs the process. Indeed, the Rayleigh timescale does not depend on viscosity of the fluid. It was also observed, that good printability was achieved even fairly beyond the border predicted for viscous liquids in the sense of higher jetting velocities than should work properly. As one may expect, that the polymer solution of composition near to first critical concentration is not purely Newtonian fluid due to hydrodynamic screening and polymer interchain interactions, it was hypothesized that there is possibly another source of relaxation and the only plausible is the elastic energy.

Based on above described consideration of intermediate results, the drop watch camera integrated in the printer was used not only to empirical optimization of pulse driving voltage waveform to generate ink drop but a series of chronophotographic images was taken in order to analyse the process in more depth with the full awareness of the relatively low quality of that optical device. Therefore, the information extracted from the images was used to analysis of the process' dynamics in terms of energy balance and developing a basic scheme of acting forces. All steps of drop formation typical for weakly viscoelastic liquid were captured by the camera. Volume, surface and related surface energy and kinetic energy was obtained from image analysis using replacement of the liquid shapes by simple geometric shapes for dimension quantifications. Velocity of the main drop and the satellite (once formed a sphere) was analysed from the time dependence of position from the nozzle. The kinetic energy of both the main drop and the satellite was calculated and their changes compared with the changes of surface energy. It was concluded that there is a significant yet not prevailing contribution of elastic energy to the recombination of the satellite with the main drop, which is the key of successful printing in the regime when Rayleigh break up occurs. The estimation of the elastic energy contribution has a relatively large error present already in the measurement but increased by its propagation during subtraction, therefore the result is of rather qualitative or semi-quantitative than quantitative character.

The clear evidence for presence of two driving mechanism of the satellite recombination with the main drop was given. Surface tension is the force causing relaxation of perturbed surface (related with the capillary time scale) working against the action of viscosity and the elastic force causes relaxation of tension present in liquids under stress due to interactions of polymer chains at the molecular level (related to the polymer relaxation time). This led to refinement of the dimensionless number evaluation; however, the state of the art of this analytical framework for printing of viscoelastic fluids is much less developed in contemporary literature. First, it must be noted, that adopted approaches using polymer relaxation time calculated according the Zimm theory failed and it must be so, because the Zimm theory was developed for evaluation of the longest relaxation time in infinite diluted polymer solutions only. (In other words, this approach can be useful for printing of trace amounts of polymer.) Instead, it was shown that relaxation time scale calculation based on the Kuhn segment length gives comparable values to those obtained for surface (interface) relaxation. Indeed, the value of Wi indicated the regime when stretched molecules rather than random coils are present in the liquid under stress which again point towards importance of molecular models based on polymer chain reptation. Also the value of El indicated moderate but still not prevailing contribution of elasticity. The relative importance of elastic component of viscoelastic liquid against capillary relaxation may be assessed with the help of plotting De vs. Oh which was conceptualised by McKinley [103]. However, the former approach does not

include process dynamics and uses material-property based criteria only and cancels the Rayleigh timescale from the consideration. The graph was improved by inclusion of El and Ec isolines (although both are again a material-property based grouping). Ec number shows the relative importance of elastic and capillary effects with respect to viscous stresses and El number compares the importance of elastic to inertial effects. In terms of physical quantities, it means, that for given solution, the nozzle dimension can only be varied as El and Ec numbers are quite tightly bound together through three shared parameters. However, sliding along the Ec isoline can be viewed as variation of the Rayleigh timescale as well if the polymer and capillary timescale are kept constant. Indeed, there is less freedom in moves along isolines in the graph than in the similarly appearing one (Re vs. Ca with We and Oh^{-2} isolines) developed for Newtonian fluids in this Thesis. The original McKinley's approach was further developed by Clasen *et al.* [162] who logically added a dynamic (velocity including) number because any dispensing operation can be fully described by any set of two material-property based and one dynamic non-dimensional groups while the remaining groups can be calculated (for example for known Oh , De , and We one obtains $Ca = Oh \cdot We^{1/2}$, $Wi = De \cdot We^{1/2}$, and $Ec = De/Oh$). The investigation was performed over a large range of involved parameters. The price for it is that they created a three dimensional space and their predictions estimate only the transition between dripping and jetting and are too coarse to catch and distinguish various printing modes. Construction of a plot of Oh vs. We or Re vs. Ca with De as a parameter for borderlines between printing regime areas would be therefore highly desirable but is beyond the scope of this Thesis, experimental and numerical techniques, and even time available to the author.

Gathered experience may invoke reconsideration of the initial assumption that viscosity of investigated solutions can be approached by the low shear rate measurements. For weakly viscoelastic liquids, it seems that even such values can be used for evaluation of the system utilising overall dimensionless criteria. However, it is correct to use high shear rate rheometers if available.

In the last step of the work, testing patterns were printed to demonstrate the suitability of prepared ink for printing. A suitable general waveform was proposed for ejection of drops from nozzles of the printing head. However, the voltage at each nozzle was finely modified (tailored) to achieve uniform drop velocity. Other parameters involved the cartridge and substrate temperature, printing height (stand-off), the choice of substrate and its surface energy, and the angle of print-head that is attributed to certain resolution of printed patterns. The patterns were prepared in various shapes from basic elemental patterns (dots, dots array) up to rectangle or grid-shape patterns. The surface morphologies were studied by optical microscopy, AFM and profilometry.

Finally, the experience gathered during the work on this dissertation was embodied into a short step by step summary of practical advices for preparation of polymer based inks.

10. CLOSING REMARKS

10.1 Contribution to Science and Practice

This study performed on exemplary water soluble polymer Poly(vinyl alcohol) contributed to science and practice mainly in following areas:

Properties of PVA solutions in the water/DMSO co-solvent system and its aging were studied and interpreted with respect to the solvent-solvent, solvent-polymer and polymer-polymer interactions on molecular level. The interpretational framework of ink formulation's impact on its printability was enriched in the field of both Newtonian and non-Newtonian fluid analytical approaches although there still remains a wide gap between them. Analysis of causes of recombination of a satellite with the main drop during printing which is one of the conditions for good printability demonstrated the importance of surface relaxation as well as elastic relaxation in the overall assessment, evaluation and development of polymer solution based ink and in engineering and control of printing process. Concepts using the Zimm relaxation time were dismissed in favour of real chain and reptation based models that hold best for parameter ranges applying in DOD printing. As the only future viable approach was identified joining of material-property and characteristic length based criteria including all relevant timescales with a dynamic criterion which includes (jetting) velocity of the fluid as the main parameter describing the printing process.

Other contribution includes the acquirement of useful skills in inkjet technology application, as printing can be considered perspective deposition technique that has already been implemented into various sector of industry. In many cases, the dispersions containing different nano-particles are investigated but there is relatively little number of published papers focused on preparation and characterization of polymer-based patterns and devices, especially based on water-soluble polymer. Therefore, this work described comprehensively the selection, preparation, characterization and deposition of chosen polymer (exemplified on PVA) for their processing by DOD inkjet technology.

Moreover, the work gives practical information and guideline for preparation of polymer solution based inkjet inks. The application potential of prepared inks includes patterning of flexible as well as rigid substrates and controlled modification of their surfaces.

Finally, obtained results of this work were presented in the international scientific journals and conferences and a manuscript covering yet unpublished work is in preparation too.

10.2 Ongoing Research and Future Prospective

In the field of theory

Definition and development of a practical map of printing regimes suitable for (weakly) viscoelastic liquids (namely polymer solutions) will be the paramount of ongoing activity, since the ideal goal has been already defined and prerequisite step stones have been laid. However, there is still a lot to be done to obtain a general evaluation framework applicable for viscoelastic fluids with Newtonian printability map as the limit case. Serious effort has to be spent both in the development of experimental techniques and theoretical work on interpretational framework of dimensionless groupings. A good sign is that all relaxation times playing role in expectable range of liquids for digital DOD printing are of similar magnitude and no extremes will need to be covered.

In the field of applied research

As was demonstrated, the patterns based on PVA were prepared. It is expected the proposed waveform could be used also for other water-soluble polymer-based inkjet inks. Thus, the printability of polyvinylpyrrolidone (PVP) will be investigated in the next step. Moreover, the hitherto gathered knowledge can be utilised effectively to obtain the PVP ink faster as it was in the case of PVA. The PVP can be used as a dielectric layer during preparation of TFT(s) or capacitors. Moreover, it can be cross-linked in more controllable and simpler manner than PVA which represents an important feature for preparation permanent patterns.

Other potential research includes: preparation of permanent patterns from poly(vinyl alcohol) and their resistance tests (resistance to water, adhesion and abrasive tests and other); continuation in preparation and characterization of water-soluble polymer ink for DOD material printing; and preparation, characterization and testing of a new inks depending on the current needs of the research at the Centre of Polymer Materials of the Tomas Bata University in Zlín.

REFERENCES

1. LEACH, R. H., PIERCE, R. J., HICKMAN, E. P., MACKENZIE, M. J. and SMITH, H. G. *The Printing Ink Manual*. 5th. Edition. Dordrecht: Springer Netherlands. 1993. ISBN 978-0-948905-81-0.
2. VISUALY, Inc. *Printing History Timeline* [online]. printcountry.com, October 2012 [cit. 20.7.2016]. Available in: <http://visual.ly/printing-history-timeline>.
3. BOVEY, F. A. and WINSLOW, F. H. Chapter 1 - the Nature of Macromolecules. *In Macromolecules: An introduction to polymer science*. BOVEY, F. A. and WINSLOW, F. H. Eds. New York: Academic Press. 1979. p. 1-21. ISBN 978-0-12-119755-1.
4. HEGEMANN, D., BRUNNER, H. and OEHR, C. Plasma treatment of polymers for surface and adhesion improvement. *Nuclear Instruments & Methods in Physics Research Section B-Beam Interactions with Materials and Atoms*. 2003, vol. 208, p. 281-286. ISSN 0168-583X.
5. SHI, J. X., LI, H. and HE, P. S. Micro- and nano-patterning of polymers. *Chinese Science Bulletin*. 2004, vol. 49, no. 14, p. 1431-1436. ISSN 1001-6538.
6. COENEN, M. J. J., SLAATS, T. M. W. L., EGGENHUISEN, T. M. and GROEN, P. Inkjet printing the three organic functional layers of two-colored organic light emitting diodes. *Thin Solid Films*. 2015, vol. 583, p. 194-200. ISSN 0040-6090.
7. CHEN, C. Inkjet Printing of Microcomponents: Theory, Design, Characteristics and Applications. *In Features of liquid crystal display materials and processes*. KAMANINA, N. V. Eds. InTech. 2011. p. 43. ISBN 978-953-307-899-1.
8. TEKIN, E., SMITH, P. J. and SCHUBERT, U. S. Inkjet printing as a deposition and patterning tool for polymers and inorganic particles. *Soft Matter*. 2008, vol. 4, no. 4, p. 703-713. ISSN 1744-683X.
9. LI, J., ROSSIGNOL, F. and MACDONALD, J. Inkjet printing for biosensor fabrication: combining chemistry and technology for advanced manufacturing. *Lab on a Chip*. 2015, vol. 15, no. 12, p. 2538-2558. ISSN 1473-0197.
10. ANDÒ, B., BAGLIO, S., DI PASQUALE, G., POLLICINO, A., D'AGATA, S., GUGLIUZZO, C., LOMBARDO, C. and RE, G. Euroensors 2015 An

- Inkjet Printed CO₂ Gas Sensor. *Procedia Engineering*. 2015, vol. 120, p. 628-631. ISSN 1877-7058.
11. DANKOCO, M. D., TESFAY, G. Y., BENEVENT, E. and BENDAHAN, M. Temperature sensor realized by inkjet printing process on flexible substrate. *Materials Science and Engineering B-Advanced Functional Solid-State Materials*. 2016, vol. 205, p. 1-5. ISSN 0921-5107.
 12. LI, Y., TORAH, R., BEEBY, S. and TUDOR, J. An all-inkjet printed flexible capacitor on a textile using a new poly(4-vinylphenol) dielectric ink for wearable applications. 2012. p. 2066-2069. ISBN 978-1-4577-1766-6, ISSN 1930-0395.
 13. GRADDAGE, N., CHU, T., DING, H., PY, C., DADVAND, A. and TAO, Y. Inkjet printed thin and uniform dielectrics for capacitors and organic thin film transistors enabled by the coffee ring effect. *Organic Electronics*. 2016, vol. 29, p. 114-119. ISSN 1566-1199.
 14. SIMAITE, A., MESNILGRETE, F., TONDU, B., SOUERES, P. and BERGAUD, C. Towards inkjet printable conducting polymer artificial muscles. *Sensors and Actuators B-Chemical*. 2016, vol. 229, p. 425-433. ISSN 0925-4005.
 15. KWON, J., EOM, S. H., MOON, B. S., SHIN, J., KIM, K., LEE, S. and LEE, Y. Studies on Printing Inks Containing Poly[2-methoxy-5-(2-ethylhexyloxy)-1,4-phenylenevinylene] as an Emissive Material for the Fabrication of Polymer Light-Emitting Diodes by Inkjet Printing. *Bulletin of the Korean Chemical Society*. 2012, vol. 33, no. 2, p. 464-468. ISSN 0253-2964.
 16. VILLANI, F., VACCA, P., NENNA, G., VALENTINO, O., BURRASCA, G., FASOLINO, T., MINARINI, C. and DELLA SALA, D. Inkjet Printed Polymer Layer on Flexible Substrate for OLED Applications. *Journal of Physical Chemistry C*. 2009, vol. 113, no. 30, p. 13398-13402. ISSN 1932-7447.
 17. VOIGT, A., OSTRZINSKI, U., PFEIFFER, K., KIM, J. Y., FAKHFOURI, V., BRUGGER, J. and GRUETZNER, G. New inks for the direct drop-on-demand fabrication of polymer lenses. *Microelectronic Engineering*. 2011, vol. 88, no. 8, p. 2174-2179. ISSN 0167-9317.
 18. DERBY, B. Bioprinting: inkjet printing proteins and hybrid cell-containing materials and structures. *Journal of Materials Chemistry*. 2008, vol. 18, no. 47, p. 5717-5721. ISSN 0959-9428.

19. XU, T., JIN, J., GREGORY, C., HICKMAN, J. J. and BOLAND, T. Inkjet printing of viable mammalian cells. *Biomaterials*. 2005, vol. 26, no. 1, p. 93-99. ISSN 0142-9612.
20. ZHENG, Q., LU, J., CHEN, H., HUANG, L., CAI, J. and XU, Z. Application of inkjet printing technique for biological material delivery and antimicrobial assays. *Analytical Biochemistry*. 2011, vol. 410, no. 2, p. 171-176. ISSN 0003-2697.
21. MOLINA-LOPEZ, F., BRIAND, D. and DE ROOIJ, N. F. Inkjet and microcontact printing of functional materials on foil for the fabrication of pixel-like capacitive vapor microsensors. *Organic Electronics*. 2015, vol. 16, p. 139-147. ISSN 1566-1199.
22. LEE, D., LIM, K., PARK, E., KIM, J. and KIM, Y. Optimized ink-jet printing condition for stable and reproducible performance of organic thin film transistor. *Microelectronic Engineering*. 2013, vol. 111, p. 242-246. ISSN 0167-9317.
23. DE GANS, B. J., DUINEVELD, P. C. and SCHUBERT, U. S. Inkjet printing of polymers: State of the art and future developments. *Advanced Materials*. 2004, vol. 16, no. 3, p. 203-213. ISSN 0935-9648.
24. SOLTMAN, D. and SUBRAMANIAN, V. Inkjet-printed line morphologies and temperature control of the coffee ring effect. *Langmuir*. 2008, vol. 24, no. 5, p. 2224-2231. ISSN 0743-7463.
25. WANG, T., ROBERTS, M. A., KINLOCH, I. A. and DERBY, B. Inkjet printed carbon nanotube networks: the influence of drop spacing and drying on electrical properties. *Journal of Physics D-Applied Physics*. 2012, vol. 45, no. 31, p. 315304. ISSN 0022-3727.
26. TSAI, M. H., HWANG, W. S., CHOU, H. H. and HSIEH, P. H. Effects of pulse voltage on inkjet printing of a silver nanopowder suspension. *Nanotechnology*. 2008, vol. 19, no. 33, p. 335304. ISSN 0957-4484.
27. MARTIN, G. D., HOATH, S. D. and HUTCHINGS, I. M. Inkjet printing - the physics of manipulating liquid jets and drops. *Engineering and Physics - Synergy for Success*. 2008, vol. 105, p. 012001. ISSN 1742-6588.
28. HUDD, A. Inkjet Printing Technologies. *In The chemistry of inkjet inks*. MAGDASSI, S. Eds. Singapore: World Scientific. 2010. p. 3-18. ISBN 978-981-281-821-8.

29. MARTIN, G. D. and HUTCHINGS, I. M. Fundamentals of Inkjet Technology. *In Inkjet technology for digital fabrication. HUTCHINGS, I. M. and MARTIN, G. D. Eds.* Chichester, West Sussex, United Kingdom: Wiley. 2013. p. 21-44. ISBN 978-0-470-68198-5.
30. ORLANDINI, J. O., NIESSEN, V., SCHAPER, J. N., PETERSEN, J. H. and BINGS, N. H. Development and characterization of a thermal inkjet-based aerosol generator for micro-volume sample introduction in analytical atomic spectrometry. *Journal of Analytical Atomic Spectrometry.* 2011, vol. 26, no. 9, p. 1781-1789. ISSN 0267-9477.
31. MORITA, N. Thermal Inkjet. *In Inkjet-based micromanufacturing. KORVINK, J. G., SMITH, P. J. and SHIN, D. -. Eds.* Weinheim, Germany: Wiley-VCH Verlag GmbH & Co. KGaA. 2012. p. 41-56. ISBN 9783527647101.
32. SETTI, L., FRALEONI-MORGERA, A., MENCARELLI, I., FILIPPINI, A., BALLARIN, B. and DI BIASE, M. An HRP-based amperometric biosensor fabricated by thermal inkjet printing. *Sensors and Actuators B-Chemical.* 2007, vol. 126, no. 1, p. 252-257. ISSN 0925-4005.
33. SETTI, L., FRALEONI-MORGERA, A., BALLARIN, B., FILIPPINI, A., FRASCARO, D. and PIANA, C. An amperometric glucose biosensor prototype fabricated by thermal inkjet printing. *Biosensors & Bioelectronics.* 2005, vol. 20, no. 10, p. 2019-2026. ISSN 0956-5663.
34. CUI, X. and BOLAND, T. Human microvasculature fabrication using thermal inkjet printing technology. *Biomaterials.* 2009, vol. 30, no. 31, p. 6221-6227. ISSN 0142-9612.
35. XU, T., GREGORY, C. A., MOLNAR, P., CUI, X., JALOTA, S., BHADURI, S. B. and BOLAND, T. Viability and electrophysiology of neural cell structures generated by the inkjet printing method. *Biomaterials.* 2006, vol. 27, no. 19, p. 3580-3588. ISSN 0142-9612.
36. VIJAYA, M. S. *Piezoelectric Materials and Devices: Applications in Engineering and Medical Sciences.* Boca Raton: CRC Press, 2013. ISBN 978-1439887868.
37. WIJSHOFF, H. Cross Talk in Piezo Inkjet. *In Inkjet-based micromanufacturing. KORVINK, J. G., SMITH, P. J. and SHIN, D. -. Eds.* Weinheim, Germany: Wiley-VCH Verlag GmbH & Co. KGaA. 2012. p. 73-86. ISBN 978-3-527-64710-1.

38. YOSHIMURA, K., KISHIMOTO, M. and SUEMUNE, T. *Inkjet Printing Technology*. OKI Technical Review: Oki Electric Industry Co., Ltd., 1998 [cit. 28.6.2016]. Available in: <http://www.oki.com/en/otr/downloads/otr-161-10.pdf>.
39. Anonymous. *FUJIFILM Dimatix Materials Printer DMP-2800 Series User Manual*. User Manual ed. U.S.A.: FUJIFILM Dimatix, Inc., 2010.
40. YAMAGUCHI, S., UENO, A., AKIYAMA, Y. and MORISHIMA, K. Cell patterning through inkjet printing of one cell per droplet. *Biofabrication*. 2012, vol. 4, no. 4, p. 045005. ISSN 1758-5082.
41. CUMMINS, G., KAY, R., TERRY, J., DESMULLIEZ, M. P. Y. and WALTON, A. J. *Optimization and characterization of drop-on-demand inkjet printing process for platinum organometallic inks*. Singapore IEEE 13th Electronics Packaging Technology Conference 2011. p. 256-261. ISBN 978-1-4577-1982-0. Available in: <http://ieeexplore.ieee.org/xpl/articleDetails.jsp?arnumber=6184427>.
42. GAN, H. Y., SHAN, X., ERIKSSON, T., LOK, B. K. and LAM, Y. C. Reduction of droplet volume by controlling actuating waveforms in inkjet printing for micro-pattern formation. *Journal of Micromechanics and Microengineering*. 2009, vol. 19, no. 5, p. 055010. ISSN 0960-1317.
43. LIU, Y., PAI, Y., TSAI, M. and HWANG, W. Investigation of driving waveform and resonance pressure in piezoelectric inkjet printing. *Applied Physics A-Materials Science & Processing*. 2012, vol. 109, no. 2, p. 323-329. ISSN 0947-8396.
44. KIM, S., SUNG, J. and LEE, M. H. *Development of inkjet nozzle driven by double piezo actuators*. Minsk, Belarus. 15th International Symposium on Flow Visualization 2012 [cit. 30.6.2016]. Available in: <http://itmo.by/pdf/isfv/ISFV15-063.pdf>.
45. KIM, Y., SON, S., CHOI, J., BYUN, D. and LEE, S. Design and Fabrication of Electrostatic Inkjet Head using Silicon Micromachining Technology. *Journal of Semiconductor Technology and Science*. 2008, vol. 8, no. 2, p. 121-127. ISSN 1598-1657.
46. KAWAMOTO, H. *Electronic circuit printing, 3D printing and film formation utilizing electrostatic inkjet technology*. Anchorage, AK NIP 23, 23rd International Conference on Digital Printing Technologies, and Digital Fabrication 2007. Society for Imaging Science and Technology 2007. p. 961-964.

47. CHOI, J., KIM, Y., SON, S. U., KIM, Y., NGUYEN, V. D., LEE, S., BYUN, D. and KO, H. S. *Electrostatic induced inkjet printing system for micro patterning and drop-on-demand jetting characteristics*. United States: CRC Press 2008. p. 277-280. ISBN 978-1-4200-8505-1. . Available in: <http://www.nsti.org/publications/Nanotech/2008/pdf/1015.pdf>.
48. KAMYSHNY, A. and MAGDASSI, S. Inkjet Ink Formulations. *In Inkjet-based micromanufacturing*. KORVINK, J. G., SMITH, P. J. and SHIN, D. -. Eds. Weinheim, Germany: Wiley-VCH Verlag GmbH & Co. KGaA. 2012. p. 173-190. ISBN 9783527647101.
49. PEKAROVICOVA, A., BHIDE, H., FLEMING, P. D. and PEKAROVIC, J. Phase-change inks. *Journal of Coatings Technology*. 2003, vol. 75, no. 936, p. 65-72. ISSN 0361-8773.
50. YEATES, S. G., XU, D., MADEC, M. -, CARAS-QUINTERO, D., ALAMRY, K. A., MALANDRAKI, A. and SANCHEZ-ROMAGUERA, V. Fluids for Inkjet Printing. *In Inkjet technology for digital fabrication*. HUTCHINGS, I. M. and MARTIN, G. D. Eds. Chichester, West Sussex, United Kingdom: Wiley. 2013. p. 87-112. ISBN 978-0-470-68198-5.
51. KUSCER, D., STAVBER, G., TREFALT, G. and KOSEC, M. Formulation of an Aqueous Titania Suspension and its Patterning with Ink-Jet Printing Technology. *Journal of the American Ceramic Society*. 2012, vol. 95, no. 2, p. 487-493. ISSN 0002-7820.
52. JEONG, S., SONG, H. C., LEE, W. W., LEE, S. S., CHOI, Y., SON, W., KIM, E. D., PAIK, C. H., OH, S. H. and RYU, B. Stable Aqueous Based Cu Nanoparticle Ink for Printing Well-Defined Highly Conductive Features on a Plastic Substrate. *Langmuir*. 2011, vol. 27, no. 6, p. 3144-3149. ISSN 0743-7463.
53. LIU, Z., SU, Y. and VARAHRAMYAN, K. Inkjet-printed silver conductors using silver nitrate ink and their electrical contacts with conducting polymers. *Thin Solid Films*. 2005, vol. 478, no. 1–2, p. 275-279. ISSN 0040-6090.
54. Hewlett-Packard Company. *Water based ink for ink-jet printing*. MEICHSNER, R. and SCHMICKL, W. Int. Cl.: 009D 11/02, U.S. Cl.:106/22 K; 106/20 D. US5183502 A. Available in: <https://www.google.com/patents/US5183502> .
55. ADVANCED PRODUCTS, Inc. *Water-based polymer thick film conductive ink*. BUCKLEY, M. S. and BOWNS, R. E. Int. Cl.:H01B 1/00; H01B 1/20; H01B 1/22; H01B 1/24; U.S. Cl.: 252/502; 252/511; 252/512; 252/514;

- 252/518; 106/ 1.18; 106/1.25; 524/501; 524/503. US5286415 A. Available in: <https://www.google.com/patents/US5286415> .
56. ANGELO, P. D., KRONFLI, R. and FARNOOD, R. R. Synthesis and inkjet printing of aqueous ZnS:Mn nanoparticles. *Journal of Luminescence*. 2013, vol. 136, p. 100-108. ISSN 0022-2313.
57. KAMYSHNY, A., BEN-MOSHE, M., AVIEZER, S. and MAGDASSI, S. Ink-jet printing of metallic nanoparticles and microemulsions. *Macromolecular Rapid Communications*. 2005, vol. 26, no. 4, p. 281-288. ISSN 1022-1336.
58. SAMUEL, J. and EDWARDS, P. Solvent-Based Inkjet Inks. *In The chemistry of inkjet inks*. MAGDASSI, S. Eds. Singapore: World Scientific. 2010. p. 141-160. ISBN 978-981-281-821-8.
59. Kiiian S.p.A. *Solvent Based Inkjet Ink Formulation*. VANINI, C. Int. Cl.: C09D 11/00; U.S. Cl.: 347/100; 106/31.13. US7950794 B2. Available in: <https://www.google.com/patents/US7950794> .
60. Markem-Image Corporation. *Solvent-based inkjet ink formulations*. BROWN, B. J., WOUDEBERG, R. C., LARSON JR, R. J., BENJAMIN, A. and WILLIAMS, C. Int. Cl.: B41J 2/015; C08L 33/08; C08L 61/00; C08L 71/10; U.S. Cl.: 347/20; 524/556; 524/592; 524/611. US20110012954 A1. Available in: <http://www.google.com/patents/US20110012954> .
61. CHOVANCOVA, V., PEKAROVICOVA, A. and FLEMING, P. *Hot melt inks for 3D printing*. Baltimore, MD: 21st International Conference on Digital Printing Technologies (NIP21) / International Conference on Digital Fabrication Technologies. Soc Imaging Sci & Technol, Imaging Soc Japan 2005. p. 147. ISBN 0-89208-258-5.
62. ZHAI, D., ZHANG, T., GUO, J., FANG, X. and WEI, J. Water-based ultraviolet curable conductive inkjet ink containing silver nano-colloids for flexible electronics. *Colloids and Surfaces A-Physicochemical and Engineering Aspects*. 2013, vol. 424, p. 1-9. ISSN 0927-7757.
63. KARIM, M. N., AFROJ, S., RIGOUT, M., YEATES, S. G. and CARR, C. Towards UV-curable inkjet printing of biodegradable poly (lactic acid) fabrics. *Journal of Materials Science*. 2015, vol. 50, no. 13, p. 4576-4585. ISSN 0022-2461.

64. MAGDASSI, S. Ink Requirements and Formulation Guidelines. *In The chemistry of inkjet inks*. MAGDASSI, S. Eds. Singapore: World Scientific. 2010. p. 19-42. ISBN 978-981-281-821-8.
65. SOCHI, T. Flow of Non-Newtonian Fluids in Porous Media. *Journal of Polymer Science Part B-Polymer Physics*. 2010, vol. 48, no. 23, p. 2437-2467. ISSN 0887-6266.
66. AKAY, M. *Introduction to Polymer Science and Technology*. Mustafa Akay & Ventus Publishing ApS, 2012. 269 p. ISBN 978-87-4030-087-1.
67. PRAMANIK, S. Casson fluid flow and heat transfer past an exponentially porous stretching surface in presence of thermal radiation. *Ain Shams Engineering Journal*. 2014, vol. 5, no. 1, p. 205-212. ISSN 2090-4479.
68. AL-SHAMMARI, B., AL-FARISS, T., AL-SEWAILM, F. and ELLEITHY, R. The effect of polymer concentration and temperature on the rheological behavior of metallocene linear low density polyethylene (mLLDPE) solutions. *Journal of King Saud University - Engineering Sciences*. 2011, vol. 23, no. 1, p. 9-14. ISSN 1018-3639.
69. MUNOZ, J., RINCON, F., ALFARO, M. C., ZAPATA, I., DE LA FUENTE, J., BELTRAN, O. and DE PINTO, G. L. Rheological properties and surface tension of Acacia tortuosa gum exudate aqueous dispersions. *Carbohydrate Polymers*. 2007, vol. 70, no. 2, p. 198-205. ISSN 0144-8617.
70. DUAN, X., XU, J., HE, B., LI, J. and SUN, Y. Preparation and Rheological Properties of Cellulose/chitosan Homogeneous Solution in Ionic Liquid. *Bioresources*. 2011, vol. 6, no. 4, p. 4640-4651. ISSN 1930-2126.
71. MORA, A., SKURTYYS, O. and OSORIO, F. Rheological Characterization of Polyoxyethylene (POE) and Carboxymethyl Cellulose (CMC) Suspensions with Added Solids. *1st International Conference on Rheology and Modeling of Materials (Ic-Rmm1)*. 2015, vol. 602, p. 012013. ISSN 1742-6588.
72. MONKOS, K. Viscosity analysis of the temperature dependence of the solution conformation of ovalbumin. *Biophysical Chemistry*. 2000, vol. 85, no. 1, p. 7-16. ISSN 0301-4622.
73. OLIVEIRA, J., BRICHI, G. S., MARCONCINI, J. M., CAPPARELLI MATTOSO, L. H., GLENN, G. M. and MEDEIROS, E. S. Effect of Solvent on The Physical and Morphological Properties of Poly(Lactic Acid) Nanofibers Obtained by Solution Blow Spinning. *Journal of Engineered Fibers and Fabrics*. 2014, vol. 9, no. 4, p. 117-125. ISSN 1558-9250.

74. GONZALEZTELLO, P., CAMACHO, F. and BLAZQUEZ, G. Density and Viscosity of Concentrated Aqueous-Solutions of Polyethylene-Glycol. *Journal of Chemical and Engineering Data*. 1994, vol. 39, no. 3, p. 611-614. ISSN 0021-9568.
75. JAKUBKA, F., SCHIESSL, S. P., MARTIN, S., ENGLERT, J. M., HAUKE, F., HIRSCH, A. and ZAUMSEIL, J. Effect of Polymer Molecular Weight and Solution Parameters on Selective Dispersion of Single-Walled Carbon Nanotubes. *Acs Macro Letters*. 2012, vol. 1, no. 7, p. 815-819. ISSN 2161-1653.
76. SPERLING, L. H. *Introduction to Physical Polymer Science*. 4th. Hoboken, New Jersey: Wiley, 2006. 613-686 p. ISBN 978-0-471-70606-9.
77. GILLES, K. B. Rheology and Surface Chemistry. In *Coatings technology handbook*. TRACTON, A. A. Eds. 3rd. Boca Raton, Florida: CRC Press. 2005. ISBN 978-1-4200-2732-7.
78. KRONBERG, B., HOLMBERG, K. and LINDMAN, B. *Surface Chemistry of Surfactants and Polymers*. Chichester, West Sussex, United Kingdom: Wiley, 2014. ISBN 978-1-119-96124-6.
79. MAZANDARANI, M. T., ELIASSI, A. and FAZLOLLAHNEJAD, M. *Experimental data and correlation of surface tension of binary polymer solutions at different temperatures and atmospheric pressure*. Copenhagen European Congress of Chemical Engineering (ECCE-6) 2007. Available in: http://www.nt.ntnu.no/users/skoge/prost/proceedings/ecce6_sep07/upload/1745.pdf.
80. VARGAFTIK, N., VOLKOV, B. and VOLJAK, L. International Tables of the Surface-Tension of Water. *Journal of Physical and Chemical Reference Data*. 1983, vol. 12, no. 3, p. 817-820. ISSN 0047-2689.
81. BRUNCHI, C., BERCEA, M., MORARIU, S. and DASCALU, M. Some properties of xanthan gum in aqueous solutions: effect of temperature and pH. *Journal of Polymer Research*. 2016, vol. 23, no. 7, p. 1-8.
82. BLANCO, L. H., VARGAS, O. M. and SUAREZ, A. F. Effect of temperature on the density and surface tension of aqueous solutions of HMT. *Journal of Thermal Analysis and Calorimetry*. 2011, vol. 104, no. 1, p. 101-104. ISSN 1388-6150.
83. MOHAMMAD, A. A., ALKHALDI, K. H. A. E., ALTUWAIM, M. S. and AL-JIMAZ, A. S. Effect of temperature and chain length on the viscosity and

- surface tension of binary systems of N,N-dimethylformamide with 1-octanol, 1-nonanol and 1-decanol. *Journal of Chemical Thermodynamics*. 2014, vol. 74, p. 7-15. ISSN 0021-9614.
84. ABBAS, K., IRAM, B., SEEMAB, P., KHALID, M., MOHAMMAD, S. and MOHAMMAD, S. Surface tension, density and viscosity studies on the associative behaviour of oxyethylene-oxybutylene diblock copolymers in water at different temperatures. *International Journal of Organic Chemistry*. 2012, vol. 2, no. 1, p. 82-92. ISSN 2161-4695.
85. KHAN, M. Y., SAMANTA, A., OJHA, K. and MANDAL, A. Interaction between aqueous solutions of polymer and surfactant and its effect on physicochemical properties. *Asia-Pacific Journal of Chemical Engineering*. 2008, vol. 3, no. 5, p. 579-585. ISSN 1932-2143.
86. STAMM, M. Polymer Surface and Interface Characterization Techniques. *In Polymer surfaces and interfaces: Characterization, modification and applications*. STAMM, M. Eds. 1st. Berlin, Heidelberg: Springer. 2008. p. 1-16. ISBN 978-3-540-73864-0.
87. NODA, I. Surface-Hydrophilic Elastomers. *In Polymer solutions, blends, and interfaces*. NODA, I. and RUBINGH, D. N. Eds. Amsterdam, The Netherlands: Elsevier. 1992. p. 1-22. ISBN 0-444-89397-0.
88. YUAN, Y. and LEE, T. R. Contact Angle and Wetting Properties. *In Surface science techniques*. BRACCO, G. and HOLST, B. Eds. Berlin, Heidelberg: Springer. 2013. p. 3-34. ISBN 978-3-642-34242-4.
89. MORRISON, N. F. and HARLEN, O. G. Viscoelasticity in inkjet printing. *Rheologica Acta*. 2010, vol. 49, no. 6, p. 619-632. ISSN 0035-4511.
90. TULADHAR, T. R. and MACKLEY, M. R. Filament stretching rheometry and break-up behaviour of low viscosity polymer solutions and inkjet fluids. *Journal of Non-Newtonian Fluid Mechanics*. 2008, vol. 148, no. 1-3, p. 97-108. ISSN 0377-0257.
91. RAYLEIGH, L. On the instability of jets. *Proceedings of the London Mathematical Society*. 1878, vol. 1, no. 1, p. 4-13.
92. KIM, E. and BAEK, J. Numerical study on the effects of non-dimensional parameters on drop-on-demand droplet formation dynamics and printability range in the up-scaled model. *Physics of Fluids*. 2012, vol. 24, no. 8, p. 082103. ISSN 1070-6631.

93. HARTMAN, R., BRUNNER, D., CAMELOT, D., MARIJNISSEN, J. and SCARLETT, B. Jet break-up in electrohydrodynamic atomization in the cone-jet mode. *Journal of Aerosol Science*. 2000, vol. 31, no. 1, p. 65-95. ISSN 0021-8502.
94. DONG, H., CARR, W. W. and MORRIS, J. F. An experimental study of drop-on-demand drop formation. *Physics of Fluids*. 2006, vol. 18, no. 7, p. 072102. ISSN 1070-6631.
95. JANG, D., KIM, D. and MOON, J. Influence of Fluid Physical Properties on Ink-Jet Printability. *Langmuir*. 2009, vol. 25, no. 5, p. 2629-2635. ISSN 0743-7463.
96. DERBY, B. Inkjet Printing of Functional and Structural Materials: Fluid Property Requirements, Feature Stability, and Resolution. *Annual Review of Materials Research*. 2010, vol. 40, p. 395-414. ISSN 1531-7331.
97. FROMM, J. E. Numerical-Calculation of the Fluid-Dynamics of Drop-On-Demand Jets. *Ibm Journal of Research and Development*. 1984, vol. 28, no. 3, p. 322-333. ISSN 0018-8646.
98. REIS, N. and DERBY, B. Ink jet deposition of ceramic suspensions: Modelling and experiments of droplet formation. *Solid Freeform and Additive Fabrication-2000*. 2000, vol. 625, p. 117-122. ISSN 0272-9172.
99. McKINLEY, G. H. and RENARDY, M. Wolfgang von Ohnesorge. *Physics of Fluids*. 2011, vol. 23, no. 12, p. 127101. ISSN 1070-6631.
100. NALLAN, H. C., SADIE, J. A., KITSOMBOONLOHA, R., VOLKMAN, S. K. and SUBRAMANIAN, V. Systematic Design of Jettable Nanoparticle-Based Inkjet Inks: Rheology, Acoustics, and Jettability. *Langmuir*. 2014, vol. 30, no. 44, p. 13470-13477. ISSN 0743-7463.
101. MUN, R., BYARS, J. and BOGER, D. The effects of polymer concentration and molecular weight on the breakup of laminar capillary jets. *Journal of Non-Newtonian Fluid Mechanics*. 1998, vol. 74, no. 1-3, p. 285-297. ISSN 0377-0257.
102. DE GANS, B., XUE, L., AGARWAL, U. and SCHUBERT, U. Ink-jet printing of linear and star polymers. *Macromolecular Rapid Communications*. 2005, vol. 26, no. 4, p. 310-314. ISSN 1022-1336.
103. McKINLEY, G. H. Dimensionless groups for understanding free surface flows of complex fluids. *Soc.Rheol.Bull*. 2005, vol. 2005, p. 6-9.

104. VADILLO, D. C., TULADHAR, T. R., MULJI, A. C., JUNG, S., HOATH, S. D. and MACKLEY, M. R. Evaluation of the inkjet fluid's performance using the "Cambridge Trimaster" filament stretch and break-up device. *Journal of Rheology*. 2010, vol. 54, no. 2, p. 261-282. ISSN 0148-6055.
105. ARNOLDS, O., BUGGISCH, H., SACHSENHEIMER, D. and WILLENBACHER, N. Capillary breakup extensional rheometry (CaBER) on semi-dilute and concentrated polyethyleneoxide (PEO) solutions. *Rheologica Acta*. 2010, vol. 49, no. 11-12, p. 1207-1217. ISSN 0035-4511.
106. WHEELER, J. S. R. and YEATES, S. G. Polymers in Inkjet Printing. *In Fundamentals of inkjet printing: The science of inkjet and droplets*. HOATH, S. D. Eds. First. Weinheim: Wiley-VCH Verlag GmbH & Co. KGaA. 2016. p. 117-140. ISBN 978-3-527-33785-9.
107. DEGENNES, P. Coil-Stretch Transition of Dilute Flexible Polymers Under Ultrahigh Velocity-Gradients. *Journal of Chemical Physics*. 1974, vol. 60, no. 12, p. 5030-5042. ISSN 0021-9606.
108. BAZILEVSKII, A. V., MEYER, J. D. and ROZHKOVA, A. N. Dynamics and Breakup of Pulse Microjets of Polymeric Liquids. *Fluid Dynamics*. 2005, vol. 40, no. 3, p. 376-392. ISSN 0015-4628.
109. EBEWELE, R. O. and EBEWELE, R. O. *Polymer science and technology*. Boca Raton: CRC press, 2000. ISBN 9781420057805.
110. REINER, M. The Deborah number. *Physics Today*. 1964, vol. 17, no. 1, p. 62.
111. SAKAGUCHI, Y., SAWADA, Z., KOIZUMI, M. and TAMAKI, K. Effect of the Kind of Bases on Hydrolysis Rate of Polyvinyl Acetate. *Kobunshi Kagaku*. 1966, vol. 23, no. 260, p. 890-894.
112. MARIN, E., ROJAS, J. and CIRO, Y. A review of polyvinyl alcohol derivatives: Promising materials for pharmaceutical and biomedical applications. *African Journal of Pharmacy and Pharmacology*. 2014, vol. 8, no. 24, p. 674-684.
113. KHANA, K., NTHOIWA, M., DIAZ, C. A. and CHAUDHARI, Y. Vinyl Alcohol Polymers. *In Handbook of thermoplastic, second edition*. OLABISI, O. and ADEWALE, K. Eds. Boca Raton: CRC Press. 2015. p. 53-88. ISBN 978-1-4665-7722-0.

114. ROWE, R. C., SHESKEY, P. J. and QUINN, M. E. *Handbook of Pharmaceutical Excipients*. 6th. Edition. London: Pharmaceutical Press. 2009. ISBN 9780853697923.
115. YUN, Y. H., KIM, J. D., LEE, B. K., CHO, Y. W. and LEE, H. Y. Polymer Inkjet Printing: Construction of Three-Dimensional Structures at Micro-Scale by Repeated Lamination. *Macromolecular Research*. 2009, vol. 17, no. 3, p. 197-202. ISSN 1598-5032.
116. SALAORU, I., ZHOU, Z., MORRIS, P. and GIBBONS, G. J. Inkjet printing of polyvinyl alcohol multilayers for additive manufacturing applications. *Journal of Applied Polymer Science*. 2016, vol. 133, no. 25, p. 43572. ISSN 0021-8995.
117. FINCH, C. A. *Polyvinyl Alcohol - Developments*. 2nd. Edition. Wiley. 1992.
118. ENDRES, H. and SIEBERT-RATHS, A. Engineering Property Profiles of Biopolymers. In *Engineering biopolymers*. ENDRES, H. and SIEBERT-RATHS, A. Eds. Hanser. 2011. p. 149-224. ISBN 9783446424036.
119. BAKER, M. I., WALSH, S. P., SCHWARTZ, Z. and BOYAN, B. D. A review of polyvinyl alcohol and its uses in cartilage and orthopedic applications. *Journal of Biomedical Materials Research Part B-Applied Biomaterials*. 2012, vol. 100B, no. 5, p. 1451-1457. ISSN 1552-4973.
120. MARTEN, F. L. Vinyl Alcohol Polymers. In *Kirk-othmer encyclopedia of chemical technology*. John Wiley & Sons, Inc. 2000. ISBN 9780471238966.
121. MARTEN, F. L. Vinyl Alcohol Polymers. In *Encyclopedia of polymer science and technology*. John Wiley & Sons, Inc. 2002. ISBN 9780471440260.
122. SMALLWOOD, I. M. *Handbook of organic solvent properties*. London, Great Britain: ARNOLD, 1996. ISBN 0-340-64578-4.
123. SPEIGHT, J. G. *Lange's Handbook of Chemistry*. 16th, 70th anniversary ed. New York, United States: McGraw-Hill, 2005. ISBN 0-07-143220-5.
124. VOHLIDAL, J., STULIK, K. and JULAK, A. *Chemicke a analytické tabulky*. (Chemical and analytical tables, in Czech). Praha: Grada, 1999. ISBN 80-7169-855-5.
125. SULY, P., KRČMAR, P., MASLÍK, J., URBANEK, P. and KURITKA, I. Poly(vinyl alcohol): Formulation of a Polymer Ink for the Patterning of

- Substrates with a Drop-On-Demand Inkjet Printer. *Materiali in Tehnologije*. 2017, vol. 51, no. 1, p. 41-48. ISSN 1580-2949.
126. AL-FARISS, T. and AL-ZAHRANI, S. Rheological behaviour of some dilute polymer solutions. *Engineering Sciences*. 1993, vol. 5, no. 1, p. 95-109.
127. WANG, X., CARR, W. W., BUCKNALL, D. G. and MORRIS, J. F. High-shear-rate capillary viscometer for inkjet inks. *Review of Scientific Instruments*. 2010, vol. 81, no. 6, p. 065106. ISSN 0034-6748.
128. DAKHIL, H. and WIERSCHEM, A. Measuring Low Viscosities and High Shear Rates with a Rotational Rheometer in a Thin-Gap Parallel-Disk Configuration. *Applied Rheology*. 2014, vol. 24, no. 6, p. 10-15. ISSN 1430-6395.
129. PAN, L. and ARRATIA, P. E. A high-shear, low Reynolds number microfluidic rheometer. *Microfluidics and Nanofluidics*. 2013, vol. 14, no. 5, p. 885-894. ISSN 1613-4982.
130. NIE, X., WANG, H. and ZOU, J. Inkjet printing of silver citrate conductive ink on PET substrate. *Applied Surface Science*. 2012, vol. 261, p. 554-560. ISSN 0169-4332.
131. LAMONT, C. A., EGGENHUISEN, T. M., COENEN, M. J. J., SLAATS, T. W. L., ANDRIESSEN, R. and GROEN, P. Tuning the viscosity of halogen free bulk heterojunction inks for inkjet printed organic solar cells. *Organic Electronics*. 2015, vol. 17, p. 107-114. ISSN 1566-1199.
132. DRABKOVA, S. *Mechanika Tekutin (Fluid Mechanics, in Czech)*. 1st. Edition. Ostrava: VSB - Technicka univerzita Ostrava. 2007. ISBN 978-80-248-1508-4.
133. NAKAYAMA, Y. *Introduction to Fluid Mechanics*. BOUCHER, R. F. Ser. Ed. Oxford: Butterworth-Heinemann. 1999. ISBN 0340676493.
134. YIANNOURAKOU, M., ROUSSEAU, B., PANNACCI, N. and HERZHAFT, B. Rheological behavior of aqueous polyacrylamide solutions determined by dissipative particle dynamics and comparison to experiments. *Epl*. 2012, vol. 97, no. 3, p. 34007. ISSN 0295-5075.
135. PIPE, C. J., MAJMUDAR, T. S. and McKINLEY, G. H. High shear rate viscometry. *Rheologica Acta*. 2008, vol. 47, no. 5-6, p. 621-642. ISSN 0035-4511.

136. GALINDO-ROSALES, F. J., ALVES, M. A. and OLIVEIRA, M. S. N. Microdevices for extensional rheometry of low viscosity elastic liquids: a review. *Microfluidics and Nanofluidics*. 2013, vol. 14, no. 1-2, p. 1-19. ISSN 1613-4982.
137. International Union of Pure and Applied Chemistry. Commission on Macromolecular Nomenclature. *Compendium of Macromolecular Nomenclature*. METANOMSKI, W. V. Ser. Ed. Oxford: Blackwell Scientific. 1991. ISBN 0632028467.
138. LĂMĂȚIC, I., BERCEA, M. and MORARIU, S. Intrinsic viscosity of aqueous polyvinyl alcohol solutions. *Revue Roumaine De Chimie*. 2009, vol. 54, no. 11-12, p. 981-986.
139. WANG, B. Viscometric, light scattering, and size-exclusion chromatography studies on the structural changes of aqueous poly(vinyl alcohol) induced by γ -ray irradiation. *Journal of Polymer Science. Part B, Polymer Physics*. 2000, vol. 38, no. 1, p. 214-221. ISSN 0887-6266.
140. TACX, J. C. J. F., SCHOFFELEERS, H. M., BRANDS, A. G. M. and TEUWEN, L. Dissolution behavior and solution properties of polyvinylalcohol as determined by viscometry and light scattering in DMSO, ethyleneglycol and water. *Polymer*. 2000, vol. 41, no. 3, p. 947-957. ISSN 0032-3861.
141. HUGGINS, M. L. The Viscosity of Dilute Solutions of Long-Chain Molecules. IV. Dependence on Concentration. *Journal of the American Chemical Society*. 1942, vol. 64, no. 11, p. 2716-2718. ISSN 0002-7863.
142. SCHULZ, G. V. and BLASCHKE, F. Eine Gleichung zur Berechnung der Viscositätszahl für sehr kleine Konzentrationen, [Molekulargewichtsbestimmungen an makromolekularen Stoffen, IX]. *Journal Für Praktische Chemie*. 1941, vol. 158, no. 1-8, p. 130-135. ISSN 0021-8383.
143. KRAEMER, E. O. Molecular Weights of Celluloses and Cellulose Derivates. *Industrial & Engineering Chemistry*. 1938, vol. 30, no. 10, p. 1200-1203. ISSN 0019-7866.
144. HELLER, W. Treatment of viscosity data on polymer solutions (an analysis of equations and procedures). *Journal of Colloid Science*. 1954, vol. 9, no. 6, p. 547-573. ISSN 0095-8522.

145. LEWANDOWSKA, K., STASZEWSKA, D. U. and BOHDANECKY, M. The Huggins viscosity coefficient of aqueous solution of poly(vinyl alcohol). *European Polymer Journal*. 2001, vol. 37, no. 1, p. 25-32. ISSN 0014-3057.
146. SCHOFF, C. K. Concentration Dependence of the Viscosity of Dilute Polymer Solutions: Huggins and Schulz-Blaschke Constants. In *Polymer handbook*. BRANDRUP, J., IMMERGUT, E. H., GRULKE, E. A., ABE, A. and BLOCH, D. R. Eds. 4th. New York, United States: Wiley. 1999. p. VII/265. ISBN 0-471-16628-6.
147. ABDEL-AZIM, A. A. A., ATTA, A. M., FARAHAT, M. S. and BOUTROS, W. Y. Determination of intrinsic viscosity of polymeric compounds through a single specific viscosity measurement. *Polymer*. 1998, vol. 39, no. 26, p. 6827-6833. ISSN 0032-3861.
148. VOLLMERT, B. *Grundriss der Makromolekularen Chemie*. Berlin Heidelberg GMBH: Springer-Verlag, 1962. ISBN 978-3-662-23601-7.
149. WONG, D. B., SOKOLOWSKY, K. P., EL-BARGHOUTHI, M. I., FENN, E. E., GIAMMANCO, C. H., STURLAUGSON, A. L. and FAYER, M. D. Water Dynamics in Water/DMSO Binary Mixtures. *Journal of Physical Chemistry B*. 2012, vol. 116, no. 18, p. 5479-5490. ISSN 1520-6106.
150. WRIGHT, E. J., ANDREWS, G. P., McCOY, C. P. and JONES, D. S. The effect of dilute solution properties on poly(vinyl alcohol) films. *Journal of the Mechanical Behavior of Biomedical Materials*. 2013, vol. 28, p. 222-231. ISSN 1751-6161.
151. GUPTA, P., ELKINS, C., LONG, T. and WILKES, G. Electrospinning of linear homopolymers of poly(methyl methacrylate): exploring relationships between fiber formation, viscosity, molecular weight and concentration in a good solvent. *Polymer*. 2005, vol. 46, no. 13, p. 4799-4810. ISSN 0032-3861.
152. RWEI, S. and HUANG, C. Electrospinning PVA solution-rheology and morphology analyses. *Fibers and Polymers*. 2012, vol. 13, no. 1, p. 44-50. ISSN 1229-9197.
153. XU, D., SANCHEZ-ROMAGUERA, V., BARBOSA, S., TRAVIS, W., DE WIT, J., SWAN, P. and YEATES, S. G. Inkjet printing of polymer solutions and the role of chain entanglement. *Journal of Materials Chemistry*. 2007, vol. 17, no. 46, p. 4902-4907. ISSN 0959-9428.

154. HONG, P., CHOU, C. and HE, C. Solvent effects on aggregation behavior of polyvinyl alcohol solutions. *Polymer*. 2001, vol. 42, no. 14, p. 6105-6112. ISSN 0032-3861.
155. HOSHINO, H., OKADA, S., URAKAWA, H. and KAJIWARA, K. Gelation of poly(vinyl alcohol) in dimethyl sulfoxide/water solvent. *Polymer Bulletin*. 1996, vol. 37, no. 2, p. 237-244. ISSN 0170-0839.
156. HONG, S., HUANG, H. and HONG, P. Effects of solvent adsorption on solution properties of poly(vinyl alcohol)/dimethylsulfoxide/water ternary systems. *Journal of Applied Polymer Science*. 2004, vol. 92, no. 5, p. 3211-3217. ISSN 0021-8995.
157. TAKAHASHI, N., KANAYA, T., NISHIDA, K. and KAJI, K. Effects of cononsolvency on gelation of poly(vinyl alcohol) in mixed solvents of dimethyl sulfoxide and water. *Polymer*. 2003, vol. 44, no. 15, p. 4075-4078. ISSN 0032-3861.
158. HONG, S., HONG, P., CHEN, J. and SHIH, K. Effect of mixed solvent on solution properties and gelation behavior of poly(vinyl alcohol). *European Polymer Journal*. 2009, vol. 45, no. 4, p. 1158-1168. ISSN 0014-3057.
159. Anonymous. *Jetable Fluid Formulation Guidelines*. FUJIFILM Dimatix, Inc., May 16, 2013 [cit. 10.7.2017]. Available in: https://www.fujifilmusa.com/shared/bin/Dimatix_Materials_Printer_Jetable_Fluid_Formulation_Guidelines_05-13.pdf.
160. SMITH, P. J. The Behaviour of a Droplet on the Substrate. *In The chemistry of inkjet inks*. MAGDASSI, S. Eds. Singapore: World Scientific. 2010. p. 55-72. ISBN 978-981-281-821-8.
161. SHARMA, P. and FANG, T. Breakup of liquid jets from non-circular orifices. *Experiments in Fluids*. 2014, vol. 55, no. 2, p. 1666. ISSN 0723-4864.
162. CLASEN, C., PHILLIPS, P. M., PALANGETIC, L. and VERMANT, J. Dispensing of rheologically complex fluids: The map of misery. *AICHE Journal*. 2012, vol. 58, no. 10, p. 3242-3255. ISSN 0001-1541.
163. HUTCHINGS, I. M., MARTIN, G. D. and HOATH, S. D. Introductory Remarks. *In Fundamentals of inkjet printing: The science of inkjet and droplets*. HOATH, S. D. Eds. Weinheim: Wiley-VCH Verlag. 2016. p. 1-12. ISBN 978-3-527-33785-9.

164. ZHANG, F., TUCK, C., HAGUE, R., HE, Y., SALEH, E., LI, Y., STURGESS, C. and WILDMAN, R. Inkjet printing of polyimide insulators for the 3D printing of dielectric materials for microelectronic applications. *Journal of Applied Polymer Science*. 2016, vol. 133, no. 18, p. 43361. ISSN 0021-8995.
165. HE, Y., WILDMAN, R. D., TUCK, C. J., CHRISTIE, S. D. R. and EDMONDSON, S. An Investigation of the Behavior of Solvent based Polycaprolactone ink for Material Jetting. *Scientific Reports*. 2016, vol. 6, p. 20852. ISSN 2045-2322.
166. TSAI, M. and HWANG, W. Effects of pulse voltage on the droplet formation of alcohol and ethylene glycol in a piezoelectric inkjet printing process with bipolar pulse. *Materials Transactions*. 2008, vol. 49, no. 2, p. 331-338.
167. WU, H. and LIN, H. Effects of Actuating Pressure Waveforms on the Droplet Behavior in a Piezoelectric Inkjet. *Materials Transactions*. 2010, vol. 51, no. 12, p. 2269-2276. ISSN 1345-9678.
168. BISSANNAGARI, M. and KIM, J. Inkjet printing of NiZn-ferrite films and their magnetic properties. *Ceramics International*. 2015, vol. 41, no. 6, p. 8023-8027. ISSN 0272-8842.
169. ARIN, M., LOMMENS, P., HOPKINS, S. C., POLLEFEYT, G., VAN DER EYCKEN, J., RICART, S., GRANADOS, X., GLOWACKI, B. A. and VAN DRIESSCHE, I. Deposition of photocatalytically active TiO₂ films by inkjet printing of TiO₂ nanoparticle suspensions obtained from microwave-assisted hydrothermal synthesis. *Nanotechnology*. 2012, vol. 23, no. 16, p. 165603. ISSN 0957-4484.
170. TIRTAATMADJA, V., MCKINLEY, G. and COOPER-WHITE, J. Drop formation and breakup of low viscosity elastic fluids: Effects of molecular weight and concentration. *Physics of Fluids*. 2006, vol. 18, no. 4, p. 043101. ISSN 1070-6631.
171. LI, H., ZHANG, W., ZHANG, X., SHEN, J., LIU, B., GAO, C. and ZOU, G. Single molecule force spectroscopy on poly(vinyl alcohol) by atomic force microscopy. *Macromolecular Rapid Communications*. 1998, vol. 19, no. 12, p. 609-611. ISSN 1022-1336.
172. HOATH, S. D., VADILLO, D. C., HARLEN, O. G., McILROY, C., MORRISON, N. F., HSIAO, W., TULADHAR, T. R., JUNG, S., MARTIN, G. D. and HUTCHINGS, I. M. Inkjet printing of weakly elastic polymer

solutions. *Journal of Non-Newtonian Fluid Mechanics*. 2014, vol. 205, p. 1-10. ISSN 0377-0257.

173. VADILLO, D. C., MATHUES, W. and CLASEN, C. Microsecond relaxation processes in shear and extensional flows of weakly elastic polymer solutions. *Rheologica Acta*. 2012, vol. 51, no. 8, p. 755-769. ISSN 0035-4511.
174. POOLE, R. J. The Deborah and Weissenberg numbers. *The British Society of Rheology, Rheology Bulletin*. 2012, vol. 53, no. 2, p. 32-39.
175. HWANG, G., LEE, C., AHN, I. K. -. and MHIN, B. J. Determination of reliable Lewis acid-base surface tension components of a solid in LW-AB approach. *Journal of Industrial and Engineering Chemistry*. 2011, vol. 17, no. 1, p. 125-129. ISSN 1226-086X.

APPENDIX – SUPPLEMENTARY DATA

The original from rheological measurements of PVA solutions prepared in water and in mixture of water/DMSO at defined temperatures.

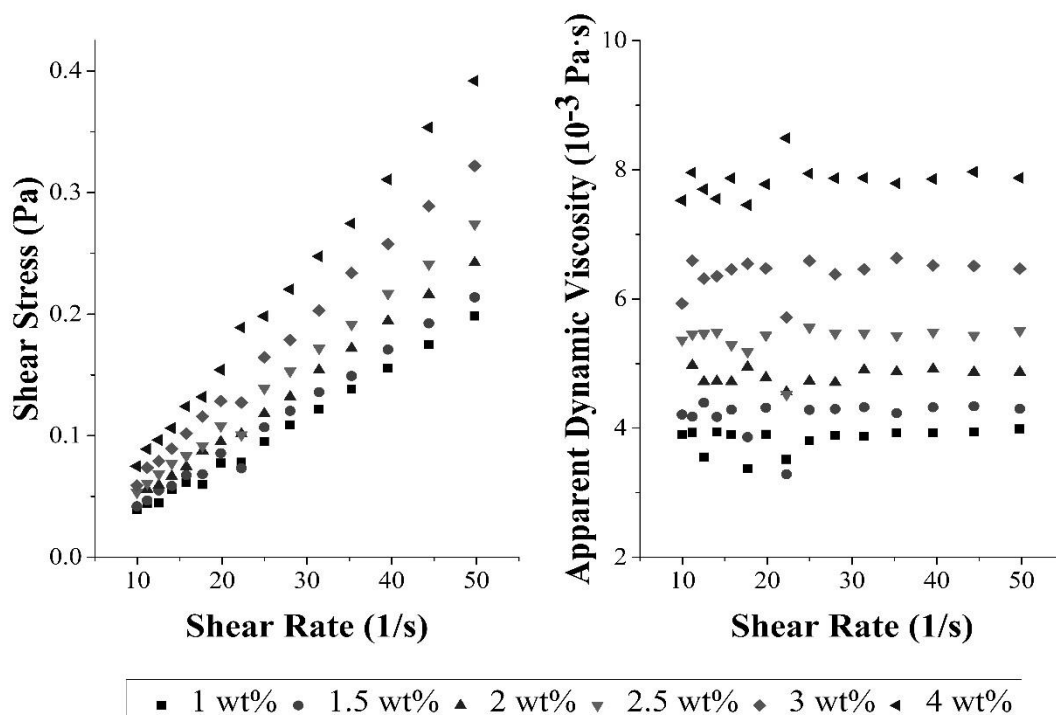


Figure 56. Shear stress vs. shear rate (left) and viscosity vs. shear rate (right) plots of aqueous PVA solutions at 10 °C.

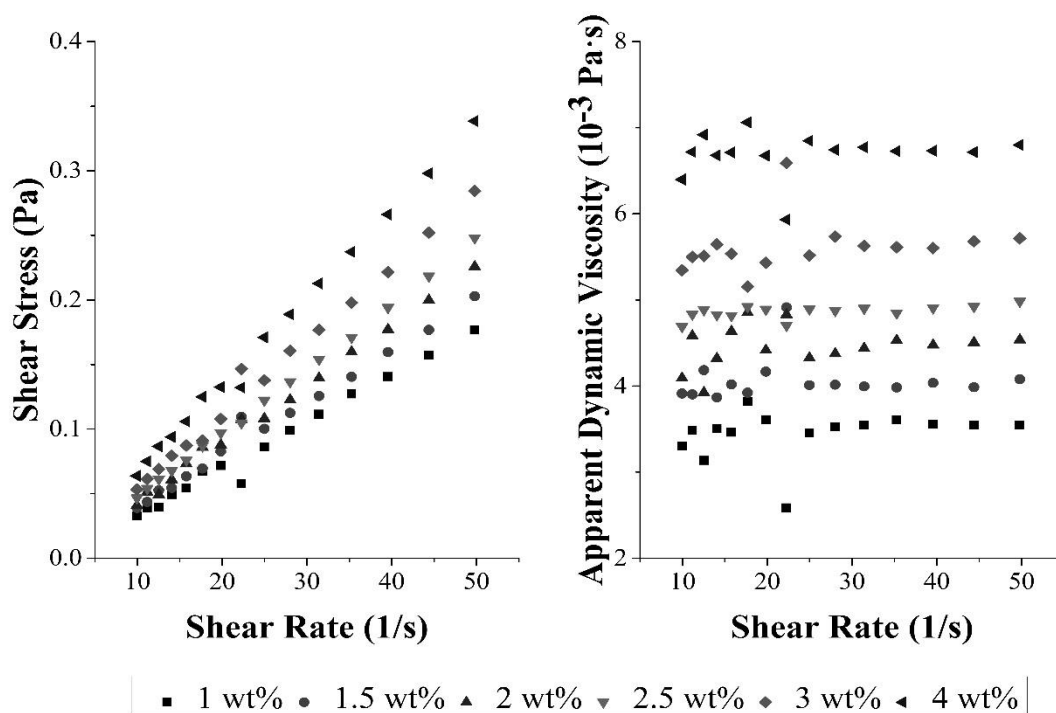


Figure 57. Shear stress vs. shear rate (left) and viscosity vs. shear rate (right) plots of aqueous PVA solutions at 15 °C.

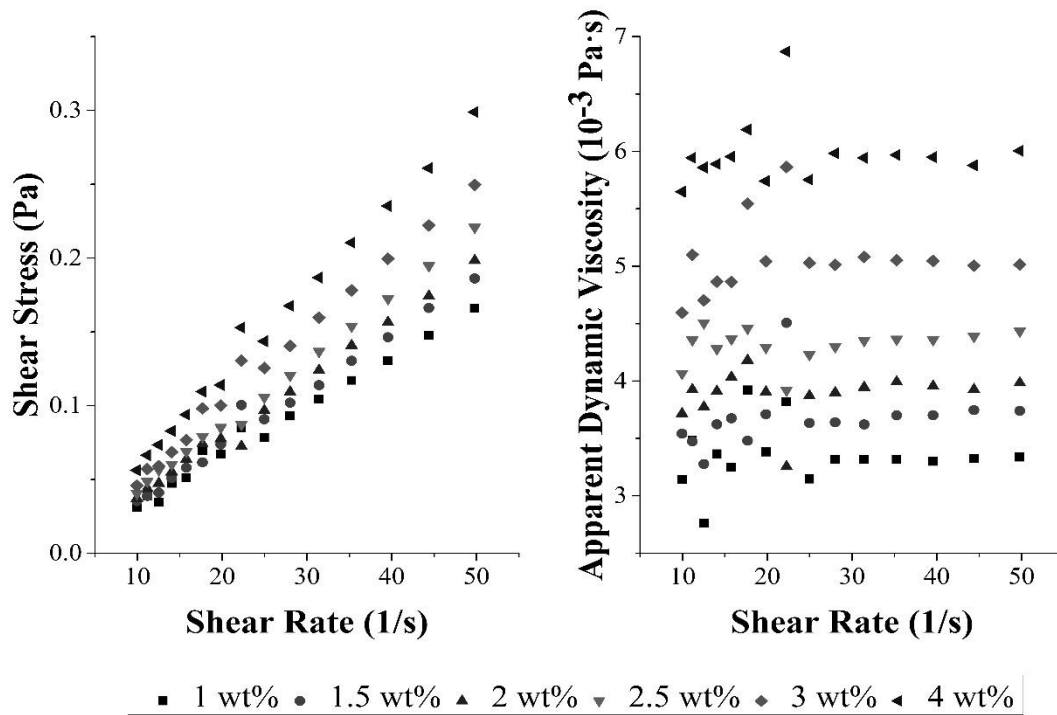


Figure 58. Shear stress vs. shear rate (left) and viscosity vs. shear rate (right) plots of aqueous PVA solutions at 20 °C.

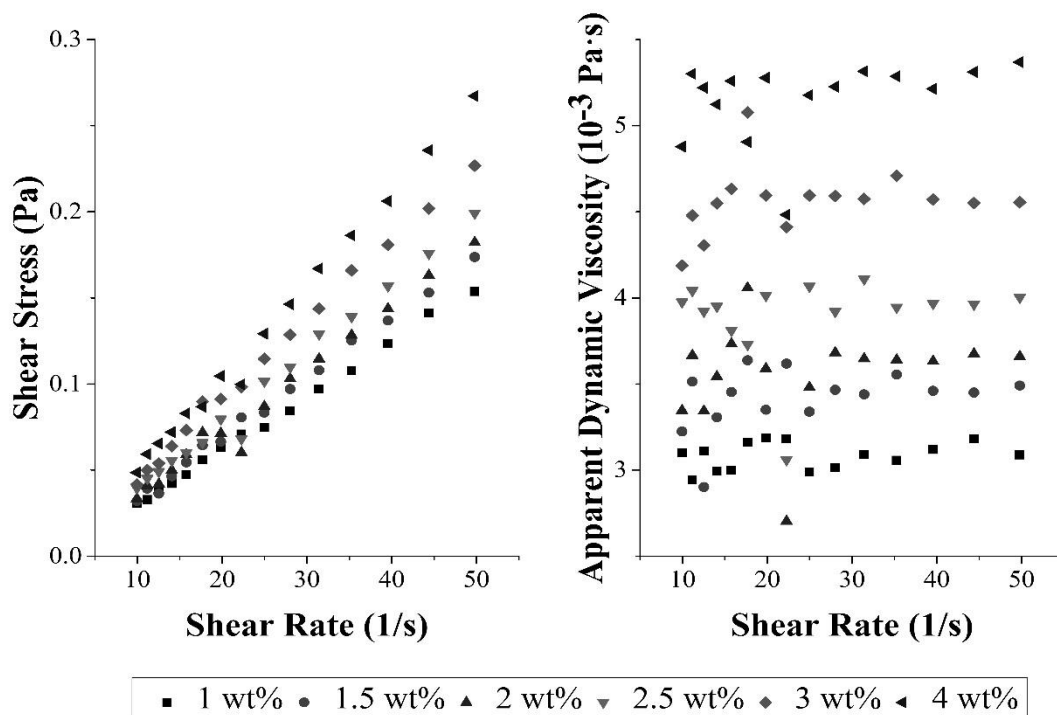


Figure 59. Shear stress vs. shear rate (left) and viscosity vs. shear rate (right) plots of aqueous PVA solutions at 25 °C.

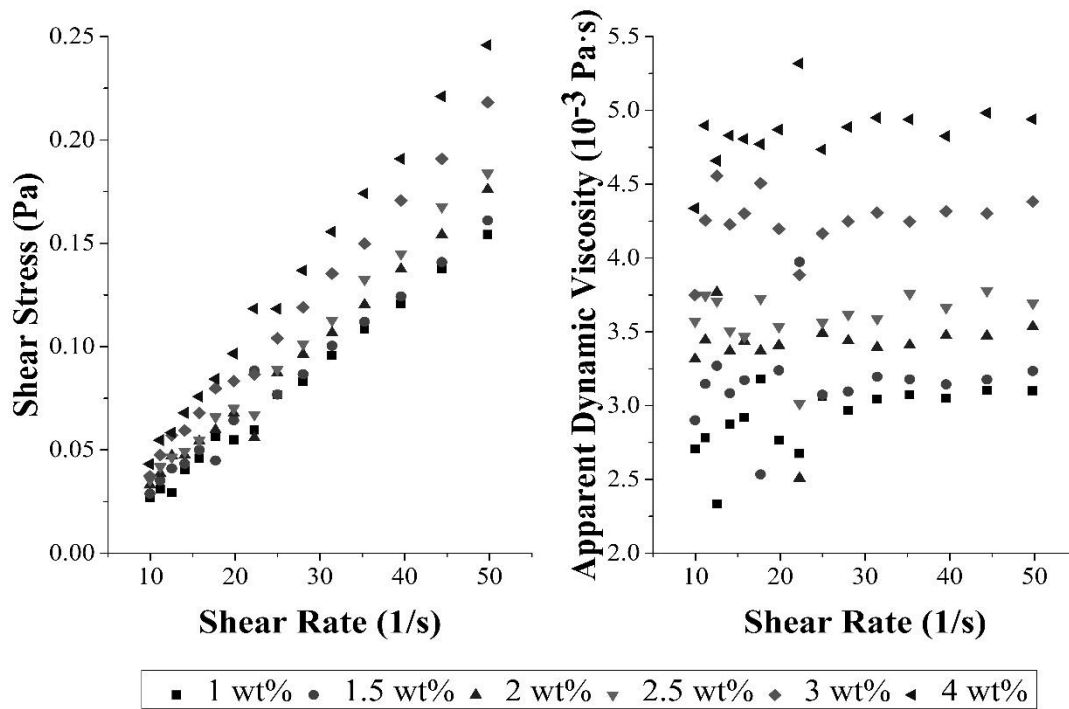


Figure 60. Shear stress vs. shear rate (left) and viscosity vs. shear rate (right) plots of aqueous PVA solutions at 30°C.

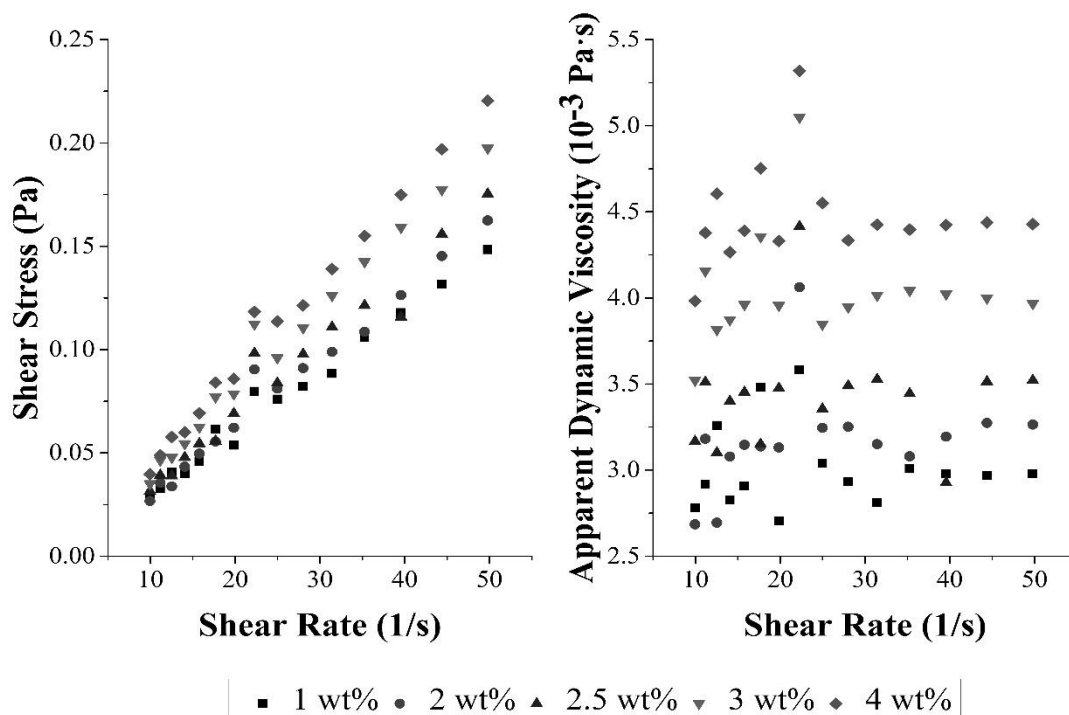


Figure 61. Shear stress vs. shear rate (left) and viscosity vs. shear rate (right) plots of aqueous PVA solutions at 35 °C.

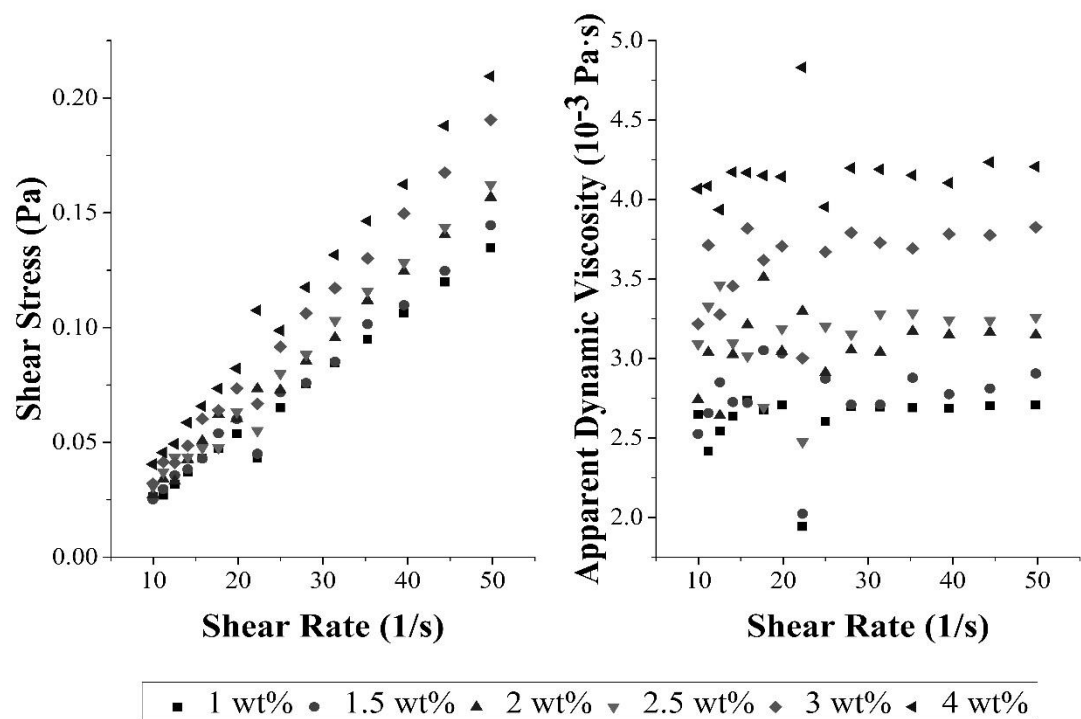


Figure 62. Shear stress vs. shear rate (left) and viscosity vs. shear rate (right) plots of aqueous PVA solutions at 40 °C.

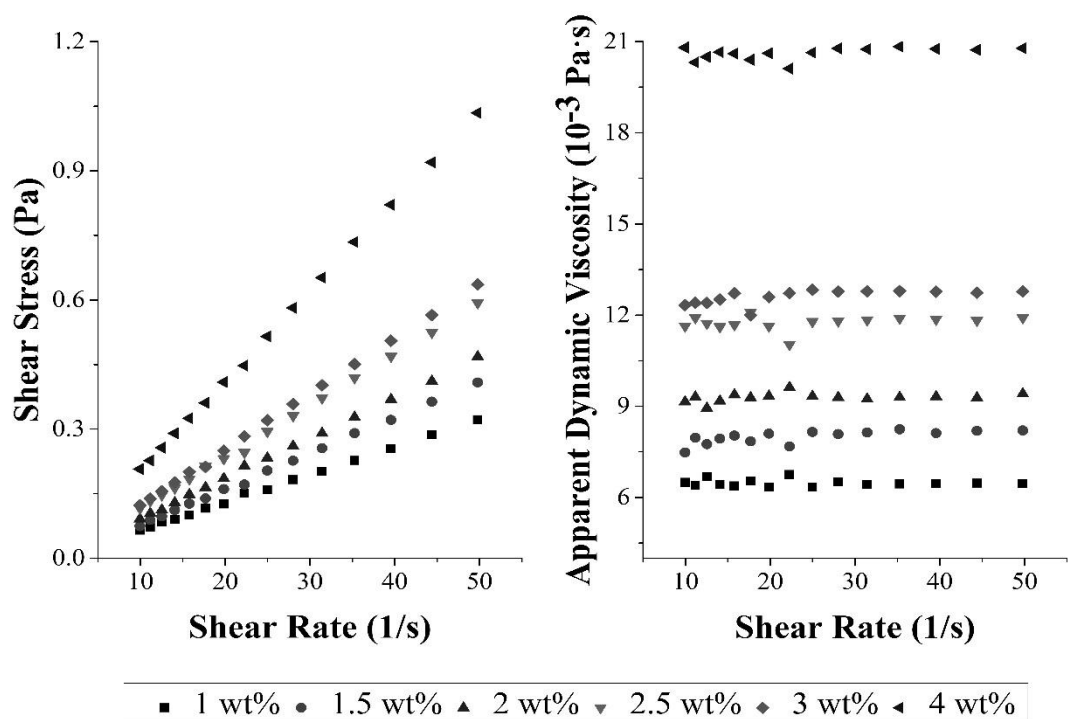


Figure 63. Shear stress vs. shear rate (left) and viscosity vs. shear rate (right) plots of PVA solutions prepared in mixture of water/DMSO at 10 °C.

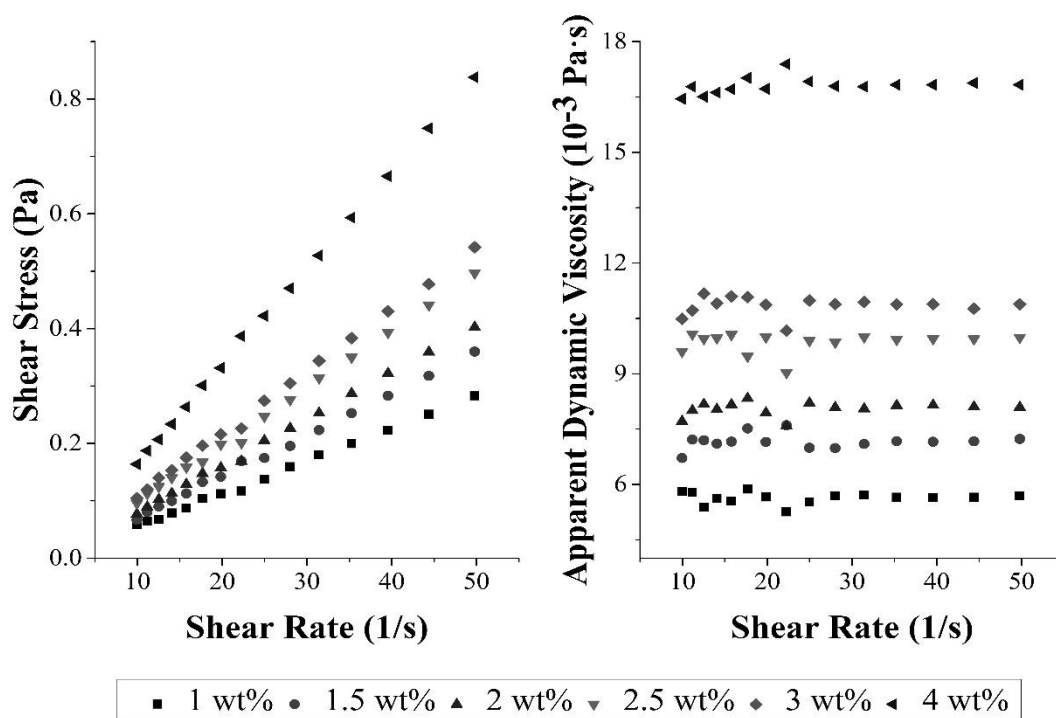


Figure 64. Shear stress vs. shear rate (left) and viscosity vs. shear rate (right) plots of PVA solutions prepared in mixture of water/DMSO at 15 °C

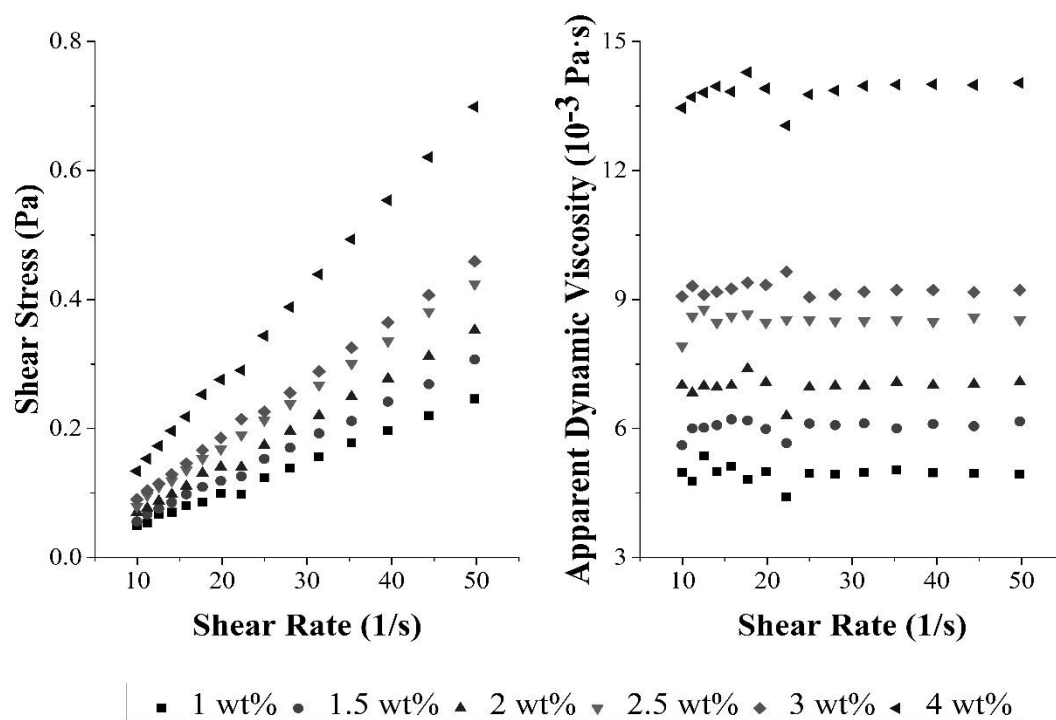


Figure 65. Shear stress vs. shear rate (left) and viscosity vs. shear rate (right) plots of PVA solutions prepared in mixture of water/DMSO at 20 °C

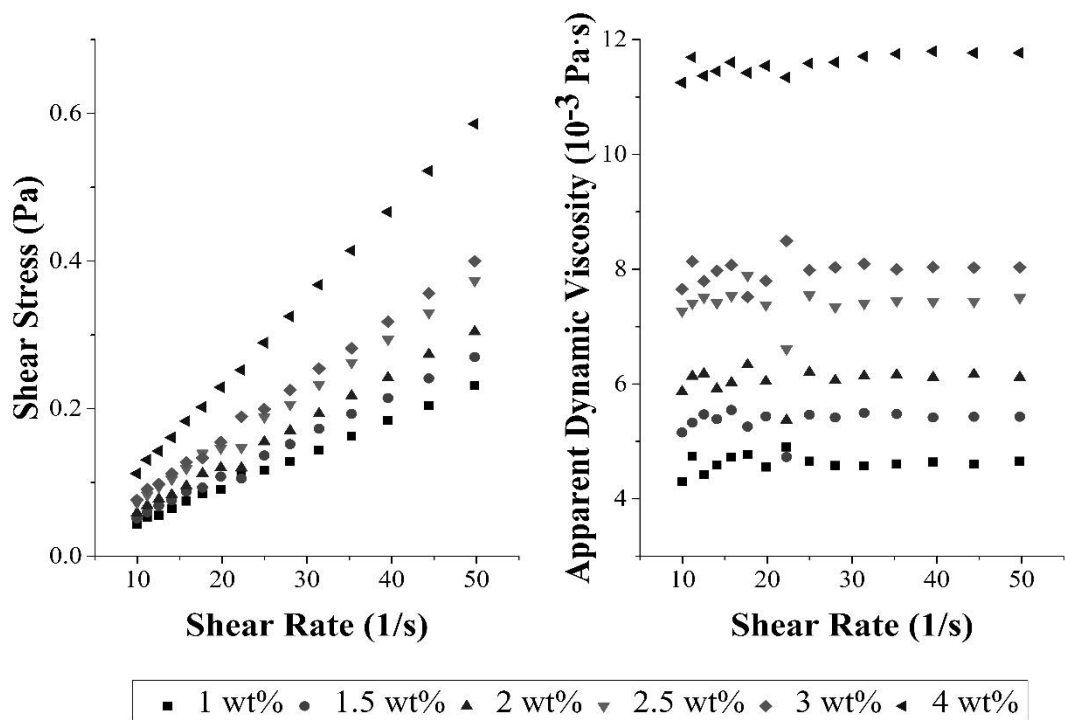


Figure 66. Shear stress vs. shear rate (left) and viscosity vs. shear rate (right) plots of PVA solutions prepared in mixture of water/DMSO at 25 °C.

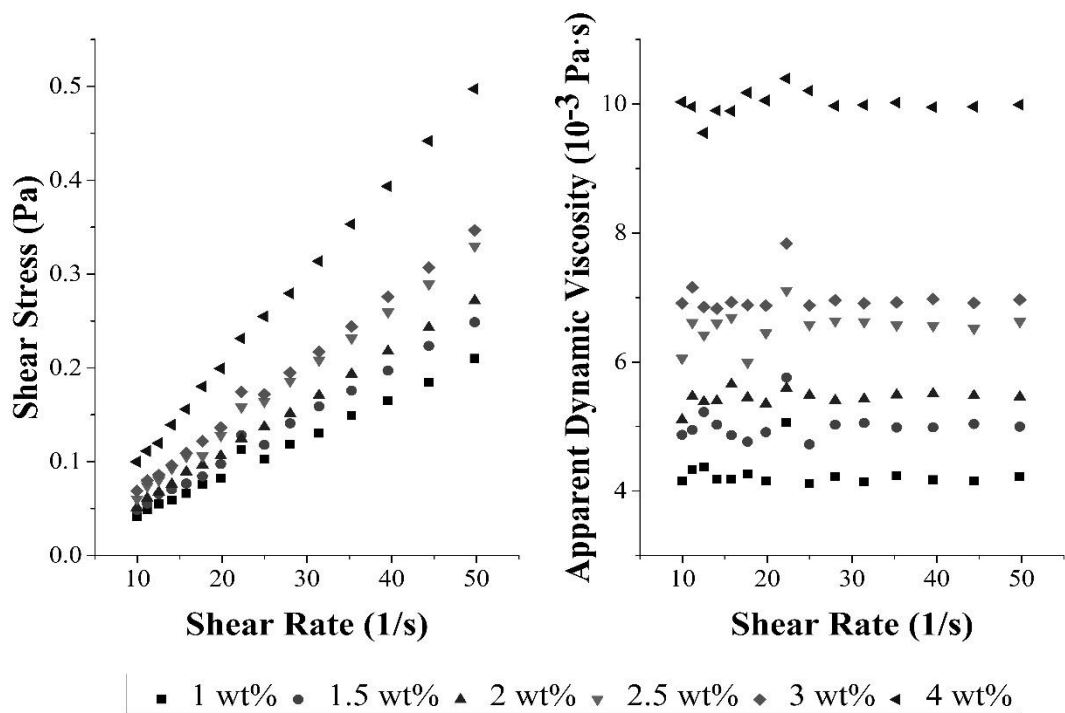


Figure 67. Shear stress vs. shear rate (left) and viscosity vs. shear rate (right) plots of PVA solutions prepared in mixture of water/DMSO at 30 °C

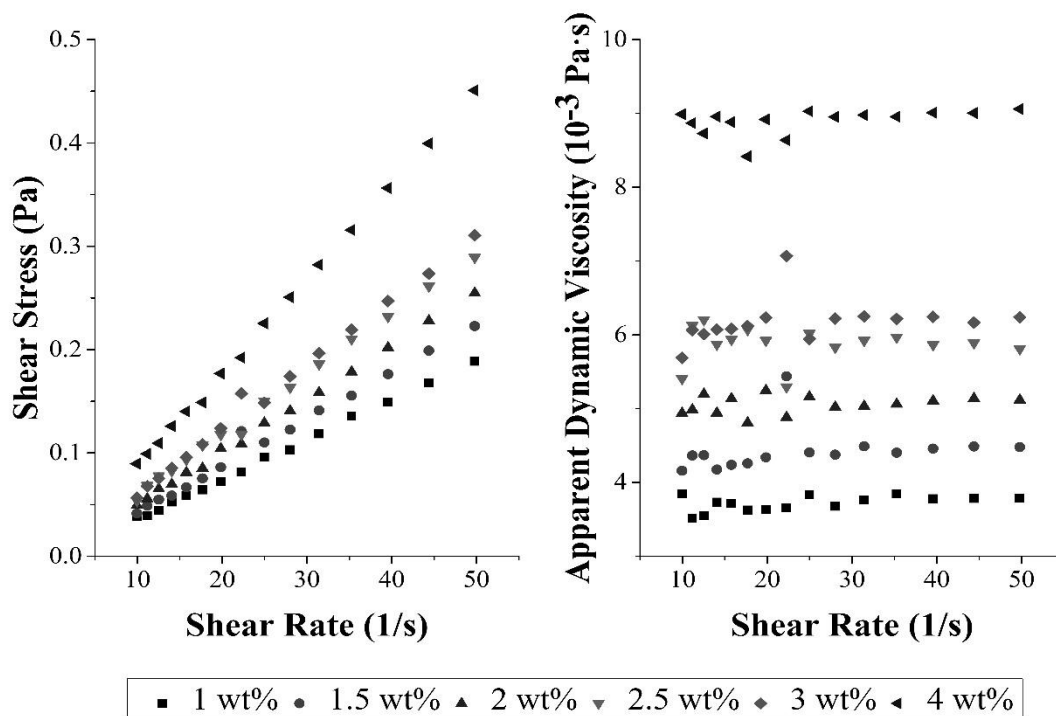


Figure 68. Shear stress vs. shear rate (left) and viscosity vs. shear rate (right) plots of PVA solutions prepared in mixture of water/DMSO at 35 °C

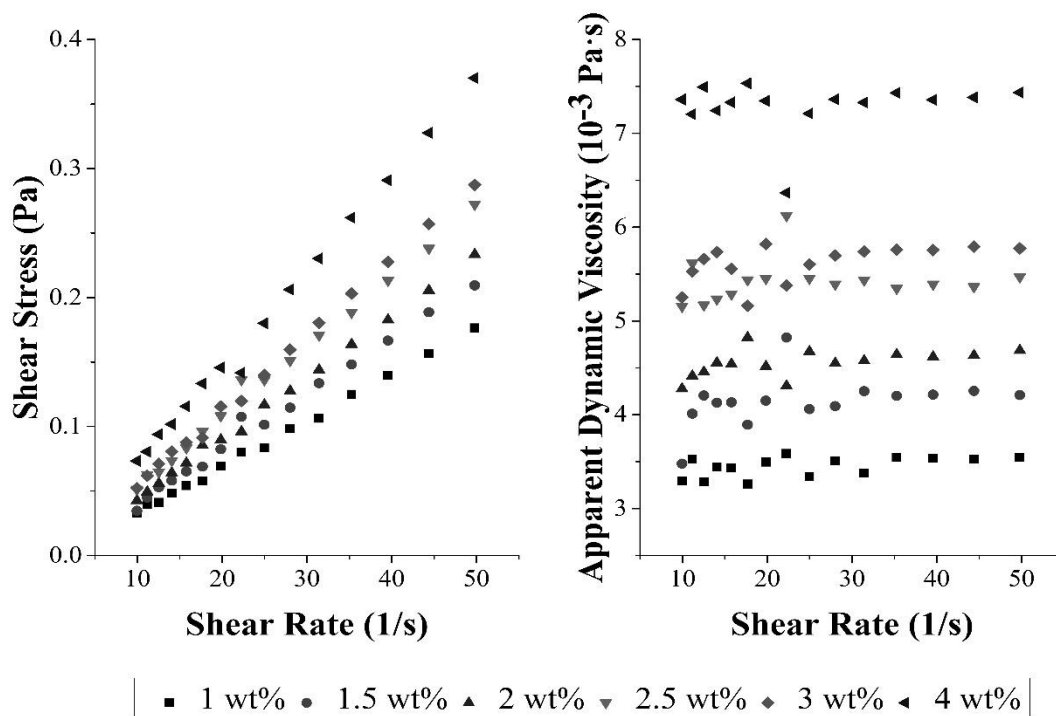


Figure 69. Shear stress vs. shear rate (left) and viscosity vs. shear rate (right) plots of PVA solutions prepared in mixture of water/DMSO at 40 °C.

LIST OF FIGURES

<i>Figure 1. Major parts of inkjet printing process. [7]</i>	8
<i>Figure 2. Scheme of relationship between resolution and drop spacing.</i>	10
<i>Figure 3. Scheme of continuous inkjet printing.[9]</i>	11
<i>Figure 4. Basic principle of the thermal inkjet printing process.[30]</i>	12
<i>Figure 5. Mechanism of jetting in thermal inkjet printing in relation with different parameters.[31]</i>	13
<i>Figure 6. The effects of electric field and poling direction in piezoelectric material. Standby position (A); shear mode (B); and thickness deformation mode (C).[29]</i>	14
<i>Figure 7. Principle of print-head with piezoelectric crystal on both sides of the ink pressure chamber.[38]</i>	15
<i>Figure 8. The proposed segments of pulse waveform (A), and the pumping chamber of piezoelectric print-head (B).[39]</i>	16
<i>Figure 9. Experimental set-up of electrostatic ink-jet printing. (1-pin electrode, insulating capillary tube filled with liquid, 2-metal plate electrode).[46]</i>	18
<i>Figure 10. The main classifications of inkjet ink.[48]</i>	19
<i>Figure 11. Flow curves for various time-independent materials. A represents Newtonian fluid; B, a dilatant fluid; C, a pseudo-plastic fluid; D, a Bingham fluid; E, a pseudo-plastic fluid with yield stress; and F, a dilatant fluid with yield stress.[65]</i>	25
<i>Figure 12. Effect of polymer molecular weight and concentration on viscosity of cellulose ester in γ-butyrolactone.[50]</i>	27
<i>Figure 13. Surface tension of PEG 300 in water at different temperatures and concentrations. [79]</i>	29
<i>Figure 14. Illustration of a contact angle formed by a sessile drop on smooth homogeneous solid surface. [88]</i>	30
<i>Figure 15. Three jet break-up modes, the axisymmetric varicose break-up ($m=0$), the lateral kink break-up ($m=1$), and the ramified jet break-up ($m=2$). [93]</i>	32
<i>Figure 16. Illustration of drop ejection and formation.</i>	33
<i>Figure 17. Original schematic diagrams showing the operating regime for stable operation of DOD ink-jet printing according to McKinley and Renardy. [99]</i>	35
<i>Figure 18. Original Kim and Baeks Capillary-Weber diagram.[92]</i>	36
<i>Figure 19. Shear stress vs. shear rate (left) and viscosity vs. shear rate (right) plots of aqueous PVA solutions at 25 °C.</i>	51
<i>Figure 20. Shear stress vs. shear rate (left) and viscosity vs. shear rate (right) plots of PVA solutions prepared in mixture of water/DMSO at 25 °C.....</i>	51

<i>Figure 21. Temperature dependence of apparent dynamic viscosity of PVA solutions (left) in water, and (right) in water/DMSO mixture. Multiple lines show result of theoretical global fits of unlimited region of experimental data by equation (7.2).</i>	52
<i>Figure 22. Temperature dependence of dynamic viscosity of PVA solutions (left) in water, and (right) in water/DMSO mixture. Multiple lines show result of theoretical global fits of selected region of experimental data by equation (7.2).</i>	54
<i>Figure 23. Plots of reduced viscosity against mass concentration of PVA solutions (left-Huggins plot) and reduced viscosity against specific viscosity (right-Schulz-Blaschke plot), respectively.</i>	58
<i>Figure 24. Turbidity of PVA solutions in water/DMSO obtained by naked eye observation. The “-” sign means no change, “turb” stands for turbidity and “gel” indicates formation of a gel)</i>	62
<i>Figure 25. Temperature-concentration dependence of surface tension of prepared PVA solutions in water/DMSO mixture.</i>	67
<i>Figure 26. Capillary-Weber diagram showing the position of prepared PVA solution in water/DMSO.</i>	71
<i>Figure 27. Reynolds-Capillary number diagram 1</i>	74
<i>Figure 28. Reynolds-Capillary number diagram 2.</i>	75
<i>Figure 29. The waveform used for inkjet printing of 2.5 wt% PVA solution in water/DMSO.</i>	78
<i>Figure 30. Cartridge settings for inkjet printing of 2.5 wt% PVA solution in water/DMSO.</i>	78
<i>Figure 31. Drop formation and ejection of 2.5 wt% of PVA in water/DMSO mixture, firing (jetting) voltage 34 V, cartridge temperature 35 °C.</i>	79
<i>Figure 32. Relationship between drop distance from nozzle against time in the case of 2.5 wt% PVA solution prepared in water/DMSO.</i>	80
<i>Figure 33. The analysis of surface energy and elastic energy</i>	84
<i>Figure 34. Analysis of drop ejection and formation based on captured images shown in Figure 31. Upper graph shows the position of the center of the main or final drop (open square with central dot) and satellite drop (open triangle with central dot) once formed. The middle gallery shows schematics of simplified geometric shapes used for image analysis. Lower graph: stacked bars show the volume and surface energy for the main drop (evaluated as a sphere, represented by grey bar) and its tail, thread, dumbbell or satellite (represented by red bar). The final drop property is than represented by the grey bar only after merging (from 63 μs). The kinetic energy is shown for main (grey bar) and satellite drop (from 41 μs, i.e. after its formation), the energy of the final drop is represented by the gray bar only after 63 μs. The time x-axis is common for both graphs.</i>	85
<i>Figure 35. Diagram of Deborah number against Ohnesorge number sketched by McKinley. [103]</i>	93

Figure 36. Replotted diagram of De number against Oh number showing the position of prepared solutions of PVA in water/DMSO.	94
Figure 37. Shape of the nozzles as seen by optical microscopy.	96
Figure 38. Cross-section of cartridge part containing the profile – optical microscopy.	96
Figure 39. The shape of ink channel in the bottom part of prepared sample – optical microscopy.	97
Figure 40. The shape of ink channel in the bottom part of prepared sample – optical microscopy.	97
Figure 41. The shape of ink channel in the bottom part of prepared sample – optical microscopy.	97
Figure 42. The picture of cartridge part containing ink channels captured from the top view (X - Y axes) obtained by x-ray analysis.	98
Figure 43. The picture of cartridge part containing ink channels captured from the side view (X - Z axes) obtained by x-ray analysis.	98
Figure 44. The picture of cartridge part containing ink channels captured from the side view (Y - Z axes) obtained by x-ray analysis.	99
Figure 45. Ink channel determined by SEM.	99
Figure 46. Ending of ink channel and its connection to nozzle captured by SEM. D.	100
Figure 47. Ink channel outlets with piezoelements captured by SEM. E.	100
Figure 48. The scheme of cross-section of cartridge part containing ink channel. The grey filled area stands for the piezoelectric element. Arrows show the liquid flow direction.	101
Figure 49. The set of bands printed from 3 wt% aqueous polymer solution PVA 4-98, magnified (A) 40 times, and (B) 100 times, respectively.	103
Figure 50. The set of bands printed from 2.5 wt% polymer solution PVA 4-98 in water/DMSO mixture, magnified (A) 40 times, and (B) 100 times, respectively.	104
Figure 51. Set of patterns prepared from 2.5 wt% PVA solution in mixture of water/DMSO with different drop spacing and number layers: 10 μm – one run (A), 10 μm – overprint (B), 17 μm – one run (C), and 17 μm – overprint (D).	105
Figure 52. Grid-shape pattern prepared from 2.5wt% PVA solution in mixture of water/DMSO. The black border rectangle shows area, where the profilometry measurement was performed.	106
Figure 53. A height profile of grid-shape pattern determined in the selected area.	106
Figure 54. Single drops patterns prepared at 254 μm (A) and 79 μm (B) drop spacing, respectively.	107
Figure 55. AFM topographic images of single drop of PVA printed on polymer substrate (left) with the cross-sectional profile (right) at 45 μm position in y axis.	108

<i>Figure 56. Shear stress vs. shear rate (left) and viscosity vs. shear rate (right) plots of aqueous PVA solutions at 10 °C.....</i>	<i>138</i>
<i>Figure 57. Shear stress vs. shear rate (left) and viscosity vs. shear rate (right) plots of aqueous PVA solutions at 15 °C.....</i>	<i>138</i>
<i>Figure 58. Shear stress vs. shear rate (left) and viscosity vs. shear rate (right) plots of aqueous PVA solutions at 20 °C.....</i>	<i>139</i>
<i>Figure 59. Shear stress vs. shear rate (left) and viscosity vs. shear rate (right) plots of aqueous PVA solutions at 25 °C.....</i>	<i>139</i>
<i>Figure 60. Shear stress vs. shear rate (left) and viscosity vs. shear rate (right) plots of aqueous PVA solutions at 30°C.....</i>	<i>140</i>
<i>Figure 61. Shear stress vs. shear rate (left) and viscosity vs. shear rate (right) plots of aqueous PVA solutions at 35 °C.....</i>	<i>140</i>
<i>Figure 62. Shear stress vs. shear rate (left) and viscosity vs. shear rate (right) plots of aqueous PVA solutions at 40 °C.....</i>	<i>141</i>
<i>Figure 63. Shear stress vs. shear rate (left) and viscosity vs. shear rate (right) plots of PVA solutions prepared in mixture of water/DMSO at 10 °C.</i>	<i>141</i>
<i>Figure 64. Shear stress vs. shear rate (left) and viscosity vs. shear rate (right) plots of PVA solutions prepared in mixture of water/DMSO at 15 °C</i>	<i>142</i>
<i>Figure 65. Shear stress vs. shear rate (left) and viscosity vs. shear rate (right) plots of PVA solutions prepared in mixture of water/DMSO at 20 °C</i>	<i>142</i>
<i>Figure 66. Shear stress vs. shear rate (left) and viscosity vs. shear rate (right) plots of PVA solutions prepared in mixture of water/DMSO at 25 °C.</i>	<i>143</i>
<i>Figure 67. Shear stress vs. shear rate (left) and viscosity vs. shear rate (right) plots of PVA solutions prepared in mixture of water/DMSO at 30 °C</i>	<i>143</i>
<i>Figure 68. Shear stress vs. shear rate (left) and viscosity vs. shear rate (right) plots of PVA solutions prepared in mixture of water/DMSO at 35 °C</i>	<i>144</i>
<i>Figure 69. Shear stress vs. shear rate (left) and viscosity vs. shear rate (right) plots of PVA solutions prepared in mixture of water/DMSO at 40 °C.</i>	<i>144</i>

LIST OF TABLES

<i>Table 1. The general composition of water-based inkjet ink. [50]</i>	20
<i>Table 2. Solvent-based ink formulation for both CIJ and DOD inkjet printing.[58, 59]</i>	21
<i>Table 3. Typical UV-curable monomer properties as a function of acrylate functionality.[50]</i>	23
<i>Table 4. Values of yield stress (τ_0) and flow behaviour index (n) for various materials. [65]</i>	26
<i>Table 5. The most common polar solvents and their selected properties such as boiling point, density, surface tension and dynamic viscosity [122-124]</i>	49
<i>Table 6. Model parameters for PVA solutions obtained by using equation (7.2) fitted into full data range shown in Figure 21.</i>	54
<i>Table 7. Model parameters for PVA solutions obtained by using equation (7.2) fitted into the selected data range shown in Figure 22.</i>	54
<i>Table 8. The observed data from determination of intrinsic viscosity as slope, intercept, correlation coefficient, Huggins (K_H) and Schulz-Blaschke (K_{SB}) constants for PVA.</i>	58
<i>Table 9. Dimensionless concentrations of prepared solutions PVA in water/DMSO (2:1 v/v) mixture.</i>	61
<i>Table 10. The gelation of PVA solutions prepared in solvents mixture water/DMSO.</i>	62
<i>Table 11. Surface tension of PVA solutions prepared in water/DMSO mixture at 25 °C.</i>	66
<i>Table 12. Surface tension of aqueous PVA solutions as well as used solvents measured at laboratory temperature of 28 °C.</i>	66
<i>Table 13. Experimental values of viscosity (η), SFT (σ) and density (ρ) of PVA in water/DMSO all obtained at 35°C. Density is expressed with 5 valid digits as this precision is given by the specification of the producer (Anton Paar.)</i> 68	
<i>Table 14. Calculated dimensionless criteria: the Reynolds number (Re), the Weber number (We), the Ohnesorge number (Oh), the Z-value and the Capillary number (Ca) of prepared solutions of PVA in water/DMSO mixture for 35 °C.</i>	69
<i>Table 15. Calculated viscoelastic criteria: the Rayleigh time (t_c), the Relaxation time according to Kuhn segment (λK), the Deborah number (De), the Ohnesorge number (Oh), the Elasticity number (El), and the Elasto-Capillary number (Ec) of prepared solutions of PVA in water/DMSO mixture for 35 °C.</i>	91
<i>Table 16. Surface energy of printed media PET substrate evaluated by See systems.</i>	102
<i>Table 17. Resolutions relationship of Dimatix material printer DMP-2800 Series.[39]</i>	103

LIST OF ABBREVIATIONS

Alphabetically ordered.

3D	Three-dimensional
AFM	Atomic force microscopy
ASH	Average step height
CaBER	Capillary break-up extensional rheometry
CIJ	Continuous inkjet
CMC	Critical micelle concentration
DH	Degree of hydrolysis
DP	Polymerization degree
DMSO	Dimethyl sulfoxide
DOD	Drop-on-Demand
DPI	Dots per inch
IJP	Inkjet printing
ITO	Indium tin oxide
LW/AB	Lifshitz-Van der Waals/acid-base
mLLDPE	Metallocene linear low-density polyethylene
MPR	Multipass rheometer
MSD	Minimum stand-off distance
OLED	Organic light-emitting diode
PEDOT	Poly(3,4-ethylenedioxythiophene)
PEG	Poly(ethylene glycol)
PET	Poly(ethylene terephthalate)
PIJ	Piezoelectric inkjet
PLED	Polymer light-emitting diode
PPM	Parts per million
PTFE	Polytetrafluoroethylene
PVA	Poly(vinyl alcohol)
PVP	Polyvinylpyrrolidone
PZT	Lead zirconium titanate
R2R	Roll-to-Roll
s.d.	Standard deviation
s.e.	Standard error
SEE System	Surface energy evaluation system
SEM	Scanning electron microscopy
SFT	Surface tension
SWCNT	Single-wall carbon nanotube
TIJ	Thermal inkjet
UV	Ultraviolet

LIST OF SYMBOLS

Alphabetically ordered.

A	Characteristic length
a, b, c	Constants (in equation 3.4)
A_1, B_1, C_1, D_1	Constants (in equation 7.1)
a_{MD}	Acceleration of main drop
a_S	Acceleration of long tail
C	Constant (in equation 3.3)
c	Mass concentration
c^*	Critical concentration
d	Pipe diameter (in equation 7.4 and 7.5)
D_0	Diameter of ink drop
F_{MD}	Elastic force of main drop
F_S	Elastic force of long tail
g	Gravitational acceleration
g_i^{total}	Total surface energy of i-th material
g_i^{LW}	Apolar part of surface energy of i-th material
g_i^{AB}	Polar part of surface energy of i-th material
g_i^+	Acid part of polar part of surface energy of i-th material
g_i^-	Base part of polar part of surface energy of i-th material
K	Constant (in equation 7.1)
K_H	Huggins constant
K_{SB}	Schulz-Blaschke constant
M_{MD}	Centre of gravity of main drop
M_S	Centre of gravity of satellites
M_V	Viscosity-average molecular weight
M_W	Weight-average molecular weight
n	Flow behaviour index
Q	Volumetric flow rate
R	Capillary radius
T	Temperature
t_c	Capillary break up time
t_v	Viscous break up time
V	Molar volume (in equation 3.3)
V	Voltage
v	Velocity
v/v	Volume/volume ratio
w	Mass fraction
$w/v \%$	Weight/volume percentage
$wt\%$	Percentage by mass
x_r	Inlet length (in equation 7.4 and 7.5)

γ	Surface tension (in equation 3.5)
γ_{LV}	Liquid-vapour interfacial tensions (in equation 3.5)
γ_{SL}	Solid-liquid interfacial tensions (in equation 3.5)
γ_{SV}	Solid-vapour interfacial tensions (in equation 3.5)
$\dot{\gamma}$	Shear rate
δ	Solubility parameter
η	Shear viscosity
η_{sp}	Specific viscosity
$\eta_{sp}/c, \eta_r$	Reduced viscosity
$[\eta]$	Intrinsic viscosity
θ	Theta – contact angle
λ	Relaxation time
λ_E	Extensional relaxation time
λ_K	Kuhn relaxation time
λ_{LVM}	Linear relaxation time
λ_Z	Zimm relaxation time
π	Mathematical constant
ρ	Density
σ	Surface tension
τ	Shear stress
τ_0	Yield stress
τ_d	Time constant (in equation 3.7)

LIST OF DIMENSIONLESS NUMBERS

Alphabetically ordered.

<i>Bo</i>	Bond number
<i>Ca</i>	Capillary number
<i>De</i>	Deborah number
<i>Ec</i>	Elasto-capillary number
<i>El</i>	Elasticity number
<i>La</i>	Laplace number
<i>Oh</i>	Ohnesorge number
<i>Re</i>	Reynolds number
<i>We</i>	Weber number
<i>Wi</i>	Weissenberg number
<i>Z</i>	Z number, Reciprocal Ohnesorge number

LIST OF UNITS

Alphabetically ordered.

°C	degree celsius
μm	micrometre
g	gravitational acceleration
g/cm ³	gram per cubic centimetre
kDa ²	kilo-Dalton
kg/cm ³	kilogram per cubic centimetre
m/s	metre per second
mm	millimetre
mN/m	milliNewtons per meter
mol %	molar percentage
mPa·s	milliPascal second
nm	nanometre
s	second
s ⁻¹	reciprocal second

² Although Dalton is a non-SI unit, it is widely accepted for use with the SI among units with experimentally determined values, better known as unified atomic mass unit (with the symbol u).

LIST OF PUBLICATIONS

Journal articles

1. SÚLY P., P. KRČMAR, J. MASLÍK, P. URBÁNEK, and I. KURITKA, Poly(vinyl alcohol): Formulation of a Polymer Ink for the Patterning of Substrates with a Drop-On-Demand Inkjet Printer. *Materials and Technology*. 2017, vol. 51, no. 1, s. 41-48. ISSN 1580-2949.
2. SÚLY P., P. KRČMAR, J. MASLÍK, P. URBÁNEK, and I. KURITKA, PVA Water/DMSO solution Ink for Digital Printing. Manuscript is prepared for submitting.
3. PLACHÝ T., M. MRLÍK, Z. KOZÁKOVÁ, P. SÚLY, M. SEDLÁČEK, V. PAVLÍNEK, and I. KURITKA, The Electrorheological Behavior of Suspensions Based on Molten-Salt Synthesized Lithium Titanate Nanoparticles and Their Core-Shell Titanate/Urea Analogues. *ACS Appl. Mater. Interfaces*. 2015, vol. 7, no. 6, pp. 3725–3731, DOI: 10.1021/am508471f
4. SEDLÁK J., I. KURITKA, M. MACHOVSKÝ, P. SÚLY, P. BAZANT, and T. SEDLÁČEK, Zinc oxide nanoparticles with surface modified by degradation of capping polymers in situ during microwave synthesis. *Advanced Powder Technology*. 2015, vol. 26, no. 4, pp. 1064-1071, DOI: 10.1016/j.apt.2015.04.016
5. KUCHARCZYK P., J. KALOUS, P. SÚLY and N. MISKOLCZI, Poly(1-butene) as a modifier of polylactide properties. *Polymer Science Series A*. 2015, vol. 57, no. 6, pp. 799-810, DOI: 10.1134/S0965545X15070081
6. HRABALÍKOVÁ M., P. HOLCÁPKOVÁ, P. SÚLY, and V. SEDLÁČEK, Immobilization of bacteriocin nisin into a poly(vinyl alcohol) polymer matrix crosslinked with nontoxic dicarboxylic acid. *Journal of Applied Polymer Science*. 2016, vol. 133, no. 28, 43674, DOI: 10.1002/app.43674
7. BONDAREV D., R. SIVKOVÁ, P. ŠÚLY, M. POLÁŠKOVÁ, O. KREJČÍ, R. KŘÍKAVOVÁ, Z. TRÁVNÍČEK, A. ZUKAL, M. KUBŮ, and J. SEDLÁČEK, Microporous conjugated polymers via homopolymerization of 2,5-diethynylthiophene, *European Polymer Journal*. 2017, vol. 92, no. 213-219, DOI: 10.1016/j.eurpolymj.2017.04.042.

Conference contributions

1. Jakub Ševčík, Pavel Urbánek, Pavol Šuly, Michal Urbánek, Jan Mašlík, Jan Antoš, Ivo Kuřitka, Preparation and characterization of nanostructured thin films applicable in polymer light emitting devices; 8th International Conference on Nanomaterials - Research and Application, NANOCON 2016, 2016, ISBN 978-808729471-0
2. Pavol Šuly, Petr Krčmář, Jan Mašlík, Pavel Urbánek and Ivo Kuřitka; Poly(vinyl alcohol): Formulation of a Polymer Ink for the Patterning of Substrates with a Drop-On-Demand Inkjet Printer; 23rd International Conference on Materials and Technology, 2015, ISBN 978-961-92518-8-1.
3. Petr Krčmář, Pavel Urbánek, Ivo Kuřitka, Jan Mašlík and Pavol Šuly; The preparation and characterization of CuO inkjet inks for gas sensors; Lopec 2014 7th International Exhibition and Conference for the Printed Electronics Industry
4. Jan Mašlík, Pavel Urbánek, Ivo Kuřitka, Petr Krčmář, Pavol Šuly and Michal Machovský; The preparation and characterization of ITO ink for gas sensing; Lopec 2014 7th International Exhibition and Conference for the Printed Electronics Industry
5. Pavel Urbánek, Jakub Ševčík, Jan Mašlík, Petr Krčmář, Ivo Kuřitka, Pavol Šuly, Barbora Hanulíková; The influence of ZnO nanoparticles content on the luminescence of the MEH-PPV in OLED devices; International Conference Plastko 2014, ISBN-978-80-7454-335-7.

Patent applications and Utility models

1. Utility model Nr. 26391 “Inorganic ink based on nanoparticles, intended especially for material printing.” Ivo Kuřitka, Pavel Urbánek, Petr Krčmář, Jan Mašlík, Pavol Šuly.
2. Inorganic ink for material printing applications, comprises copper oxide nanoparticles, polymeric dispersant and rest of water. Krčmář, P, Kuřitka, I, Mašlík J, Šuly P, Urbánek P. Patent application: CZ201301022-A3

CURRICULUM VITAE

Name: Pavol Šuly

Date of birth: 9th February 1988

Place of birth: Bánovce nad Bebravou, Slovakia

Permanent address: Ozorovská Hlavná 826/48, 95701 Bánovce nad Bebravou, Slovakia

Affiliation: Centre of Polymer Systems, Tomas Bata University in Zlín, tř. T. Bati 5678, 76001 Zlín, Czech Republic

Polymer Centre, Faculty of Technology, Tomas Bata University in Zlín, náměstí T.G. Masaryka 275, 76272 Zlín, Czech Republic

Telephone: (+420) 57-603-8128

E-mail: suly@utb.cz

Education: 2012 – to date
Tomas Bata University in Zlín, Faculty of Technology, Ph.D. studies in Chemistry and Materials Technology, Specialization: Technology of Macromolecular Compounds

2010 – 2012
Tomas Bata University in Zlín, Faculty of Technology, Master`s degree in Chemistry and Materials Technology, Specialization: Polymer Engineering

2007 – 2010
Tomas Bata University in Zlín, Faculty of Technology, Bachelor`s degree in Chemistry and Materials Technology, Specialization: Polymeric Materials and Technologies

2003 – 2007
Secondary vocational school clothing, Bánovce nad Bebravou, Specialization: Technician of Shoes Manufacturing, GCSE

Projects:

CZ.01.1.02/0.0/0.0/15_019/0004549 – Imflamable systems according to EN 45545 for composite fabrication (2016-2019) - member of the research team

CZ.01.1.02/0.0/0.0/15_019/0005090 – Stenopeic aperture for correction of presbyopy (2016-2019) - member of the research team

CZ.1.05/2.1.00/03.0111 – Centre of Polymer Systems (2011-2015) - member of the research team

LO 1504 – Centre of Polymer Systems Plus (2015-2020) - member of the research team

IGA/CPS/2016/007 – “Preparation and characterization of functional polymer materials for thin films applicable in printed electronics and sensor technology” - member of the research team

IGA/CPS/2015/006 – “Preparation of functional inks for material inkjet printing and their applications in printed electronics and sensors”- member of the research team

IGA/FT/2014/006 – “The modification of polymer substrates and new materials for inkjet printing of sensors” - member of the research team

IGA/FT/2013/025 – “The material printing of polymeric and inorganic inks for advance applications” - member of the research team